Dissecting the role of adaptor protein complex 4 (AP-4) on development and protein sorting in *Arabidopsis thaliana*

Studien zur Rolle des Adapter Protein Komplexes 4 (AP-4) für die Entwicklung und Proteinsortierung in Arabidopsis thaliana

Der Naturwissenschaftlichen Fakultät
der Friedrich-Alexander-Universität
Erlangen-Nürnberg
zur
Erlangung des Doktorgrades Dr. rer. nat.

vorgelegt von
Christina Margarete **Müdsam**
aus Neustadt an der Aisch

Als Dissertation genehmigt
von der Naturwissenschaftlichen Fakultät
der Friedrich-Alexander-Universität Erlangen-Nürnberg

Tag der mündlichen Prüfung:	22.11.2017
Vorsitzender des Promotionsorgans:	Prof. Dr. Georg Kreimer
Gutachter:	Prof. Dr. Norbert Sauer
	Prof. Dr. Andreas Burkovski

Parts of this work correspond to the pre-peer reviewed version of the following article:
Müdsam, C., Wollschläger, P., Sauer, N., Schneider, S. (2018). Sorting of Arabidopsis NRAMP3 and NRAMP4 depends on adaptor protein complex AP4 and a dileucine-based motif. Traffic (*Accepted for publication: 16 March 2018*), which has been/will be published in the final form at https://doi.org/10.1111/tra.12567.

Table of contents

Summary

The heterotetrameric adaptor protein complexes (AP-1 to AP-5) represent essential components of the protein sorting machinery in all eukaryotes. Nevertheless, the role of AP-4 remains comparatively poorly understood. Through fundamental characterization of *Arabidopsis* loss-of-function mutants and examination of subcellular targeting of numerous transmembrane proteins, this work aims to provide further insights into AP-4 dependent sorting processes and its effects on plant development.

In addition to *Arabidopsis* mutants either deficient for one of the large (AP4ß), or the medium (AP4µ) subunit of the complex, a corresponding double mutant line was established. Comparison of the different mutant lines with wildtype plants subsequently revealed that AP-4 affected plant growth throughout different developmental stages. More precisely, *ap4* mutants showed reduced growth of roots and of etiolated hypocotyls, and developed abnormal leaf trichomes with aberrant branches. Moreover, mutation of AP-4 subunits severely impaired pollen tube growth *in vitro*, and, correspondingly, reduced paternal transmission of the mutant alleles *in vivo*. Furthermore, *ap4* mutants showed defects in primary shoot growth, with a concomitant disruption of apical dominance. While auxin is known to suppress the outgrowth of lateral buds in the wild-type, the abnormal shoot growth of the mutant was not found to be associated with an altered distribution of the plant hormone. Further, disruption of AP-4 subunits altered the concentration of *myo*-inositol, glucose and fructose, and resulted in chlorosis, accompanied by a reduced chlorophyll content in mutant seedlings compared to the wildtype.

Overall, the double mutant as well as the single mutants, showed a highly pleiotropic, but identical phenotype, suggesting that the functionality of the complex is completely disrupted in the absence of any of the subunits. Importantly, stable reintroduction of *AP4µ* fused to *-GUS* or *-GFP*, expressed under control of an *AP4µ-promoter* fragment, completely restored the wildtype phenotype in *ap4µ* mutant plants. In agreement with other recently published data, AP4µ-GFP was localized to small punctate intracellular compartments. Promoter activity was detected almost ubiquitously throughout plant growth, but markedly peaked in newly developing tissue, which was overall consistent with the various defects observed in the loss-of-function mutants.

Finally, live cell imaging of *Arabidopsis* mesophyll protoplasts transiently overexpressing fluorophore-fusions of potential cargos, revealed that the subcellular distribution of several transmembrane proteins was drastically altered in the absence of a functional AP-4 complex. For one, the absence of AP-4 impaired sorting of a fluorescently labeled aquaporin, GFP-PIP2;1, to the plasma membrane. And secondly, possibly correlating with the chlorotic appearance of *ap4* mutants, tonoplast targeting of GFP-fusions of the metal-ion transporters NRAMP3 and NRAMP4, as well as of the molybdate transporter MOT2, was substantially disturbed in the absence of AP-4. Colocalization studies further demonstrated a partial relocation of these proteins to the plasma membrane in *ap4*

mutants. In contrast, targeting of a GFP-fusion of inositol transporter INT1 to the vacuolar membrane was not affected by mutations in AP-4. This observation, in turn, confirmed that missorting of NRAMP3-, NRAMP4, or MOT2-GFP in the *ap4* mutants was specific, and not due to a general disruption of tonoplast targeting. Altogether, these results are the first to demonstrate that AP-4 affects subcellular sorting of specific vacuolar transmembrane proteins.

Closer inspection of the mechanisms behind sorting of NRAMP3 and NRAMP4 additionally revealed that tonoplast localization of each of the proteins strictly required a dileucine-based motif within their amino acid sequence. Finding that exchange of the critical leucine-pair for an alanine-duplet, or disruption of the AP-4 complex, both induced relocation of the metal-ion transporters to the plasma membrane, finally allowed for the hypothesis of a direct participation of the AP-4 complex in dileucine motif dependent protein sorting in the plant system.

Zusammenfassung

Die heterotetrameren Adapter Protein Komplexe (AP-1 bis AP-5) repräsentieren essentielle Komponenten der eukaryotischen Proteinsortierungsmaschinerie. Nichtsdestotrotz ist die Rolle des AP-4 Komplexes, insbesondere im pflanzlichen System, nach wie vor noch verhältnismäßig wenig untersucht. Eine grundlegende Charakterisierung entsprechender *Arabidopsis* Funktionsverlustmutanten und die Untersuchung der subzellulären Verteilung von zahlreichen Transmembranproteinen, sollten daher im Rahmen der vorliegenden Studie Einblicke in AP-4-abhängige Sortierungsprozesse und deren Auswirkungen auf die pflanzliche Entwicklung geben.

Zusätzlich zu Einzelmutanten, in denen jeweils entweder die Expression einer der großen Untereinheiten (*AP4ß*), oder die der mittleren Untereinheit (*AP4µ*) des AP-4 Komplexes durch T-DNA Insertion verhindert war, wurde die entsprechende Doppelmutante generiert. Der Vergleich der verschiedenen Mutantionslinien zum Wildtyp machte anschließend deutlich, dass der Komplex das Pflanzenwachstum über die verschiedenen Entwicklungsstadien hindurch beeinflusst. Konkret äußerte sich dies bei den Mutanten in einem reduzierten Wachstum von Wurzeln und von etiolierten Hypokotylen, sowie in der Entwicklung morphologisch abnormaler Trichome. Außerdem waren Mutationen in den Untereinheiten von AP-4 *in vitro* mit einer massiven Beeinträchtigung des Pollenschlauchwachstums verbunden. In Übereinstimmung hierzu, konnte auch *in vivo* eine verminderte paternale Transmission der einzelnen Mutanten-Allele, jeweils in Konkurrenz zum Wildtyp-Allel, festgestellt werden. Weiterhin zeigten Mutanten Störungen in der primären Sprossentwicklung, sowie eine häufig damit einhergehende Aufhebung der Apikaldominanz. Während Auxin zwar bekanntermaßen an der normalerweise stattfindenden Unterdrückung des Seitentriebwachstums beteiligt ist, konnte die abnormale Sprossentwicklung der Mutanten nicht auf eine veränderte Verteilung dieses Pflanzenhormons zurückgeführt werden. Abgesehen davon, führten Mutationen in Untereinheiten von AP-4 im Vergleich zum Wildtyp zu einem veränderten Gehalt an *myo*-Inosit, Glukose und Fruktose, sowie zu Chlorose, verbunden mit einer durch Eisenmangel zusätzlich verstärkten Reduktion des Chlorophyllgehalts.
Insgesamt zeigten sowohl die Doppelmutanten, als auch die Einzelmutanten also einen zwar stark pleiotropen, aber dennoch identischen und im Hinblick auf die einzelnen Aspekte gleich stark ausgeprägten Phänotyp. Dies implizierte, dass der Komplex bereits in Abwesenheit einer der Untereinheiten nicht mehr funktional ist. Darüber hinaus konnte in *ap4µ* Mutanten, durch stabile Expression der mit *-GFP* oder *-GUS* fusionierten, genomischen *AP4µ*-Sequenz unter Kontrolle eines *AP4µ*-Promoterfragments, ein zum Wildtyp identischer Phänotyp vollständig wiederhergestellt werden. In der entsprechenden Komplementationslinie konnte AP4µ-GFP anschließend an kleinen, punktförmigen, intrazellulären Strukturen detektiert werden, was mit den Ergebnissen

einer kürzlich veröffentlichen Studie konform ist, in der AP4µ am *trans*-Golgi Netzwerk nachgewiesen werden konnte. Promotoraktivität ließ sich weiterhin beinahe ubiquitär über das gesamte Wachstum hinweg detektieren, zeigte dabei jedoch vor allem in jungem Gewebe deutliche Maxima, was sich insgesamt mit der Polyphänie der Funktionsverlustmutanten deckte.

Im weiteren Verlauf der Arbeit, sollten Transmembranproteine identifiziert werden, die AP-4-abhängigen Sortierungsmechanismen unterliegen. Dazu wurden Fluorophor-Fusionen zahlreicher potentieller Cargos generiert und diese jeweils transient in *Arabidopsis* Mesophyllprotoplasten überexprimiert. Nach konfokalmikroskopischer Untersuchung konnten so später diejenigen Fusions-Proteine identifiziert werden, deren subzelluläre Verteilung in Abhängigkeit von AP-4 verändert war. In *ap4* Mutanten war hierbei im Vergleich zum Wildtyp zum einen die Sortierung eines fluoreszenzmarkierten Aquaporins, GFP-PIP2;1, zur Plasmamembran beeinträchtigt. Zum anderen zeigten mehrere, im Wildtyp am Tonoplasten lokalisierte Proteine, eine deutliche Verschiebung zu anderen Kompartimenten. So war in Abwesenheit des Komplexes, möglicherweise in Zusammenhang mit der in *ap4* Mutanten beobachteten Chlorose, sowohl die Sortierung von GFP-Fusionen der Metallionentransporter NRAMP3 und NRAMP4, als auch die des Molybdattransporters MOT2 zur Vakuolenmembran substanziell gestört. Weiterhin bestätigten Kolokalisationsstudien eine partielle Umsteuerung dieser Proteine zur Plasmamembran der Mutante. Im Gegensatz dazu, zeigte eine GFP-Fusion des Inositoltransporters INT1 in *ap4* Mutanten keinerlei Beeinträchtigung in Bezug auf die Sortierung zum Tonoplast. Das wiederum machte deutlich, dass die Umsteuerung von NRAMP3-, NRAMP4- und MOT2-GFP in der *ap4* Mutante spezifisch, und nicht auf eine generelle Störung der Proteinsortierung zur Vakuole zurückzuführen war.
Eine genauere Untersuchung von Mechanismen hinter der Sortierung von NRAMP3 und NRAMP4 zeigte außerdem, dass der Transport der beiden Proteine zum Tonoplasten jeweils streng von einem dileucin-basierten Motiv in deren Peptidsequenz abhängig war. Die Beobachtung, dass sowohl der Austausch des kritischen Leucinpaars gegen ein Alanindublett, als auch die Abwesenheit eines funktionalen AP-4 Komplexes, jeweils eine Umsteuerung der Metallionentransporter zur Plasmamembran zu Folge hatte, erlaubte schließlich die Hypothese einer direkten Beteiligung des AP-4 Komplexes bei der dileucin-motiv-abhängigen Proteinsortierung im pflanzlichen System.

1 Introduction

1.1 Protein trafficking along the secretory and endocytic pathway: the central role of adaptor protein complexes in post-Golgi sorting

All eukaryotic cells depend on a system to sort newly synthesized proteins to their specific target compartment(s) and to retrieve proteins for recycling or degradation - all while retaining the integrity and specific function of individual organelles of the endomembrane system. Although also tubular intermediates or even transient direct connections between compartments are postulated to contribute to the distribution of proteins, the relocation along the anterograde or secretory pathway and back along the retrograde or endocytic pathway mainly occurs via transport vesicles (reviewed by Watson and Stephens, 2005; Robinson et al., 2015), which mediate the shuttling between different organelles.

Proteins following the secretory pathway are initially (usually co-translationally) translocated into the endoplasmic reticulum (ER) (reviewed by Zimmermann et al., 2011). Transmembrane (TM) proteins, on which this work will mainly focus, become directly inserted into the ER membrane and keep their lumenal-to-cytosolic orientation throughout successive sorting steps. After passing ER-specific processing, such as particular glycosylations (Vitale, 1999), most proteins to travel further are integrated into vesicles via the coat protein complex COPII. These vesicles then follow the anterograde pathway to the *cis*-Golgi (Kreis et al., 1995; Hanton et al., 2005a; Watson and Stephens, 2005; Brandizzi and Barlowe, 2013). Alternatively, some proteins like the H^+-ATPase VHA-a3, have been shown to leave the ER independent of COPII- and are thought to reach their destination, the tonoplast (TP), without passing through the Golgi (Richter et al., 2007; Viotti, 2014). From the Golgi, ER-resident proteins that had escaped their target compartment can follow the retrograde pathway back to the ER via COPI, which also participates in *intra*-Golgi traffic (Kreis et al., 1995; Hanton et al., 2005a; Béthune et al., 2006; Szul and Sztul, 2011; Spang, 2013). Having passed the *cis*-, *medial*, and *trans*-cisternae of the Golgi, proteins finally reach the *trans*-Golgi network (TGN), which is often termed the major sorting station for protein trafficking (Keller and Simons, 1997; Traub and Kornfeld, 1997; Gu et al., 2001).

Via the TGN, TM proteins can be targeted to different endosomal compartments, to the plasma membrane (PM) or to the TP in plants, and to the equivalent lysosomal and vacuolar membrane in animals and yeasts, respectively. PM and vacuolar membranes collectively represent possible final destinations of the biosynthetic route. Contributing to the complexity of the subcellular sorting network (for a schematic overview, see Figure 1) they can be reached either directly, or via endosomal intermediates, intersecting the endocytic pathway (reviewed for example in Jürgens, 2004; Robinson et al., 2008; Richter et al., 2009; Drakakaki and Dandekar, 2013; Xiang et al., 2013; Gershlick et al., 2014a). Distinct routes, particularly those leading to the TP will be detailed in section 1.5.

PM localized proteins that are to be degraded, or to be recycled back to the PM later-on, enter the endocytic pathway. Removal receptors, channels, or transporters from any particular membrane, for example, provides a means to regulate signaling events and to quickly react to external stimuli (McMahon and Boucrot, 2011; Li et al., 2012; Paez Valencia et al., 2016). Representing the entrance to the endocytic pathway, the early endosome (EE) is defined as the first organelle to be reached after uptake from the PM. Whereas EEs are regarded as independent organelles in other organisms, the plant EE is often considered as an equivalent to the TGN, and therefore termed TGN/EE. This is largely based on experiments with the commonly used endocytic tracer FM4-64, which, directly upon endocytosis from the PM, appears to coincide with the TGN in plant cells (Dettmer et al., 2006; Viotti et al., 2010).

After its uptake, a protein can pass recycling endosomes for temporal storage prior to retransfer to the PM (Ang et al., 2004; Maxfield and McGraw, 2004; Taguchi, 2013). Alternatively, endocytosis can be followed by vacuolar or lysosomal degradation. Along this pathway, proteins are transported via the EE to the prevacuolar compartment (PVC), which corresponds to late endosomes (LE) (Lam et al., 2007), or multivesicular bodies (MVB) (Tse et al., 2004). There, the endosomal sorting complexes required for transport (ESCRT)-machinery mediates integration of the proteins to be degraded into internal vesicles (Hurley, 2008) prior to hydrolysis in the vacuole (Winter and Hauser, 2006).

The majority of all post-Golgi sorting steps described in the above paragraphs depends on adaptor protein (AP) complexes (Boehm and Bonifacino, 2001; Nakatsu and Ohno, 2003; Bassham et al., 2008; Robinson, 2015). Five AP complexes, termed AP-1 to AP-5, have been identified to date (Pearse and Robinson, 1990; Le Borgne et al., 1996; Dell'Angelica et al., 1997, 1999, Hirst et al., 1999, 2011). In addition to a more distantly related complex termed TSET (Van Damme et al., 2011; Gadeyne et al., 2014; Hirst et al., 2014), and some alternative monomeric adaptors, AP complexes can be recruited from the cytosol to distinct membranes, where they act as the hub between the proteins that are to be sorted to another compartment and numerous components of the vesicle coat machinery (which will be covered in more detail in sections 1.3.2 and 1.4).

In a way, AP complexes resemble logistics companies in that they recognize and accumulate their cargo to finally direct cargo-loaded vesicles along a specific route to their destination. Likewise, each AP complex is considered to act at distinctive cellular compartments from where it mediates specific transport steps for selected cargo proteins. Specific sorting routes of the endomembrane system of a plant cell and the corresponding AP complexes are depicted in Figure 1. Notably, the function of each AP complex, or more specifically, the routes on which it operates and the cargo-types it recognizes, is often conserved between different eukaryotic species.

In plants, AP-1 localizes to the TGN/EE and has been shown to participate in transport to the PVC or the vacuolar membrane (Park et al., 2013; Teh et al., 2013; Wang et al., 2013, 2014). In addition to its role in anterograde sorting, animal homologs of AP-1 have further been suggested to participate in transport to the PM of polarized cells, and to facilitate bi-directional trafficking between endosomes and the TGN (Hirst et al., 2012; Nakatsu et al., 2014). AP-2 participates in endocytosis from the PM in plants (Fan et al., 2013; Kim et

al., 2013; Yamaoka et al., 2013) and particularly during cell plate formation, it is considered to act together with TSET/TPLATE (Van Damme et al., 2006, 2011; Gadeyne et al., 2014). Similar to its yeast and animal homologs, plant AP-3 has been shown to be required for sorting of specific proteins to the vacuolar membrane (Wolfenstetter et al., 2012; Ebine et al., 2014). Agreeing with its role in vacuolar sorting, the complex is further considered to participate in the biogenesis of lytic vacuoles (Niihama et al., 2009; Feraru et al., 2010; Zwiewka et al., 2011). In animals, AP-4 participates in sorting from the TGN to endosomes (Burgos et al., 2010), and AP-5 has been shown to localize to late endosomal compartments and is thus considered to contribute to endosomal sorting (Hirst et al., 2011).

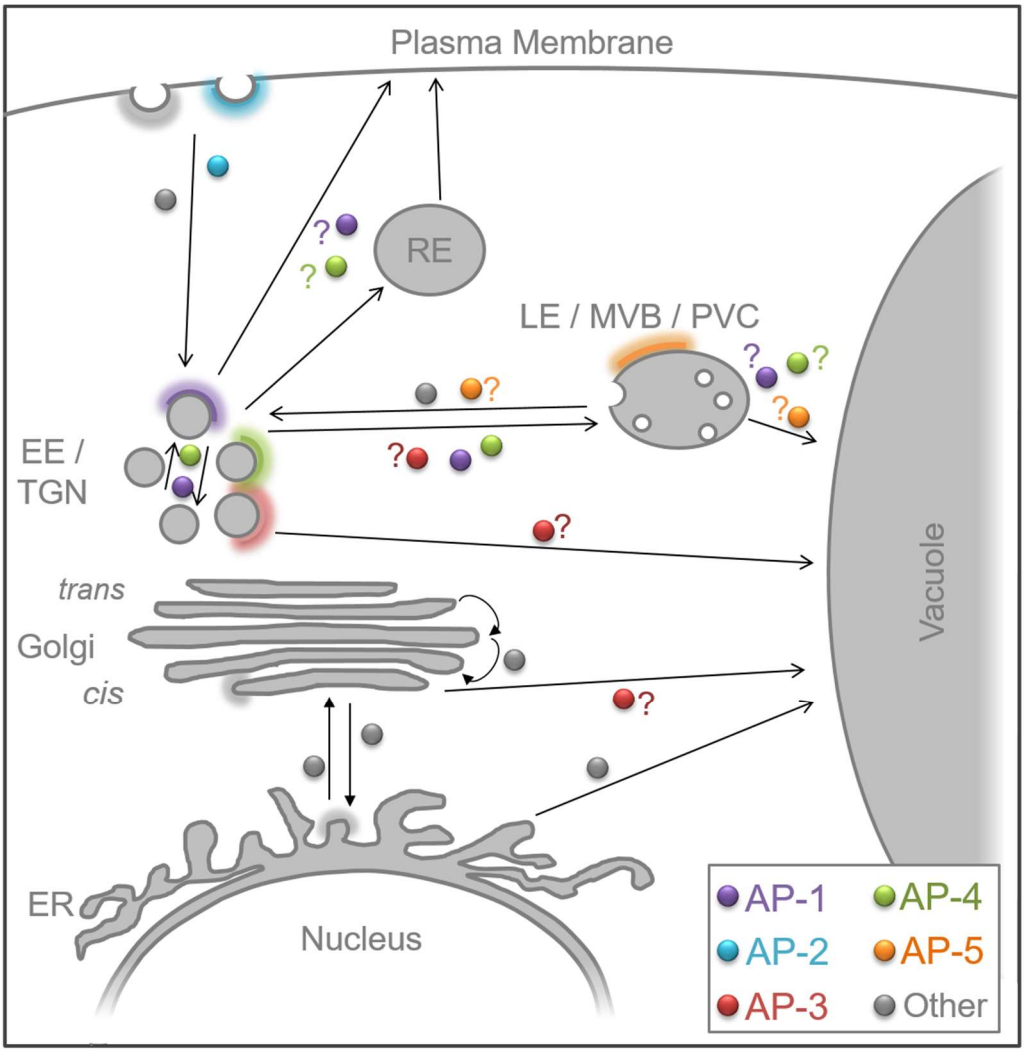

Figure 1: Vesicle trafficking pathways along the secretory and endocytic pathway with corresponding adaptors known or postulated to act at each step.

Small circles represent coated vesicles (see inset for color-code of adaptors/coat). Labeled organellar membranes represent preferential localization of each AP complex (same color-code).

Newly synthesized transmembrane proteins are transported from the ER to the Golgi. Alternatively, specific proteins are sorted from the ER directly to the TP. Retrograde Golgi to ER and intra-Golgi trafficking is mediated by COPI (herein labeled as "other" adaptor). Arrows between TGN/EE components indicate trafficking steps postulated for animal cells, where TGN and EE are considered independent organelles: AP-1 is thought to mediate bidirectional (TGN-to-EE and EE-to-TGN) transport (together with clathrin), whereas AP-4 participates in TGN-to-EE directed sorting. From the early endosome, shown as the plant equivalent TGN/EE, proteins may be transported to the PM (probably via AP-1 and/or

AP-4 vesicles) or to the vacuolar membrane, either directly (probably via AP-3), or passing the LE/MVB/PVC (again via AP-1 or AP-4). AP-5 is thought to act in endsosomal sorting at the LE. From the PM, proteins can be internalized via AP-2 (clathrin coated) vesicles (or the TSET complex) back to the TGN/EE (or EE in animals), from where they may either be recycled back to the PM (possibly via AP-1 or AP-4), or to the LE/PVC/MVB. AP-: adaptor protein complex; EE: early endosome; ER: endoplasmic reticulum; LE: late endosome; MVB: multivesicular body; PVC: prevacuolar compartment; RE: recycling endosome; TGN: *trans*-Golgi network.

1.2 Components of the protein sorting machinery

Of course, an AP complex alone does not make a vesicle. Nevertheless, the characteristic structure of the adaptor proteins allows them to interconnect individual components of the vesicle trafficking machinery.

1.2.1 Composition and structure of AP complexes and adaptins

Except for the trimeric *Arabidopsis* AP-5, all other AP complexes are heterotetrameric. As depicted in Figure 2, each ~270 kDa complex comprises two large (γ/α/δ/ε/ζ and ß1-5, ~100 kDa each), one medium (µ1-5, ~50 kDa), and one small (σ1-5, or in *Arabidopsis* σ1-4, ~20 kDa) subunit (reviewed in Kirchhausen, 1999; Boehm and Bonifacino, 2001), collectively referred to as adaptins. Each AP complex has the overall structure of a "head". Its "ears" are formed by the *N*-terminal domain of the large subunits, which are connected to the "trunk" via a flexible "hinge" region.

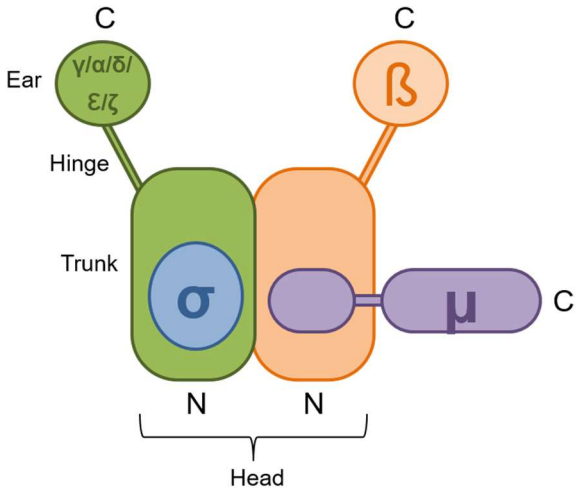

Figure 2: Schematic representation of the general arrangement of the different adaptins in AP complexes.
Each AP complex (with the exception of *Arabidopsis* AP-5) is heterotetrameric, consisting of two large (γ, α, δ, ε, or ζ, and one of ß1-5, each 90 –130 kDa), one medium (µ1-5, ~50 kDa) and one small (σ1-5, in *Arabidopsis* restricted to σ1-4, ~20 kDa) subunit. Each large subunit forms an *N*-terminal "trunk" and a *C*-terminal "ear"-domain, connected via a flexible "hinge" region. The "trunk" domains of both large adaptins, the small adaptin and the *N*-terminal domain of the medium subunit collectively represent the "head" of the complex. Figure modified from Boehm and Bonifacino (2001).

All five AP complexes occur conserved among all eukaryotic lineages, although some clades have secondarily lost individual complexes or, more rarely, a single subunit of a specific complex. Homologs of all five are for example present in mice and humans, whereas *Saccharomyces cerevisiae* and *Drosophila melanogaster* lack AP-4 and AP-5 (Hirst et al., 1999, 2011; Boehm and Bonifacino, 2002). Genes encoding the subunits for all five AP complexes, with the exception of σ5, have also been identified in the *Arabidopsis* genome (Pearse and Robinson, 1990; Le Borgne et al., 1996; Dell'Angelica et al., 1997, 1999, Hirst et al., 1999, 2011; Bassham et al., 2008). Not only the orthologs of distinct species, but also paralogous adaptins of AP-1, AP-2, AP-3 and AP-4 share some similarity

(21–83% identity at the amino acid level). The subunits of AP-5 on the other hand are less well conserved (< 10% sequence identity), but share key features for example with respect to secondary structure and size (Hirst et al., 2011). Despite their homology, subunits of different AP complexes are usually not interchangeable. Exceptions are, for example, the ß-subunits of *Arabidopsis* AP-1 and AP-2. It has been proposed that each of them can be a component of AP-1 and AP-2, and accordingly they are termed ß1/2A and ß1/2B (Boehm and Bonifacino, 2001; Dietel, 2012).

Subunits of several complexes are encoded by two or more genes, yielding different isoforms of a specific adaptin. Different isoforms further may confer distinct selectivity towards cargos or other interactors when integrated into the respective complex (Mattera et al., 2011; Guo et al., 2013). Mammalian AP-1 for example has two isoforms coding for the medium subunit and three isoforms coding for the small subunit. Whereas one *μ1* isoform (*μ1A/AP1M1*) is ubiquitously expressed, the other (*μ1B/AP1M2*) is functionally present in epithelial cells only (Pearse and Robinson, 1990; Kirchhausen, 1999; Ohno et al., 1999). Mutations of the single *σ1* isoforms have further been shown to cause distinct phenotypes in humans (Tarpey et al., 2006; Montpetit et al., 2008; Setta-Kaffetzi et al., 2014). In contrast, the isoforms of *μ1* in *Arabidopsis* show different expression levels (*AP1M*2 being the more highly expressed), but are otherwise thought to act redundantly (Park et al., 2013). Even more diversity results from the fact that multiple splice variants are thought to occur for several adaptins (Boehm and Bonifacino, 2001).

As already implied in this paragraph, AP complexes and their adaptins are denoted with slight variations throughout the literature. This work will follow a nomenclature, in which the complexes are denoted as AP-1, AP-2 etc. and the adaptins are denoted without hyphenation and using the appropriate Greek lower-case letters to indicate individual subunits (except AP1/2A and AP1/2B; see above).

1.2.2 Alternative adaptors involved in post-Golgi protein sorting

In addition to the similarities between homologous adaptins, they further share some similarity to subunits of the heteroheptameric COPI (16–21% identity at the amino acid level). COPI consists of two subcomplexes termed F-COPI and B-COPI, which in turn comprise four (F-COPI: ß-, γ-, δ-, and ζ-COP) or three (B-COPI: α-, ß'- and ε-COP) subunits (Fiedler et al., 1996). Whereas ß- and γ-COP are distantly related to the large adaptins, δ- and ζ-COP relate to the medium and small adaptins, respectively (Duden et al., 1991; Kreis et al., 1995). B-COPI components do not show any homology to adaptins, instead they are thought to function as scaffolds, similar to clathrin (Malhotra et al., 1989; Waters et al., 1991).

Some eukaryotes additionally possess monomeric adaptors of the GGA (Golgi-localizing, γ-adaptin ear homology, ARF-binding proteins), and/or the stonin family, which show some similarity to certain adaptin domains (Boehm and Bonifacino, 2001; Robinson and Bonifacino, 2001; Bonifacino, 2004; Robinson, 2004, 2015). Similar to AP complexes, they are able to recognize specific cargo and to recruit clathrin (Costaguta et al., 2001; Puertollano et al., 2001b; Zhu et al., 2001; Doray et al., 2008), but also interact with AP

complexes (Doray et al., 2002; Bai et al., 2004). Since no homologs of these monomeric adaptors are present in plants, they will not be described any further at this point.
Members of the monomeric epsinR/epsin and the clathrin-assembly lymphoid myeloid leukemia protein/assembly protein 180 kDa (CALM/AP180)-family on the other hand do have homologs in plants (Zouhar and Sauer, 2014). They contain ENTH (epsin *N*-terminal homology) or ANTH (AP180 *N*-terminal homology) domains, respectively, which characteristically bind specific phospholipids and thereby partially deform membranes (De Camilli et al., 2002; Legendre-Guillemin et al., 2004). Some of them additionally have been shown to interact with AP complexes (Song et al., 2006; Lee et al., 2007; Song et al., 2012) or to bind soluble NSF attachment protein receptor (SNARE)-proteins (Miller et al., 2007, 2011), which in turn are required for vesicles to fuse with a specific target membrane.

1.3 Sorting vesicles

This paragraph will briefly describe the process of vesicle trafficking and mainly focus on interactions of AP complexes with other components of transport vesicle formation and trafficking machinery. Interactions with the cargo proteins themselves will be covered in section 1.4.

1.3.1 Vesicle formation and delivery

Vesicle trafficking from one compartment to the other generally comprises multiple steps (Rothman and Wieland, 1996; Schmid, 1997; Borgne and Hoflack, 1998; Bonifacino and Glick, 2004). Just like sending a parcel requires preparation of the package and including an address label, before it can be pre-sorted and shipped to its destination, a vesicle needs to be formed, transported and delivered. The first step of vesicle formation, i.e. the coating at and budding from the donor membrane, requires the presence of cargo molecules, specific lipids and small GTPases for recruitment of the vesicle coat machinery (reviewed by Hwang and Robinson, 2009). This machinery in turn comprises AP complexes, monomeric adaptors, members of the Rab-family and scaffold proteins like clathrin (McMahon and Mills, 2004). Together, they concertedly cause the donor membrane to deform yielding a coated bud, which is finally detached via the action of members of the dynamin superfamily causing scission of the vesicle (Praefcke and McMahon, 2004; Ramachandran, 2011; Fujimoto and Tsutsumi, 2014). Next, the vesicle is transported to the acceptor compartment and the coat is removed. Transport is at least partially thought to occur along components of the cytoskeleton (Horgan and McCaffrey, 2011), agreeing with the direct interactions found between AP complexes and members of the kinesin superfamily (Nakagawa et al., 2000). Lastly, the vesicle tethers, docks and fuses to the target membrane, which is mostly achieved by interactions between compatible SNAREs on the vesicle and the target membrane (reviewed by Hong, 2005; Nelson et al., 2007).

1.3.2 Interactions between AP complexes and other components of the vesicle trafficking machinery

Their ability to interlink the different molecules makes AP complexes indispensable for many vesicle trafficking events. As already mentioned, some AP complexes are able to interact with clathrin, which forms the lattice around clathrin-coated vesicles (CCV). In fact, AP-1 and AP-2 were actually first identified in an attempt to dissect individual components isolated together with CCVs (reviewed by Robinson, 2015). It is now known that the interaction between AP complexes and clathrin occurs via a short stretch of amino acids within the "hinge" region of some ß-adaptins (Shih et al., 1995). This clathrin-box is present in AP-1, AP-2 (LLNLD) and, species-dependent but with a slight sequence modification, also in AP-3 (LLDLD) (Dell'Angelica et al., 1998; ter Haar et al., 2000). Nevertheless, AP-3 is considered to be able to act independently of clathrin at least to some extent (Seeger and Payne, 1992). Both AP-4 and AP-5 do not interact with clathrin, and accordingly cannot be detected as CCV components, although one study found AP-4 to localize on clathrin coated membranes (Barois and Bakke, 2005). So far, it is not known which alternative scaffold proteins are used by these complexes.

Apart from clathrin, AP complexes have been shown to interact with several other components of the vesicle trafficking machinery. The initial recruitment of an AP complex to a membrane is generally mediated through interactions with specific small GTPases, most notably ADP-ribosylation factor 1 (Arf1) (Ooi et al., 1998; Boehm et al., 2001; Ren et al., 2013). In its active (GTP-bound) state, Arf1 is able to associate with membranes (Randazzo et al., 1995; Antonny et al., 1997), to interact with lipid-modifying enzymes (Cockcroft et al., 1994; Honda et al., 1999; Jones et al., 2000), and most notably has been shown to allow for AP-1 to bind cargo proteins (Stamnes and Rothman, 1993). An interaction between Arf1(-GTP) and the ß- (and γ-) subunit of AP-1 results in a conformational change, allowing access to cargo-binding sites within the AP complex (Ren et al., 2013). Accordingly, membrane association of some AP complexes is disrupted, when Arf1 is forced to remain in its inactive form either by expression of a dominant-negative Arf1 mutant or by inhibiting GDP to GTP exchange through use of Arf-guanine nucleotide exchange factor(GEF)-inhibitors like Brefeldin A (Guo et al., 2013). The hydrolysis of GTP to GDP on the other hand, is later required to remove the vesicle coat to allow it to fuse with the acceptor membrane (Tanigawa et al., 1993; Lanoix et al., 1999; Meyer et al., 2005). GTP hydrolysis in turn is achieved (or at least accelerated) by Arf-GTPase activating proteins (GAPs) (Donaldson and Jackson, 2000; Meyer et al., 2005; Nie and Randazzo, 2006; Inoue and Randazzo, 2007).

AP complexes and some monomeric adaptors (see section 1.2.2) are further capable of directly binding certain phospholipids that either occur specifically or are enriched in the membrane of distinct organelles. In mammalian cells, an interaction between the γ-subunit of AP-1 and phosphatidylinositol 4-phosphate is for example necessary for AP-1 association to the TGN (Wang et al., 2003), and phosphatidylinositol 4,5-bisphosphate contributes to the targeting of AP-2 to the PM (Rohde et al., 2002; Höning et al., 2005; Jost et al., 1998).

Overall, transport of a cargo protein to its destination therefore depends on AP complexes to integrate the multitude of individual parameters, which synergistically result in vesicle formation and transport of the cargo to its destination.

1.4 Sorting motifs

A particular focus of this work is to elucidate how AP complexes, particularly AP-4, recognize or select specific transmembrane cargo. Sorting motifs, which usually comprise short linear peptide sequences within the cargo, play the major role in this process, because they act as address labels and thus, to a large extent, determine how and whereto the protein is targeted. Early in the secretory pathway, specific sorting motifs can be recognized by COPI or COPII complexes (Hanton et al., 2005a; Hwang and Robinson, 2009). Diacidic motifs for example are in some cases required for ER release (Hanton et al., 2005b; Dunkel et al., 2008; Zelazny et al., 2009; Cai et al., 2011; Sorieul et al., 2011). By interacting with monomeric adaptors and/or particularly AP complexes, several other sorting motifs direct cargos through almost all post-Golgi sorting steps. The following paragraphs will focus, with few exceptions, on common sorting motifs which contribute to AP dependent targeting throughout the eukaryotic lineages. Most studies on that topic have been conducted on animal cells or on yeasts. Although several of those signals have by now also been identified in plant proteins, comprehensive data are still scarce.
Generally, sorting motifs are positioned in the cytosolic domains of transmembrane proteins since they must be accessible to the respective AP complex. Often, sorting signals have to meet additional, signal-type specific, positional requirements regarding their distance from the next TM domain or the protein-terminus. They are classified according to their respective consensus sequence, usually comprising few invariant amino acids, which are generally large and hydrophobic and mediate association to AP complexes, as well as variable amino acids that often modulate binding preferences towards specific adaptors. The best characterized sorting signals relevant to post-Golgi sorting of transmembrane proteins by AP complexes, i.e. tyrosine-based and dileucine-based motifs, will be elaborated in more detail in the following. Prior, acidic clusters and ubiquitin-conjugation as signals for protein sorting will be described, briefly. An overview of this section is further presented in Table 1 (p. 10).

1.4.1 Acidic clusters

Consisting of glutamate- and/or aspartate-rich clusters together with phosphorylatable residues, acidic clusters are thought to mediate endosome to TGN retrieval of several transmembrane proteins in animals and yeasts which cycle between both compartments and show a TGN localization at steady state (Marcusson et al., 1994; Jones et al., 1995). The activity of the motif appears to be dependent on phosphorylation of its serine or threonine residues by the kinase CKII (Jones et al., 1995). In animals, phosphorylation of the motif brings about recruitment of phosphofurin acidic cluster sorting protein 1 (PACS-1) (Wan et al., 1998), which in turn is able to connect or transfer the cargo to AP-1 or AP-3 (Crump et al., 2001; Scott et al., 2003).

1.4.2 Ubiquitin-conjugation as a signal for protein sorting

Conjugation of one or more ubiquitin molecules to lysine residues of membrane proteins can act as a signal for endocytosis prior to lysosomal or vacuolar degradation, or can cause retention of a tagged protein to a specific compartment (Hicke and Dunn, 2003; Piper and Luzio, 2007; Scheuring et al., 2012). Initially this was demonstrated for the G-protein-coupled pheromone receptors Step2p and Step3p in yeasts (Hicke and Riezman, 1996; Roth and Davis, 1996), and in several receptors in animals, for example the growth hormone- or the epidermal growth factor-receptor (Strous et al., 1996; Levkowitz et al., 1999). In *Arabidopsis*, turnover of iron transporter IRT1 is mediated by ubiquitinylation of several cytosolic lysine residues (Barberon et al., 2011). Similarly, boron dependent mono- or di-ubiquitinylation has been shown to drive vacuolar degradation of the boron transporter BOR1 (Takano et al., 2010; Kasai et al., 2011). Whereas endocytosis of BOR1 from the PM actually depends on a tyrosine-based motif (Yoshinari et al., 2012), ubiquitinylation in this case mediates further sorting to the LE and the vacuole. The signal can be recognized by ubiquitin-interacting motifs, which initially have been identified in components of the 26S proteasome of yeasts. They are, however, also present in components of the protein sorting machinery of different species, for example within specific subunits of the ESCRT-I complex, or in some epsins (Young et al., 1998; Hofmann and Falquet, 2001).

1.4.3 Tyrosine-based motifs

1.4.3.1 The NPXY motif

The tyrosine-based NPXY motif solely acts as signal for endocytosis (Chen et al., 1990; Bonifacino and Traub, 2003), and further appears to be limited to certain type I, i.e. single-pass transmembrane proteins with an extracellular *N*-terminus (Bonifacino and Traub, 2003). For example, it is required for internalization of low density lipoprotein (LDL)-receptors (Davis et al., 1986). NPXY motifs can bind proteins with a phosphotyrosine binding domain (Santolini et al., 2000; Chen et al., 2006; Smith et al., 2006), which in turn interact with AP-2 (Morris and Cooper, 2001; He et al., 2002).

1.4.3.2 The YXXϕ motif

Tyrosine-based motifs of the YXXΦ-type (where Y is tyrosine, X any amino acid and Φ a bulky, hydrophobic amino acid, often methionine, phenylalanine, leucine, isoleucine or valine) can fulfill a broader function. Generally, they bind to the μ-adaptins of AP complexes. The X-residues as well as the amino acid preceding the tyrosine often contribute to binding preferences towards a specific μ-adaptin (Ohno et al., 1995; Stephens et al., 1997; Owen and Evans, 1998; Stephens and Banting, 1998). In polarized epithelial cells, they may contribute to basolateral sorting of PM localized proteins (Hunziker et al., 1991; Rajasekaran et al., 1994). In addition, they act as signals for

endocytosis, particularly when they are positioned 10-40 amino acids away from a transmembrane domain, but not in the *C*-terminus of the cargo (Bonifacino and Traub, 2003). YXXΦ motifs acting as lysosomal sorting signals, on the other hand (Williams and Fukuda, 1990; Harter and Mellman, 1992; Marks et al., 1996; Gough et al., 1999), are usually positioned in the *C*-terminus, with 6–9 amino acids distance to the neighboring transmembrane domain (Rohrer et al., 1996), and are often directly preceded by a glycine (Harter and Mellman, 1992) and with acidic amino acids occupying the X positions (Rous et al., 2002). Likewise, YXXΦ motifs of plant proteins have been shown to trigger endocytosis, and to contribute to polar localization of, for example, the boron transporter BOR1 (Bar and Avni, 2009; Takano et al., 2010). YXXΦ motifs in BP80 and VSR1 direct these sorting receptors to the PVC (Ron and Avni, 2004; daSilva et al., 2006), thereby adding to the repertoire of vacuolar targeting signals.

1.4.4 Dileucine-based motifs

1.4.4.1 The DXXLL motif

DXXLL type motifs occur at the *C*-terminus in some transmembrane receptors, such as the vertebrate mannose-6-phosphate-receptors, and in other transmembrane proteins shuffling between the TGN and endosomes, whereby they mediate the anterograde transport from TGN to endosomes (Zhu et al., 2001; Puertollano et al., 2001a; Doray et al., 2002; Puertollano et al., 2003). Since the aspartate residue often resides within a cluster of other acidic residues, it is sometimes referred to as an acidic cluster dileucine motif (Bonifacino and Traub, 2003). It should be highlighted, however, that DXXLL signals appear to bind AP complexes not directly (Höning et al., 1997; Puertollano et al., 2001a; Zhu et al., 2001). Instead, they interact with the VHS-domain (name derived from their occurrence in VPS-27, Hrs and STAM) of the monomeric GGAs (Nielsen et al., 2001; Puertollano et al., 2001a; Takatsu et al., 2001; Zhu et al., 2001; Shiba et al., 2002), which do not have homologs in plants.

1.4.4.2 [D/E]XXXL[L/I]-type motifs

In animals, dileucine motifs of the [D/E]XXXL[L/I]-type act as signals for basolateral targeting or endocytosis, and mediate localization to late endosomes, melanosomes, or lysosomes (Letourneur and Klausner, 1992; Sandoval et al., 2000; Bonifacino and Traub, 2003). They often occur at *C*- or *N*-terminal positions (Bonifacino and Traub, 2003), but seem to be functional also in other soluble domains, as exemplified by the dileucine motif in a cytosolic loop of ocular albinism type 1 (Piccirillo et al., 2006). This motif can either be positioned 6-11 amino acids away from neighboring transmembrane domains, or, particularly in proteins targeted to the LE or to lysosomes, may be located close to the *C*- or *N*-terminus (Bonifacino and Traub, 2003). Whereas the first leucine generally is strictly required, the second leucine can often be exchanged for isoleucine without affecting the

functionality of the motif (Letourneur and Klausner, 1992). Sometimes referred to as acidic dileucine motifs (≠ acidic cluster dileucine motif), LE- or lysosome-directing dileucine motifs seem to strictly require an acidic amino acid at position -4 from the first leucine (Sandoval et al., 2000), which is often preceded by further acidic residues or a phosphoacceptor (Bonifacino and Traub, 2003). In contrast, acidic residues preceding the dileucine (including the glutamate or aspartate at position -4) are no strict prerequisite for motifs to mediate internalization in animals (Pond et al., 1995; Sandoval et al., 2000). Although several dileucine-based motifs have been identified in plant proteins, it has yet to be clarified whether the presence of specific residues affects their function in similar ways (see section 3.3 for a discussion on that topic). Generally, [D/E]XXXL[L/I] motifs have been shown to interact with animal AP-1, AP-2, or AP-3, particularly with hemicomplexes consisting of the large γ/α/δ- and the corresponding σ1-3 subunits (Janvier et al., 2003; Doray et al., 2007; Lindwasser et al., 2008; Mattera et al., 2011).

In *Arabidopsis*, dileucine-based motifs have been found to be essential for the sorting of inositol transporter 1 (INT1; Wolfenstetter et al., 2012), vacuolar iron transporter 1 (VIT1; Wang et al., 2014), molybdate transporter 2 (MOT2; Gasber et al., 2011), the monosaccharide transporter ERD-6-LIKE1 (ESL1; Yamada et al., 2010), the two-pore channel TPC1 (Larisch et al., 2012), and the peptide transporters PTR2, PTR4, and PTR6 (Komarova et al., 2012).

However, for numerous proteins sorting signals have not been identified yet. Moreover, the presence of a dileucine motif does not guarantee localization to any specific compartment. The mammalian glucose transporters GLUT8 and GLUT12 for example do possess [D/E]XXXL[L/I] motifs (Augustin et al., 2005; Flessner and Moley, 2009), but localize to lysosomes, or to the PM and Golgi, respectively (Flessner and Moley, 2009). Similarly, GFP-fusions of murine TPC1 and TPC2 show isoform specific subcellular distributions, even in *Arabidopsis* protoplasts, where MmTPC1-GFP localizes to endosomal membranes, whereas MmTPC2-GFP localizes to the TP (Larisch et al., 2012), although both contain a dileucine motif.

Table 1: Overview of common signals involved in post-Golgi sorting of transmembrane proteins.

Sorting motif	Positional requirements	Function	Known adaptors
Acidic cluster	variable	endosome-to-TGN sorting	PACS-1 (AP-1, AP-3)
Ubiquitin-tag	variable (lysine residues)	endocytosis, endosomal sorting	Proteins with ubiquitin-interacting motif
NPXY	>10 amino acids distance to neighboring TM domains	endocytosis, receptor internalization	Proteins with phosphotyrosine-binding domain (AP-2)
YXXϕ	10–40 amino acids distance to TM domains; not in *C*-terminus	endocytosis	μ-adaptins of AP-1, AP-2, AP-3, AP-4
	6–9 amino acids distance to TM domains; in *C*- or *N*-terminus	sorting to lysosome, lysosome-related organelles, PVC, vacuole	
	variable	basolateral sorting	
[D/E]XXXL[L/I]	6–11 amino acids distance to TM domains	endocytosis	γ/σ1, α/σ1, and/or δ/σ3 of AP-1, AP-2, AP-3
[D/E]XXXL[L/I]	6–11 amino acids distance to TM domains, or near *C*- or *N*-terminus	sorting to lysosome, late endosome, or lysosome-related-organelles	
DXXLL	1–2 amino acids away from *C*-terminus	TGN-to-endosome sorting	VHS domain of GGAs

The single letter code is given for all amino acids. Further, positions labeled with "X" can be occupied by any amino acid, and ϕ indicates a bulky, hydrophobic amino acid (e.g. phenylalanine, isoleucine, leucine, methionine, valine). Positional requirements refer to cytosolic domains only. Crucial amino acids that cannot be exchanged for any other without impairing the functionality of a motif are given in red. Table modified from Wolfenstetter (2012).

1.5 The role of AP complexes in plant development and protein trafficking

Compared to their animal and yeast counterparts, the function of plant AP complexes and their preferences towards specific sorting signals is generally less well understood. And of all five AP complexes, AP-1, AP-2 and AP-3 have been examined in greater detail, whereas only little is known about the more recently identified AP-4 and AP-5. (Dell'Angelica et al., 1999; Hirst et al., 1999, 2011). Only within the recent years, genes encoding *Arabidopsis* adaptin homologs could be assigned to the respective complex, and several publications have since then illuminated the function of AP-1, AP-2 and AP-3 in *Arabidopsis*: like it does in other organisms, *Arabidopsis* AP-1 was shown to localize to the TGN (Park et al., 2013; Teh et al., 2013). Usually, the complete loss of an AP-1 adaptin is lethal to multicellular organisms (Boehm and Bonifacino, 2001; Robinson, 2004; Ohno, 2006). *Arabidopsis ap1m2* mutants only lack the more highly expressed isoform of the μ-subunit and are

viable. They were found to develop unbranched trichomes and to show defects in root growth, male fertility, and cytokinesis (Johnson et al., 2004; Park et al., 2013; Teh et al., 2013; Wang et al., 2013). AP-2 was shown to be recruited to the PM, to contribute to endocytosis (Fan et al., 2013; Kim et al., 2013; Yamaoka et al., 2013). In contrast to the detrimental effects of mutations in adaptins of AP-1 or AP-2, mutations in subunits of AP-3 do not cause any detectable morphological defects in *Arabidopsis* when plants are grown on soil (Niihama et al., 2009; Feraru et al., 2010; Zwiewka et al., 2011; Müdsam, 2012). However, AP-3 was found to be involved in the transition from protein storage to lytic vacuoles (Niihama et al., 2009; Feraru et al., 2010; Zwiewka et al., 2011).
It is by now well established that multiple sorting pathways may guide to one and the same compartment, but involve different AP complexes (and sorting motifs), as exemplary shown for different vacuolar (membrane) proteins in Figure 3. For example, AP-1 (but not AP-3) has recently been demonstrated to interact with the dileucine motif of VIT1, which reaches the TP via the TGN and the PVC (Wang et al., 2014). INT1 appears to follow this route, as well (Wolfenstetter et al., 2012; Wang et al., 2014). TP localization of sucrose transporter 4 (SUC4) on the other hand, strictly requires AP-3 (Wolfenstetter et al., 2012). The sorting motif(s) required for targeting of *Arabidopsis* SUC4 to the vacuolar membrane are so far unknown. Although VSR1 cycles between the TGN and the PVC (unlike VIT1, INT1 and SUC4 which all localize to the TP in *Arabidopsis*), soluble cargo bound by the receptor (12S globulin, 2S albumin) is finally targeted to the vacuole (Ahmed et al., 2000; Shimada et al., 2003). Sorting of the receptor requires a tyrosine-based sorting motif, which was shown to interact with the μ-subunit of AP-4 (Fuji et al., 2016).

As depicted in Figure 3, the subcellular localization of cargo can be differentially affected by the absence of the corresponding AP complex. In cells depleted for AP-1, fluorophore-fusions of INT1 or VIT1 are mostly relocated to the PM (Wang et al., 2014). Fluorescently labeled cargo of VSR1, which in turn interacts with AP-4, was found to be secreted into the extracellular space of mutants lacking any of the subunits of AP-4 (Fuji et al., 2016). Although this might suggest that the receptor itself is, similar to AP-1 cargo, relocated to the PM without its adaptor, the localization of VSR1 in *ap4* mutants has not been determined experimentally. In contrast to these examples, GFP-SUC4 was shown to localize exclusively to the *cis*-Golgi in mutants lacking the ß-subunit of AP-3 (Wolfenstetter et al., 2012).

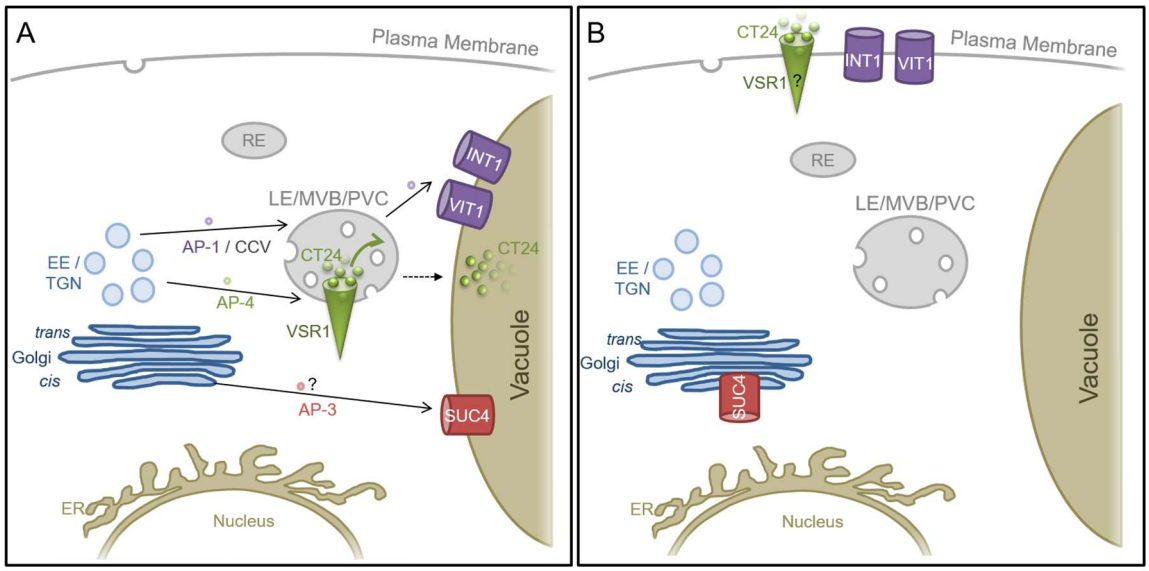

Figure 3: Known vacuolar (membrane) cargo of AP complexes in *Arabidopsis* in the presence (A) and absence (B) of their sorting adaptor.

(A) VIT1 and INT1 reach the TP via an interaction between AP-1 and their dileucine motif (Wang et al., 2014). VIT1 was shown to pass Golgi, TGN, and PVC *en route* to the TP. SUC4 reaches the TP in the presence of AP-3 (Wolfenstetter et al., 2012). VSR1 interacts with (the µ-subunit of) AP-4 via its cytosolic tyrosine motif. The receptor cycles between the TGN and the PVC, localizing primarily to the PVC at steady-state. In the presence of AP-4, soluble cargo of VSR1 reaches the vacuole (Fuji et al., 2016).

(B) INT1 and VIT1 are rerouted to the PM in the absence of AP-1 (or if their dileucine motif is mutated) (Wang et al., 2014). SUC4 localizes to the *cis*-Golgi in *ap3ß* mutants (Wolfenstetter et al., 2012). Artificial cargo of VSR1 (CT24) is released into the apoplast in *ap4* mutants (Fuji et al., 2016). VSR1 and a subset of its endogenous cargo was shown to accumulate in *ap4* mutants, but the specific localization of the receptor in the mutant has not been determined.

AP-: adaptor protein complex; EE: early endosome; ER: endoplasmic reticulum; LE: late endosome; MVB: multivesicular body; PVC: prevacuolar compartment; RE: recycling endosome; TGN: *trans*-Golgi network.

1.6 Aims of this work

Based on a prior study performing initial experiments on *Arabidopsis* mutants with T-DNA insertions in the gene coding for the putative ß-subunit of AP-4 (Müdsam, 2012), this work was aimed at a comprehensive characterization of the AP-4 complex of *Arabidopsis*, including the identification of cargo proteins of the complex.

Elucidation of the function of plant AP-4 and the assignment of adaptins to the complex initially required the establishment of additional plant lines homozygous for mutations in putative *AP4-adaptins*. At that point, general dwarfed growth of one *ap4ß* mutant-line was the only morphological difference to wild-type (WT) plants that had already been described (Müdsam, 2012). A fundamental comparison between putative *ap4-adaptin* mutants and the WT, as well as the creation and analysis of reporter-gene constructs should therefore reveal the significance of the AP-4 complex for plant development in *Arabidopsis*. Growth and morphology of *ap4* mutant seedlings were to be examined under various conditions, for example with respect to root growth, or organ development.

Focusing on transmembrane proteins, cargos that require AP-4 for sorting to their target compartment should then be identified. Partially, this was based on the coincidence of one or more characteristic AP-4 dependent traits in a potential cargo-mutant.

Additionally, proteomic data from the group of Waltraud Schulze (University of Hohenheim) should provide the basis for identification, and/or validation of further proteins requiring AP-4 to reach their destination. As a side project, putative cargo of the AP-3 complex, similarly suggested through proteomic data obtained in analogous experiments (again by the group of Waltraud Schulze) was examined. To test whether possible cargo was in fact sorted via AP-4 (or AP-3), GFP-candidate-fusions were generated, allowing examination of the subcellular targeting of the fluorescently labeled protein using confocal imaging. Altered localization in the absence of the corresponding adaptor should finally reveal proteins that are subject to AP-4 (or AP-3) dependent sorting. Identification of sorting motifs required for regular targeting of identified cargo should provide insights into possible preferences of AP-4 (or AP-3) towards specific proteins or sorting signals.

In the course of this work, some aspects have been examined by other groups. Gershlick et al. (2014b) detected an interaction of the cytosolic domain of VSR2 with AP-4. Moreover, Fuji et al. (2016) were able to identify and assign the individual adaptins of *Arabidopsis* AP-4 in a screen for mutants with defects in receptor dependent sorting of soluble cargo. They could further demonstrate that AP4µ localizes to the TGN and interacts with *Arabidopsis* VSR1 via a tyrosine-based (YMPL) motif of the receptor.

2 Results

2.1 Genotypic analysis of mutant lines with T-DNA insertions in genes coding for adaptins of AP-4

When this study was launched, *Arabidopsis* homologs of putative adaptins had already been assigned to the different AP complexes (Bassham et al., 2008). But apart from AP-3 components, experimental data validating the proposed complex-compositions were limited, or in case of AP-4, entirely absent from the literature. To allow functional investigation of *Arabidopsis* AP-4, mutant lines with T-DNA insertions in genes coding for the putative ß- and µ-subunit of the complex had to be isolated initially. Developmental and biochemical analyses of these mutants could later provide insights into the function of AP-4 and allow examination of potential defects in protein sorting.

Preliminary data was available from a previous study (Müdsam, 2012), in which homozygous knockout (ko) plants of one line, *ap4ß-1*, had already been isolated and found to be impaired in overall plant growth. In the same study, the T-DNA insertion site within *AP4ß* of another line, *ap4ß*-2, had been determined. Heterozygous plants had further been crossed back with the WT to eliminate a predicted additional insertion. Further analyses, conducted and presented in the work at hand, continued from the offspring of these crossings.

As already stated in the previous section, all *Arabidopsis* AP-4 adaptins have been identified very recently and corresponding T-DNA lines have been characterized and published by the group of Fuji et al. (2016). The mutant lines, carrying T-DNA insertions in the gene coding for AP4ß or AP4µ, which are examined in detail in this present study, are identical to the T-DNA lines already published (see section 4.1.3.3). Due to the fact that the identification of mutants among the offspring of the parental T-DNA lines was performed independently, and because these initial experiments provide the basis for subsequent analyses, the isolation of homozygous mutant plants will nevertheless be presented in the following.

2.1.1 Identification of *ap4ß-2* mutants

As already mentioned, the T-DNA line *ap4ß-1* [originating from the parental T-DNA line SAIL_781H01, corresponding to *gfs4-4* published by Fuji et al. (2016)], had already been isolated and genetically characterized in an earlier study (Müdsam, 2012).

The second mutant line, termed *ap4ß-2*, is derived from the original T-DNA line SAIL_796A10, which in turn corresponds to the *gfs4-3* mutant published by Fuji et al. (2016). Plants heterozygous for a T-DNA insertion at the desired position, i.e. in the genomic sequence of *AP4ß,* had been crossed back with Col-0 plants earlier (Müdsam, 2012). Any of the following analyses on this mutant line were performed during the present study.

Progeny obtained from back-crossing with WT plants were cultivated on soil under a short-day (SD)-regime (8 h photoperiod) for approximately five weeks before genomic

DNA was isolated. Plants among the F_1 carrying the desired insertion-allele were then selected for further cultivation. Homozygous mutants were subsequently identified among plants of the pre-selected F_2 generation. The name and binding site of each primer used for PCR-based genotyping of *ap4ß-2* are depicted in Figure 4A (in blue). The results are presented in Figure 4B. PCR with genomic *Arabidopsis* DNA as the template, and a combination of the genomic forward and reverse primer, yielded a fragment of 2079 bp in the WT control and indicated the presence of the WT-allele in several samples. The insertion allele was detected using a combination of the genomic reverse primer together with the T-DNA specific primer LB3, which binds within the left border (LB) of the T-DNA, thus yielding a fragment of approximately 1300 bp in the presence of the T-DNA insertion. Absence of this fragment in the WT control confirmed the specificity of the primer combination used.

As shown in Figure 4B (for example represented by samples #1, or #36), several plants homozygous for the T-DNA insertion, characterized by the presence of the PCR product representing the insertion allele and the absence of the band representing the WT allele, could be identified.

To test for the presence of any remaining functional transcript of *AP4ß* in the mutants, RNA was isolated from homozygous mutant plants, from which in turn cDNA was obtained via reserve transcription (see section 4.2.2.2). The cDNA was used as a template in the subsequent PCRs. Exon-binding primers (indicated in orange in Figure 4A) were combined to either amplify a fragment upstream (5'), downstream (3'), or spanning the T-DNA insertion site in the presence of *AP4ß* transcript in the samples (see also section 4.1.1.1).

To account for variances in cDNA concentration between different samples, and to identify false negatives, a fragment corresponding to *AtACT2*-transcript was amplified from each cDNA sample. Primer combinations were further selected to span intron-sequences, which allowed to detect potential contamination with genomic DNA, resulting in (additional) larger fragments, as shown for the genomic controls in Figure 4C.

Transcript corresponding to DNA sequences 5' and 3' of the T-DNA insertion was detected in all samples (Figure 4C), whereas full-length transcript (represented by the fragment amplified with a primer pair flanking the T-DNA insertion site) was only obtained from cDNA of WT (represented by #46) or heterozygous (represented by #41), but not of homozygous mutant plants. Overall, these mutants could be assumed to represent loss-of-function mutants, because translation would yield a drastically truncated AP4ß-fragment. The homozygous mutant plant #34 was cultivated further, and its progeny were used in all subsequent experiments.

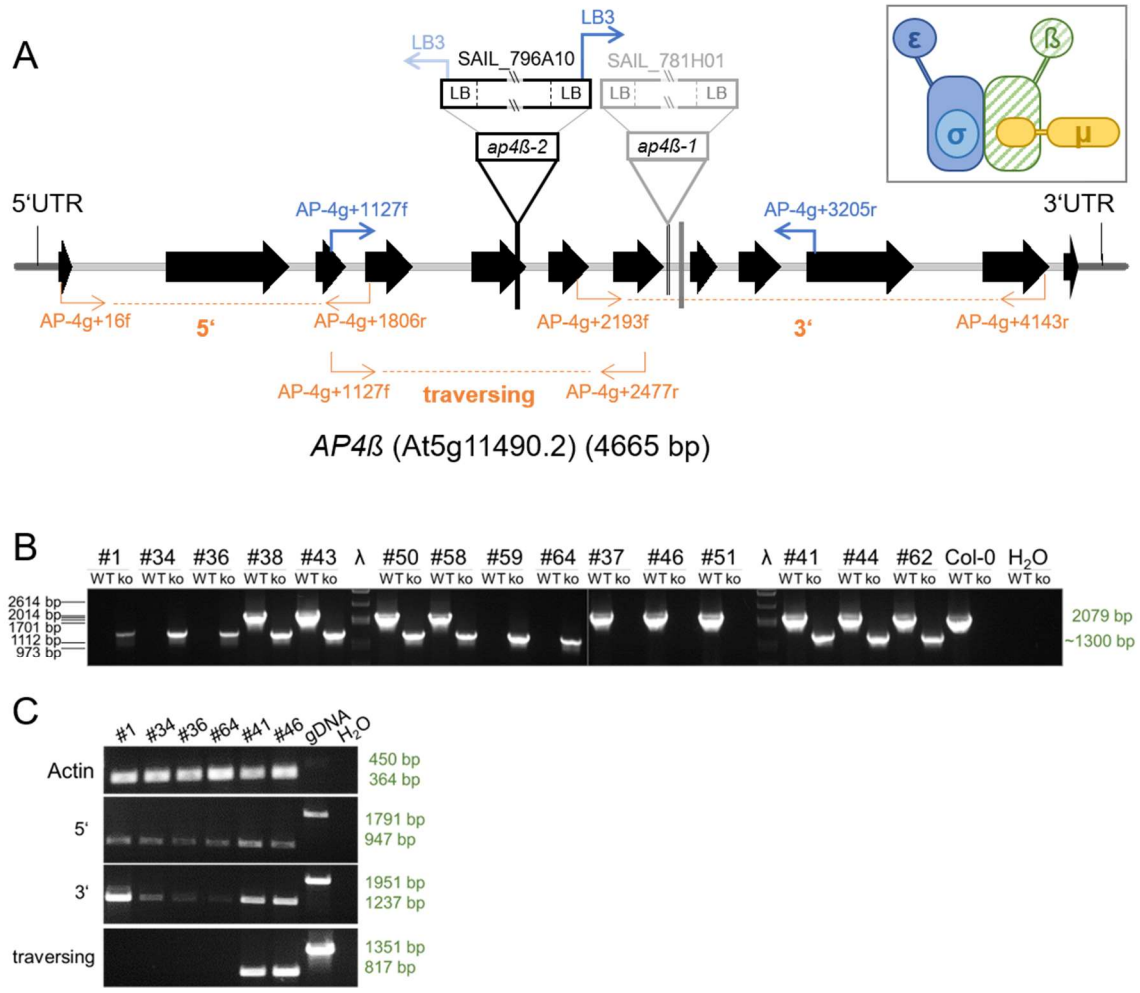

Figure 4: T-DNA lines with insertions in *AP4ß* (At5g11490). Genotypic analysis and transcript detection in plants of the T-DNA line *ap4ß-2* (SAIL_796A10).

(A) Schematic representation of the genomic sequence of *AP4ß* (At5g11490.2) (modified from Müdsam, 2012). Inset indicates mutation of ß-subunit (crosshatched) in AP-4 complex. The genomic sequence of *AP4ß* contains 4665 bp. The coding sequence is arranged in twelve exons (black arrows). T-DNA insertion sites of *ap4ß-1* (SAIL_781H01; grey) or *ap4ß-2* (SAIL_796A10; black) are indicated and have been determined earlier (Müdsam, 2012). In both lines, T-DNA insertions occur in a tandem orientation with flanking left borders (Müdsam, 2012). Binding sites of primers used for genotyping (blue arrows; lighter shades indicate alternative combinations) and for the detection of transcript in *ap4ß-2* (orange arrows) are depicted. Primer combinations used for transcript detection are indicated as dashed lines (orange), and yield fragments denoted in bold orange letters [3': 947 bp (1791 bp); traversing: 817 bp (1351 bp); 5': 1237 bp (1951); amplified from cDNA (genomic DNA)] in the presence of partial transcript, as shown in (C). UTR = untranslated region.

(B) Detection of WT- and insertion- (ko) alleles in line SAIL_796A10 using primers indicated (dark blue) in (A). Expected fragment sizes are given in green. Genomic DNA obtained from Col-0 plants served as a control for the WT allele and the specificity of the primer combination used for detection of the insertion allele. H_2O: negative control without template DNA. λ: Phage-Lambda DNA enzymatically digested with *Cla*I, used as a size marker. The ratio of homozygous to heterozygous to WT is not representative for the total of analyzed plants.

(C) Detection of *AP4ß* transcript in line SAIL_796A10, with primer pairs indicated in (A). Sample numbers correspond to those in (B). Expected fragment sizes are given in green. gDNA: genomic DNA obtained from a Col-0 plant. H_2O: negative control without any template DNA.

2.1.2 Isolation of *ap4μ* mutants

To examine whether the loss of another putative adaptin of the same complex yields different or any additional effects, mutants with a T-DNA insertion in the gene coding for the μ-subunit of AP-4 were additionally included in this study.

Two lines, each predicted to carry a T-DNA insertion in *AP4μ*, were obtained from the European *Arabidopsis* Stock Centre (NASC). Genotypes of individual plants were determined via PCR, with primer combinations depicted in Figure 5A (primer sequences are given in section 4.1.1.1).

The WT allele was detected via PCR with the primers AP4μg-933f and AP4μg+591r in line SALK_052835, yielding a 1524 bp fragment, or with AP4μg+613f and AP4μg+1921r for SALK_014326 (*ap4μ*), yielding a 1309 bp fragment in the presence of the respective WT allele (top row of Figure 5B and D). PCR fragments corresponding to the respective insertion allele could be amplified from both lines, using a combination of any of the genomic primers (forward or reverse) with the LB primer LBb1.3. The bottom row of Figure 5B and D show results of one combination for each T-DNA line, respectively. PCR products of the expected size were obtained from all (SALK_052835) or several (SALK_014326) samples, but not from WT controls, indicating that the primer combinations were specific and thus appropriate to detect the respective insertion.

In contrast, PCRs with a genomic primer and a primer binding in the right border of the T-DNA yielded no detectable products (not shown), indicating a tandem orientation of the T-DNA with LB sequences (or at least fragments thereof) facing the genomic DNA 5' and 3'. Sequencing data was in line with this observation and allowed to determine the precise T-DNA insertion site(s) within the genomic sequence of *AP4μ*. In SALK_052835, the T-DNA was found to be positioned in the 5'UTR. The obtained sequence of PCR products aligned with the genomic sequence upstream of the 5'UTR of *AP4μ*, up to -59 bp from the start-ATG (sequence of PCR product obtained with genomic forward primer and LB primer), and with the genomic sequence of *AP4μ* starting from -19 bp from the start-ATG and further downstream towards the coding sequence (CDS). This indicated a tandem insertion of the T-DNA in the 5' UTR and possibly the concomitant deletion of a small (40 bp) genomic fragment.

The T-DNA insertion site of line SALK_014326 was analogously determined and found to be positioned in the 4th intron at position +1023 bp, or +1047 bp, respectively.

Analogous to the transcript detection in *ap4ß-2* mutants (described in section 2.1.1), individual plants found to be homozygous for a T-DNA insertion in *AP4μ* were then tested for the presence of corresponding transcript via RT-PCR. Primer combinations are indicated in Figure 5A. Because the T-DNA is located within the 5'UTR of *AP4μ* in SALK_052835, transcript detection was restricted to one primer combination (AP4μg+613f + AP4μg+996r, yielding a product corresponding to fragment "A").

As shown in Figure 5C, *AP4μ* transcript was still detected in heterozygous (represented by #1), as well as in homozygous plants of SALK_052835 (represented by #3, #8, #12, #17). Due to the position of the T-DNA in the untranslated region, the transcript is likely to yield a functional adaptin. This was further corroborated by the WT-like habitus of these mutants (Figure 5C, right), contrasting the altered morphology of the (*ap4ß* and) *ap4μ*

mutants (*cf.* Figure 5E, right). Thus, line SALK_052835 was excluded from further experiments presented in this work.

Plants from line SALK_014326 also seemed to transcribe RNA sections 5' and 3' of the T-DNA insertion. However, a fragment representing the full-length transcript, could not be obtained from cDNA of homozygous individuals (represented by #6, #9, #17, #25). Accordingly, it can be assumed that these mutants lack the full-length AP4µ protein. The homozygous mutant SALK_014326 #9 was cultivated further, and the progeny used in subsequent experiments. In the following, this mutant line will be referred to as *ap4µ.*

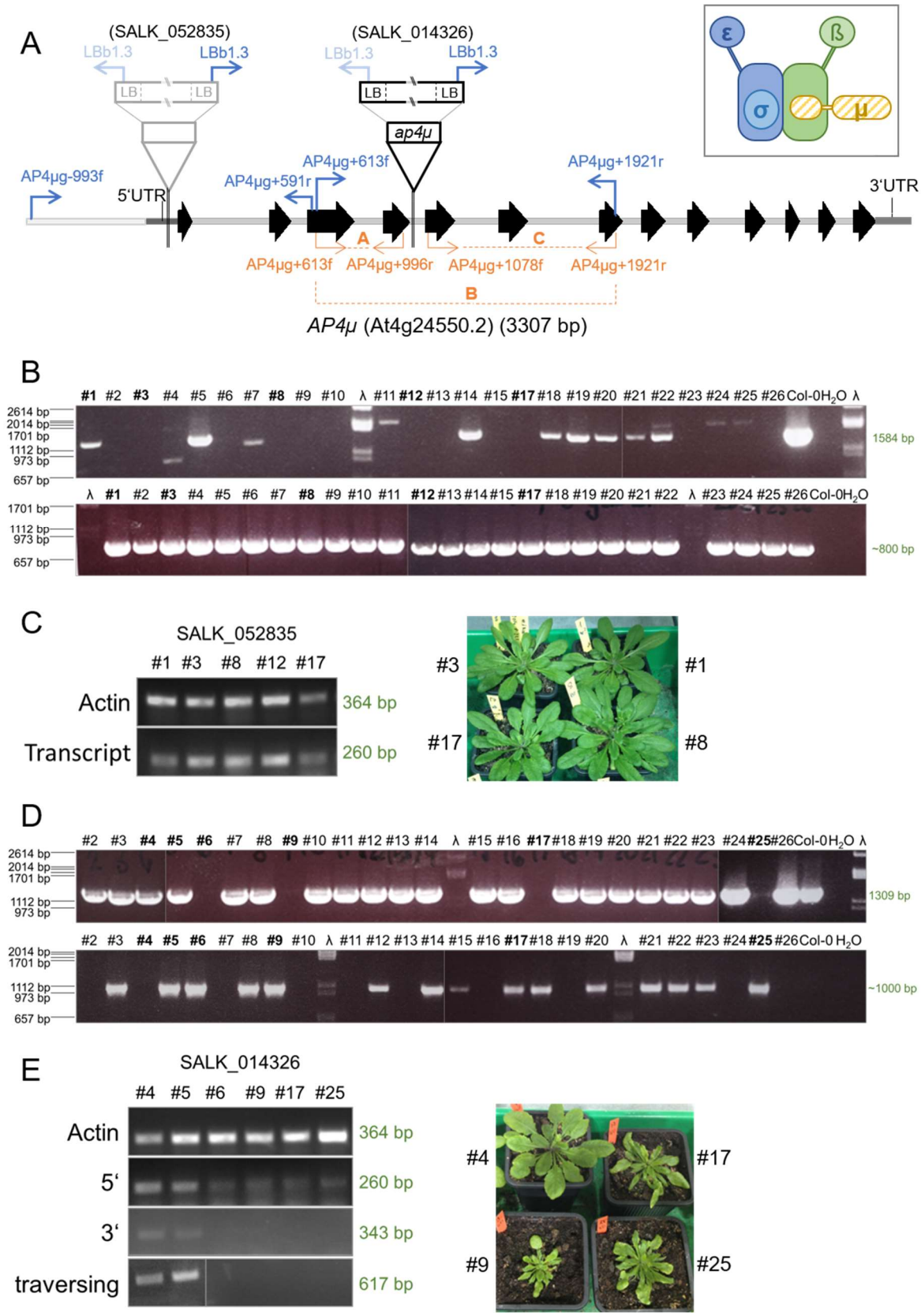

Figure 5: T-DNA lines with insertions in *AP4μ* (At4g24550).

(A) Schematic representation of the genomic sequence of *AP4μ* (At4g24550.2). Inset indicates mutation of μ-subunit (crosshatched) in AP-4 complex. Bold black arrows represent exons. T-DNA insertion sites, and the orientation of the T-DNA, are indicated in grey (SALK_052835), or black (SALK_014326; *ap4μ*). Blue arrows indicate binding sites of primers used for genotyping, lighter shades represent alternative combinations not represented in (B) or (D). Orange arrows indicate binding sites of primers used for detection of transcript. The corresponding fragments are denoted in orange

capital letters (A: 260 bp; B: 588 bp; C: 343 bp; amplified from cDNA). UTR = untranslated region. Inset depicts AP-4 complex and indicates μ-subunit in a crosshatched pattern.
(B) Detection of WT (upper row) and insertion (lower row) alleles in plants of line SALK_052835. WT and insertion alleles were detected via PCR as indicated in (A). Expected fragment sizes are given in green on the right. The ratio of homozygous to heterozygous to WT is not representative for the total of analyzed plants. Bold numbers indicate individuals also examined in (C). Genomic DNA obtained from Col-0 plants served as a control for the WT allele and the specificity of the primer combination used for detection of the insertion allele. H_20: negative control without template DNA. λ: Phage-λ DNA enzymatically digested with *Cla*I, used as a size standard.
(C) Detection of *AP4μ* transcript in line SALK_052835. A*ctin* (*AtACT2*) was used as a loading control (expected fragments: cDNA 364 bp). Sizes of expected fragments are given in green. Partial transcript was detected via PCR with the primers flanking fragment "A" as indicated in panel (A).
(D) Detection of WT (upper row) and insertion (lower row) alleles in plants of line SALK_014326. WT and insertion alleles were detected via PCR, using (dark blue) primers indicated in (A). Expected size of PCR products is given in green on the right. Bold numbers correspond to plants also represented in (E). Genomic DNA obtained from Col-0 plants served as a control for the WT allele and the specificity of the primer combination used for detection of the insertion allele. H_20: negative control without template DNA. λ: Phage-λ DNA enzymatically digested with *Cla*I, used as a size standard (fragment sizes are indicated on the left).
(E) Detection of AP4μ transcript in progeny of a heterozygous parent of line SALK_014326. *Actin* (*AtACT2*) was used as a loading control (expected fragments: cDNA 364 bp). Transcript corresponding to sequences upstream (5'), downstream (3'), or traversing the T-DNA insertion site, was detected as indicated in panel (A), yielding fragments corresponding to "A", "C", and "B", respectively. H_2O: negative control without template DNA.

2.1.3 Generation of a *ap4ß-2 ap4μ* double knockout line

In order to test whether the loss of a second adaptin enhances any effects observed in the single mutants, or results in any additional defects, a double ko line, lacking both the ß- and the μ-adaptin of AP-4, was generated. To obtain double mutants, stigmata of homozygous *ap4μ* plants were pollinated with pollen from homozygous *ap4ß-2* plants and *vice versa*. Double ko plants, homozygous for T-DNA insertions in both genes, were selected in the F_2 generation via PCR-based genotyping.

2.2 Expression pattern and subcellular localization of AP-4

To give insights on the role of AP-4 for plant growth at different developmental stages and to yield cues on its function in subcellular protein sorting, different reporter lines for the μ-subunit of AP-4 were analyzed.
At this point it has to be emphasized that the subcellular localization of AP-4 has been examined independently in another study (Fuji et al., 2016), using a construct analogous to the *AP4μ$_{Pro}$:AP4μ-GFP*-fusion herein described. Therefore, the corresponding data on the subcellular localization of AP-4 obtained in the course of this present study is only briefly described. The tissue and organ specific expression pattern of *AP4μ* (or any other AP-4 adaptin from *Arabidopsis*), on the other hand, has not been examined so far and represents entirely novel data.
To generate suitable reporter plants, the genomic sequence of *AP4μ* was genetically fused to either *GUS* or *GFP*. Expression of the fusion was driven by the endogenous *AP4μ* promoter, represented by a fragment comprising 1800 bp of the genomic sequence upstream of the start-ATG of *AP4μ*. The vectors carrying these constructs were used to stably transform homozygous *ap4μ* mutants, and the stably transformed plants were

examined. The mutant background was chosen for several reasons: For one, the functionality of the reporter-fusions can be validated by their ability to restore any potential defect that might be present in the uncomplemented mutant. Secondly, complementation of any mutant defect by the *reporter-gene*-fusion could simultaneously confirm that the observed defect was in fact due to the mutation of the gene examined. And lastly, integration of the artificial adaptin-fusion into the AP-4 complex, and hence possibly also the protein level obtained, is likely to be affected by the presence of endogenous AP4µ.
Transformants were selected via the herbicide resistance encoded on the T-DNA vector carrying the *AP4µ-reporter*-fusion. From the T_1 generation, 24 resistant plants per line were grown until maturity. These plants resembled the WT, and none of them displayed the dwarfed growth observed in the parental mutant line (T_0). Segregation of the herbicide resistance was examined along two following generations of individual T_1 plants, to eventually isolate lines, homozygous for a single insertion of the respective reporter-construct. In the following, these lines are referred to as *ap4µ/AP4µ$_{Pro}$:AP4µ-GFP* and *ap4µ/AP4µ$_{Pro}$:AP4µ-GUS*, respectively.
For details on the cloning strategy, see section 4.2.6.1.

2.2.1 Histochemical analyses of the expression pattern of *AP4µ*

To examine the expression pattern of *AP4µ*, *ap4µ/AP4µ$_{Pro}$:AP4µ-GUS* plants were stained using the procedure described in section 4.2.4.1. Since *GUS* expression in the *ap4µ/AP4µ$_{Pro}$:AP4µ-GUS* plants is determined by the activity of the *AP4µ* promoter (and in this case additionally coupled to the actual AP4µ-level), a blue staining indicates tissues or cell types, in which the examined gene, *AP4µ*, is expressed. As shown in Figure 6, blue staining could be detected at different developmental stages in the analyzed *ap4µ/AP4µ$_{Pro}$:AP4µ-GUS* line: in young seedlings (Figure 6G), as well as in etiolated seedlings (Figure 6A), staining was dominant in the stele of the roots and hypocotyls, and further detected in the cotyledons. In older seedlings, GUS staining showed a marked peak in stipules (Figure 6F), and at the meristematic zone of primary roots and side roots (Figure 6B), decreasing towards the columella and towards the elongation zone. Weaker staining was further observed in cotyledons (Figure 6D) and true leaves (Figure 6E), where it dominated along the vasculature. Inflorescences displayed no GUS-activity in sepals, weak staining in petals, but clearly showed blue staining of pistils and stamen (Figure 6C). There, GUS-activity was mostly restricted to the stigma, and the filaments and pollen within the anthers. In later experiments, AP-4 dependent sorting was to be analyzed in transiently transformed protoplasts. To confirm that AP-4 is actually present in these cells and the system therefore suited to examine AP-4 dependent sorting, GUS activity was further specifically examined in mesophyll cells of *ap4µ:AP4µPro:AP4µ-GUS* plants. As shown in Figure 6H, the soluble blue 5,5'-Dibrom-4,4'-dichlor-indigo had diffused into the supernatant of a preparation of *ap4µ:AP4µPro:AP4µ-GUS* protoplasts, whereas no unspecific staining was observed of equally treated *ap4µ:AP4µPro:AP4µ-GFP* mesophyll protoplasts.

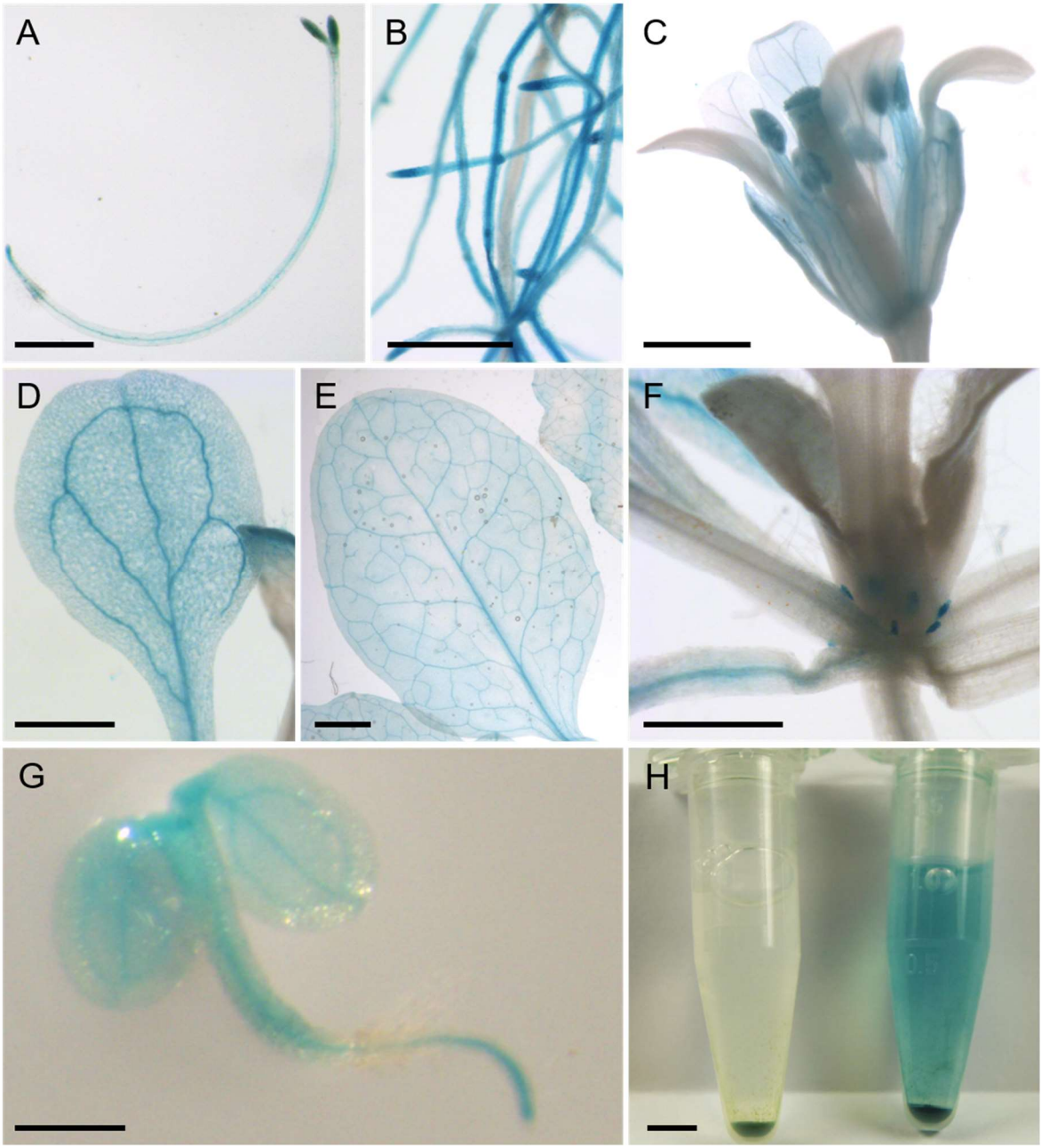

Figure 6: Tissue specific expression of *AP4μ*.
(A) In stably transformed *ap4μ/AP4μ*$_{Pro}$*:AP4μ-GUS* plants, GUS-staining is observed in roots, cotyledons and in the hypocotyl of etiolated seedlings.
(B) Strong staining is detected in roots, particularly in the meristematic zone of primary roots and side roots.
(C) Inflorescences show weak GUS activity in sepals, and strong GUS staining in anthers.
(D) and (E) GUS staining is visible in cotyledons **(D)** and true leaves **(E)**, with increased staining in the vasculature.
(F) Strong GUS staining is visible in stipules of older seedlings.
(G) Except for root hairs, blue staining can be observed in all organs of young seedlings.
(H) GUS staining of mesophyll protoplasts isolated from *ap4μ/AP4μ*$_{Pro}$*:AP4μ-GUS* (right) yields a blue supernatant, which is absent from the negative control (*ap4μ/AP4μ*$_{Pro}$*:AP4μ-GFP*) (left).
Scale bars: **(A)**: 1 mm; **(B), (C), (D)** and **(F)**: 100 µm; **(E)**: 200 µm; **(G)**: 500 µm, **(H)**: 5 mm.

2.2.2 Subcellular localization of AP4µ

To examine the subcellular localization of AP4-adaptins and the AP-4 complex, *N*- or *C*-terminal GFP-fusions of the ß- and µ-subunit were examined. To generate vectors for transient expression in mesophyll protoplasts, the CDS of *AP4ß* or *AP4µ* was fused to the open reading frame of *GFP.* In this case, expression was driven by the strong, constitutive *35S*-promoter ($35S_{Pro}$). Primer combinations, donor and resulting expression vectors are given in sections 4.1.1.2 and 4.1.2.2.

The vectors carrying the different constructs were then used to transiently transform *Arabidopsis* mesophyll protoplasts of WT, *ap4ß-1*, or *ap4µ* (see section 4.2.3.3), and the localization of the GFP-fusions was analyzed via confocal microscopy. In line with the fact that AP complexes are generally soluble before being recruited to a specific membrane, overexpression of the *GFP*-fusions in WT cells, generally yielded strong fluorescent labeling of the cytosol (Figure 7). AP4ß-GFP was additionally detected in punctate structures, possibly corresponding to the TGN. Interestingly, (except for *GFP-AP4µ*) overexpression of the same constructs in protoplasts derived from the respective mutant lines yielded much weaker GFP-fluorescence overall, and signals were mostly restricted to small distinct puncta, whereas cytosolic GFP-signals were only occasionally observed.

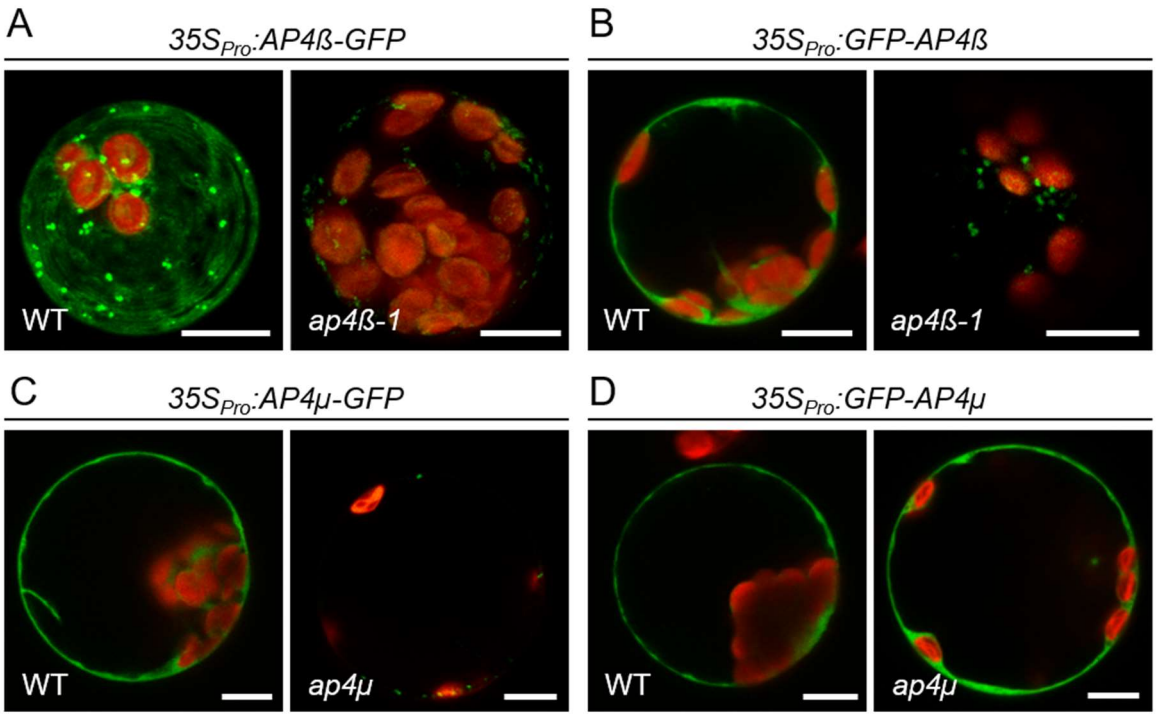

Figure 7: WT and *ap4* mesophyll protoplasts transiently transformed with *C*- or *N*-terminal *GFP*-fusions of *AP4ß* or *AP4µ*.

Protoplasts expressing *GFP*-fusions of *AP4ß* are presented in **(A)** (maximum projection; *C*-terminal GFP) and **(B)** (confocal single section; *N*-terminal GFP). Confocal single sections of protoplasts expressing *GFP*-fusions of *AP4µ* are presented in **(C)** (*C*-terminal GFP) and **(D)** (*N*-terminal GFP). GFP-fluorescence is shown in green, chlorophyll autofluorescence in red. Scale bars represent 10 µm.

As opposed to a cytosolic localization, the observed GFP-labeling in mutant protoplasts resembled that of fluorophore-fusions of *Arabidopsis* AP1-adaptins published earlier (Park

et al., 2013; Teh et al., 2013; Wang et al., 2013), and also corresponds to the localization of animal AP4-adaptins to the TGN (Hirst et al., 1999).

As already mentioned, overexpression of a single subunit of the heterotetrameric complex might produce false results, due to artificial free adaptin(-GFP), which cannot be integrated into a functional complex. On the other hand, this does not explain why the same constructs yielded a partially different (and weaker) labeling when expressed in the mutants. To eliminate the potential influence of overexpression, subcellular localization of AP4µ was studied in *ap4µ* mutant plants stably expressing a *GFP*-fusion of the genomic *AP4µ* sequence under control of the *AP4µ* promoter. In line with the GUS-assay, GFP-fluorescence was detectable in mesophyll protoplasts of the analogous GFP-reporter-line (*ap4µ/AP4µ$_{Pro}$:AP4µ-GFP*; Figure 8H). Although fluorescence appeared to be quite weak in most protoplasts, signals were still detectable in almost every cell. Importantly, the GFP-fluorescence was restricted to punctate structures without obvious GFP-fluorescence in the cytosol, indicating that the cytosolic signals observed in WT cells overexpressing *GFP-adaptin*-fusions did not represent the actual localization of the AP-4 complex, appropriately.

Punctate labeling was also observed in other tissues of *ap4µ/AP4µ$_{Pro}$:AP4µ-GFP*. When seedlings of this line were grown on MS plates for three to seven days, GFP-fluorescence was clearly detectable in roots (Figure 8A–C). Agreeing with the results obtained with the GUS-marker line (section 2.2.1), GFP-signals were particularly pronounced at the meristematic zone of primary roots and side roots, and decreased at the columella (Figure 8A and B). Although, using whole mount samples, the relatively weak GFP-signals were difficult to detect in tissues with a strong fluorescent background, as for example caused by autofluorescence of chlorophyll, AP4µ-GFP was also visible in aerial organs. This is represented by confocal images obtained from cotyledons of dark-grown seedlings and of the pistil of a light grown seedling shown in Figure 8D–F. In the latter, AP4µ-GFP produced pronounced fluorescence in the stigmatic papillae, again corresponding to the GUS-activity of the analogous reporter line in this tissue. To determine whether the punctate structures labeled by AP4µ-GFP corresponded to an endosomal compartment, roots of young *ap4µ/AP4µ$_{Pro}$:AP4µ-GFP* seedlings were treated with the styryl dye FM4-64. This lipophilic dye is known to initially label the PM before being endocytosed, thereby successively labeling different endosomal compartments and finally the vacuolar membrane. As shown in Figure 8G, fluorescent signals of FM4-64 did partially colocalize with AP4µ-GFP labeled intracellular compartments. Mesophyll protoplasts derived of the same plant line were further isolated and transiently transformed with the marker CD3-967 (Nelson et al., 2007), which codes for an mCherry-fusion of a 49-amino-acid-fragment of mannosidase 1 (Man1) and labels the *cis*-Golgi. In agreement with AP-4 localization to (the TGN or) an endosomal compartment, AP4µ-GFP did not colocalize with this marker (Figure 8H).

Shortly after these experiments were performed, Fuji et al. (2016) confirmed a partial colocalization of FM4-64 positive endosomes with a very similar AP4µ-GFP construct, and further published AP4µ to be specifically localized to the TGN/EE, where they found it to preferentially colocalize with the TGN marker mRFP-syntaxin of plants 43 (SYP43; Uemura

et al., 2012). Due to these results, the subcellular localization of AP-4 was not further analyzed in this work.

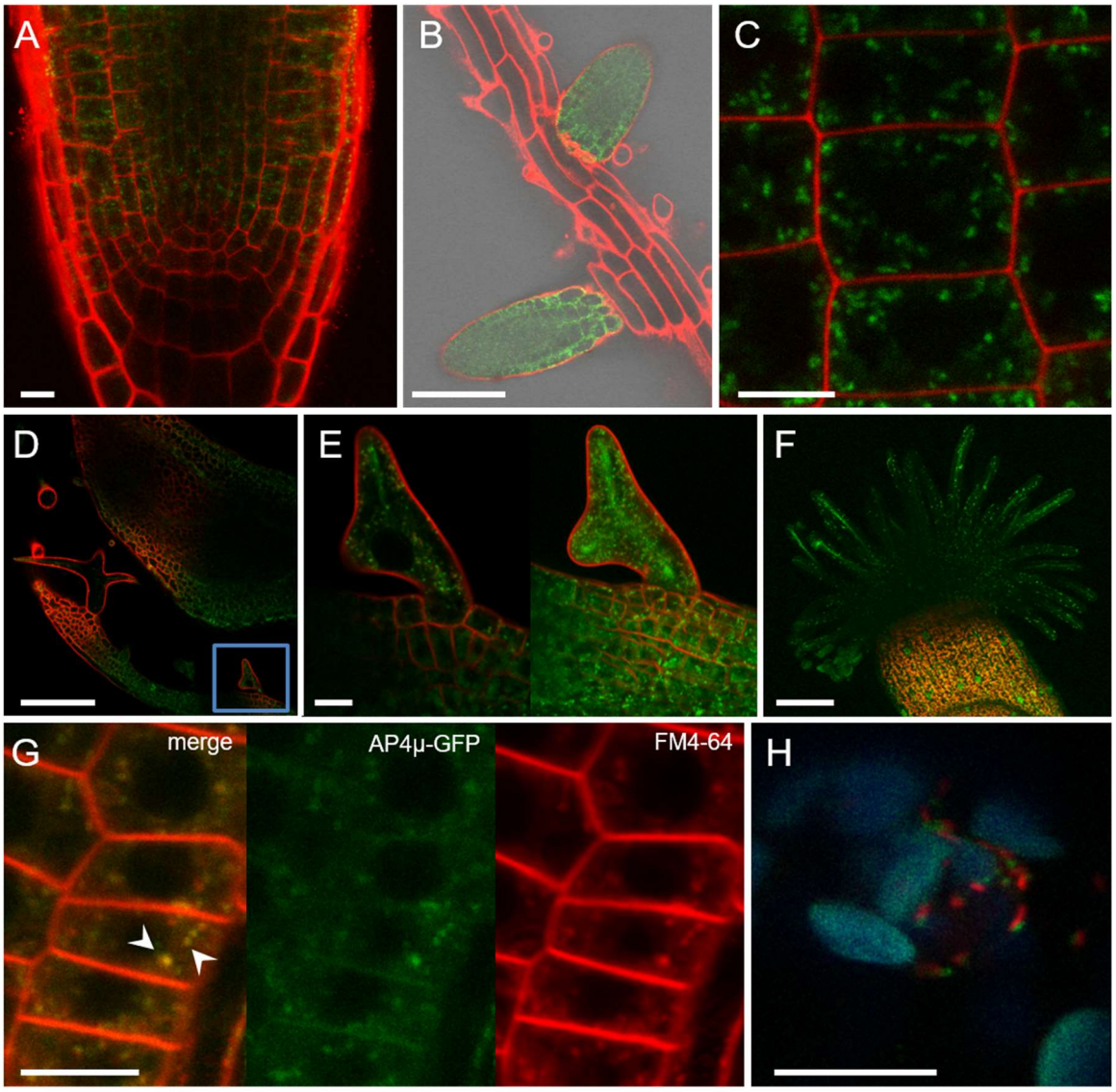

Figure 8: Tissue specific expression and subcellular localization of *AP4µ-GFP*.
GFP fluorescence is shown in green. Red represents fluorescence of propidium iodide [(A) to (C)], of FM4-64 [(D), (E) and (G)], of mCherry (H), or chlorophyll autofluorescence (F).
(A) to **(C)** Confocal single sections of roots of *ap4µ/AP4µ$_{Pro}$:AP4µ-GFP* seedlings. GFP fluorescence is particularly strong in the meristematic zone of primary roots (A) and in young side roots (B), localizing to punctate structures (C).
(D) and **(E)** In cotyledons of dark grown seedlings, AP4µ-GFP is detectable in epidermal cells (D) and developing trichomes [(D), (E)]. (E) shows a higher magnification of the trichome marked by a blue box in (D) as a confocal single section (left) and the corresponding maximum projection (right).
(F) AP4µ-GFP is visible in stigmatic papillae of *ap4µ/AP4µ$_{Pro}$:AP4µ-GFP* plants.
(G) AP4µ-GFP colocalizes with FM4-64 in endocytic compartments (white arrows) in root epidermal cells of *ap4µ/AP4µ$_{Pro}$:AP4µ-GFP* seedlings.
(H) AP4µ-GFP does not colocalize with the *cis*-Golgi marker CD3-967 in mesophyll protoplasts. Chlorophyll autofluorescence is shown in blue.
Scale bars: (A), (C), (E), (G), (H): 10 µm. (B), (D), (F): 100 µm

2.3 Developmental abnormalities of *ap4* mutants

To examine the role of AP-4 for plant development, *ap4ß-1, ap4ß-2*, and *ap4µ* single mutants (section 2.1.1 and 2.1.2) and *ap4ß-2 ap4µ* double ko plants (section 2.1.3) were compared to the WT at different developmental stages. Under the assumption that the affected adaptins, in fact, constitute components of the same complex, all single, as well as the double mutants, should display identical defects. However, that is only unless the complex retains some functionality in the absence of a single adaptin. In that case, double mutants were expected show additional defects compared to the corresponding single ko plants. To further validate the functionality of the AP4µ-reporter-constructs, the *ap4µ* mutants stably expressing *AP4µ* fused to *GUS* or *GFP* under control of the *AP4µ*-promoter were also included in these experiments.
Apart from the dwarfism of *ap4ß-1* mutants described earlier (Müdsam, 2012), no information on any abnormalities of *ap4* mutants in *Arabidopsis* was available at the time these experiments were performed. Therefore, subsequent analyses aimed to investigate the significance of AP-4 for plant development in greater detail. Initially, anatomical and biochemical studies should reveal insights on the role of AP-4, for example by examination of root-growth and trichome-morphology, or by measuring carbohydrate- and chlorophyll- contents. The results could then provide potential cues towards possible AP-4 cargo and allow to identify transmembrane proteins, which might require the complex to be sorted to their target-compartment.
By now, the dwarfism described for *ap4ß-1* mutants (Müdsam, 2012), was confirmed and published to also occur in single mutants of other AP4-adaptins (Fuji et al., 2016). In addition, Pertl-Obermeyer et al. (Pertl-Obermeyer et al., 2016) from the group of W. Schulze at the University of Hohenheim, reported a short-root phenotype for one mutant line (*ap4ß-1*).

2.3.1 Reduced growth of roots and etiolated hypocotyls

To analyze root growth, seeds of WT, *ap4ß-1*, *ap4ß-2*, *ap4µ*, *ap4ß-2 ap4µ*, and *ap4µ/AP4µ$_{Pro}$:AP4µ-GFP,* or *-GUS*, were sterilized and plated on half-strength MS-medium supplemented with 0%, 1% or 2% (w/V) sucrose (see sections 4.1.4.2, 4.2.1.2 and 4.2.4.4). Under each condition, single and double mutants developed significantly shorter roots compared to WT seedlings (Figure 9). Although at later stages (seven or ten days after transfer to the growth-chamber), differences between mutants and WT seedlings grown on medium without sucrose, were not found to be significant (Figure 9B), this is likely due to the large variation in WT root-growth in the absence of added sucrose.
Particularly on medium supplemented with 1% or 2% sucrose, the root-growth-reduction, i.e. the ratio of mutant and corresponding WT root-lengths, appeared to be consistent irrespective of the external sugar supply or the seedling-age.

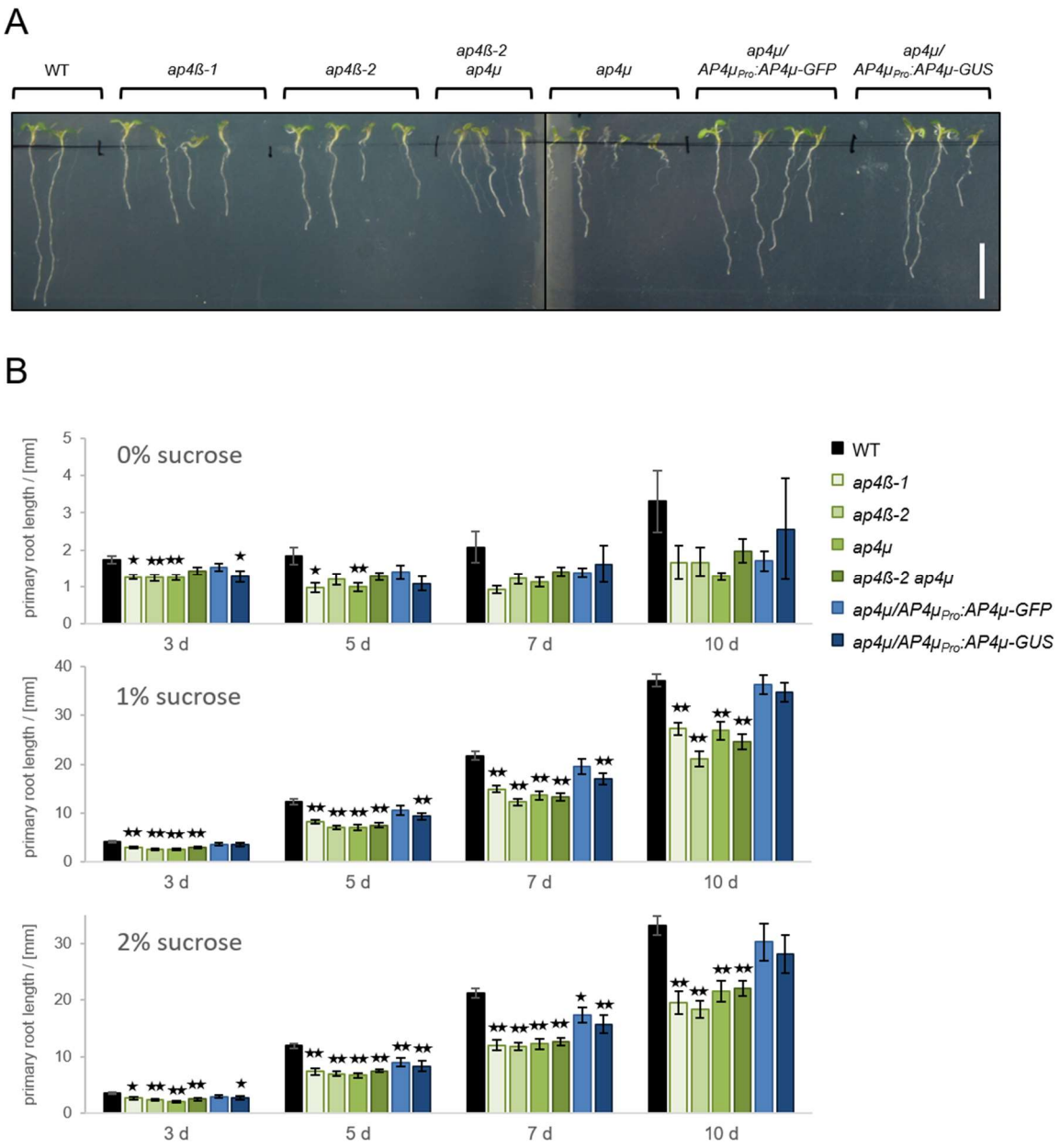

Figure 9: Decreased root growth of *ap4* mutants.
(A) *Arabidopsis* WT, *ap4ß-1, ap4ß-2, ap4µ, ap4ß-2 ap4µ*, *ap4µ/AP4µ$_{Pro}$:AP4µ-GFP* and *ap4µ/AP4µ$_{Pro}$:AP4µ-GUS* seedlings grown for seven days on ½ strength MS supplemented with 2% sucrose. Scale bar represents 1 cm. **(B)** Primary root lengths of *Arabidopsis* WT, *ap4ß-1, ap4ß-2, ap4µ, ap4ß-2 ap4µ*, *ap4µ/AP4µ$_{Pro}$:AP4µ-GFP* and *ap4µ/AP4µ$_{Pro}$:AP4µ-GUS* grown for three, five, seven, or ten days on half-strength solid MS supplemented with 0%, 1% or 2% sucrose. Columns represent means ± SE (n ≥ 12 for each genotype and condition). Asterisks indicate significant (*, $p < 0.05$) or highly significant (**, $p < 0.01$) differences compared to the WT (Student's t-test). WT is shown in black, a*p4* mutants are given in green tones, complemented *ap4µ* mutants are given in blue tones as indicated in the legend.

Reduced root growth might be due to decreased meristem activity and/or defects in cell elongation. As presented in an earlier section (2.2.1), *AP4µ* was quite strongly expressed in the meristematic zone of seedling roots (Figure 6). Therefore, the loss of a subunit of AP-4 was expected to rather impair cell division instead of elongation. To test this hypothesis, root architecture was inspected in three-day-old *ap4ß-1*, *ap4ß-2* and WT seedlings, using confocal imaging. Cell walls were labeled by incubation with propidium iodide. As presented in Figure 10, meristem size was not altered in *ap4ß-1* and *ap4ß-2*

mutant roots. In contrast, the length of fully differentiated epidermal root cells was significantly reduced in both mutants compared to WT. Instead of impairment of cell division, the reduced overall root-length accordingly rather correlates with decreased cell expansion in *ap4* mutants.

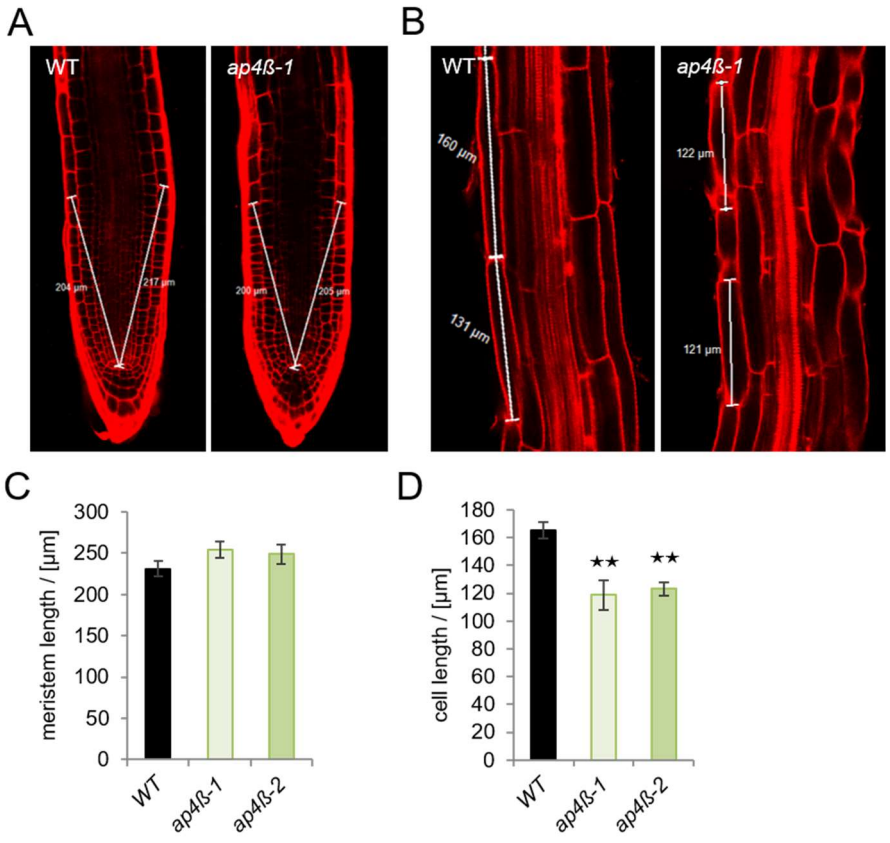

Figure 10: Decreased cell size in roots of *ap4ß-1* mutants.

(A) Confocal images of primary roots of three-day-old WT and *ap4ß-1* seedlings stained with propidium iodide. Meristem length was measured from the quiescent centre to the last not clearly elongated epidermal cell. Two measurements (indicated by white bars) were performed per root. The mean of both measurements represents one root in (C).

(B) Confocal images of the differentiation zone of primary roots of 3-day-old WT and *ap4ß-1* seedlings stained with propidium iodide. Cell lengths, presented in (D), were measured as indicated (white bars).

(C) Meristem lengths in primary roots of WT, *ap4ß-1* and *ap4ß-2*. Measurement was conducted as presented in (A). Columns represent means ± SE (n ≥ 11 roots per genotype). Asterisks indicate significant (*, $p < 0.05$) or highly significant (**, $p < 0.01$) differences compared to the WT (Student's t-test).

(D) Lengths of differentiated root epidermal cells of WT, *ap4ß-1* and *ap4ß-2*. Measurements were performed as represented in (B). Columns represent means ± SE (n ≥ 11 cells from at least four individual seedlings per genotype). Asterisks indicate significant (*, $p < 0.05$) or highly significant (**, $p < 0.01$) differences compared to the WT (Student's t-test).

Further, all single and double ko lines showed significantly shorter hypocotyls compared to the WT (Figure 11), when seedlings were grown in the dark for seven days, irrespective of the sucrose concentration in the medium.

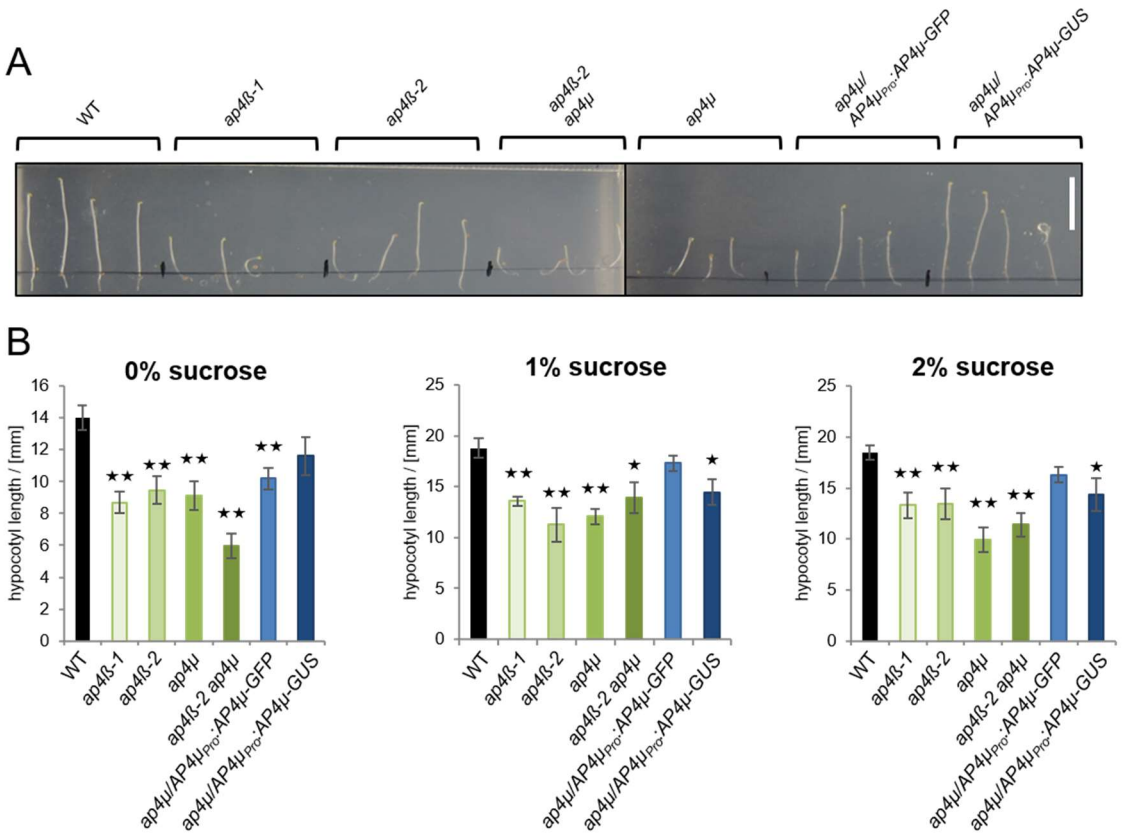

Figure 11: Reduced growth of etiolated hypocotyls in *ap4* mutants.
(A) *Arabidopsis* seedlings grown in the dark for seven days on ½ strength MS medium with 2% sucrose. Scale bar represents 1 cm.
(B) Hypocotyl lengths of etiolated seedlings grown in the dark for seven days on ½ strength MS medium with 0%, 1%, 2% sucrose. Columns represent means ± SE (n ≥ 9 for each genotype). Asterisks indicate significant (*, $p < 0.05$) or highly significant (**, $p < 0.01$) differences compared to the WT (Student's t-test).

Importantly, WT-like growth was to the most extent restored in roots and hypocotyls of *ap4µ* mutants stably transformed with *AP4µ$_{Pro}$:AP4µ-GFP* or *-GUS* constructs (Figure 9 and Figure 11), demonstrating that the *APµ*-fusions are functional *in vivo*. It is further noteworthy, that overall, a double ko of the *ß*- and *µ*-subunit did not enhance the growth defects of the single mutants.

2.3.2 Supernumerary trichome branching

An additional observation was that *ap4* mutants showed supernumerary branching of leaf trichomes (epidermal hair). Typically, most leaf trichomes of Col-0 plants show three branches forming a stellate shape as represented for example by the WT trichomes shown in Figure 12A. In contrast, *ap4* mutants often developed trichomes with four or more branches. To quantify these observations, mutant and WT plants were grown in a checkerboard arrangement (for about four weeks) to eliminate positional effects. Then, every visible trichome of a third or fourth true leaf was classified according to its branch number. Figure 12B shows the distribution of different trichome classes as percentages of

the total trichome population per leaf. Confirming the initial observations, three-branched trichomes accounted for approximately 80% of the total trichome populations on WT, as well as on the complemented *ap4μ* mutant leaves, but only for 50% in *ap4ß-1*, *ap4ß-2*, *ap4μ*, or *ap4ß-2 ap4μ* plants. Instead, higher branch numbers, present in only ~ 15% of the trichomes on leaves of WT and complemented mutant plants, were observed in more than 40% of the trichomes in mutant lines. Trichome clustering was not observed in WT or mutants, i.e. trichomes did not have another trichome as a neighboring cell (Figure 12A). Moreover, mutant trichomes developed morphologically normal papillae, as shown on the surface of trichome stalks of WT and *ap4ß-1* in Figure 12C.

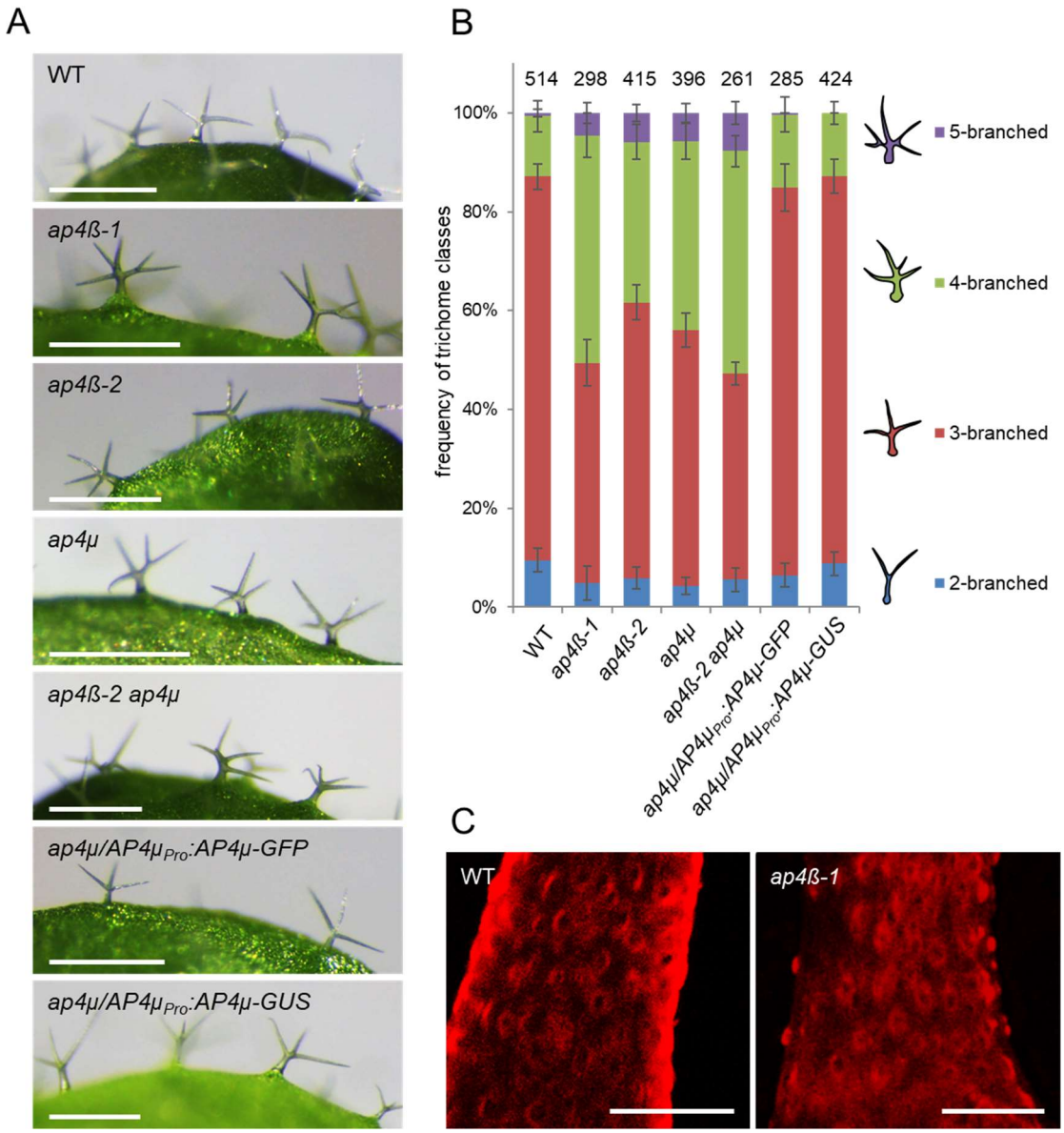

Figure 12: *Ap4* mutants show supernumerary branching of leaf trichomes.

(A) Trichomes on leaves of the indicated genotypes. Scale bars represent 500 µm.

(B) Quantitative distribution of trichome classes. Columns represent means ± SE of at least 7 leaves per genotype. The total number of trichomes of which branches were counted is indicated on top. Based on a Kruskal-Wallis one-way ANOVA on ranks and an all pairwise multiple comparison test (Dunn's Test), branch counts of the WT and the complemented lines (*ap4μ/AP4μ$_{Pro}$:AP4μ-GFP* and *ap4μ/AP4μ$_{Pro}$:AP4μ-GUS)* differ significantly from *ap4ß-1*, *ap4ß-2*, *ap4μ* and *ap4ß-2 ap4μ* ($P < 0.01$).

(C) Maximum projections of stalks of isolated trichomes of WT and *ap4ß-1* stained with FM4-64. Scale bars represent 25 µm.

2.3.3 Impaired male fertility of *ap4* mutants

Like trichomes, pollen tubes require concentrated action of cytoskeletal rearrangements and vesicle trafficking to allow for rapid and extensive growth. As represented by the low prevalence of homozygous mutants among the offspring of heterozygous *ap4μ* plants (section 2.1.2, Figure 5D), mutant alleles seemed to occur with a lower frequency than what would be expected for a regular Mendelian segregation. Moreover, *ap4ß-1* and *ap4ß-2* plants were found to develop significantly shorter siliques than the WT, which was further accompanied by a reduction in the number of seeds in each silique (Figure 13A and B), indicating reproductive impairment. Alexander staining of pollen of *ap4ß-1*, *ap4ß-2* and WT, which can be used to differentiate between unaborted (purple) and aborted (green) pollen (Alexander, 1969), indicated that mutant pollen was generally viable (Figure 13C). To evaluate, whether low inheritance of the *ap4* mutant allele nevertheless resulted from defects of the male gametophyte, pollen tube growth was analyzed *in vitro*. A protocol is given in section 4.2.4.5. Pollen of different *ap4* lines and of WT plants were incubated on synthetic medium for 4.5 h to determine the pollen germination rate, or for 2.5 h to measure pollen tube growth. Although the pollen germination rate was generally low on the synthetic medium, also in the WT control, an even larger proportion *ap4ß-1* and *ap4ß-2* pollen failed to germinate, even after 4.5 h of incubation (Figure 13D). After 2.5 h incubation, the pollen tubes of *ap4ß-1*, *ap4ß-2*, *ap4μ*, or *ap4ß-2 ap4μ* mutants reached only half the length of WT or of complemented mutant pollen tubes (about 100 µm vs. over 200 µm; Figure 13E and F).

Impaired male fertility of the mutant was additionally confirmed *in vivo*, via segregation analyses of the *ap4ß-1*, *ap4ß-2* and *ap4μ* mutant alleles. To this end, pollen from heterozygous (*AP4ß/ap4ß* or *AP4μ/ap4μ*) plants, were used to pollinate WT (= *AP4ß/AP4ß* or *AP4μ/AP4μ*) pistils, and the genotype of the descendants was analyzed. To exclude that a ko of *AP4ß* or *AP4μ* additionally interfered with female fertility, crossings were additionally performed *vice versa* (e.g. pistils from heterozygous plants were pollinated with WT pollen). Segregation analysis of the *ap4μ* allele was performed by PCR-based genotyping (analogous to 2.1.2) of the F_1 generation. For segregation analyses of the *ap4ß-1* or *ap4ß-2* allele, progeny were selected via the Basta-resistance encoded on the T-DNA (vector pDAP101; McElver et al., 2001). The ratio of heterozygous to WT progeny was calculated for each parental silique. Among the descendants obtained from the WT siliques that had been pollinated with pollen from heterozygous plants, heterozygous:WT plants occurred in a ratio of ~ 15:85. This indicates a drastically reduced fertility of the mutant pollen, because WT-like fertility would instead yield a 50:50 ration in the F_1 generation. The descendants of the *vice versa* experiments, however, did show an approximate 50:50 ratio, suggesting that a disruption of the *ß*- or *μ*-subunit of AP-4 does not interfere with female fertility.

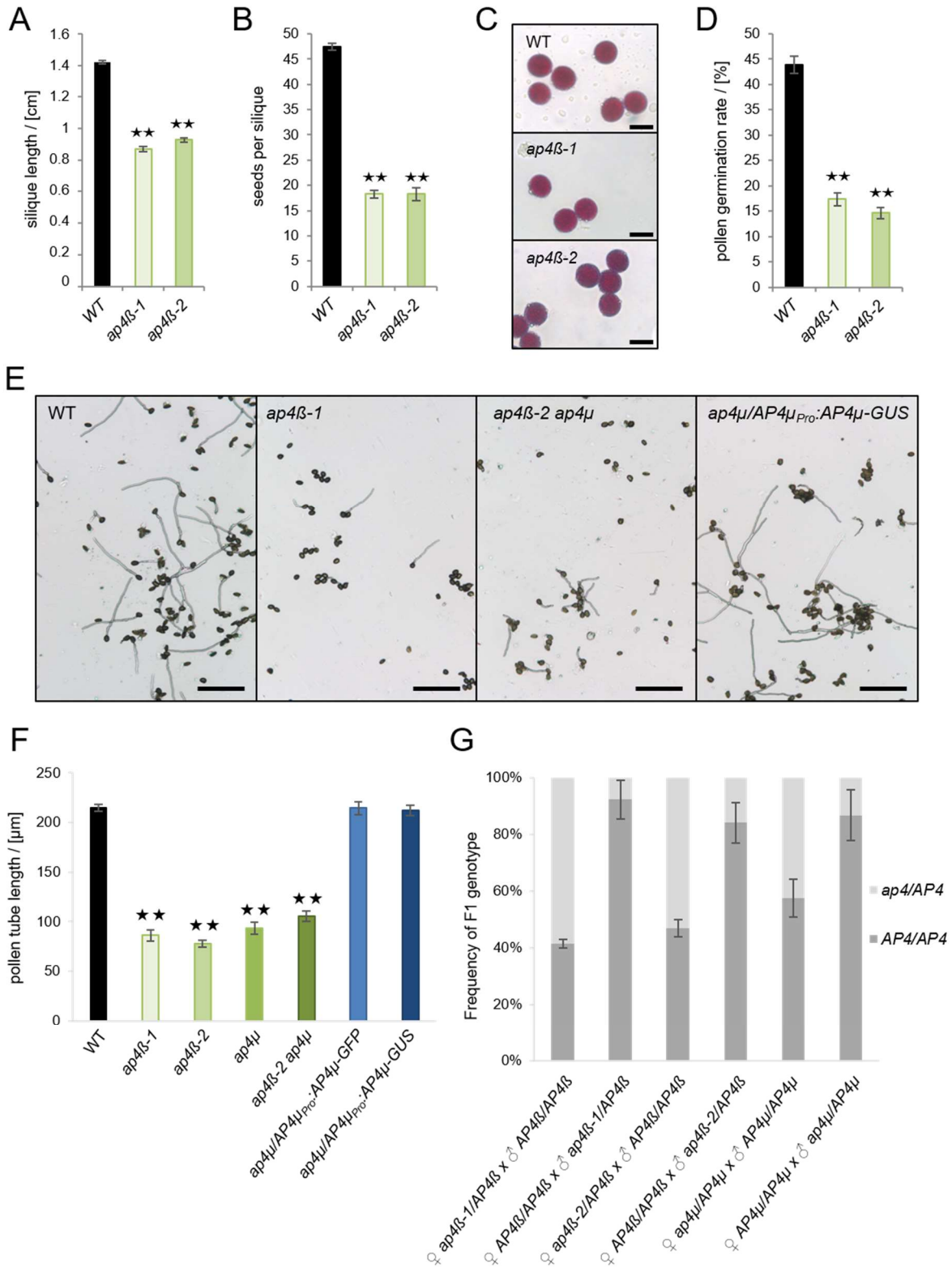

Figure 13: Pollen tube growth and male fertility are impaired in *ap4* mutants.
(A) Length of mature siliques of WT, *ap4ß-1*, and *ap4ß-2* plants grown on soil. Columns represent means ± SE (n > 129 siliques for each genotype).
(B) Number of seeds per silique in mature siliques of WT, *ap4ß-1*, and *ap4ß-2* plants grown on soil. Columns represent the mean number of seeds per silique ± SE in n > 26 mature siliques per genotype.
(C) Pollen viability as indicated by Alexander staining of WT, *ap4ß-1*, and *ap4ß-2* pollen. Purple staining indicates viable pollen. Pollen of two flowers from three individual plants (grown on soil) per genotype were treated, all pollen showed purple coloration. Representative images of WT, *ap4ß-1*, and *ap4ß-2* are shown. Scale bars represent 20 µm.

(D) Germination rate of WT, *ap4ß-1*, and *ap4ß-2* pollen on synthetic medium after 4.5 h incubation. Columns represent mean percentage ± SE of germinated pollen per image (n ≥ 38 images per genotype with at least 14 pollen per image).
(E) Bright field images of *in vitro* germinated pollen after 2.5 h incubation on medium. Scale bars represent 200 µm.
(F) Lengths of pollen tubes as treated in (E). Columns represent means ± SE (n > 90 pollen tubes for each genotype from three biological replicates in total).
(G) Genotypes regarding *AP4ß* and *AP4µ* alleles in the F_1 descendants of cross-pollination experiments with WT (*AP4/AP4*) pistils and pollen from heterozygous (*ap4/AP4*) plants, or *vice versa*. Bars represent mean values ± SD of the percentage of each genotype in the F_1 generation from two (♀ *ap4ß-1/AP4ß* x ♂ *AP4ß/AP4ß* and ♀ *ap4ß-2/AP4ß* x ♂ *AP4ß/AP4ß*) or four (all other) independent crossing-experiments. At least 28 siliques were obtained per combination. All seeds (from each of these siliques) were grown and analyzed.

2.3.4 Loss of apical dominance

When grown until maturity, *Arabidopsis* WT (Col-0) plants develop a tall primary shoot, which in turn is thought to suppress the outgrowth of axillary buds (reviewed in Cline, 1997; Domagalska and Leyser, 2011). In contrast, apical dominance was regularly lost in *ap4* mutant plants (Figure 14A). However, the percentage of mutants with secondary shoots overgrowing the primary shoot, varied greatly between several trials. Moreover, as exemplified by individual *ap4ß-1* mutant plants in Figure 14B, parameters, such as the proportion of primary to secondary shoot length, was highly inconsistent between individual plants. Further, terminal flowers or inflorescences of primary shoots sometimes became necrotic and began to wilt even prior to any fruit development (top row of Figure 14B). Of course, WT plants were generally grown side-by-side with the mutants to eliminate positional effects.

Figure 14: Irregular loss of apical dominance in *ap4ß-1* mutants.
(A) Flowering WT (left) and *ap4ß-1* (right) plant grown under identical conditions.
(B) Total lengths of primary shoots and proportions of primary- to secondary-shoot-length vary largely between individual *ap4ß-1* mutant plants. Images at the top show a higher magnification of the primary inflorescence of the plant in the image below (red arrows indicate the position of corresponding inflorescences).

2.3.5 Altered carbohydrate contents

To obtain further hints to possible cargo proteins of AP-4, the carbohydrate content of *ap4ß-1* and *ap4ß-2* seedlings, and of rosette leaves of *ap4ß-1*, *ap4ß-2* and *ap4µ* plants was measured by ion chromatography. Extracts were obtained as described in section 4.2.4.3; concentrations of *myo*-inositol, glucose, fructose and sucrose were determined. As presented in Figure 15, sucrose contents were generally unaffected by the absence of any of the AP-4 subunits. In both seedlings and rosette leaves, representing sink and source tissue, respectively, levels of m*yo*-inositol were found to be significantly reduced in all mutants compared to the WT. Measurement of fructose and glucose concentrations yielded differential results for sink (seedlings) and source (rosette leaves) tissue: compared to the WT, fructose concentrations were specifically elevated in mutant seedlings, but were found to be at WT-level in rosette leaves. Glucose, similar to fructose, also appeared to accumulate in mutant seedlings, but compared to the WT, the glucose concentrations in rosette leaves were, in fact, found to be significantly reduced in the mutants.

With respect to the role of AP-4 in the subcellular sorting of transmembrane proteins, this data indicate that the complex might be involved in the trafficking of specific sugar transporters to their target compartment. In many cases, however, different sugar transporters show a high degree of redundancy and overlapping substrate specificities. Moreover, the loss of an AP-4 subunit might exert secondary effects on sugar biosynthesis. It is therefore difficult to anticipate potential AP-4 targets based only on the ion chromatography data.

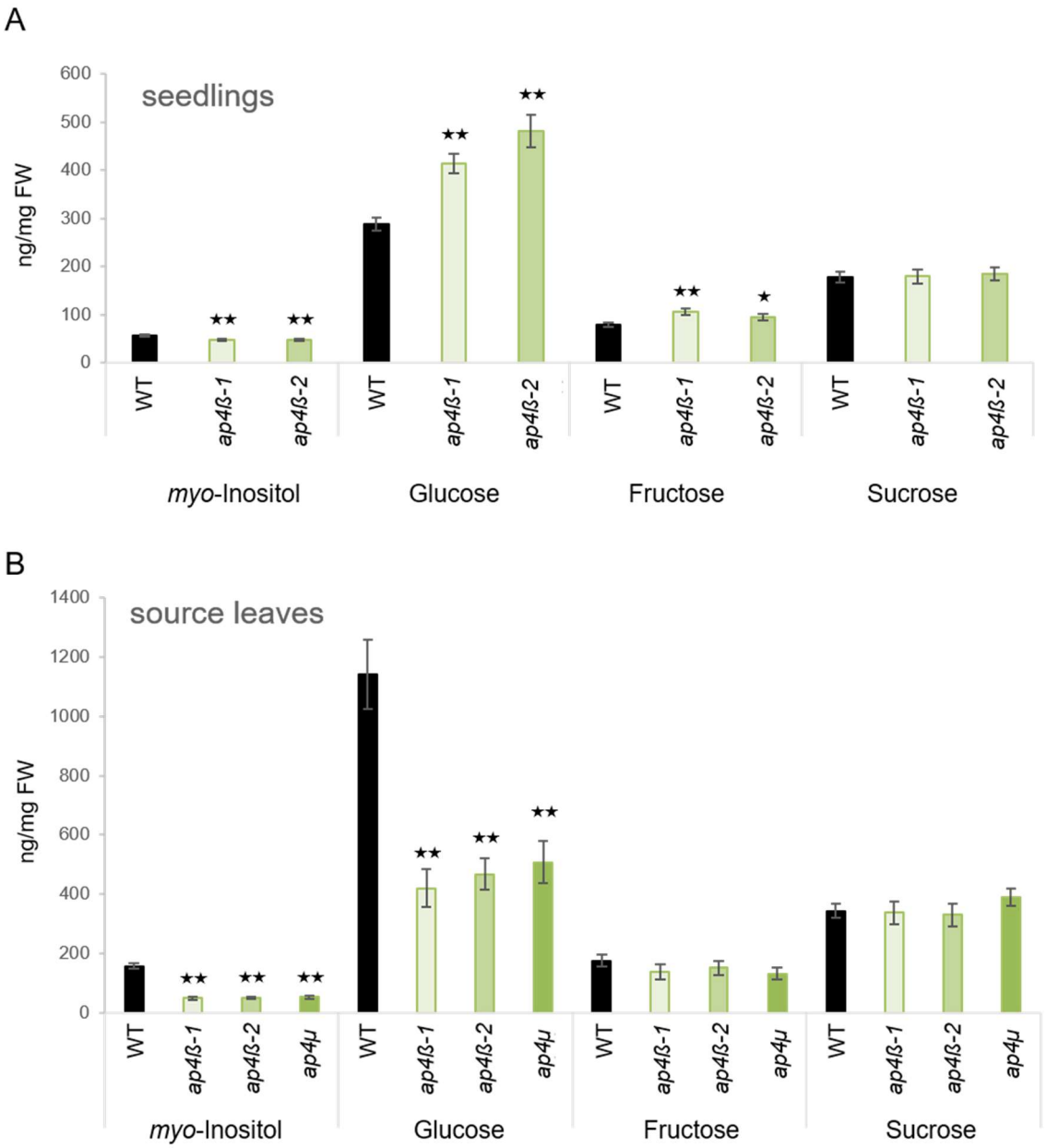

Figure 15: Sugar and sugar-alcohol content of WT and *ap4* mutants.
(A) Concentration of different carbohydrates in 19-day-old WT, *ap4ß-1* and *ap4ß-2* seedlings as determined by ion chromatography. Per sample, 9-16 seedlings were cut off directly above the soil. Columns represent means ± SE (n ≥ 18 samples per genotype from three independent experiments, in total).
(B) Carbohydrate concentrations in leaves of seven-week-old WT, *ap4ß-1*, *ap4ß-2* and *ap4μ* plants. Per sample, three fully expanded leaves (of one plant) were harvested. Columns represent means ± SE [n ≥ 18 for each genotype. Results from two (*ap4μ*) or three (*ap4ß-1*, *ap4ß-2*) or five (WT) independent experiments are shown]. Asterisks indicate significant (*, $p < 0.05$) or highly significant (**, $p < 0.01$) differences compared to the WT. FW = fresh weight.

2.3.6 Chlorosis

When *ap4* mutants were cultivated in growth chambers on soil, slight chlorosis was sometimes observed in leaves of the mutants. This could indicate iron-deficiency. To examine the development of *ap4* mutant seedlings with respect to metal supply in more detail, seedlings were grown on synthetic medium to be able to control iron-sufficient and

iron-deficient conditions more precisely. ABIS medium was either supplemented with 50 µM FeHBED (+Fe), or with 50 µM ferrozine (-Fe) which chelates residual iron in the medium and renders it inaccessible to the plants (see section 4.1.4.2). As a control, *nramp4-1* single ko, and *nramp3-1 nramp4-1* double ko plants (all in the Col-0 background) were grown together with *ap4* mutants and WT seedlings. For *nramp* mutants, characteristic iron-dependent phenotypes have been described earlier (Lanquar et al., 2005; Mary et al., 2015). In WT plants, NRAMP3 and NRAMP4 localize to the TP, and mediate the release of divalent cations (including iron) to the cytosol (Thomine et al., 2003; Lanquar et al., 2005). Because early seedling development requires remobilization of iron from the vacuole, the absence of both transporters results in chlorosis in young plants if iron is limited, i.e. cannot be taken up from the growth medium (Mary et al., 2015).

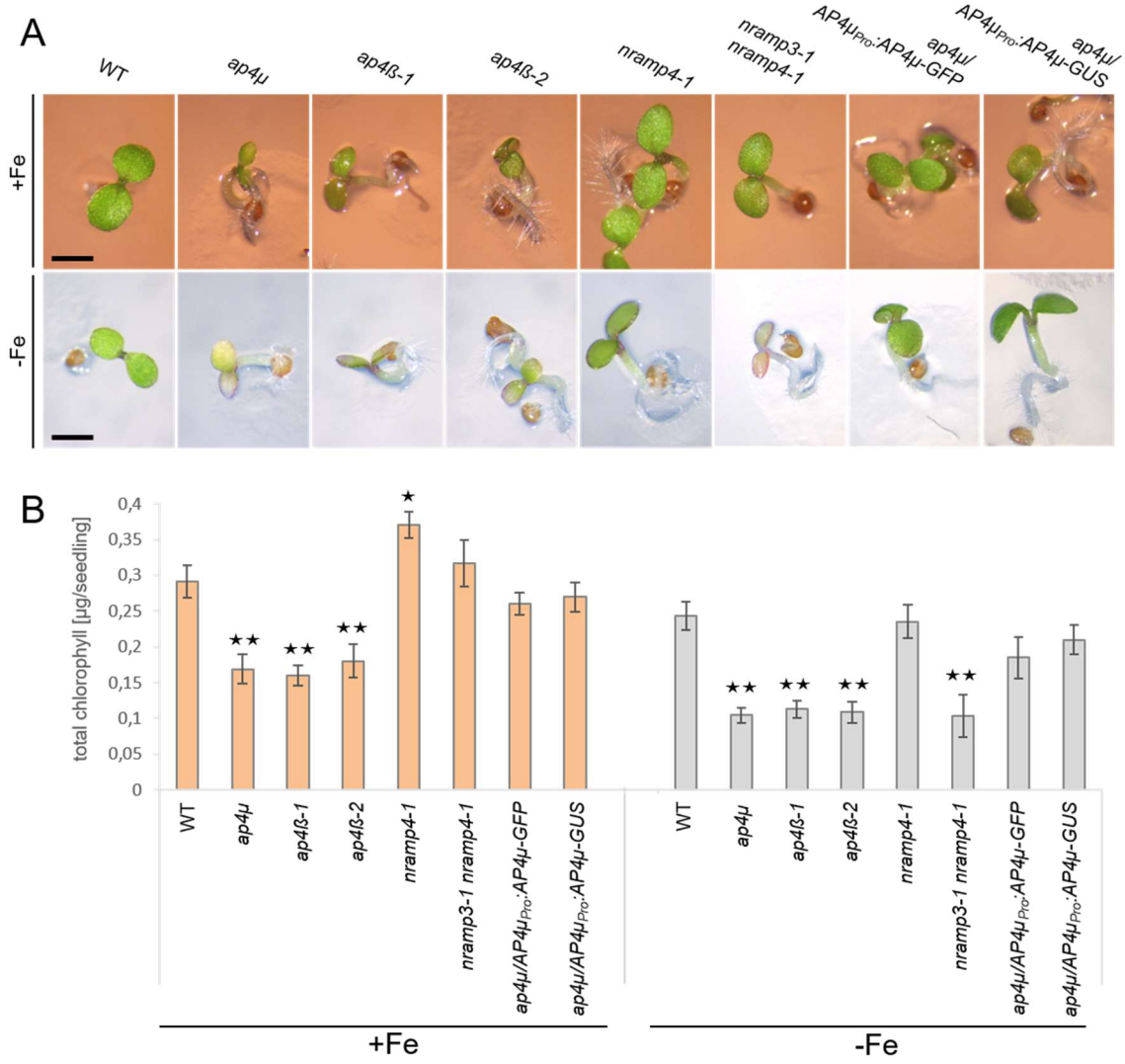

Figure 16: *Ap4* mutant seedlings show reduced chlorophyll content.
(A) Seedlings grown under iron-sufficient (+Fe, top row) and iron-deficient (-Fe, bottom row) conditions. Under iron-sufficient conditions, growth of *ap4* mutants is delayed, cotyledons appear smaller, but are similarly greened after four days compared to *nramp4-1*, *nramp3-1 nramp4-1*, or WT. Under iron-deficiency, *ap4* mutants develop chlorosis comparable to the *nramp3-1 nramp4-1* double mutant. Scale bars represent 1 mm.

(B) *Ap4* mutants show reduced chlorophyll content per seedling compared to the WT. Under limited iron, values of *ap4* mutants are comparable to those of *nramp3-1 nramp4-1* double mutants. The means ± SE of four independent experiments are shown (n > 11 samples in total per genotype and iron-condition). Asterisks indicate significant (*, $p < 0.05$) or highly significant (**, $p < 0.01$) differences compared to the WT (Student's t-test).

On ABIS medium supplemented with iron (+Fe), cotyledons of *ap4ß-1*, *ap4ß-2* and *ap4µ* mutant seedlings appear slightly smaller than those of the WT, which is in agreement with the observations already described (Müdsam, 2012) and which by now has been published by Fuji et al. (2016). Qualitatively, greening appeared to be mildly impaired in these lines (Figure 16A; top row). When grown under limited iron (-Fe), *ap4* single mutant lines developed chlorosis comparable to *nramp3-1 nramp4-1* double mutants (Figure 16A; bottom row). Spectrophotometrical determination of the chlorophyll content confirmed these observations, and revealed that pigment levels of *ap4* mutants were, in fact, reduced under both conditions (Figure 16B). When iron was supplemented, the chlorophyll content per seedling of *nramp4-1* was measured to be slightly above WT level. Consistent to Mary et al. (2015), *nramp3-1 nramp4-1* developed severe chlorosis only under iron limitation with a pigment content of 42% compared to WT, whereas no significant decrease was measured in *nramp4-1* single mutants. Chlorophyll contents of complemented *ap4µ* mutants (*ap4µ/AP4µ$_{Pro}$:AP4µ-GFP* and *ap4µ/AP4µ$_{Pro}$:AP4µ-GUS*) were not significantly different from the WT. *Ap4ß-1*, *ap4ß-2* and *ap4µ* reached about 58% of the respective WT level of total chlorophyll per seedling when iron was supplemented, but showed a further decrease to approximately 45% under iron-limitation.

2.4 Protein sorting in *Arabidopsis ap3* and *ap4* mutants

Attempts to identify AP-4 cargo were based on several different preliminary considerations. Sorting of human amyloid precursor protein (HsAPP) is known to depend on AP-4. Both, individual sorting steps of APP along the secretory pathway, as well as the interaction between HsAPP and AP-4, are quite well studied (Burgos et al., 2010; Choy et al., 2012). To initially examine whether *Arabidopsis* AP-4 presents comparable specificities towards the heterologous cargo, *35S$_{Pro}$:HsAPP-GFP* was expressed in *Arabidopsis* mesophyll protoplasts of WT and *ap4* mutant plants. Provided that the sorting of HsAPP-GFP was altered in *Arabidopsis ap4* mutants, cargo of the complex could possibly be identified based on a homology to APP. Moreover, it might allow to determine the specific route(s) on which AP-4 mediates intracellular sorting specifically in plants.
Secondly, candidates identified via a proteomics approach in cooperation with the University of Hohenheim (Pertl-Obermeyer et al., 2016) were cloned and their subcellular localization was analyzed.
Finally, possible transmembrane cargos of *Arabidopsis* AP-4 were selected based on mutant phenotypes of the respective genes. Under the assumption that a protein cannot fulfill its specific function if it fails to reach its target compartment, wrong subcellular sorting of the protein of interest would cause the same effect as a ko of the corresponding gene. As a consequence, any ko phenotype of this cargo would also occur in *ap4* mutants.

Therefore, potential cargo was chosen according to mutant phenotypes of the respective gene corresponding to (or at least not contradicting) an *ap4* phenotype.

2.4.1 Sorting of human APP in *ap4* mutants of *Arabidopsis*

HsAPP had already been shown to be sorted by AP-4 via an interaction between the YKFFE-motif of HsAPP and the μ-subunit of AP-4 (Burgos et al., 2010; Ross et al., 2014). When this interaction is abolished, either by mutation of the motif or by depletion of AP4μ, HsAPP localization shifts from endosomes to the TGN (Burgos et al., 2010). To analyze whether human APP was similarly sorted in *Arabidopsis*, *GFP* was fused to a modified CDS of *HsAPP* (codon-optimized for expression in plants, synthesized by Eurofins Genomics; see section 4.2.6.3) and transiently overexpressed ($35S_{Pro}$) in *Arabidopsis* mesophyll protoplasts.

Mesophyll protoplasts of WT or *ap4μ* plants, transiently overexpressing *HsAPP-GFP* showed fluorescence mostly in small puncta (Figure 17A). To study the localization in more detail, markers for different compartments were transformed together with *HsAPP-GFP*. When coexpressed with *SYP32-mCherry* (wave22R; Geldner et al., 2009), pronounced overlap of the Golgi-marker with HsAPP-GFP was neither observed in WT, nor in *ap4μ* mutants (Figure 17B). Coexpression with *VTI12-mCherry* (wave13R; Geldner et al., 2009), on the other hand, resulted in parallel labeling of the TGN/EE by both fluorophore-fusions, but again, no obvious difference between *ap4μ* and the WT was observed.

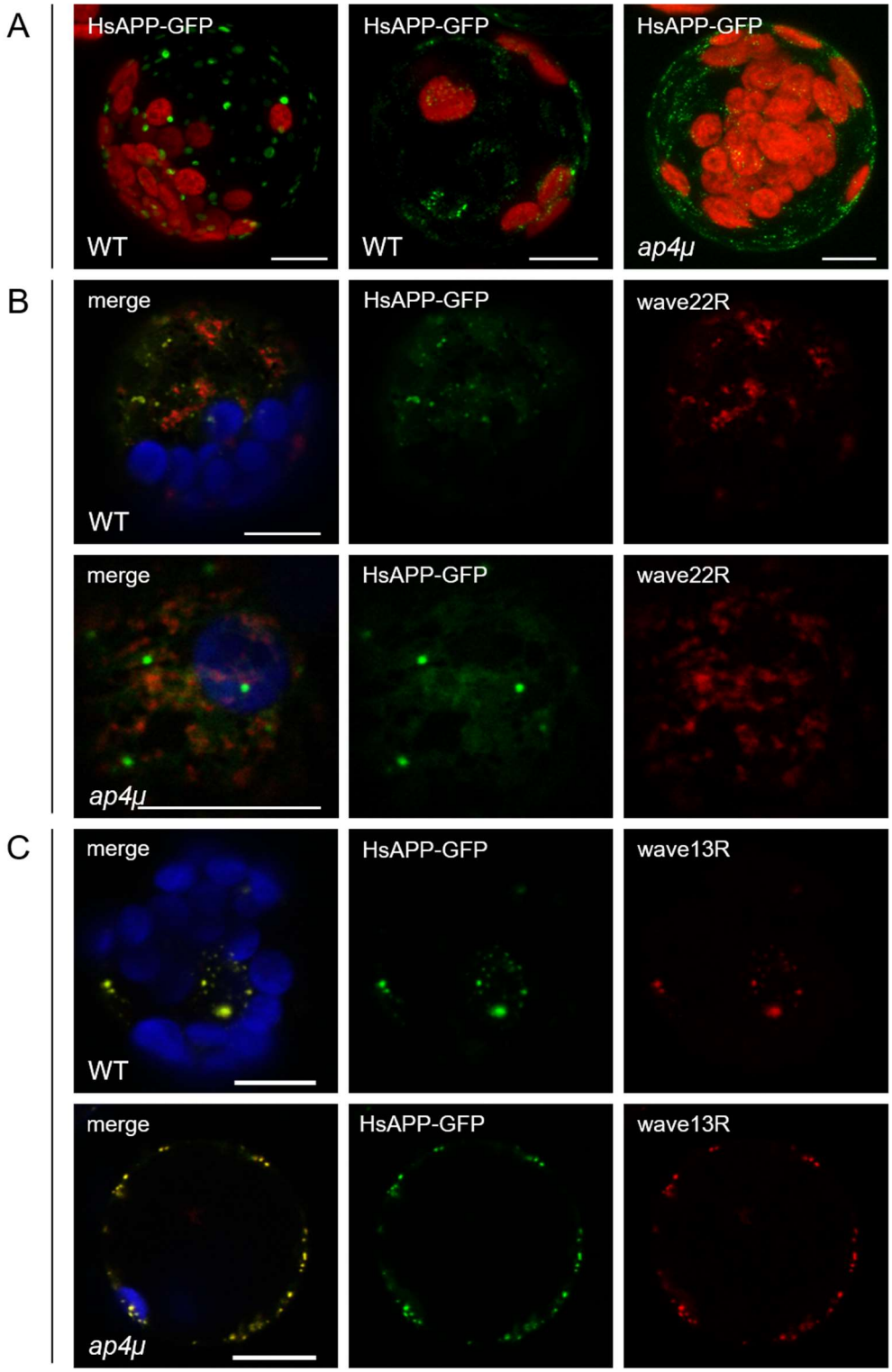

Figure 17: Localization of HsAPP-GFP in mesophyll protoplasts of WT and *ap4μ*.
(A) Maximum projections of WT (left and middle) and *ap4μ* (right) mesophyll protoplasts expressing *HsAPP-GFP*. HsAPP-GFP localizes to small disk-shaped structures (left), or puncta (middle and right). GFP is shown in green, chlorophyll autofluorescence in red. Scale bars represent 10 µm.
(B) HsAPP-GFP does not show any obvious colocalization with the Golgi marker SYP32-mCherry (wave22R) in WT (top) or *ap4μ* (bottom) mesophyll protoplasts. GFP fluorescence is shown in green, mCherry is shown in red, chlorophyll autofluorescence is shown in blue. Scale bars represent 10 µm.
(C) HsAPP-GFP colocalizes with the TGN/EE marker VTI12-mCherry (wave13R) in WT (top) and *ap4μ* (bottom) mesophyll protoplasts. GFP fluorescence is shown in green, mCherry is shown in red, chlorophyll autofluorescence is shown in blue. Scale bars represent 10 µm.

2.4.2 Subcellular localization of GFP-fusions of cargo candidates identified by sucrose gradient profiling

In a proteomics approach, possible cargo of *Arabidopsis* AP-4 and/or AP-3 was identified via sucrose gradient profiling performed and published by Pertl-Obermeyer et al. (Pertl-Obermeyer et al., 2016). Briefly, proteins of WT, *ap4ß-1* and *ap3ß* mutant plants were radioactively labeled *in vivo*. The full proteome was then fractionated along a sucrose gradient yielding soluble fractions, as well as individual (hydrophobic) interphases, each thought to be enriched for specific membrane compartments. Mass spectrometry was then used to identify protein compositions of the individual interphases in WT and mutant. Based on the relative abundance of a protein of interest in each interphase, a characteristic distribution profile of this protein along interphases of the mutant or the WT gradient was obtained. The presence of marker proteins in an individual interphase further allowed assignment of a given fraction to specific cellular compartments. Potential AP-3 or AP-4 cargos, being missorted in the mutants, were thus expected to show an altered distribution profile compared to WT. Alternatively, cargos might be depleted from the mutant proteome due to degradation after mistargeting.

To validate that the subcellular localization of a protein identified as a possible AP-3 or AP-4 cargo was, in fact, altered in the mutant, the corresponding CDS was genetically fused to *GFP*, and sorting of the GFP-fusion was examined in mesophyll protoplasts of WT, *ap3ß*, and/or *ap4ß-1*.

The following candidates, identified as possible cargo of AP-3 and/or AP-4 by the group of Waltraud Schulze (University of Hohenheim), were cloned and their subcellular targeting examined: cationic amino acid transporter 9 (CAT9), aluminium sensitive 1 (ALS1), sugar transport protein 1 (STP1), nitrate transporter 1.1 (NRT1.1), syntaxin of plants (SYP) 122, SYP132, and plasma membrane intrinsic protein 2A (PIP2;1). Altered distribution profiles in at least one experiment had suggested CAT9 to be a putative cargo of AP-3, and ALS1, STP1, as well as NRT1.1 to be putative cargos of AP-4. Altered distribution profiles and differential phosphorylation levels had been detected for SYP122 (in *ap4ß-1* compared to WT) and SYP132 (in *ap3ß* compared to WT). Altered abundance in *ap3ß*, as well as differential phosphorylation of PIP2;1 in both mutants had further implicated a possible role for both complexes in subcellular sorting of the aquaporin.

As shown in Figure 18, GFP-fusions of the TP localized CAT9, and ALS1, were not found to be missorted in *ap3ß,* or *ap4ß-1* mesophyll protoplasts. Likewise, PM localization of GFP-fusions of STP1 (Figure 19A), NRT1.1 (Figure 19B), and the syntaxins of plants SYP122 and SYP132 (Figure 20) was neither affected by a loss of AP3ß, nor of AP4ß.

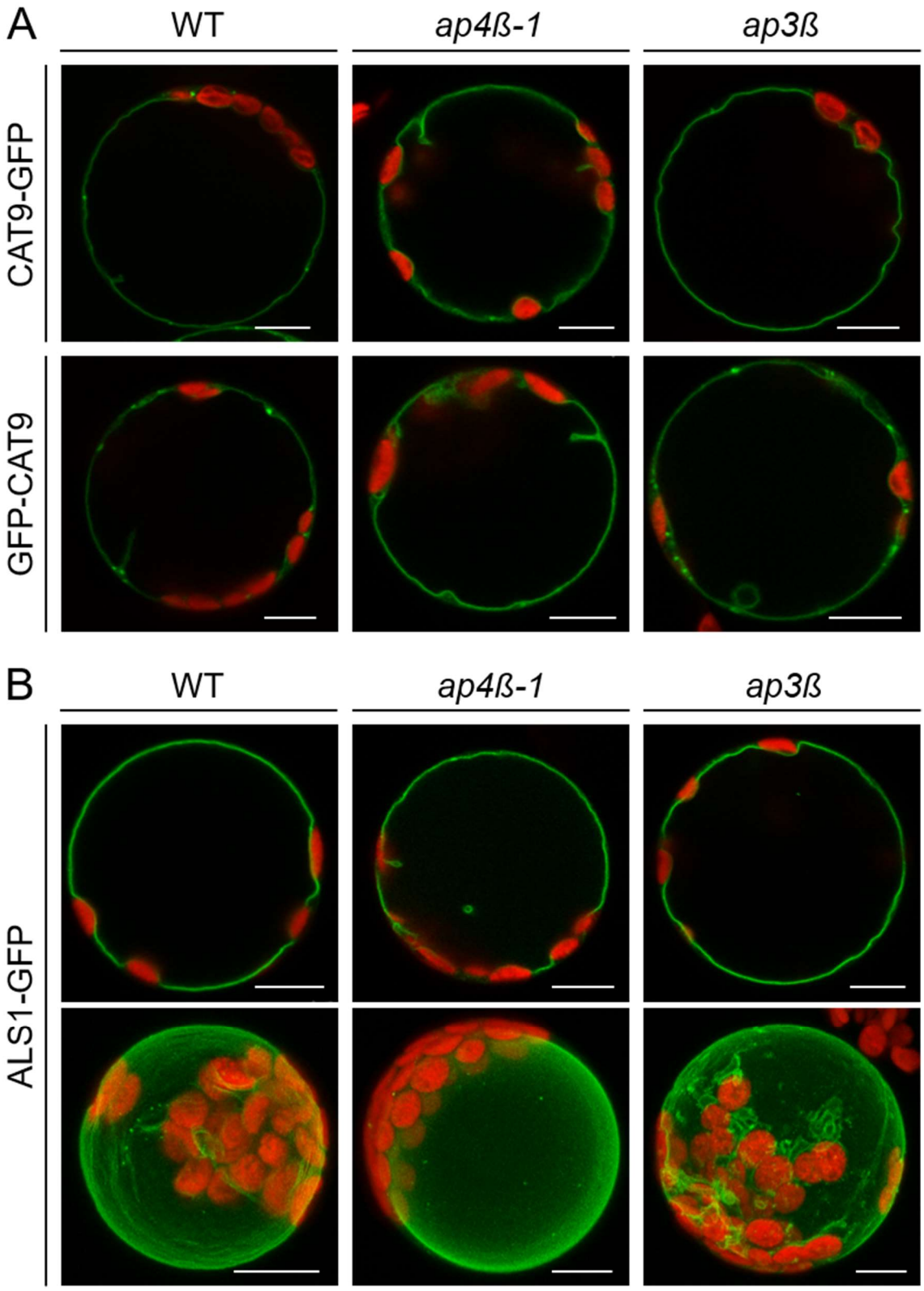

Figure 18: Subcellular localization of GFP-fusions of CAT9 and ALS1 in mesophyll protoplasts of WT, *ap3ß*, and *ap4ß-1*.

GFP is shown in green, chlorophyll autofluorescence in red. Scale bars represent 10 µm.

(A) CAT9-GFP (upper row) and GFP-CAT9 (lower row) localize to the TP in mesophyll protoplasts of WT (left), *ap4ß-1* (middle), and *ap3ß* (right).

(B) ALS1-GFP localizes to the TP in WT (left), *ap4ß-1* (middle), and *ap3ß* (right), as represented by confocal single sections (upper row), and maximum projections (lower row) of individual mesophyll protoplasts.

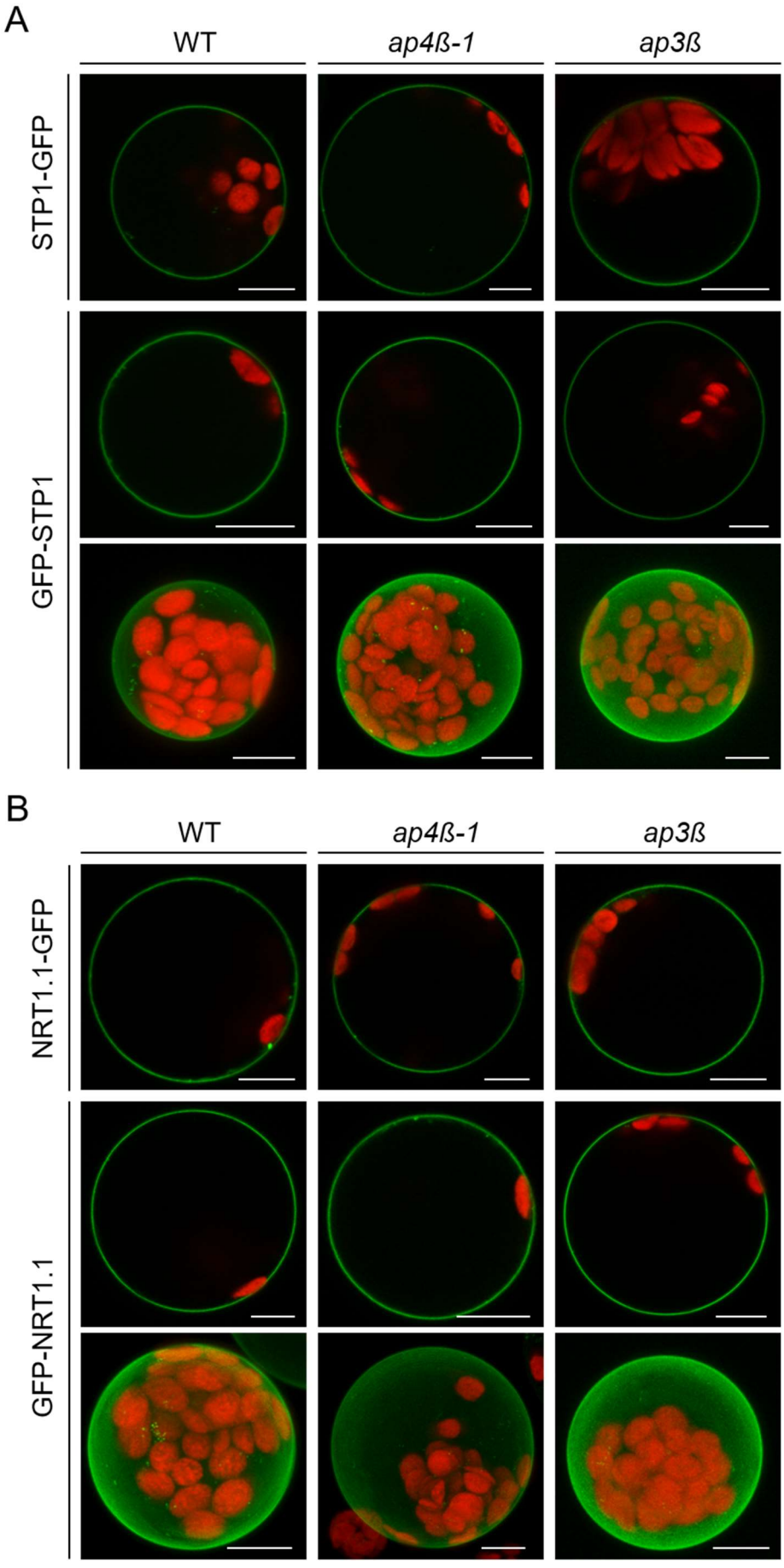

Figure 19: Subcellular localization of GFP-fusions of STP1 and NRT1.1 in mesophyll protoplasts of WT, *ap3ß*, and *ap4ß-1*.
GFP fluorescence is shown in green, chlorophyll autofluorescence in red. Scale bars represent 10 µm. Confocal single sections (upper and middle row) are shown for all GFP-fusions. Localization of *N*-terminal GFP-fusions are additionally shown as maximum projections (lower row).
(A) *C*- (upper row) and *N*-terminal (middle and lower row) GFP-fusions of STP1 localize to the PM of WT, *ap3ß*, or *ap4ß-1* mesophyll protoplasts.
(B) *C*- (upper row) and *N*-terminal (middle and lower row) GFP-fusions of NRT1.1 localize to the PM of WT, *ap3ß*, or *ap4ß-1* mesophyll protoplasts.

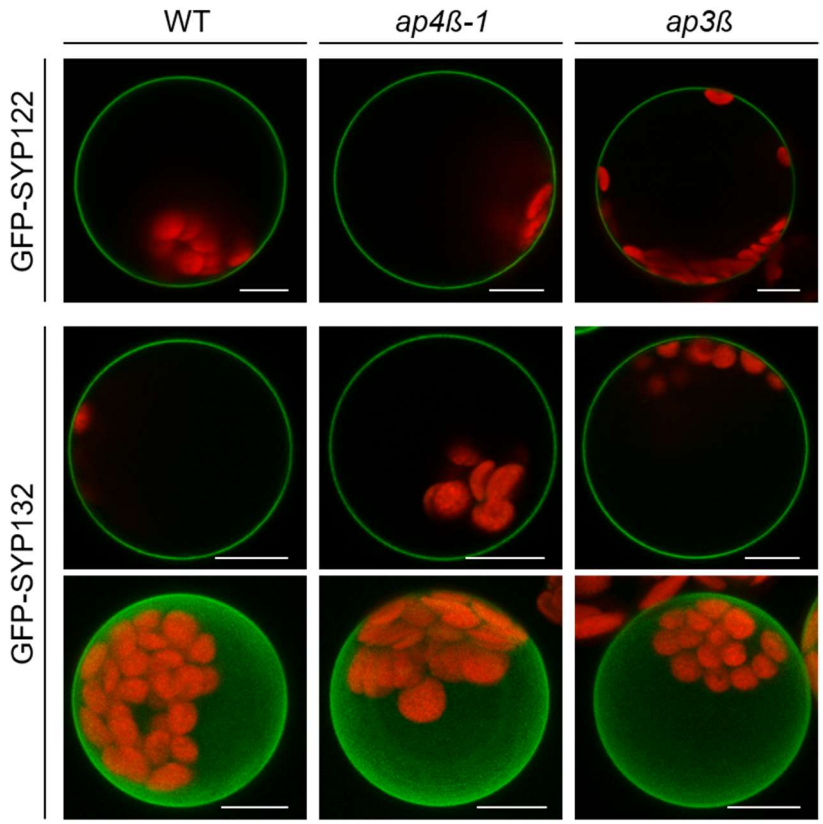

Figure 20: *N*-terminal GFP-fusions of SYP122 and SYP132 localize to the PM in mesophyll protoplasts of WT, *ap3ß*, and *ap4ß-1*.
Images in bottom row show maximum projections of protoplasts expressing *35S$_{Pro}$:GFP-SYP132*, all other show confocal single sections of protoplasts expressing *35S$_{Pro}$:GFP-SYP122* (upper row), or *35S$_{Pro}$:GFP-SYP132* (middle row). The genetic background (WT, *ap4ß-1*, *ap3ß*) is indicated at the top. GFP is shown in green, chlorophyll autofluorescence in red. Scale bars represent 10 µm.

In both, *ap3ß* and *ap4ß-1* mutants, several aquaporins were found to show altered distribution or abundance profiles and/or altered phosphorylation compared to the WT (Pertl-Obermeyer et al., 2016). Moreover, the swelling behavior of mesophyll protoplasts that had been exposed to an osmotic stimulus had revealed altered water transport rates in both mutants. To confirm that this effect was due to missorting of specific aquaporins, a GFP-fusion of the plasma membrane intrinsic protein PIP2;1 was generated and subcellular targeting was analyzed by confocal microscopy. As shown in Figure 21, GFP-PIP2;1 clearly labeled the PM in most WT and *ap3ß* mutant cells, resulting in uniform fluorescence surrounding the entire protoplast. However, in contrast to the evenly distributed fluorescence typical for PM localization, the GFP-fusion occasionally appeared in a marked patchy pattern or was concentrated in puncta or network-like structures. Although this generally was observed in all genotypes (i.e. in WT, *ap3ß*, and *ap4ß-1*), the effect seemed to be more drastic in *ap4ß-1* mesophyll protoplasts (Figure 21A). In most WT cells, coexpression of *GFP-PIP2;1* with the PM-marker *INT4-RFP* (Wolfenstetter et al., 2012) accordingly yielded overlapping GFP and RFP signals, whereas in *ap4ß-1* mutants, GFP-fluorescence was separated from the RFP-labeled PM to a substantial extent (Figure 21B). To quantify the initial observation, WT, *ap3ß-1* or *ap4ß-1* protoplasts transformed with *GFP-PIP2;1* were again recorded and each transformed cell was categorized according to the predominant localization of the GFP-fusion (Figure 21C). Because confocal single sections were often not sufficient to discriminate between an even and a patchy GFP-distribution, maximum projections were generated from z-stacks with at least 30 steps and a step size of approximately 0.5–1 µm. On these images, each showing

several transformed protoplasts, every cell with visible GFP-fluorescence was counted as either “PM” (evenly distributed GFP-fluorescence, no pronounced intracellular signals) or “other” (fluorescence predominantly concentrated in puncta, patches, or network-like structures). To exclude bias, all pictures were numbered (randomly varying the order of the genotypes) prior to analysis by a third person (single-blind). Compared to the WT, the percentage of protoplasts with a clear PM localization of GFP-PIP2;1 was, in fact, found to be significantly decreased in *ap4ß-1* protoplasts (p-value < 0.05), but not in *ap3ß* (p-value > 0.5).

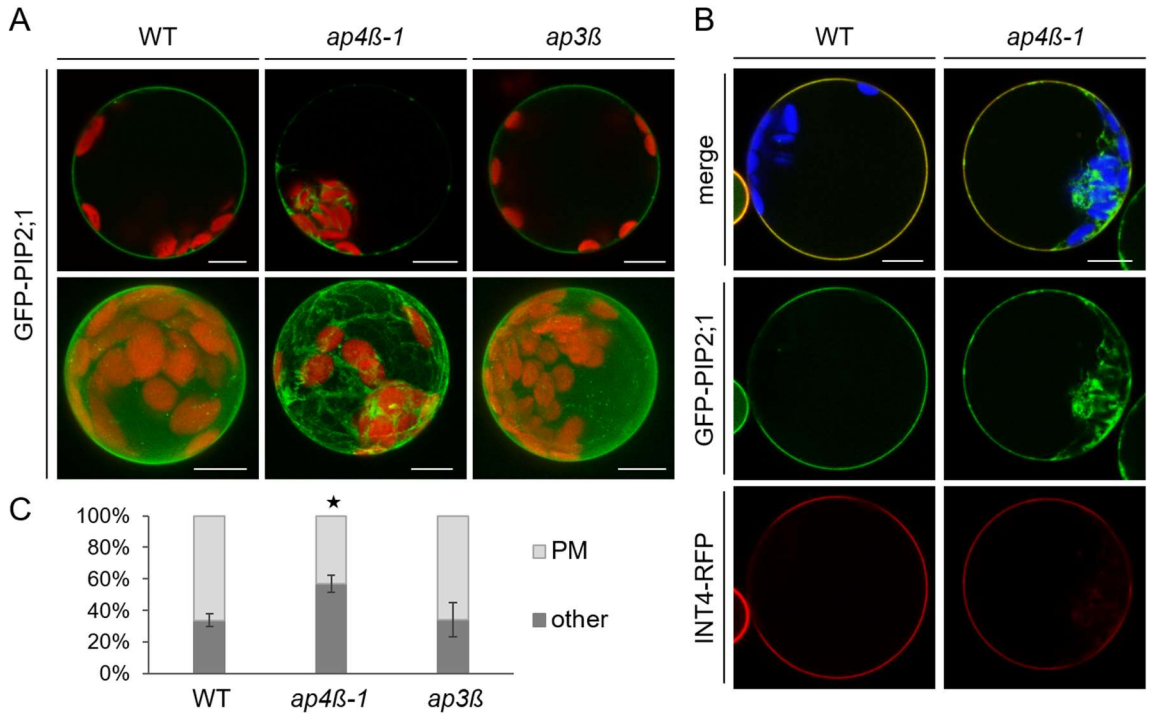

Figure 21: Localization of GFP-PIP2;1 in WT, *ap4ß-1*, and *ap3ß* mesophyll protoplasts.
(A) Single sections (top row) and maximum projections (bottom row) of representative WT (left), *ap4ß-1* (middle), and *ap3ß* (right) protoplasts expressing *35S$_{Pro}$:GFP-PIP2;1*. GFP-fluorescence is shown in green, chlorophyll autofluorescence in red. Scale bars represent 10 µm.
(B) GFP-PIP2;1 colocalizes with INT4-RFP at the PM of WT (left) mesophyll protoplasts, but additionally labels intracellular structures in *ap4ß-1* (right). GFP fluorescence is shown in green, RFP fluorescence in red. Merged images additionally show chlorophyll autofluorescence in blue. Scale bars represent 10 µm.
(C) Percentage of protoplasts with PM localization of GFP-PIP2;1 [as represented for example by WT in panel (A)]; or with predominant intracellular localization (other) of GFP-PIP2;1 [as represented by *ap4ß-1* in panel (A)]. Columns represent the means ± SE (n = 3 independent experiments). At least 55 protoplasts were scored per transformation and genotype. Asterisk indicates significant (p < 0.05) difference compared to WT. Figure modified from Pertl-Obermeyer et al., 2016 (Supplementary Figure 3).

2.4.3 Subcellular sorting of possible AP-4 targets based on consistent mutant phenotypes

2.4.3.1 Defects in AP-4 do not alter auxin distribution in plants

As shown in section 2.3.4, *ap4* mutants showed defects in shoot growth and reduction of apical dominance. The latter is thought to (at least partially) depend on the transport of auxin from the primary shoot thereby inhibiting axillary or lateral shoot growth (reviewed in Cline, 1997; Domagalska and Leyser, 2011). Based on the assumption that the loss of apical dominance observed in *ap4* might, for example, be due to missorting of a protein which mediates transport of the phytohormone, several candidates were selected from the literature, of which GFP-fusions were then created. Sorting was examined in transiently transformed mesophyll protoplasts of WT, *ap4*, and, acting as an additional control, also in *ap3ß* mutants.

Corresponding to its role in auxin transport (Bouchard et al., 2006), disruption of the multidrug resistance(MDR)-like MDR1/ABCB19/PGP19, results in reduced apical dominance (Noh et al., 2001). Moreover, *mdr1* mutants develop smaller rosettes than the WT (Lin and Wang, 2005).

A double ko of the apyrases *APY1* and *APY2* inhibits pollen germination (Steinebrunner et al., 2003), and growth of etiolated hypocotyls (Wu et al., 2007b). Further, pollen tube growth has been shown to decrease after addition of external (extracellular) anti-apyrase antibody, which indicated a role as ectoapyrases and suggested that APY1 and/or APY2 localize to (or at least transit) the PM (Wolf et al., 2007). Newer studies, however, found both apyrases to localize to the Golgi (Schiller et al., 2012; Chiu et al., 2012). Knock-down of the apyrases has been demonstrated to interfere with polar auxin transport in *Arabidopsis* (Liu et al., 2012), resulting in dwarfed growth. Whereas an *apy1 apy2* double ko results in lethality due to male infertility, pollen specific reintroduction of *APY2* yields viable plants, which show defects in cell expansion (Wolf et al., 2007). Collectively these parallels to *ap4* mutant defects suggested that APY1 and/or APY2 might represent candidates for AP-4 mediated sorting. To test, whether missorting of MDR1, APY1, or APY2 in *ap4* was causative for the possibly auxin related phenotype(s), GFP-fusions of both apyrases, and of MDR1 were generated and their subcellular sorting was analyzed.

In line with published data (Wu et al., 2007a; Chiu et al., 2012; Schiller et al., 2012), GFP-MDR1 was found to localize to the PM of WT cells, and GFP-fusions of APY1 or APY2 mostly labeled puncta, possibly corresponding to the Golgi apparatus. Importantly, subcellular targeting was not affected by mutations in *AP4ß*, or *AP3ß* (Figure 22).

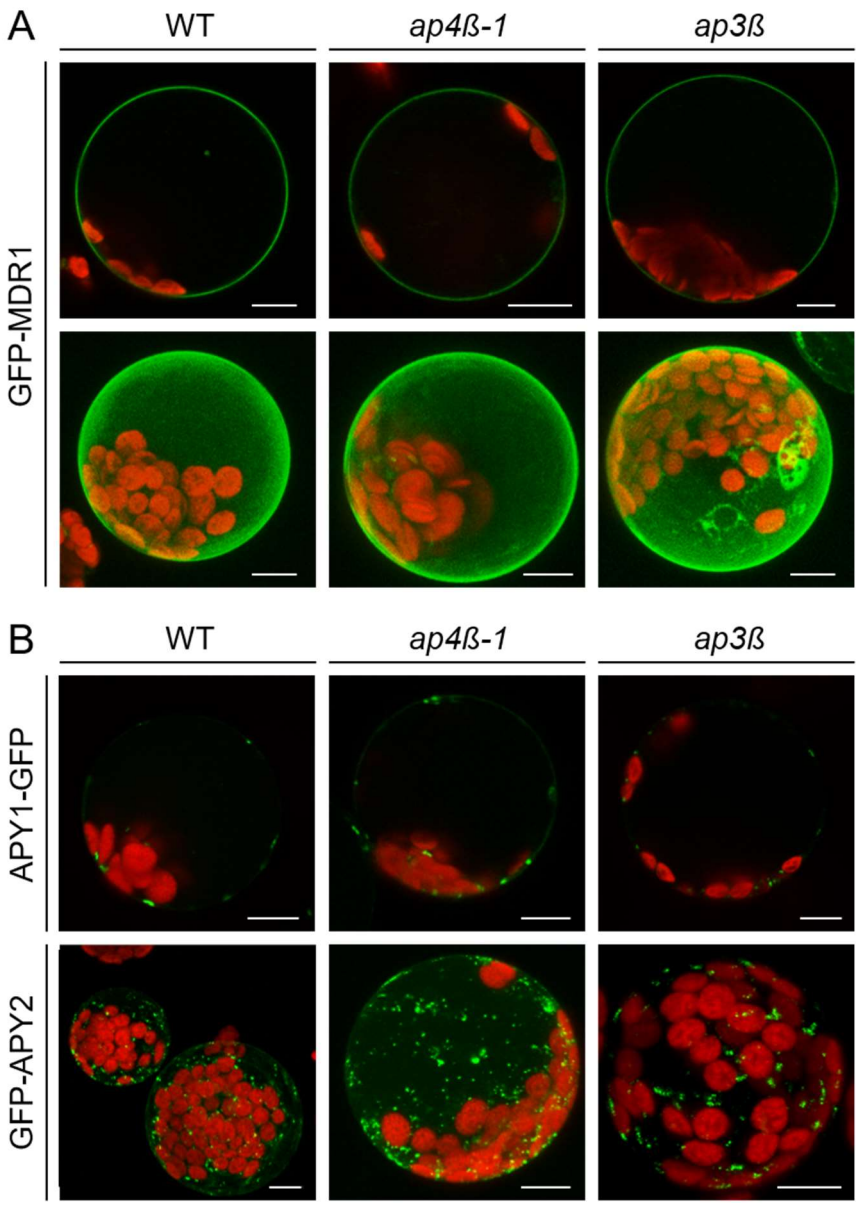

Figure 22: Subcellular localization of GFP-fusions of MDR1, APY1 and APY2 in WT, *ap3ß*, and *ap4ß-1* mesophyll protoplasts.
GFP is shown in green, chlorophyll autofluorescence in red. Scale bars represent 10 µm.
(A) GFP-MDR1 labels the PM in WT (left column), *ap4ß-1* (middle column), and *ap3ß* (right column), as represented by confocal single sections (top row), or maximum projections (bottom row) of individual mesophyll protoplasts expressing *35S$_{Pro}$:GFP-MDR1*.
(B) APY1-GFP (top row) and GFP-APY2 (bottom row) mostly label punctate structures in mesophyll protoplasts of WT (left column), *ap4ß-1* (middle column), and *ap3ß* (right column). Individual images show optical single sections of protoplasts expressing *APY1-GFP*, and maximum projections of protoplasts expressing *GFP-APY2*.

In addition, *ap4ß-1* plants were crossed with different marker lines, expressing *GFP*-fusions of the *PIN-FORMED* (*PIN*) family of auxin transporters under control of the corresponding *PIN*-promoter (for references of marker lines, please refer to section 4.1.3.3). Subcellular trafficking of PIN proteins is quite well studied (Feraru and Friml, 2008; Křeček et al., 2009; Friml, 2010; Grunewald and Friml, 2010; Kitakura et al., 2011; Luschnig and Vert, 2014; Sancho-Andrés et al., 2016), and known to depend on a tight regulation of anterograde and retrograde sorting steps, which makes them suitable candidates to study AP-4 dependent protein sorting.
To additionally monitor auxin distribution, *ap4ß-1* mutants were further crossed with reporter lines expressing *GUS* or *GFP* under the control of an auxin responsive promoter (*DR5$_{Pro}$*). Stable marker lines homozygous for mutant or WT alleles of *AP4ß* were selected in the F_2 generation. Since *AP4µ* (see section 2.2) as well as the analyzed *PIN1*, *PIN2*, *PIN3*

and *PIN7* are all strongly expressed in roots (Blilou et al., 2005; Křeček et al., 2009), expression and subcellular sorting of the different GFP-fusion proteins was observed in roots of three- to five-day-old seedlings (grown on half strength MS-medium supplemented with 2% sucrose). $DR5_{Pro}$:GUS expression was additionally examined in whole seedlings and inflorescences. Localization and expression patterns of the PIN-GFP fusions in WT roots were consistent with already published data (Benková et al., 2003; Xu and Scheres, 2005; Dello Ioio et al., 2008; Blilou et al., 2005): as presented in Figure 23, PIN1-GFP localized predominantly to the (basal) PM of root cells in the central cylinder; PIN2-GFP was observed in the (apical) PM of cells of the cortex, epidermis, and the root cap; *PIN3-GFP* was strongly expressed in the columella, where the corresponding GFP-fusion localized (apolarly) to the PM; PIN7-GFP was present in the (basal) PM of the stele and localized apolarly to the PM of columella cells. Importantly, no obvious differences could be detected between corresponding WT and *ap4ß-1* roots in any of the marker lines.

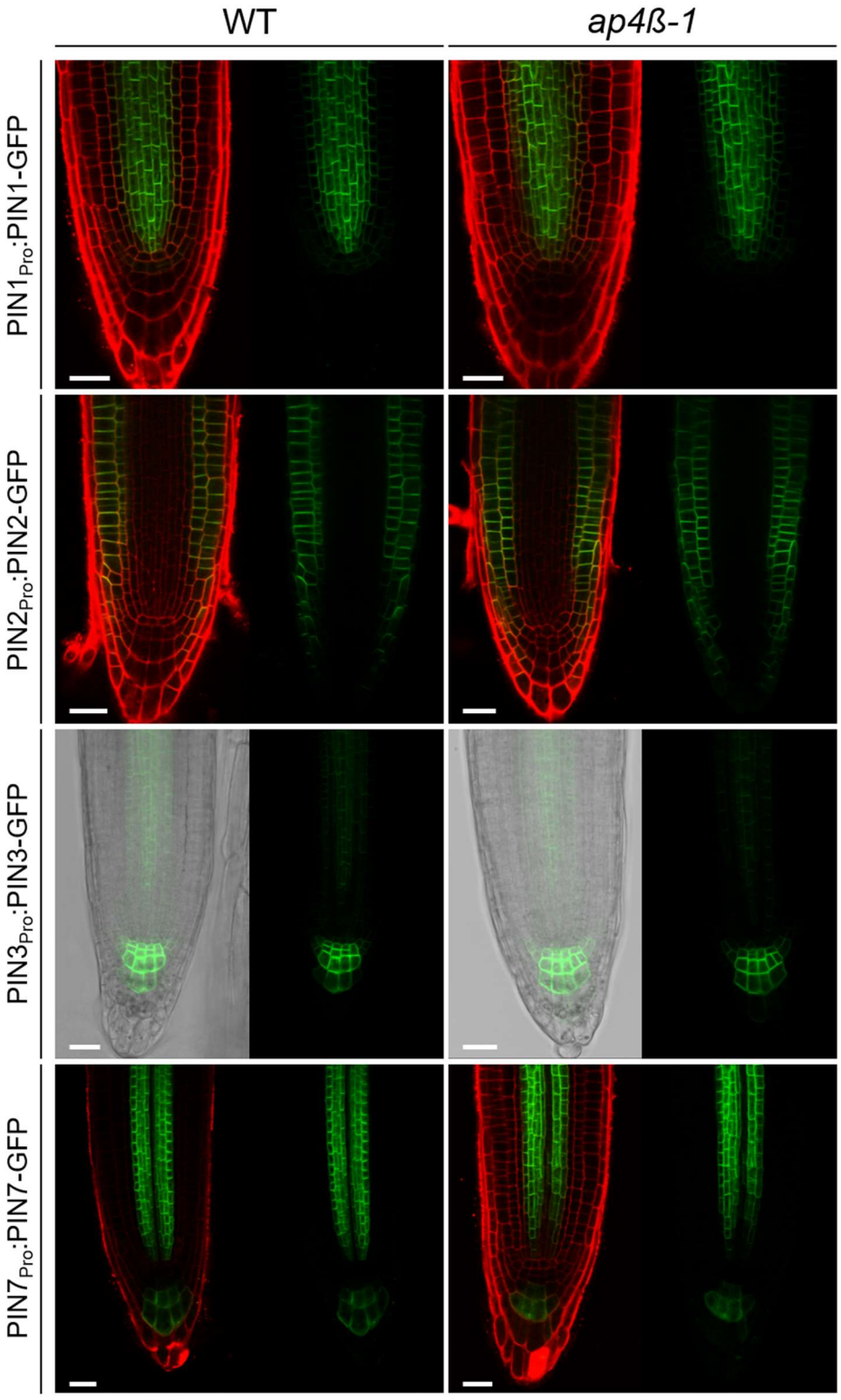

Figure 23: Expression of *GFP*-fusions of *PIN1, PIN2, PIN3* and *PIN7* is not altered in roots of *ap4ß-1* compared to the WT.

WT and *ap4ß-1* seedlings expressing *GFP*-fusions of *PIN1*, *PIN2*, *PIN3*, or *PIN7* under control of the corresponding PIN-promoter (as indicated) were grown on ½ strength MS supplemented with 2% sucrose. Confocal images of roots of 3-day-old seedlings are shown. Pictures on the right of each column show GFP-fluorescence only (in green). The picture on the left of each column shows a merge with the corresponding bright-field image (PIN3-GFP) or with propidium iodide fluorescence (red, all other). Scale bars represent 25 µm.

This was additionally reflected by the identical *GFP*-expression in roots of WT and *ap4ß-1* plants, in which HDEL-tagged *GFP* was expressed under the control of the auxin responsive $DR5_{Pro}$ (Figure 24A). Likewise, WT and *ap4ß-1* plants expressing *ß-glucuronidase* under control of the same promoter, also yielded comparable staining, which was pronounced in initials and tips of side roots, as well as in leaf primordia and in anthers of both, WT and *ap4ß-1* (Figure 24B, C).

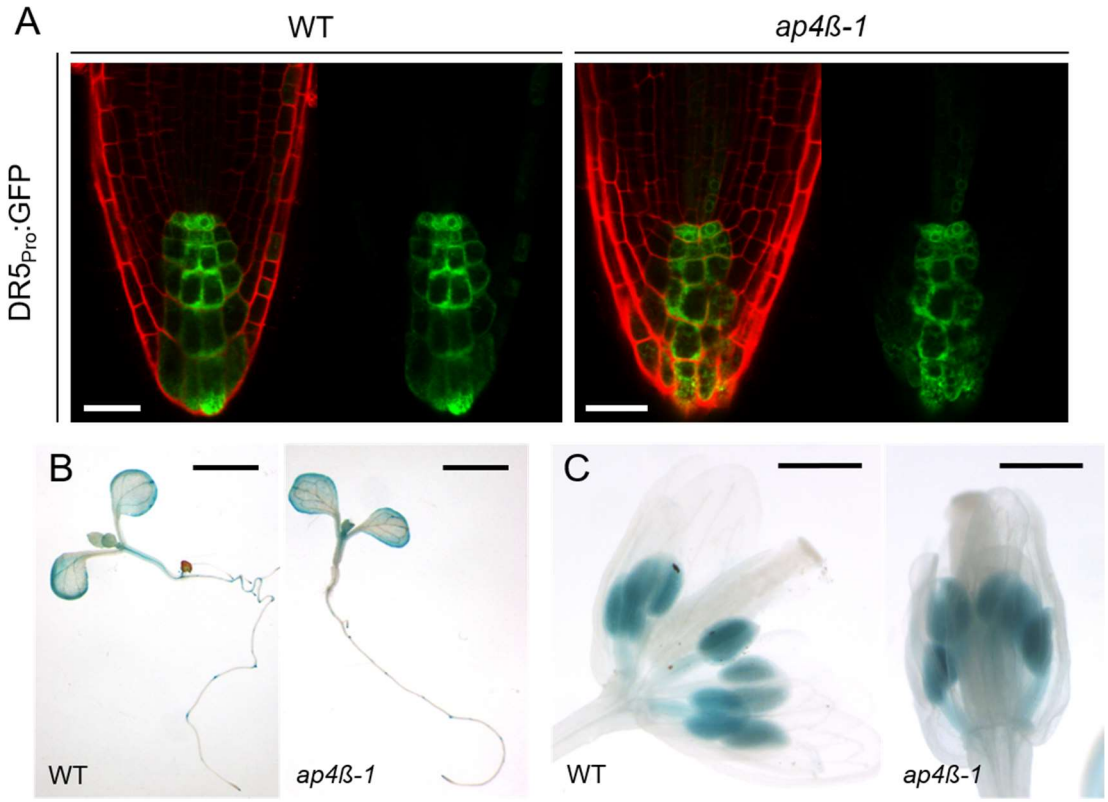

Figure 24: Expression of *GFP* or *GUS* under control of the auxin-responsive promoter $DR5_{Pro}$ is not altered in *ap4ß-1* compared to the WT.
(A) *GFP*-expression (HDEL-tagged to confer ER localization) under control of $DR5_{Pro}$ in root tips of three-day-old WT and *ap4ß-1* seedlings. Seedlings were grown on ½ strength MS supplemented with 2% sucrose. Cell walls were stained with propidium iodide prior to confocal analysis. GFP is shown in green, propidium iodide fluorescence in red. Scale bars represent 25 µm.
(B) and **(C)** GUS staining of WT and *ap4ß-1* expressing *GUS* under control of $DR5_{Pro.}$ Seedlings in (B) were cultivated on ½ strength MS for seven days prior to analysis. Inflorescences in (C) originate from soil-grown-plants.
Scale bars represent 2 mm in (B), or 0.5 mm in (C).

Collectively, these results demonstrate that auxin distribution was undisturbed in *ap4ß-1* mutants and that moreover, AP-4 did not notably contribute to polar trafficking of PINs, or to apolar trafficking of MDR1 at steady-state. Therefore, the altered shoot morphology observed in *ap4* mutants, is unlikely to result from an impairment of auxin trafficking, or of (polar) sorting of PIN1, PIN2, PIN3, or PIN7.

2.4.3.2 *GFP-fusions of NRAMP3, NRAMP4 and MOT2 are partially missorted in* ap4 *mutant protoplasts*

As presented in section 2.3.6, *ap4* mutants developed chlorosis as represented by the reduced chlorophyll content of seedlings grown on medium with and particularly without iron. Under iron deficiency, the pigment levels of *Arabidopsis ap4* mutants further resembled those of double mutants lacking both TP localized members of the NRAMP-family of metal transporters (NRAMP3 and NRAMP4). Possibly, this similarity might result from a participation of the AP-4 complex in sorting of NRAMP3 and/or NRAMP4. To test this hypothesis, the subcellular localization of both transporters was examined in the absence of a functional AP-4 complex. Because not only iron depletion, but also deficiencies for other metal-ions can result in chlorosis, some other transmembrane proteins known to be involved in metal homeostasis, were additionally examined.

GFP-fusions of metal tolerant protein 1 (MTP1; Desbrosses-Fonrouge et al., 2005; Kobae et al., 2004) and zinc induced facilitator 1 (ZIF1; Haydon and Cobbett, 2007) have been shown to localize to the TP in *Arabidopsis* and mediate metal uptake into the vacuole. MTP1 and ZIF1 confer tolerance to excess zinc (Desbrosses-Fonrouge et al., 2005; Haydon and Cobbett et al., 2007), and a more recent study showed *zif1* mutants to also be hypersensitive to Fe deficiency (Haydon et al., 2012), implicating a role for ZIF1 in iron-homeostasis. In studies performed by Pertl-Obermeyer et al. (2016), MTP1 was depleted from *ap4ß-1* in at least one experiment, which, in general, might be due to degradation of a falsely localized protein.

Consistent with already published data, overexpression of *MTP1-GFP* or *ZIF1-GFP* yielded fluorescent labeling of the vacuolar membrane in WT protoplasts (Figure 25). TP localization was not found to be impaired by a loss of AP3ß, and also appeared to be entirely unaffected by mutation of *AP4ß*.

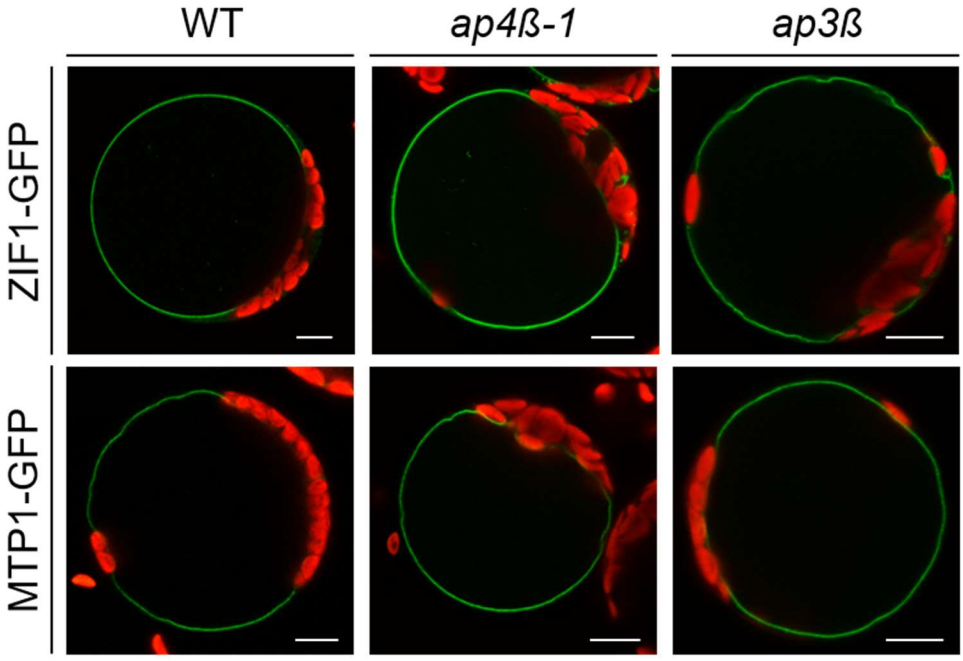

Figure 25: *C*-terminal GFP-fusions of the zinc transporters ZIF1 (top row) and MTP1 (bottom row) localize to the TP of WT (left), *ap4ß-1* (middle), and *ap3ß* (right) mesophyll protoplasts. GFP fluorescence is shown in green, chlorophyll autofluorescence in red. Scale bars represent 10 µm.

Subsequent experiments aimed at a comprehensive analysis of the subcellular sorting of NRAMP3- and NRAMP4-GFP, particularly with respect to a potential participation of AP-4. Again, trafficking was initially examined in mesophyll protoplasts transiently overexpressing a *GFP-fusion* of the possible cargo. In addition to WT and *ap4*, sorting of NRAMP3- and NRAMP4-GFP was examined in *ap3ß* mutants due to the known role of AP-3 in protein sorting to the TP (Wolfenstetter et al., 2012), which in turn is known to represent the target membrane of NRAMP3 and NRAMP4 (Thomine et al., 2003; Lanquar et al., 2005). To exclude that potential missorting was due to general tonoplastic sorting defects of the mutant, *35S$_{Pro}$:GFP-INT1* was transformed as a control. For one, sorting of the TP-localized inositol transporter has already been shown to be independent of AP-3 (Wolfenstetter et al., 2012). And secondly, Wang et al. (2014) had identified AP-1 as the adaptor responsible for the sorting of INT1 to the TP, so the absence of AP-4 seemed unlikely to additionally alter INT1 localization. Moreover, a GFP-fusion of the molybdate transporter MOT2 was included in the experiment.

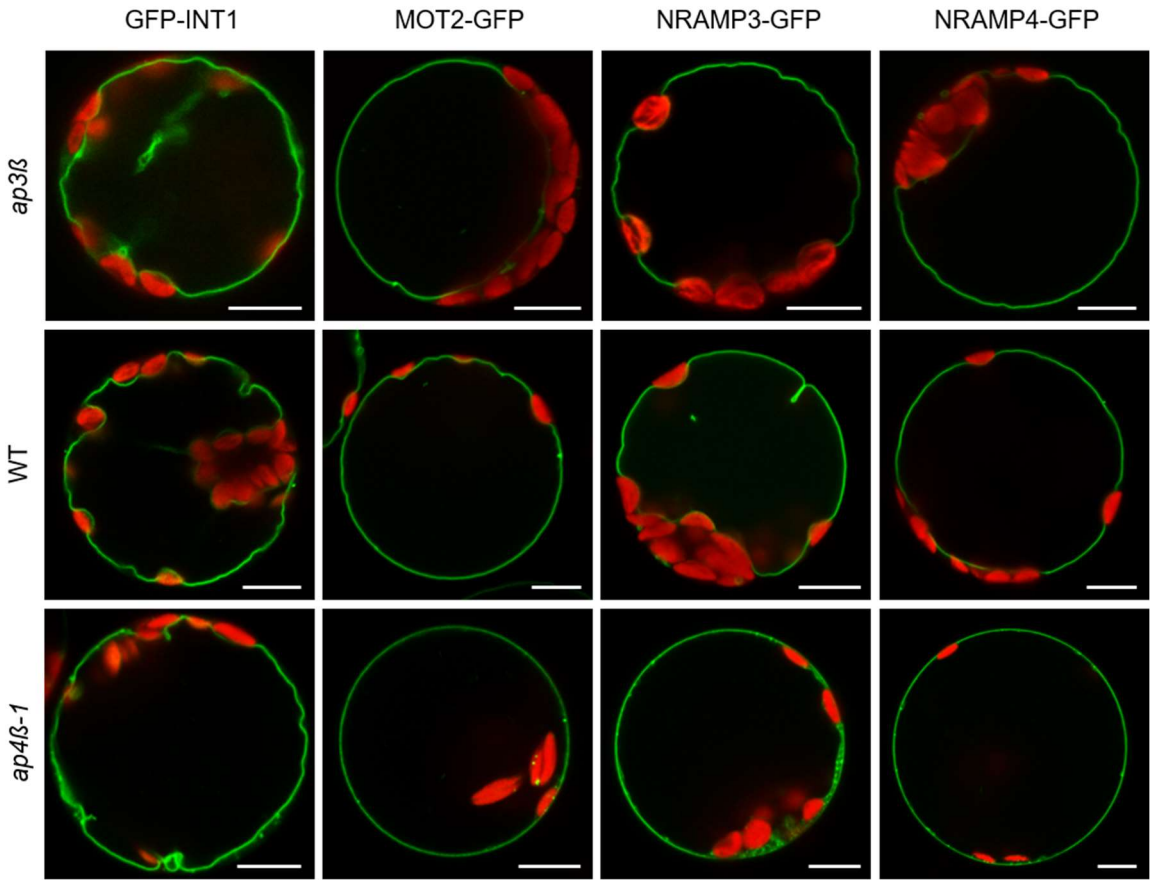

Figure 26: Subcellular localization of GFP-fusions of INT1, MOT2, NRAMP3 and NRAMP4 in mesophyll protoplasts of WT, *ap3ß*, and *ap4ß-1*.
Representative confocal single sections of *Arabidopsis ap3ß* (top), WT (middle) and *ap4ß-1* (bottom) mesophyll protoplasts expressing *GFP*-fusions of *INT1, MOT2, NRAMP3* and *NRAMP4* (from left to right), respectively. GFP fluorescence is shown in green, chlorophyll autofluorescence in red. Scale bars represent 10 µm.

In agreement with published data, GFP-INT1 (Wolfenstetter et al., 2012), MOT2-GFP (Gasber et al., 2011), NRAMP3-GFP (Thomine et al., 2003) and NRAMP4-GFP (Lanquar et al., 2005) localized to the TP in WT mesophyll protoplasts (Figure 26, middle row). A lack

of the ß-subunit of AP-3 did not interfere with TP localization of GFP-INT1 (Wolfenstetter et al., 2012), or of any other of the tested GFP-fusions (Figure 26, top row). In *ap4ß-1* protoplasts, the distribution of GFP-INT1 was not significantly affected, i.e. the GFP-fusion localized to the TP, as already implied by the findings of Wang et al. (2014). In contrast, GFP-fusions of MOT2, NRAMP3 and NRAMP4 appeared to be substantially missorted in the *ap4ß-1* mutant (Figure 26, bottom row). In these mutants, GFP fluorescence originated either solely or additionally from what appeared as an even ring surrounding the entire protoplast, indicating a partial missorting to the PM. Therefore, the *GFP*-fusions were subsequently cotransformed together with a construct encoding the PM marker INT4-RFP (Wolfenstetter et al., 2012). In agreement with the previous transformation experiments, GFP- and RFP-signals did neither colocalize in WT (Figure 27 top row of A-D, respectively), nor in *ap4ß-1* protoplasts expressing *GFP-INT1* (TP) together with *INT4-RFP* (PM) (Figure 27A, bottom row). In contrast, MOT2-GFP, NRAMP3-GFP and NRAMP4-GFP showed substantial colocalization with INT4-RFP in *ap4ß-1* in a significant fraction of transformed cells, yielding a yellow ring around the protoplast (Figure 27B, C, and D). Histograms at the very right of each panel in Figure 27, were obtained with Fiji (see section 4.1.8) and depict the intensity profiles of RFP- and GFP-signals along a shared axis perpendicular to the cell surface (each x-axis is indicated by a white arrow in the corresponding confocal image). Moreover, spatial correlation between GFP and RFP is represented by scatterplots, and the corresponding Pearson correlation coefficients (r_p) and Spearman's rank correlation (r_s), which were obtained from the respective confocal image presented, and give a more quantitative measure for the degree of colocalization (see section 4.2.5). In theory, values for each of the coefficients can range from -1.0, representing perfect exclusion, to +1.0, representing perfect correlation, for example between GFP- and RFP-signals in a biological sample.

It must be emphasized, that for combinations of INT4-RFP with MOT2-, NRAMP3-, or NRAMP4-GFP in *ap4* mutants, the analysis was restricted to cells, in which GFP-fluorescence would have been attributed to the PM (see the following paragraph). At least five images per fluorophore combination (and in each genetic background) were analyzed, and all yielded comparable results, respectively.

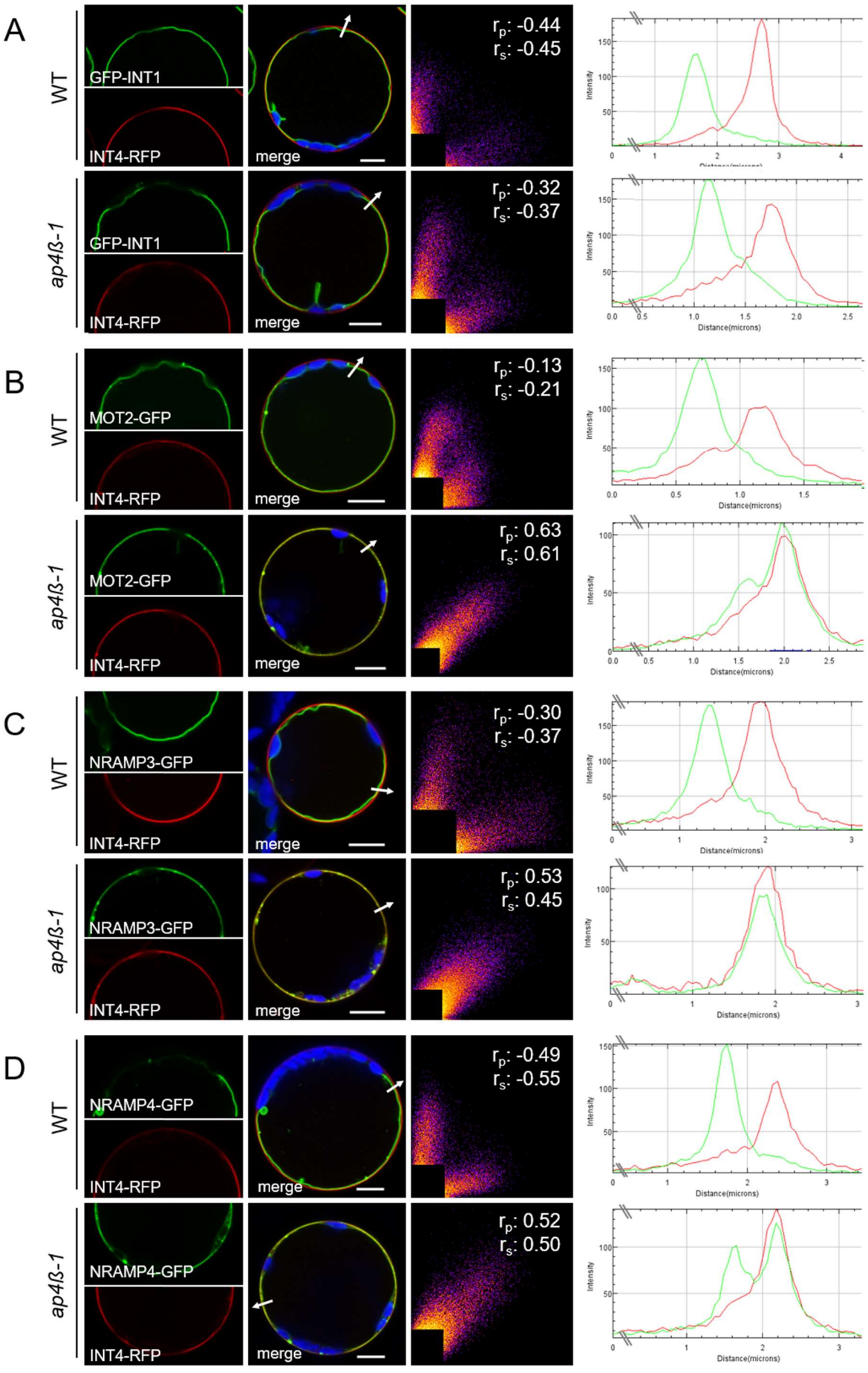
A
WT
GFP-INT1
INT4-RFP
merge
r_p: -0.44
r_s: -0.45
ap4ß-1
GFP-INT1
INT4-RFP
merge
r_p: -0.32
r_s: -0.37
B
WT
MOT2-GFP
INT4-RFP
merge
r_p: -0.13
r_s: -0.21
ap4ß-1
MOT2-GFP
INT4-RFP
merge
r_p: 0.63
r_s: 0.61
C
WT
NRAMP3-GFP
INT4-RFP
merge
r_p: -0.30
r_s: -0.37
ap4ß-1
NRAMP3-GFP
INT4-RFP
merge
r_p: 0.53
r_s: 0.45
D
WT
NRAMP4-GFP
INT4-RFP
merge
r_p: -0.49
r_s: -0.55
ap4ß-1
NRAMP4-GFP
INT4-RFP
merge
r_p: 0.52
r_s: 0.50
Intensity
Distance(microns)

Figure 27: MOT2-GFP, NRAMP3-GFP and NRAMP4-GFP are partially missorted to the PM of *ap4ß-1* mesophyll protoplasts.
GFP fluorescence is shown in green, RFP fluorescence in red. Merged images additionally show chlorophyll autofluorescence (blue) and indicate direction of fluorescence intensity measurements (white arrows). Fluorescence intensity profiles along the direction of the white arrows were obtained with ImageJ. Red lines depict RFP-intensity, green lines GFP-intensity along the same vector. Scatterplots (RFP intensity along the x-axis; GFP along the y-axis) were obtained with the Coloc2 plug-in in ImageJ. Pearson correlation coefficient (r_p) and Spearman's rank correlation (r_s) indicate the extent of colocalization (ranging from -1.0 for perfect exclusion to +1.0 for complete colocalization). Scale bars represent 10 µm.
(A) GFP-INT1 does not colocalize with the PM marker INT4-RFP, in WT (top), or in *ap4ß-1* (bottom) mesophyll protoplasts.
(B) to **(D)** In WT protoplasts MOT2-GFP [(B) top], NRAMP3-GFP [(C) top] and NRAMP4-GFP [(D) top] do not colocalize with the PM marker INT4-RFP. In *ap4ß-1* mesophyll protoplasts, the GFP-fusions of MOT2 [(B) bottom], NRAMP3 [(C) bottom] and NRAMP4 [(D) bottom] colocalize with INT4-RFP at the PM.
A revised version of this figure is published in Müdsam et al. (2018).

MOT2-GFP, NRAMP3-GFP and NRAMP4-GFP did not label exclusively the PM of mutant cells (Figure 28). Instead, within one and the same batch of transformed protoplasts, different localizations ranging from TP only, to TP with additional PM, PM only, and varying GFP fluorescence in intracellular structures or aggregates were regularly observed. As a reference, Figure 28C depicts the presence of protoplasts from each category within one transformation experiment (in this case MOT2-GFP in *ap4ß-1* protoplasts). To determine, whether those distribution patterns were characteristic and reproducible for each construct, the results were quantified by assigning each protoplast to one of the following categories (as indicated in Figure 28C): a protoplast was counted as “TP”, when localization appeared WT-like, i.e. when GFP fluorescence appeared either exclusively in the TP, or when in addition to predominant TP-fluorescence, only weak fluorescence could be observed in other intracellular compartments. Cells were counted as “PM”, whenever a clear, even ring around the entire protoplast could be detected, which includes cells with varying ratios of TP:PM labeling. And finally, GFP localization was categorized as intracellular (“IC”), when fluorescence was predominantly visible in internal structures other than the TP. Each construct was tested in *ap4µ* and *ap4µ/AP4µ$_{Pro}$:AP4µ-GUS* protoplasts in addition to WT and *ap4ß-1* (Figure 28B). While GFP-INT1 sorting in mutant protoplasts was identical to that in the WT (Figure 28A and B), quantification of MOT2-, NRAMP3- and NRAMP4-GFP locations revealed a distinct distribution pattern for each construct. NRAMP4-GFP was sorted preferentially to the PM in both *ap4* mutant lines, with less than 20% of the transformed protoplasts displaying predominant TP localization, and less than 10% in intracellular structures. In contrast, NRAMP3-GFP and MOT2-GFP sorting was generally disturbed in a smaller fraction of mutant protoplasts, but NRAMP3-GFP appeared to have a higher tendency to remain in or be missorted to intracellular structures. In each case, results were comparable between *ap4ß-1* and *ap4µ* mutants, and sorting defects were fully rescued in *ap4µ/AP4µ$_{Pro}$:AP4µ-GUS* protoplasts.

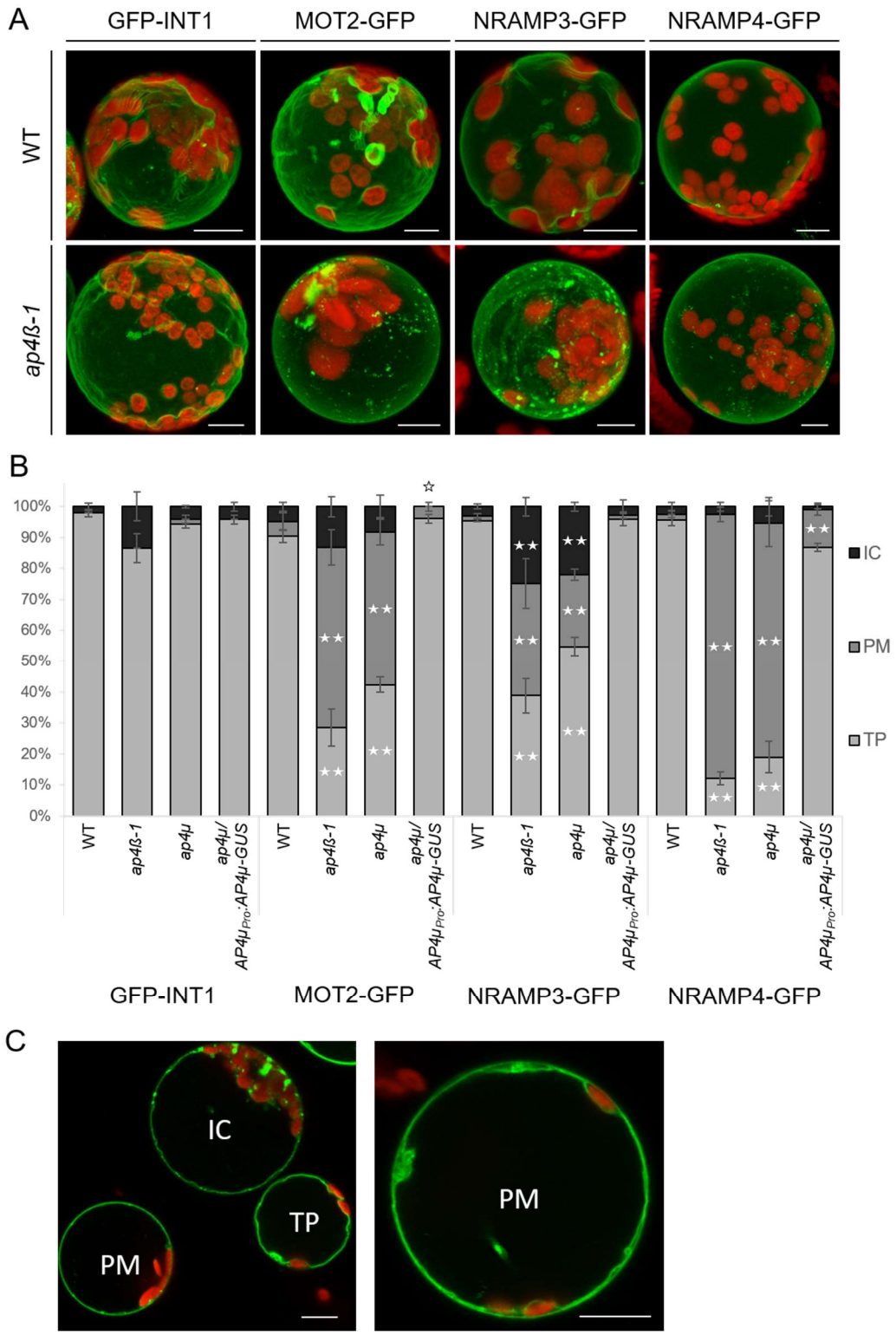

Figure 28: Differential missorting of GFP-fusions of INT1, MOT2, NRAMP3 and NRAMP4 in *ap4* mutants.
(A) Subcellular localization of GFP-fusions of INT1, MOT2, NRAMP3 and NRAMP4 in WT and *ap4ß-1* mesophyll protoplasts. Representative maximum projections *Arabidopsis* WT (upper row) and *ap4ß-1* (bottom row) mesophyll protoplasts expressing *GFP* fusions of *INT1, MOT2, NRAMP3* and *NRAMP4* (from left to right) are shown as indicated. **(B)** Distribution of GFP-INT1, MOT2-GFP, NRAMP3-GFP, and NRAMP4-GFP locations to different subcellular compartments of WT, *ap4ß-1*, *ap4µ*, or *ap4µ/AP4µ$_{Pro}$:AP4µ-GUS* in individual transformation events to the TP, PM, or intracellular compartments (IC), e.g. as represented by *ap4ß-1* protoplasts expressing *MOT2-GFP* in panel (C). Given are mean values ± SE of location counts per experiment (n ≥ 3 for each transformed construct and genotype, with ≥ 69

protoplasts counted per construct and genotype in total). Asterisks indicate significant (*, $p < 0.05$) or highly significant (**, $p < 0.01$) differences compared to the respective localization in the WT (Student's t-test).
(C) Confocal single sections of *ap4ß-1* protoplasts expressing *MOT2-GFP*, with fluorescence in different subcellular compartments. For quantification [as presented in (B)], localization was classified as "tonoplastic" (TP), whenever GFP fluorescence was limited to the vacuolar membrane, or if, in addition to the TP, internal membranes were only faintly fluorescent (represented by the indicated protoplast in the picture on the left). Whenever fluorescence was dominant in endomembrane compartments or aggregates, as represented by the protoplast on the upper half of the image, localization was counted as "intracellular" (IC). Localization was counted as "plasma membrane" (PM), whenever GFP fluorescence was clearly detectable as an even ring surrounding the cell, as represented by the protoplast on the lower left. Dual staining of TP and PM was scored as a shift to the PM, as represented by the protoplast in the picture on the right.
In (A) and (C) GFP fluorescence is shown in green, autofluorescence of chlorophyll in red. Scale bars represent 10 µm. Figure 26 and Figure 28 have been revised, adapted and modified for publication in Müdsam et al. (2018).

Altered sorting of NRAMP3-GFP and NRAMP4-GFP was also observed in *ap4µ* stably transformed with analogous constructs (*35S$_{Pro}$:NRAMP3-GFP*, or *35S$_{Pro}$:NRAMP4-GFP*). As shown in Figure 29, the GFP-fusions exclusively labeled the TP of WT and *nramp3-1 nramp4-1* leaf epidermal cells, whereas fluorescence was partially relocated to the PM in *ap4µ* in plants of the T1 generation.

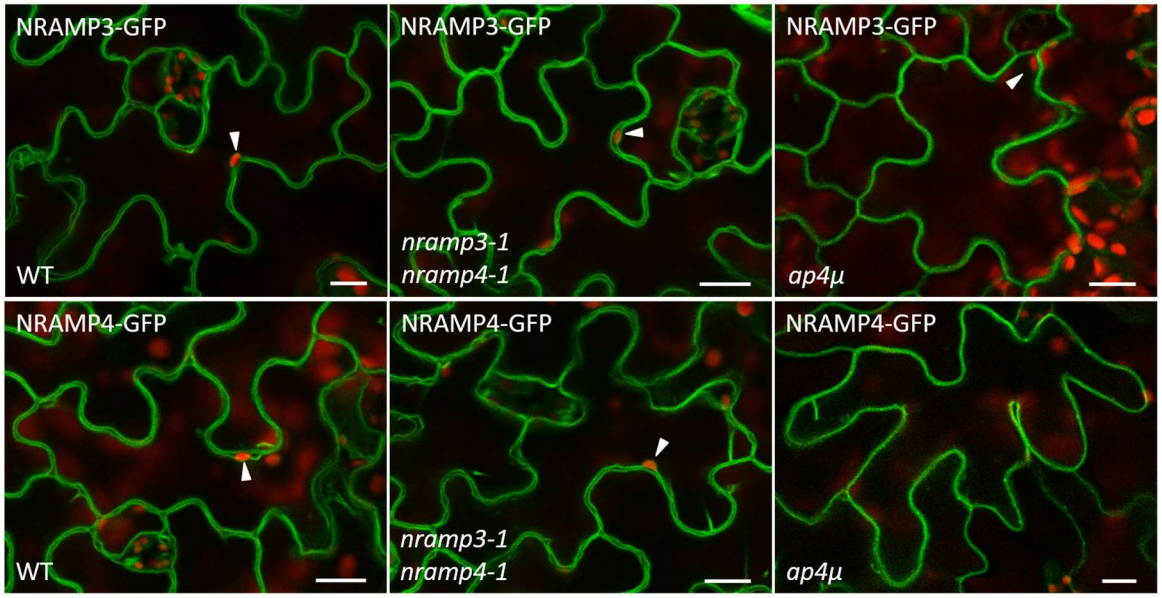

Figure 29: NRAMP3-GFP and NRAMP4-GFP in leaf epidermal cells of stably transformed WT, *nramp3-1 nramp4-1*, and *ap4µ* plants.
GFP fluorescence is shown in green, chlorophyll autofluorescence in red. White arrowheads indicate chloroplasts, excluded from the GFP-labeled TP in WT and *nramp3-1 nramp4-1* cells. Scale bars represent 10 µm. Modified from Müdsam et al. (2018).

2.4.3.3 Missorting of NRAMP3 and NRAMP4 in ap4 *mutants cannot be abolished by addition of the sorting motif of INT1*

As presented in the above sections, GFP-fusions of *Arabidopsis* NRAMP3, NRAMP4 and MOT2 were missorted in *ap4* mutants, whereas GFP-INT1 was sorted to the TP like in the WT. Wolfenstetter et al. (2012) demonstrated that the addition of the *C*-terminus of INT1 [C(INT1)], which contains the motif required for sorting of INT1 to the TP, was sufficient

to redirect non-tonoplastic proteins to the vacuolar membrane of WT cells, provided that the sorting motif of INT1 was positioned at the correct distance from the membrane. Likewise, analogous NRAMP/INT1 chimaera could possibly show WT-like TP sorting in *ap4* mutants via redirecting NRAMP trafficking to an AP-4 independent pathway mediated by the sorting information in C(INT1). Different chimaeras were therefore generated (see section 4.2.6.4), in which the CDS of *C(INT1)* was either added to the full-length *NRAMP3* or *NRAMP4* CDS (Figure 30A), or to CDS fragments corresponding to *C*-terminally truncated (ΔC) NRAMP3 or NRAMP4 (Figure 30B). As shown in Figure 30A, addition of C(INT1) to the full-length NRAMP3 or NRAMP4 sequence did not interfere with TP sorting of the GFP-fusions in WT cells, but was not able to abolish missorting in the *ap4ß-2* mutant. Truncations removed the endogenous *C*-terminus of NRAMP3 or NRAMP4 to meet the positional requirements for the sorting motif of C(INT1) in the chimeric protein. As a control, analogous truncated NRAMP-chimaera were generated, in which the endogenous NRAMP3 or NRAMP4 *C*-terminus was exchanged for the *C*-terminus of INT4 [C(INT4)]. INT4 itself localizes to the PM (Schneider et al., 2006), and it was suggested that its *C*-terminus does not to hold any information relevant to subcellular sorting (Wolfenstetter et al., 2012). Truncation of the endogenous NRAMP *C*-termini, however, resulted in ER retention of the corresponding C(INT1) and C(INT4) chimaera, already in the WT (Figure 30B and C). Accordingly, NRAMP3ΔC-C(INT1)-GFP and NRAMP4ΔC-C(INT1)-GFP were not sorted to the TP of *ap4* mutants, but also remained in the ER like in the WT (Figure 30B). This could either be due to missfolding of the resulting fusion-proteins, or alternatively indicates that the NRAMP *C*-termini might, in fact, contain sorting information required for ER-release.

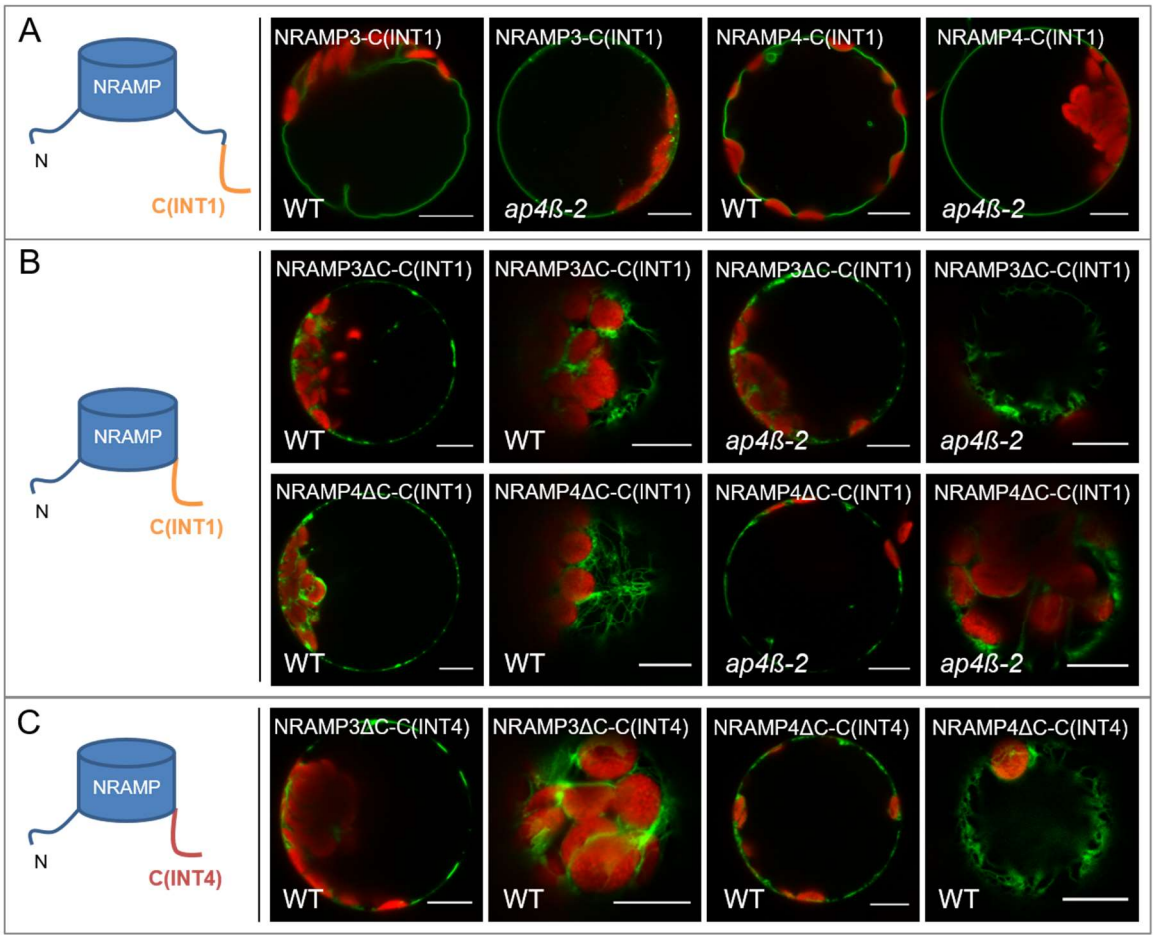

Figure 30: Subcellular localization of GFP-labeled NRAMP/INT1 and NRAMP/INT4 chimaera in WT and *ap4* mutants.
Images on the left schematically represent different chimaera. The genetic background is indicated on the lower left, chimaera and truncations of NRAMP3 and NRAMP4 are indicated on the upper left in each confocal image. ΔC indicates removal of 43 (NRAMP3) or 50 (NRAMP4) amino acids of the *C*-terminus. GFP was fused to the *C*-terminus of each chimeric or truncated protein. GFP fluorescence is shown in green, chlorophyll autofluorescence in red. Scale bars represent 10 µm.
(A) Addition of the *C*-terminus of INT1 [C(INT1)] to the *C*-terminus of NRAMP3 or NRAMP4 does not affect TP targeting of the GFP-fusions in WT, but cannot abolish missorting in *ap4* (*ap4ß-2*) mesophyll protoplasts.
(B) Exchange of endogenous *C*-termini of NRAMP3 or NRAMP4 for the *C*-terminus of INT1 yields localization of the GFP-fusions to the ER in WT and *ap4ß-2* mesophyll protoplasts. Different images of the same chimeric protein and background show optical sections through the center (left) or top (right) of a protoplast.
(C) Exchange of endogenous *C*-termini of NRAMP3 or NRAMP4 for the *C*-terminus of INT4 similarly yields localization to the ER in WT mesophyll protoplasts. Different images of the same chimaera show optical sections through the center (left) or top (right) of a protoplast.

2.4.3.4 Sorting of NRAMP3 and NRAMP4 to the tonoplast requires an N*-terminal dileucine motif*

As presented in section 2.4.3.2, correct targeting of MOT2, NRAMP3 and NRAMP4 apparently depends on the presence of a functional AP-4 complex. Next, the NRAMP-intrinsic information or sorting motifs required for the trafficking of NRAMP3 and NRAMP4 to the TP of WT cells, i.e. in the presence of AP-4, should be identified.
As shown in Figure 31A, a truncated NRAMP3ΔN-GFP, lacking 30 amino acids constituting the cytosolic *N*-terminus, did not localize to the TP in WT (or *ap4ß-2*) mutants. However,

in contrast to the *C*-terminally truncated NRAMPΔC-C(INT)-chimaera (*cf.* section 2.4.3.3, Figure 30B and C), NRAMP3ΔN-GFP was not completely retained in the ER, but also labeled dot-like structures, which suggests that the GFP-fusion reached at least the Golgi. Moreover, when GFP was fused to the *N*-terminus of NRAMP3 or NRAMP4, fluorescence was observed in the PM in addition to the TP (Figure 31B), even in the WT. Partial missorting in the presence of an *N*-terminal GFP has also been observed in TP localized members of the PTR-family (Komarova et al., 2012). This might indicate the presence of an *N*-terminal sorting motif, which is masked by the *N*-terminal fluorophore and is therefore not appropriately accessible to the recognizing adaptor.

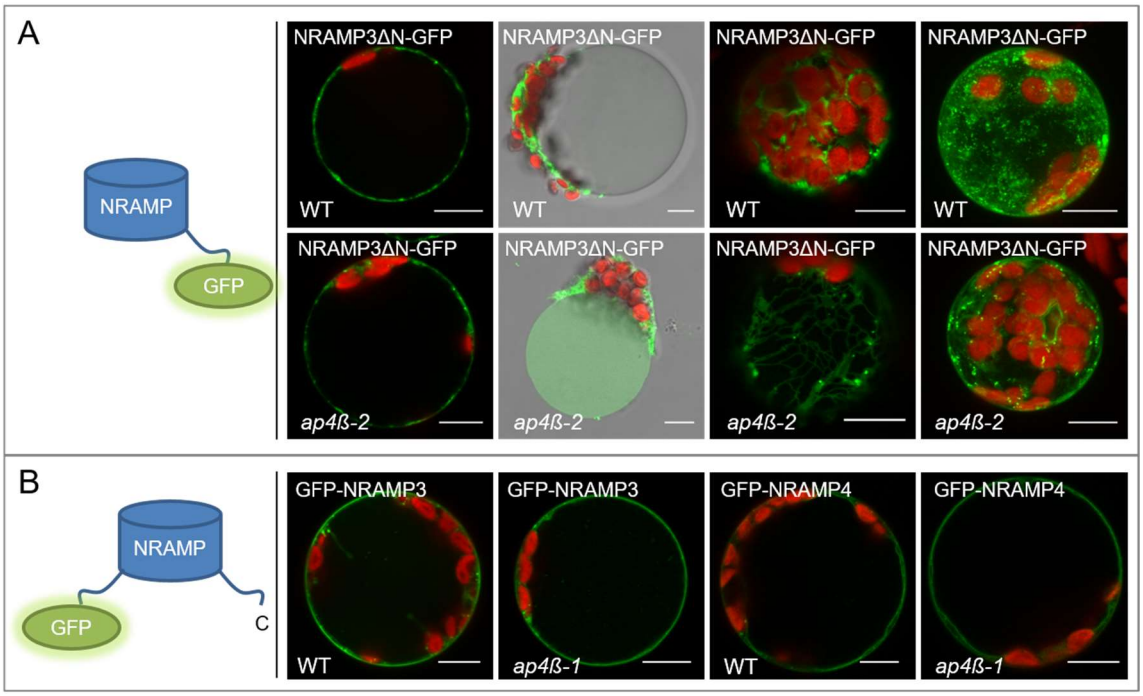

Figure 31: Trafficking of NRAMP3 (and NRAMP4) to the TP requires *N*-terminal sorting information.
Images on the left schematically represent GFP-fusions. GFP fluorescence is shown in green, chlorophyll autofluorescence in red. Scale bars represent 10 µm.
(A) Removal of the *N*-terminus of NRAMP3 (NRAMP3ΔN) results in subcellular sorting to network-like and punctate structures in WT (top row) and *ap4ß-2* (lower row). From left to right, individual images for each genetic background show: optical single sections through the center of an intact protoplast, of a lysed protoplast (overlay with bright-field image), or through the top of an intact protoplast, and a maximum projection of an intact protoplast, respectively.
(B) GFP-NRAMP3 and GFP-NRAMP4 are partially missorted in WT and *ap4ß-1* mesophyll protoplasts.

Dileucine motifs are usually described by a [D/E]XXXL[L/I] consensus sequence. Komarova et al. (2012) had recently suggested to extend the definition to [D/E]X_{3-5}L[L/I] and therefore implied the presence of one (ENNEPLLI in NRAMP3), or two (DRERPLL and EETEKVLI in NRAMP4) dileucine motifs in the cytosolic *N*-termini of NRAMP3 and NRAMP4 to be possibly relevant for the targeting of these proteins to the TP (Komarova et al., 2012; Supplemental Table 2). However, the function of these putative motifs was not experimentally confirmed. Both, MOT2 as well as INT1, are known to be sorted via dileucine-based motifs, i.e. ETTTTP**LL** in MOT2 (Gasber et al., 2011) and NMEG**LLE** in INT1 (Wolfenstetter et al., 2012) (amino acids constituent to the dileucine motif are underlined; amino acids which, in the respective publication, have been exchanged for alanines to

abolish TP sorting are highlighted in bold). But whereas MOT2, having an *N*-terminal dileucine motif, showed partial missorting in the absence of AP-4, INT1, with the sorting signal included in the *C*-terminus, did not. Moreover, a rice homolog (OsNRAMP5) with an DADDQLL peptide within the *N*-terminus conforming to the [D/E]$X_{3–5}$L[L/I] consensus, was found to localize to the PM (Ishimaru et al., 2012; Sasaki et al., 2012).

To investigate whether the putative motifs in the *N*-termini of NRAMP3 and NRAMP4 are necessary for their sorting to the TP, GFP-fusions of both proteins were generated, in which the leucine residues of individual putative [D/E]$X_{3–5}$L[L/I]-type motifs were exchanged for alanines, analogously to experiments performed by Gasber et al. (2011) and Wolfenstetter et al. (2012). An alignment of the *N*-terminal sequences of NRAMP3 and NRAMP4 is shown in Figure 32A, and Figure 33A, and introduced mutations are indicated. In case of NRAMP3, both, ENNEPLL, as well as ENNEPLLI correspond to the [D/E]$X_{3–5}$L[L/I] consensus sequence. Hence, both leucines as well as the isoleucine were replaced by alanine (LLI→AAA) (Figure 32A). Similarly, exchange of both leucines of the first, i.e. more *N*-terminal DRERPLL of NRAMP4 (LL→AA) results in an alanine-triplet. Accordingly, EETEKV**LIV** (NRAMP4) was replaced by EETEKV**AAA** (LIV→AAA) (Figure 33A). The equivalent DETEKVHIV in NRAMP3, which does not fit the dileucine consensus sequence, was further exchanged for DETEKVAAA (HIV→AAA) to serve as a negative control.

As expected, the resulting NRAMP3$_{HIV→AAA}$-GFP (like NRAMP3-GFP) clearly labeled the TP in transiently transformed WT mesophyll protoplasts, implying that introduction of an *N*-terminal alanine triplet does not *per se* influence sorting, for example due to misfolding of the protein (Figure 32B). The corresponding NRAMP4$_{LIV→AAA}$-GFP accumulated, in addition to the TP, to a large extend in the ER, as represented by net-like structures in an optical section taken from the top of a protoplast, or by the patchy and uneven GFP fluorescence in an optical section of the center of a protoplast (Figure 33B i., ii.). Yet, the fact that sorting to the TP is at least partially retained in this mutant was clearly evident when the PM was removed by osmotic lysis, leaving a GFP-labeled vacuolar membrane (Figure 33B iii., iv.).

In contrast to the unaffected targeting of NRAMP3$_{HIV→AAA}$-GFP, mutation of the LLI peptide in the putative dileucine motif of NRAMP3 (NRAMP3$_{LLI→AAA}$) drastically altered the distribution of the GFP-fusion (Figure 32C). Although protoplasts with minimal residual labeling of the TP were occasionally observed, the majority of transformed cells did not show any detectable GFP fluorescence in the vacuolar membrane, even upon osmotic lysis (Figure 32C iii., iv.). Instead, GFP fluorescence was primarily detected in the PM, as characterized by an evenly fluorescent ring around intact protoplasts. PM localization of NRAMP3$_{LLI→AAA}$-GFP was further confirmed by coexpression of the PM-marker *INT4-RFP* (Figure 32D and E), which resulted in spatially correlating GFP and RFP signals.

To determine which particular residues of the LLI triplet in NRAMP3 are critical for TP localization, alanine-scanning mutagenesis was performed, exchanging individual amino acids of the LLI peptide for alanine (Figure 32F, G and H). In WT mesophyll protoplasts, NRAMP3$_{(L10A)}$-GFP (Figure 32G), as well as NRAMP3$_{(L11A)}$-GFP (Figure 32H) essentially behaved comparable to NRAMP3$_{LLI→AAA}$-GFP, i.e. both GFP-fusions mainly localized to the

PM (residual labeling of the TP was again only observed occasionally). Additional fluorescence was sometimes observed in punctate structures within transformed cells. In contrast, alanine-exchange of the isoleucine at position 12 (NRAMP3$_{I12A}$-GFP) did not affect targeting to the TP (Figure 32F). In summary, TP localization of NRAMP3 is thus dependent on an *N*-terminal dileucine motif comprising the leucine residues at position 10 and 11, but not the isoleucine at position 12.

Alanine-substitution of the equivalent dileucine motif in NRAMP4 (NRAMP4$_{LL\rightarrow AA}$) completely abolished TP sorting, with no residual GFP fluorescence detectable in the vacuolar membrane (Figure 33C). This substitution led to sorting of the resulting GFP-fusion to the PM, as confirmed by colocalization with INT4-RFP (Figure 33D and E).

In line with these results, coexpression of *NRAMP4$_{LL\rightarrow AA}$-GFP* and native *NRAMP4-RFP*, resulted in separate GFP (PM) and RFP (TP) signals in WT protoplasts (Figure 34A and B), whereas GFP and RFP fluorescence colocalized at the PM of *ap4* mutant protoplasts transfected with the same constructs (Figure 34C and D).

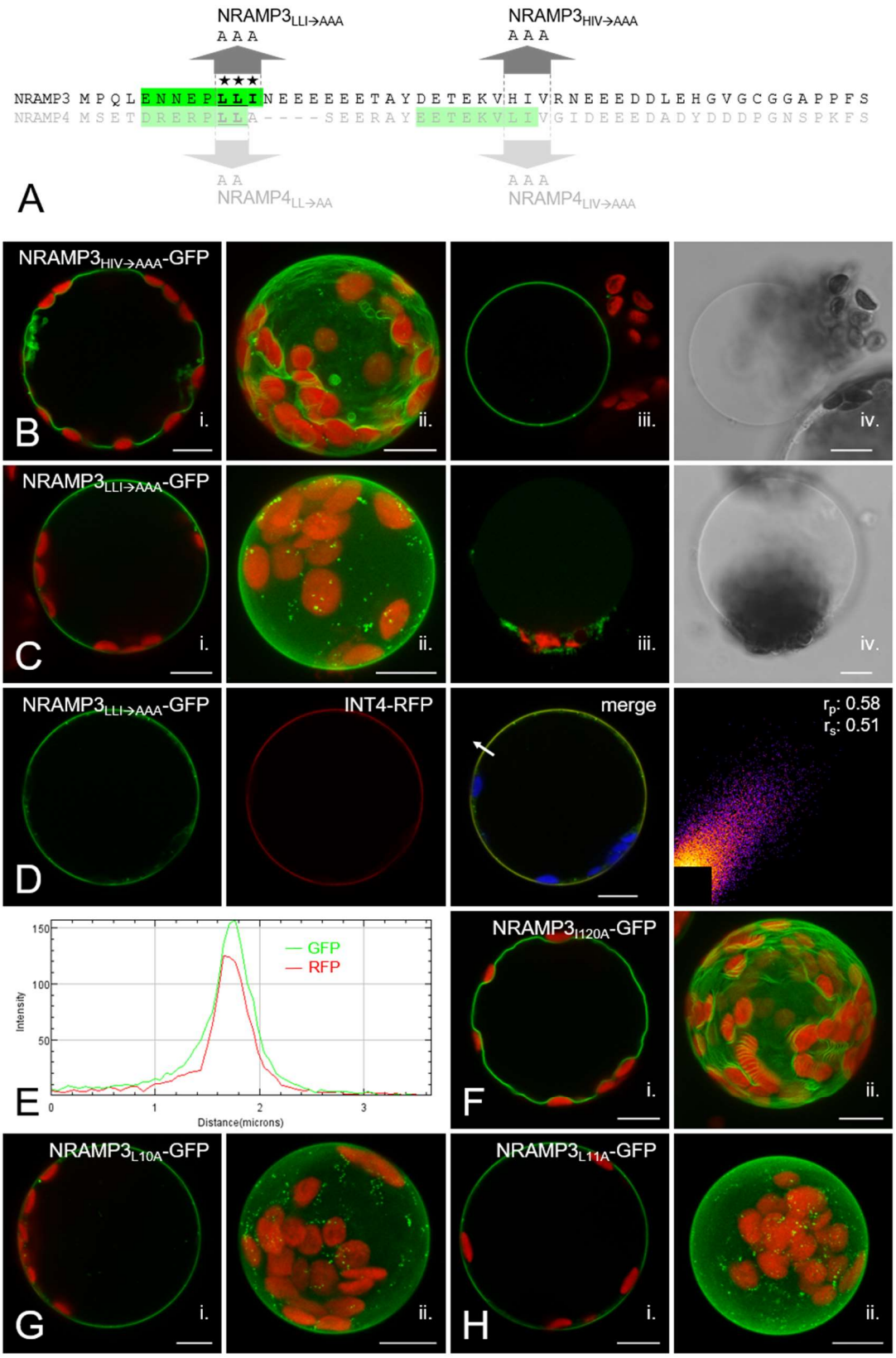

Figure 32: An *N*-terminal dileucine motif directs NRAMP3 to the TP.
(A) Sequence alignment of the *N*-termini of NRAMP3 and NRAMP4 from *Arabidopsis thaliana*. Potential dileucine motifs are highlighted in green; alanine-mutations are indicated. Amino acids in NRAMP3 marked by asterisks were additionally subjected to single alanine exchange. (The subcellular localization of the indicated NRAMP4-mutants is shown in Figure 33.)

(B) to (D) and (F) to (G) Confocal images of GFP-fusions of *N*-terminally mutated NRAMP3 in WT mesophyll protoplasts. GFP fluorescence is shown in green, chlorophyll autofluorescence in red [(B), (C) and (F)-(G)] or blue (D). Scale bars represent 10 µm. Additional labels denote confocal single sections (i.), and maximum projections (ii.) of intact protoplasts, and confocal single sections through lysed protoplasts (iii.) together with the corresponding bright-field images (iv.).

(B) Exchange of HIV (histidine-isoleucine-valine) for AAA (alanine-triplet) in the *N*-terminus of NRAMP3 does not abolish GFP-labeling of the TP.

(C) Alanine substitution of LLI (leucine-leucine-isoleucine) in the *N*-terminus of NRAMP3 diminishes TP localization of the GFP-fusion and leads to localization at the PM.

(D) $NRAMP3_{LLI\rightarrow AAA}$-GFP colocalizes with INT4-RFP at the PM. RFP fluorescence is shown in red. The merged image additionally shows chlorophyll autofluorescence (blue) and indicates direction of fluorescence intensity measurement (white arrow) shown in (E). The corresponding scatterplot (RFP intensity along the x-axis; GFP along the y-axis) was obtained with the Coloc2 plug-in in ImageJ. Pearson correlation coefficient (r_p) and Spearman's rank correlation (r_s) indicate the extent of colocalization (ranging from -1.0 for perfect exclusion to +1.0 for complete colocalization).

(E) Fluorescence intensity profiles along the direction of the white arrow shown in (D) as obtained with ImageJ. Red line depicts RFP-intensity, green line GFP-intensity along the same vector.

(F) to **(H)** Exchange of single leucine residues for alanine (L10A and L11A), but not of isoleucine (I12A) in the *N*-terminus of NRAMP3 interferes with TP localization.

(F) Mutation of isoleucine (12^{th} amino acid from the *N*-terminus) to alanine (I12A) does not interfere with sorting of the $NRAMP3_{I12A}$-GFP fusion to the TP.

(G) $NRAMP3_{L10A}$-GFP (alanine substitution of leucine at position ten of the NRAMP3 amino acid sequence) labels the PM.

(H) $NRAMP3_{L11A}$-GFP (alanine substitution of leucine at position eleven of the NRAMP3 amino acid sequence) labels the PM.

This figure was published in Müdsam et al. (2018).

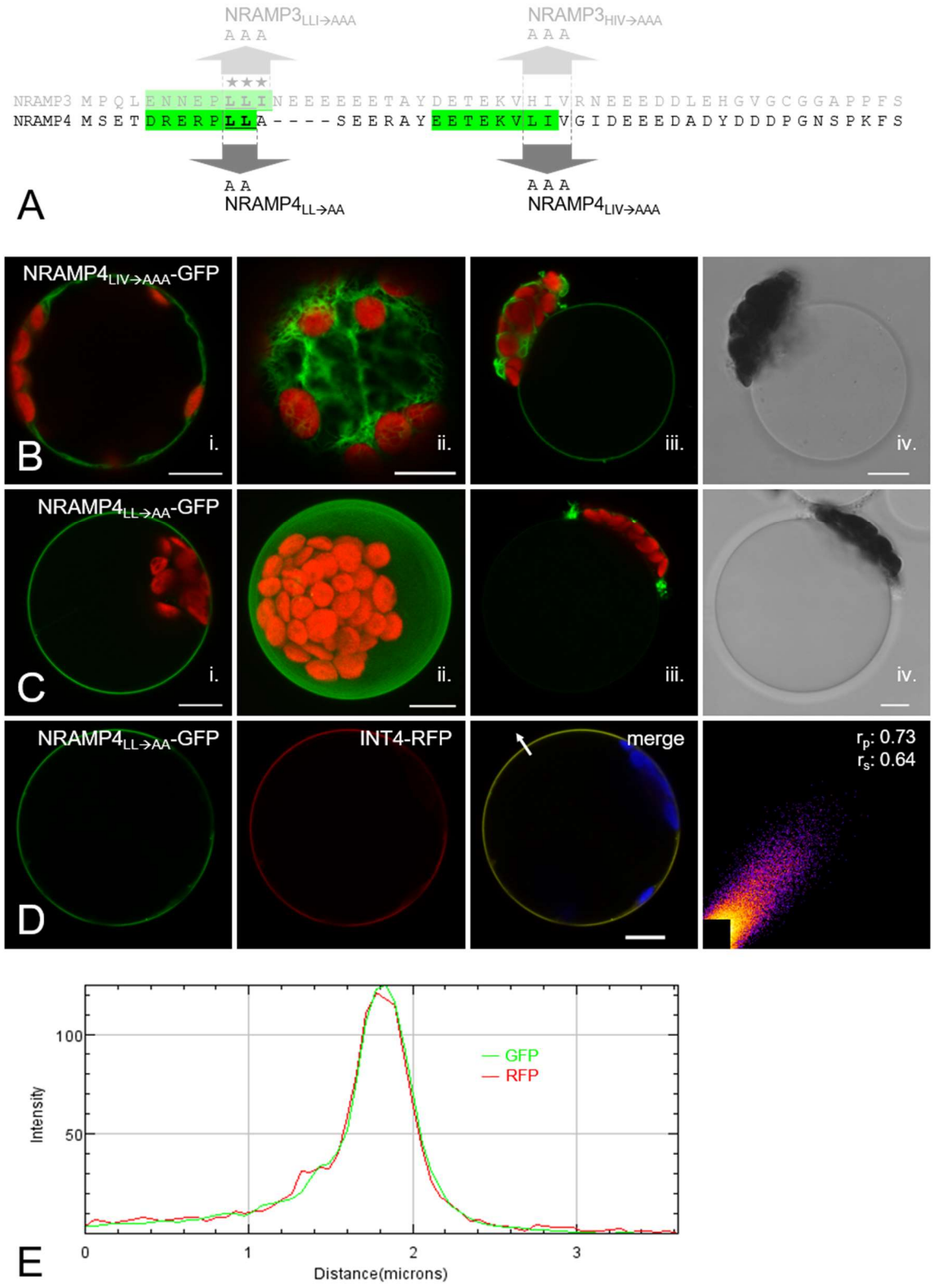

Figure 33: An *N*-terminal dileucine motif directs NRAMP4 to the TP.
(A) Sequence alignment of the *N*-termini of NRAMP3 and NRAMP4 from *Arabidopsis thaliana*. Potential dileucine motifs are highlighted in green; alanine-mutations are indicated. (Subcellular localization of NRAMP3-mutants is shown **Figure 32**.)
(B) to **(D)** Confocal images of GFP-fusions of *N*-terminally mutated NRAMP4. GFP fluorescence is shown in green, chlorophyll autofluorescence in red [(B) and (C)] or blue (D). Scale bars represent 10 µm.

(B) Mutation of the LIV-peptide (leucine-isoleucine-valine) in the *N*-terminus of NRAMP4 to AAA (alanine-triplet) does not abolish TP-sorting of the resulting NRAMP4$_{LL\rightarrow AA}$-GFP. An optical section through the centre (i.) or the top (ii.) of an intact protoplast, and a confocal single section through a lysed protoplast (iii.) and the corresponding bright-field image (iv.) are shown. Net-like structures (ii.) imply partial localization of the GFP-fusion to the ER. GFP-labeling of the TP is clearly detectable after osmotic lysis of the PM (iii. and iv.).
(C) Mutation of the more *N*-terminal potential dileucine motif of NRAMP4 abrogates TP localization of the GFP-fusion. An optical section (i.) and a maximum projection (ii.) of an intact protoplast show even GFP-labeling of the PM. After osmotic lysis of the PM (iii. and iv.) no residual GFP fluorescence is visible in the TP.
(D) NRAMP4$_{LL\rightarrow AA}$-GFP colocalizes with INT4-RFP at the PM. RFP fluorescence is shown in red. The merged image additionally shows chlorophyll autofluorescence (blue) and indicates direction of fluorescence intensity measurement (white arrow) shown in (E). The corresponding scatterplot (RFP intensity along the x-axis; GFP along the y-axis) was obtained with the Coloc2 plug-in in ImageJ. Pearson correlation coefficient (r_p) and Spearman's rank correlation (r_s) indicate the extent of colocalization (ranging from -1.0 for perfect exclusion to +1.0 for complete colocalization).
(E) Fluorescence intensity profiles along the direction of the white arrow shown in (D) as obtained with ImageJ. Red line depicts RFP-intensity, green line GFP-intensity along the same vector.
This figure was published in Müdsam et al. (2018).

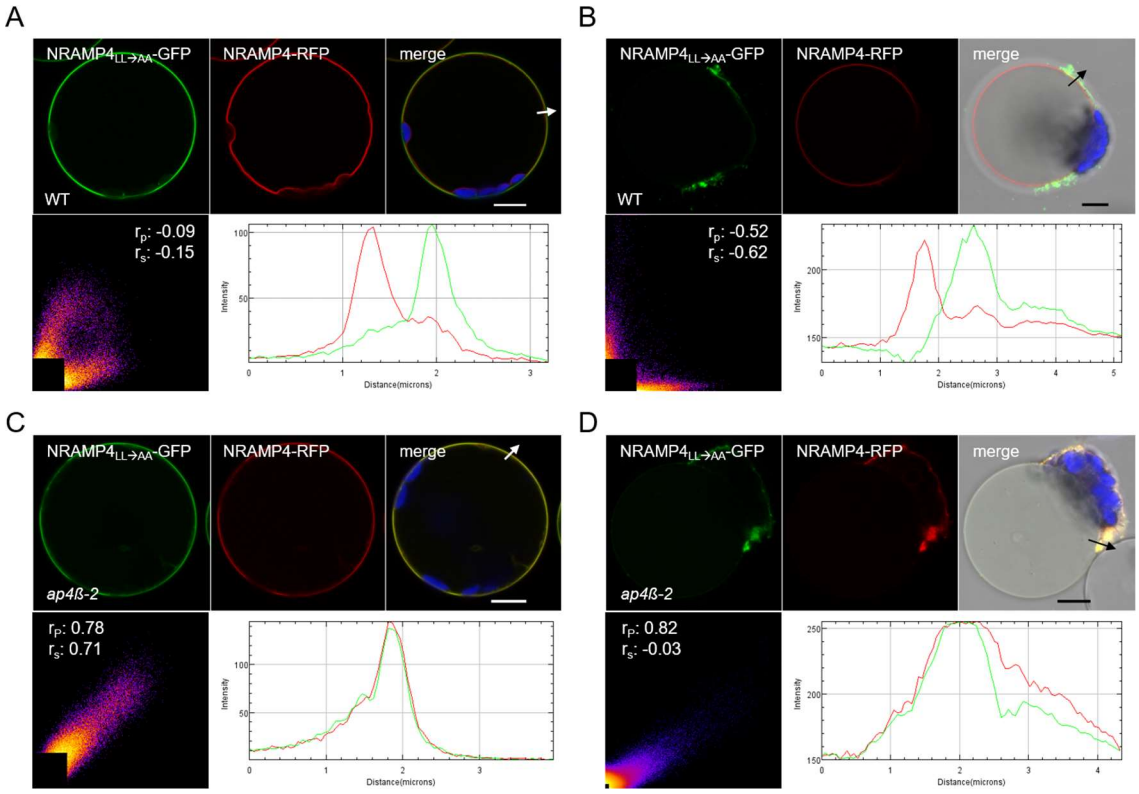

Figure 34: NRAMP4-RFP colocalizes with the NRAMP4$_{LL\rightarrow AA}$-GFP mutant at the PM of *ap4ß-2* mesophyll protoplasts.
Top row of each panel shows GFP fluorescence of NRAMP4$_{LL\rightarrow AA}$-GFP in green (left), RFP fluorescence of NRAMP4-RFP in red (middle), and a merge of GFP and RFP with chlorophyll autofluorescence in blue (right). The merged image in (B) and (D) additionally shows the corresponding bright-field image. Scale bars represent 10 µm. Bottom row of each panel shows corresponding scatterplots (RFP intensity along the x-axis; GFP along the y-axis) as obtained with the Coloc2 plug-in in ImageJ (left). Pearson correlation coefficient (r_p) and Spearman's rank correlation (r_s) indicate the extent of colocalization (ranging from -1.0 for perfect exclusion to +1.0 for complete colocalization). Fluorescence intensity profiles (right) along the direction of the white or black arrow (indicated in top row) as obtained with ImageJ. Red line depicts RFP-intensity, green line GFP-intensity along the same vector.
(A) and (B) NRAMP4$_{LL\rightarrow AA}$-GFP does not colocalize with native NRAMP4 fused to RFP in WT mesophyll protoplasts. An intact protoplast is shown in (A), a lysed protoplast is shown in (B).
(C) and (D) In *ap4ß-2* mutant protoplasts, co-transformation of the same constructs leads to colocalization of the resulting proteins at the PM. This figure was published in Müdsam et al. (2018).

2.4.3.5 Mutation of AP4ß affects sorting of PTR2- and PTR6-GFP to the tonoplast

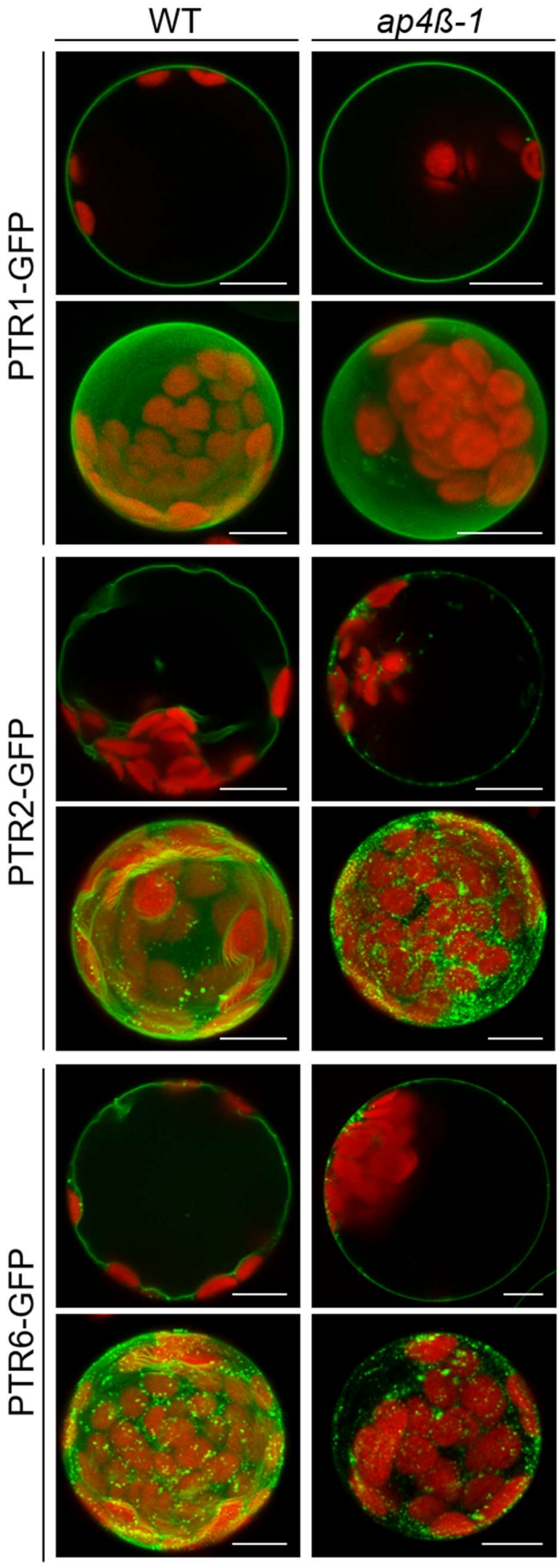

As already mentioned, dileucine-based motifs have also been shown to be required for sorting of several vacuolar transmembrane proteins in *Arabidopsis*, for example the iron transporter VIT1 (Wang et al., 2014), and the TP localized members of the peptide transporter (PTR) family in *Arabidopsis* (Komarova et al., 2012). As demonstrated above, the loss of AP4-adaptins interfered with sorting of GFP-fusions of NRAMP3, NRAMP4 and MOT2, but not INT1, although all four require dileucine based motifs for tonoplast targeting. This raised the question whether AP-4 might preferentially affect trafficking of proteins with a specific subtype of dileucine motif, and whether AP-4 shares at least some specificity towards particular sorting motifs with other AP complexes.

The paralogous vacuolar PTRs all require dileucine motifs to reach the TP (Komarova et al., 2012), while being otherwise highly conserved. Potentially altered subcellular sorting in *ap4* mutants would therefore not only corroborate the assertion that AP-4 contributes to dileucine motif dependent TP targeting, at all, but was also expected to reveal insights in specificities of AP-4 towards distinct dileucine motifs.

Figure 35: Subcellular localization of GFP-labeled members of the PTR-family in WT and *ap4ß-1* mesophyll protoplasts.
Localization of PTR1-GFP to the PM is not altered in *ap4ß-1* compared to WT. *C*-terminal GFP-fusions of PTR2 and PTR6 localize predominantly to the of TP of WT (left column), but label mostly intracellular, dot-like structures in *ap4ß-1* mesophyll protoplasts. GFP fluorescence is shown in green, chlorophyll autofluorescence in red. Scale bars represent 10 µm.

As shown in Figure 35, a GFP-fusion of the PM-localized PTR1 was still sorted correctly in *ap4ß-1*. Even more importantly, PTR2-GFP, which localized mostly to the TP in WT cells, was found to predominantly label intracellular, dot-like structures in *ap4ß-1*. Compared to the analogous PTR2-GFP, the GFP-fusion of PTR6 tended to label intracellular structures already in the WT, but again TP localization of PTR6-GFP appeared to be even less dominant in *ap4ß-1*. Although this preliminary data suggests that AP-4 also contributes to sorting of TP-localized PTRs, a more quantitative evaluation of the extent of rerouting of each PTR-GFP fusion (including PTR4, which was not examined in this study) is required to precisely derive preferences of AP-4 towards a specific PTR, or the corresponding dileucine motif for that matter.

3 Discussion

Although principal mechanisms and machineries of protein trafficking are to some extent conserved throughout all eukaryotic organisms, plants have acquired some modifications to adapt to their specific requirements (reviewed by Jürgens, 2004; Foresti and Denecke, 2008; Robinson et al., 2008). AP complexes have been identified decades ago (Robinson, 2015), but some of the functions, pathways and interactions involved in AP-mediated protein trafficking are still unknown. Particularly in plants, sorting mechanisms are just beginning to be illuminated. A comprehensive investigation of the AP-4 complex from *Arabidopsis*, particularly with respect to its role in subcellular sorting of TM-proteins, aimed to contribute to the rapidly increasing understanding of protein sorting mechanisms in plants.

3.1 *Ap4* mutants show a highly pleiotropic phenotype

Compared to subunits of AP-1, AP-2 and AP-3, adaptins of AP-4 (and AP-5) show a very low abundance in mammalian cells (Hirst et al., 2013). And although the loss of AP-4 causes severe phenotypes especially in humans, defects appear to be mostly restricted to the brain. In contrast, the expression profile of *Arabidopsis AP4μ* resembles those of *AP1μ2* and *AP2μ* in different tissues (Park et al., 2013; Supplemental Figure 3), and thus appears to be comparatively high. This is well in agreement with the severity and multitude of morphological abnormalities of *ap4* mutants that were revealed in this study, including the reduction of root growth, abnormal trichome branching, and defects in pollen tube growth and shoot development. And in turn, the phenotypes associated with the loss of *AP4ß* and/or *AP4μ* were mostly consistent with the expression of *AP4μ* (section 2.2), which was for example detectable in roots, developing trichomes and pollen grains. However, the reduction of root length was found to correlate with defects in cell elongation (section 2.3.1), which appeared to contradict the strong expression of *AP4μ* in the meristematic zone and the rather low abundance in differentiated cells. On the other hand, AP4μ was still detectable in the transition zone where it might be required for sorting of (newly synthesized) proteins which then mediate or contribute to cell elongation later in development. If such a protein failed to be sorted correctly due to the lack of AP-4, this might cause a disruption of cell elongation and thus a delayed manifestation of an *ap4* mutant phenotype.
Overall, the pleiotropic phenotype of *ap4* mutants reflect the significance of AP-4 for plant development. In addition, individual abnormalities of the mutants also allow to derive novel hypothesis regarding the function of AP-4 and possible interactions with other cellular components. These aspects will be discussed in the following paragraphs.

3.1.1 AP-4 acts as an obligatory complex

Isoforms of *AP1*-adaptins are encoded on more than a single locus in the genome of *Arabidopsis*. Disruption of a single *AP1ß*-isoform, i.e. either *AP1/2A* or *AP1/2B* causes no obvious effects in *Arabidopsis* (Boehm and Bonifacino, 2001; Dietel, 2012), whereas

mutation of *AP1μ2* (the more highly expressed isoform of *AP1μ*) interferes severely with plant growth (Johnson et al., 2004; Park et al., 2013; Teh et al., 2013; Wang et al., 2013). Null-mutation of any *AP1*-adaptin, on the other hand, is usually embryonic lethal to multicellular organisms (Boehm and Bonifacino, 2001; Robinson, 2004). In contrast to the lethality of complete *AP1-adaptin* mutations, the loss of a subunit of AP-3 usually causes rather mild defects, which mostly affect lysosomes, lysosome-related-organelles or vacuoles, which in metazoans is often manifested in some type of abnormal pigmentation (reviewed in Dell'Angelica, 2009). And despite being involved in vacuolar biogenesis, mutations in AP-3 adaptins also do not cause any detrimental morphological defects in *Arabidopsis* (Niihama et al., 2009; Feraru et al., 2010; Zwiewka et al., 2011; Müdsam, 2012). Regarding subcellular protein sorting, most known cargos of AP-3 behave identically, irrespective of which AP-3 adaptin is disrupted. For example, enhanced vacuolar accumulation of PM proteins was found to be identical in single mutants of either *ap3ß* (*pat2*), *ap3δ* (*pat4*), or of mutants overexpressing a dominant negative variant of *AP3μ* (Feraru et al., 2010; Zwiewka et al., 2011). Further, T-DNA insertions in *AP3ß*, *AP3δ*, or *AP3μ* were all found to suppress a gravitropic defect of the *zigzag* mutant (Niihama et al., 2009), which is a loss-of-function mutant of the gene encoding Qb-SNARE VTI11. On the other hand, Xiang and Van Den Ende (2013) found that vacuolar sorting of a fluorescently labeled *N*-terminal fragment of vacuolar invertase 2 was disturbed in *ap3ß*, but not in *ap3μ* T-DNA insertional mutants, suggesting that AP-3 might retain at least some functionality in the absence of the medium subunit.

As demonstrated in section 2.3, mutations affecting the *ß*- or *μ*-adaptin of AP-4 of *Arabidopsis* result in pleiotropic effects, such as reduced growth of roots, etiolated hypocotyls and pollen tubes, as well as supernumerary trichome branching, partial loss of apical dominance, altered sugar contents, and chlorosis. These developmental abnormalities, in addition to the missorting of specific tonoplastic proteins, were identical in *ap4ß* and *ap4μ*. Moreover, double mutants lacking both adaptins did not show any additive defects. First, this confirms that the T-DNA lines represent complete loss-of-function mutants. Secondly, in line with recently published data (Fuji et al., 2016), it indicates that both subunits are indeed part of one and the same complex. Thirdly, in contrast to, for example, AP1μ or AP1γ (Boehm and Bonifacino, 2001; Bassham et al., 2008), AP4ß and AP4μ appear not to be encoded on additional loci, respectively. And finally, it suggests that, as opposed to AP-3, the entire AP-4 complex is not functional if either the ß- or the μ-subunit is missing. At this point it can be argued that the experiments presented in this study might have merely failed to detect a cargo which is affected differentially by mutations in *AP4ß* or *AP4μ*. However, Pertl-Obermeyer et al. (2016) found that at least *ap4ß-1* mutants were depleted for AP4μ and AP4σ, as well. Intriguingly, the identical growth-defects of *Arabidopsis ap4ß* and *ap4μ* are in line with results obtained for mammalian AP-4. In humans, disruptions in AP-4 are linked to a subtype of hereditary spastic paraplegias, irrespective of which subunit is affected by the mutation (reviewed in Kumar et al., 2015). And in addition, patients with mutations in either *AP4ß*, *AP4μ* or *AP4ε,* show decreased protein levels of both, AP4ß and AP4ε (Verkerk et al., 2009; Abou Jamra et al., 2011; Moreno-De-Luca et al., 2011; Najmabadi et al., 2011; Bauer et

al., 2012). Unless protein levels of AP-4 adaptins are regulated differently compared to the human homologs, the absence of a single subunit of AP-4 in *Arabidopsis*, in fact, leads to degradation of the remaining subunits. In turn, this rules out the possibility that the complex retains any function, even in mutants in which only a single subunit is genetically disrupted.

3.1.2 Equivalent mutant phenotypes suggest connections between AP-4 and AP-1 pathways

It was recently demonstrated that a sudden decrease of AP-1 vesicles via a knock-sideways approach upregulates AP-4 vesicle formation in HeLa cells, which suggested a connection between AP-1 and AP-4 transport pathways in mammalian cells (Robinson et al., 2010; Hirst et al., 2012). *Arabidopsis* mutants, lacking the more highly expressed isoform of *AP1μ* have been examined in several recent studies. Although trichome branching seems to be opposingly affected by a depletion of AP-4 or AP-1 (*cf.* supernumerary trichome branching of *ap4* mutants presented in section 2.3.2 vs. reduced trichome branching in *ap1μ* mutants presented in Teh et al., 2013; Wang et al., 2013), other developmental defects observed in the *ap4* mutant lines resemble those described for *ap1m2 (ap1m2-1* and *hap13-1)* mutants. For example, as shown in sections 2.3.1 and 2.3.3, depletion of AP-4 results in root-growth-retardation and fertilization defects, which similarly has been shown for *Arabidopsis ap1m2* mutants (Johnson et al., 2004; Park et al., 2013; Wang et al., 2013). It is unlikely that single AP1-adaptins can substitute for the corresponding AP4-subunit in AP-4, or *vice versa*. If this was the case, differences would have been observed between *ap4μ* and *ap4ß*, or between single ko plants and the double mutant. Instead, the fact that growth abnormalities of *ap4* and *ap1μ* show a quite large degree of overlap, indicates that both complexes affect the same pathways, maybe by conditional recognition of overlapping sets of at least some cargo proteins. Contributing to this hypothesis, AP-1 and AP-4 have both been shown to localize to the TGN/EE in *Arabidopsis* (Park et al., 2013; Teh et al., 2013; Wang et al., 2013; Fuji et al., 2016), although they seem to reside in different subdomains and only partially colocalize with one another (Fuji et al., 2016). Moreover, both have been shown to interact with and participate in trafficking of VSRs (Gershlick et al., 2014b; Fuji et al., 2016). TP-directed sorting of dileucine motif containing multipass transmembrane proteins was so far only demonstrated to be affected by AP-1 depletion (Wang et al., 2014), but the results presented in this work clearly showed that trafficking of some of these proteins is similarly impaired by mutations in *AP4*-adaptins (the significance of the dileucine motif will be discussed in greater detail in section 3.3).

3.1.3 AP-4 might mediate vesicle trafficking along microtubules by interacting with specific kinesin-like proteins

An *Arabidopsis* (leaf) trichome represents a highly enlarged unicellular epidermal hair, arranged in a stalk with usually three (Col-0) branches forming a stellate shape. More than 40 genes are known to be involved in trichome development and morphogenesis and

grouped into different categories, according the stage or process of trichome development that is affected by their mutation (Hülskamp et al., 1994; Perazza et al., 1999; Hülskamp, 2004; Marks et al., 2009; Taheri et al., 2015). In turn, this often correlates with the particular trichome-phenotype that results from the loss (or gain) of the affected gene. Trichome initiation and thus the spatial arrangement of trichomes can be altered (Larkin et al., 1996), which is for example represented by the trichomeless *glabrous-1* mutant (Oppenheimer et al., 1991), or the *tryptichon* mutant, in which trichome initiation is increased, resulting in the development of trichome clusters or nests (Schellmann et al., 2002; Pesch and Hülskamp, 2011). Secondly, mutations affecting endoreduplication and thus the DNA content, usually affect trichome size or the number of branches per trichome. For example, reduced DNA content compared to WT correlates with a decrease in trichome branch-numbers in *glabra-3* mutants, whereas DNA levels and branch numbers are increased in *rastafari, kaktus* and *spindly* (Hülskamp et al., 1994; Perazza et al., 1999). On the other hand, mutations in *stichel*, *angustifolia*, and *zwichel* reduce, and mutations in *noeck* increase branch-numbers, without affecting the DNA content (Hülskamp et al., 1994; Folkers et al., 1997). Defects in cell expansion and directional growth following branch initiation result in a distorted trichome morphology. This can manifest in twisted appearance or bulging at branch tips, and is usually accompanied by abnormal actin organization, for example in the *crooked*, *alien*, or *wurm* mutant (Mathur et al., 1999; Schwab et al., 2003). Other mutants, for example *chablis, chardonnay* and *retsina* show defects in cell wall deposition resulting in the absence of characteristic papillae on the trichome surface (Hülskamp et al., 1994).

As presented in section 2.3.2, a*p4ß-1, ap4ß-2, ap4μ* and *ap4ß-2 ap4μ* mutants developed trichomes with an increased frequency of higher-order branch numbers, but an otherwise normal morphology, and WT-like papillae. Also, mutations in *AP4*-adaptins did not obviously affect trichome spacing or the overall trichome frequency. For one, this is in line with the expression of *AP4μ* in young, but not in mature trichomes (section 2.2.2, Figure 8E vs. Figure 6F). The nuclear DNA content of *ap4* mutants was not determined, so it is at this point unclear, whether the supernumerary branching of these mutants is, for example, accompanied by an additional round of endoreduplication. However, the frequencies of individual trichome classes (classified according to their branch-number) on *ap4* mutant leaves, are similar to those of tri- or tetraploidic Col-0 derivatives, or to *kaktus,* or *spindly* (Perazza et al., 1999). *Spindly* mutants, however, have also been shown to develop longer stems (Jacobsen, 1993), and both *spindly* and *kaktus* mutants show longer hypocotyls compared to the WT when grown in the dark (Jacobsen, 1993; El Refy et al., 2003). This inconsistency to the phenotypes of *ap4* mutant suggests that increased trichome branching in *ap4* is likely to be independent of *SPINDLY* as well as of the ubiquitin-protein ligase encoding *KAKTUS* (Downes et al., 2003; El Refy et al., 2003). Supernumerary branching, resembling that observed in *ap4ß-1, ap4ß-2, ap4μ* and *ap4ß-2 ap4μ* trichomes (see section 2.3.2), has also been described for mutants lacking the microtubule-based kinesin-like protein KIN-13A (Lu et al., 2005). It is known to destabilize microtubules at the plus-end and thereby possibly inhibits the formation of additional branch points in trichomes (Oda and Fukuda, 2013). It has further been suggested to be

involved in cell elongation in rice and also in *Arabidopsis* (Kitagawa et al., 2010; Mucha et al., 2010; Fujikura et al., 2014; Deng et al., 2015), and was found to localize to the Golgi or to Golgi derived vesicles (Lu et al., 2005; Wei et al., 2009), indicating that the kinesin might participate in anterograde protein trafficking. In addition to the similar effects of mutations in *KIN-13A* or *AP4*, i.e. reduction of cell length and increase of trichome branch numbers, this suggests that both might concertedly mediate cell elongation or regulate trichome branching in *Arabidopsis*.

3.2 AP-4 participates in sorting of transmembrane proteins

Although the experiments presented in this work could not identify additional cargo of AP-3, the subcellular sorting of several transmembrane proteins was revealed to be dependent on AP-4. So far, the repertoire of known AP-4 cargo in plants was limited to VSR1 and some soluble ligands of the receptor, which have been shown to be secreted into the apoplast in *ap4* mutants (Fuji et al., 2016). In their publication, Fuji et al. (2016) actually studied AP-4 dependent sorting starting from the cargo and searching for mutants, in which the cargo, VSR1, or rather a GFP-tagged ligand of VSR1, was secreted instead of reaching the vacuolar lumen (see also Fuji et al., 2007). In contrast, this thesis basically followed the opposite approach, starting from the *ap4* mutant(s) in an attempt to identify its cargo. Quite surprisingly, the proteins that were missorted in the absence of AP-4 localize to different compartments, i.e. the PM or the TP, in WT cells. In contrast, AP-2 is generally thought to only mediate endocytosis (Fan et al., 2013; Kim et al., 2013; Yamaoka et al., 2013), whereas AP-3 is at least primarily involved in sorting from the Golgi to the tonoplast in plants (Niihama et al., 2009; Feraru et al., 2010; Zwiewka et al., 2011; Wolfenstetter et al., 2012). So initially, this appears to contradict the notion that one AP complex generally mediates protein sorting along one specific route. On the other hand, it might suggest that AP-4 participates in a common step in indirect sorting to both the PM and the TP. Before the identified AP-4 cargos and possible routes of the complex are evaluated in more detail, the following paragraph will briefly discuss the approach that was used in this this thesis to examine AP-4 dependent sorting in *Arabidopsis*.

3.2.1 Advantages and drawbacks of the protoplast assay

To identify putative cargo of the AP-4 (and/or AP-3) complex and to validate proteomic data obtained by Pertl-Obermeyer et al. (2016), GFP-fusions of the respective candidates were (transiently) overexpressed in *Arabidopsis* mesophyll protoplasts of WT and mutant. However, missorting of most candidates, particularly those suggested by proteomic data, could not be confirmed using the protoplast-assay (section 2.4.2), and there are indeed some potential drawbacks to be discussed. For example, it could be argued that alterations of polar protein distribution would have not been detected in morphologically apolar protoplasts. Whereas GFP-fusions of, for example, MDR1 (Wu et al., 2007a) and SYP132 (Enami et al., 2009) have been shown to localize apolarly to the PM of different cell types (endogenous promoter, respectively), this argument does appear to be valid for

SYP122 and NRT1.1, which show a polar distribution at the PM, at least in some cell types (Enami et al., 2009; Krouk et al., 2010). Another potential source of error is the addition of GFP to the respective candidate. Indeed, fusion of GFP to the *N*-terminus of PTR2, PTR4 and PTR6 is known to interfere with TP-localization (Komarova et al. 2012), and similarly impaired TP-targeting of NRAMP3 and NRAMP4 (section 2.4.3.4, Figure 31), whereas both GFP-INT1 and INT1-GFP localize to the TP (Schneider et al., 2008; Wolfenstetter et al., 2012; Wang et al., 2014). To address this, *N*- and *C*-terminal fusions of each candidate were usually generated, and/or the fluorophore-position was chosen to correspond to already published data. Finally, it could be criticized that (transient) overexpression potentially affects subcellular targeting, or saturates components of the sorting machinery, and therefore might yield false-positives. Overexpression has for example been shown to affect sorting of maize PIP1;2, which requires PIP2;5 to reach the PM, but is retained in the ER if (over)expressed alone (Zelazny et al., 2007, 2009). Nevertheless, saturation of a trafficking pathway would have affected both WT and mutant cells, and therefore would not necessarily rule out the possibility to detect differences in protein sorting between WT and mutant. Further, transient overexpression in mesophyll protoplasts under control of the $35S_{Pro}$ ensured that each construct was constitutively transcribed and translated at comparable levels in the examined cell type (Wolfenstetter et al., 2012). In contrast, endogenous promoters would likely have yielded insufficient fluorescence for microscopic analyses, at least in some cases. For example, $NRAMP4_{Pro}$ has been shown to hardly drive any expression under iron-sufficient conditions in *Arabidopsis*, and even under iron-starvation, the activity of both, $NRAMP4_{Pro}$ and $NRAMP3_{Pro}$, decreases rapidly within a few days after germination (Lanquar et al., 2005). Moreover, this method allowed to study subcellular sorting of numerous proteins in the identical cell type and in a much less time-consuming manner compared to an approach with stably transformed plants.

Finally, the present study revealed the targeting of several TM proteins to be specifically altered in the absence of AP-4, and moreover, identical or similar approaches have been used successfully in earlier studies, for example to demonstrate missorting of GFP-SUC4 in *ap3ß* mutant protoplasts (Wolfenstetter et al., 2012), or of GFP-VIT1 and INT1-GFP in AP1γ-depleted cells (Wang et al., 2014).

3.2.2 Altered trafficking of GFP-PIP2;1 in *ap4ß-1*

As shown in section 2.4.2, PM localization of GFP-PIP2;1 was disturbed in the absence of AP4ß. This result suggests a participation of AP-4 in sorting of PIP2;1 (sometimes referred to as PIP2A) to the PM, which in turn was suggested to contribute to the reduced swelling of *ap4ß-1* mutant protoplasts in response to an hypoosmotic stimulus (Pertl-Obermeyer et al., 2016).

Aquaporins mediate diffusion of water, gas and specific solutes through membranes of multiple species. In *Arabidopsis* 35 homologs exist, which can be divided into seven classes according to their sequence similarity and putative subcellular localization (Johanson et al., 2001; Anderberg et al., 2011; Maurel et al., 2015). Among those, the PM intrinsic PIPs

comprise thirteen members, further subdivided into two subclasses PIP1 and PIP2, according to their sequence identity.

Although PIPs have often been used as markers for the PM, it is now well established that their localization is actually more variable than the name would suggest, since not only their activity, but also their subcellular distribution is highly dynamic and sensitive towards environmental stresses (reviewed in Maurel, 2007; Hachez et al., 2013; Chevalier and Chaumont, 2014). Corresponding to their dynamic subcellular distribution, numerous sorting motifs have by now been identified in members of the PIP family. For example, ER-release of AtPIP2;1, ZmPIP2;4 and ZmPIP2;5 was shown to depend on a strict DXE-motif in the *N*-terminus of the proteins (Zelazny et al., 2009; Sorieul et al., 2011). In case of ZmPIP2;5, ER export further appears to be regulated by a LXXXA motif in the third TM-domain (Chevalier et al., 2014), which is conserved in AtPIP2;1. In AtPIP2;1, the DXE-motif neighbors residues that have been found to be subject to methylation (Santoni et al., 2006), which might additionally influence the subcellular targeting (also discussed in Maurel et al., 2015). Abundance of *Arabidopsis* PIP2;1 at the PM can also be modified by ubiquitination via an ER-localized E3 ligase, resulting in retention of the ubiquinated PIP2;1 in the ER (Lee et al., 2009). SYP121 was shown to be required for targeting of ZmPIP2;5 to the PM, possibly via a physical interaction between the proteins (Besserer et al., 2012). And from the PM, PIPs have been shown to constitutively cycle back to and from the TGN (Luu et al., 2012). So, overall, numerous components of the sorting machinery regulate the appropriate localization of PIPs at steady-state, and in turn, AP-4 might affect PIP2;1 trafficking by interaction with one of the numerous sorting signals.

Corresponding to putative participation of AP-4 in sorting to the PM, it has been shown that animal AMPA receptors which are usually targeted to the axonal PM of neurons, accumulate intracellularly in the absence of AP-4 (Matsuda and Yuzaki, 2008; Matsuda et al., 2008; Matsuda and Yuzaki, 2009). This suggests that the PM might represent a conserved target compartment for AP-4 mediated protein sorting. On the other hand, among all the PM localized proteins examined (comprising, in addition to the aquaporin, GFP fusions of MDR1, STP1, NRT1.1; PTR1; SYP122 and SYP132, as well as PIN1, PIN2, PIN3, PIN7 and INT4-RFP), GFP-AtPIP2;1 was the only one that (partially) failed to reach its destination in the *ap4* mutant. Moreover, several alternative explanations are conceivable, in which the absence of AP-4 affects targeting of the aquaporin in an indirect matter:

For example, in addition to clathrin-coated structures, AtPIP2;1 appears to be associated with sterol-rich micro-domains at the plasma membrane (Li et al., 2011). Obermeyer et al. (2016) found that proteins associated with lipid metabolism showed altered abundance in organelle enriched membrane fractions of *ap4ß* mutants compared to the WT. Therefore, PM abundance of AtPIP2;1 might be affected by an altered lipid composition in the *ap4* mutant rather than by direct partitioning of AP-4 in targeting of GFP-PIP2;1 to the PM.

Furthermore, subcellular targeting of GFP-PIP;1 was shown to depend on the phosphorylation state (Prak et al., 2008): a construct mimicking a constitutively phosphorylated form of PIP2;1 (GFP-PIP2;1(S283D)), was sorted to the PM under normal

conditions, identically to the native protein. In contrast, the GFP-PIP2;1(S283A) mutant mimicking a constitutively dephosphorylated variant, showed intracellular localization in a diffuse pattern, or "fuzzy staining". Phosphorylation of S283 thus appeared to be required for targeting of PIP2;1 to the PM, and was further found to be altered in response to osmotic stimuli (Prak et al., 2008). The possibility that AP-4 (or AP-3) participates in sorting of specific PIP-phospho-variants has already been discussed in Pertl-Obermeyer et al. (2016). In a scenario in which AP-4 was required for sorting of PIP2;1 to the PM, this might suggest a preference of AP-4 towards a phosphorylated form of PIP2;1. In the absence of AP-4, (the phosphorylated) PIP2;1 would then accumulate intracellularly. Interestingly, Pertl-Obermeyer et al. (2016) also found that in *ap4* mutants, phosphorylation of PIP2;1 at Ser283 was significantly decreased compared to the WT. Under normal conditions, decreased phosphorylation of PIP2;1 at this serine would be expected to enhance localization to "fuzzy" structures (which is in line with the localization of GFP-PIP2A in *ap4ß-1* mutants). Together, this allows for the hypothesis that GFP-PIP2;1 was, in fact, sorted "correctly" in the *ap4* mutant, in that its localization (predominantly to fuzzy structures) is compliant to its phosphorylation state (reduced phosphorylation at Ser283). Instead of directly interacting with PIP2;1, AP-4 might instead regulate the phosphorylation of PIP2;1 by acting more upstream, e.g. by sorting of osmotic receptors or the kinase required for phosphorylation of PIP2;1. Analysis of the subcellular localization of phosphorylation mimics of PIP2;1 (S283A or S283D) might clarify whether AP-4 is directly involved in the sorting of PIP2;1, at all, and might also reveal whether sorting via AP-4 is preferential for a specific phospho-variant of PIP2;1.

As already mentioned, altered trafficking of PIP2;1 appeared to correlate with a reduction in water transport capacity in *ap4ß-1* mutants. By contrast, sorting of GFP-PIP2;1 was not found to be significantly altered in *ap3ß* mutants compared to the WT (see section 2.4.2; Figure 21), although water flux in *ap3ß* mutants was found to be decreased in the swelling assay (Pertl-Obermeyer et al., 2016). Yet, it must be emphasized that sorting of GFP-PIP2;1 was analyzed at osmotic equilibrium, while the swelling experiment probably triggers re-sorting of some PIPs including PIP2;1 in response to the osmotic stimulus applied in the assay. Therefore, it cannot be excluded that AP-3 is involved in the putative stimulus-induced trafficking step of PIP2;1, which would not have been detected in the GFP-sorting assay under the used conditions, but would have affected the behavior in the swelling assay. In fact, other publications have implicated a role for AP-3 in PIP2;1-trafficking (Feraru et al., 2010; Zwiewka et al., 2011). In these studies, a GFP fusion of PIP2;1 was found to accumulate intracellularly in vacuole-like compartments in *pat2* (the *pat2-2* mutant is equivalent to *ap3ß* mutants used in this study) and *pat4-1* (*ap3δ*) mutants, as well as in plants expressing a dominant negative mutant of *AP3μ*. The vacuolar accumulation became obvious particularly after dark-treatment (Feraru et al., 2010; Zwiewka et al., 2011), which increases the stability of GFP in lytic vacuoles (Tamura et al., 2003). Although mesophyll protoplasts used in this work were incubated in the dark after transformation, they were transferred to ambient (albeit dimmed) light 5 min to 2 hours prior to analysis. Since vacuolar GFP was found to be degraded with a half-life of about 19

min at 22°C under continuous light (150 µmol m^{-2} sec^{-1}; Tamura et al., 2003), it cannot be excluded that accumulation of GFP-PIP2;1 in vacuolar compartments of *ap3ß* was simply not observed due to the experimental setup.
On the other hand, the subcellular localization of GFP-PIP2;1 was analyzed in mesophyll protoplasts, whereas Feraru et al. (2010) and Zwiewka et al. (2011) studied sorting in *Arabidopsis* roots. Thus, the conflicting outcomes might be due to the fact that sorting of GFP-PIP2;1 was examined in different cell types. Contributing to this, intracellular accumulation of GFP-PIP2;1 in roots appeared to be more pronounced in the stele but only subtle in other root cells (Feraru et al., 2010; Zwiewka et al., 2011), corresponding to the strong expression of *AP3ß-GUS* in the stele (Feraru et al., 2010). Although sorting of GFP-SUC4 is affected in mesophyll protoplasts of *ap3ß*, the absolute or the relative expression level of *AP3*-adaptins with respect to other components of the sorting machinery might influence sorting of GFP-PIP2;1 in different tissues.

3.2.3 AP-4 affects protein trafficking to the tonoplast

In addition to interfering with PM localization of GFP-PIP2;1, defects in AP-4 resulted in aberrant sorting of GFP-fusions of specific vacuolar transmembrane proteins. Considering that the vacuolar sorting receptors VSR1 and VSR2 are known interactors of AP-4 (Gershlick et al., 2014b; Fuji et al., 2016), the missorting of tonoplast localized transmembrane proteins in *ap4* mutants might initially not appear as a novel aspect. However, contrary to what their names suggest, VSR1 and VSR2, or vacuolar sorting receptors in general, do not reach the vacuolar membrane. Instead, the soluble ligands of the receptor are released to traffic further, finally reaching the vacuolar lumen, while the receptor is recycled. There is much debate on where exactly VSRs and cargo interact or dissociate, and from (or to) where the receptor is recycled, which some authors argue to occur as early as from the TGN (for example discussed by Kang and Hwang, 2014; Robinson and Pimpl, 2014; de Marcos Lousa and Denecke, 2016; Robinson and Neuhaus, 2016). Therefore, the data presented in this study is, in fact, the first to demonstrate that AP-4 affects sorting of transmembrane proteins that are destined to the tonoplast, although, as mentioned earlier, this does not exclude the possibility of AP-4 mediating an earlier step in sorting towards the vacuolar (and/or plasma) membrane. Further, the missorting of tonoplast proteins indicates even more similarities to AP-1 dependent sorting mechanisms, which will be discussed in the following paragraphs.

3.2.3.1 NRAMP3-, NRAMP4-, and MOT2-GFP are partially missorted to the plasma membrane of ap4 mutants

As presented in section 2.4.3.2, GFP-fusions of MOT2, as well as NRAMP3 and NRAMP4 (and members of the PTR-family) were partially missorted to the PM and to intracellular compartments in *ap4ß-1* and *ap4µ* mutants. WT-like distribution of the MOT2-, NRAMP3- and NRAMP4-GFP-fusions was further reestablished in stable transformants of *ap4µ* expressing *AP4µ$_{Pro}$:AP4µ-GUS,* demonstrating that the construct is able to functionally complement the sorting defect of the *ap4µ* mutant.

Like these missorted proteins, INT1 also consists of about 500 amino acids, and localizes to the TP in WT (Thomine et al., 2003; Lanquar et al., 2005; Schneider et al., 2008; Gasber et al., 2011). In addition, NRAMP3, NRAMP4 and INT1 share a similar topology with twelve transmembrane domains and intracellular *N*- and *C*-termini. But in contrast to the missorting of MOT2-, NRAMP3-, and NRAMP4-GFP, targeting of GFP-INT1 to the TP was not significantly affected by mutations in *AP4ß* or *AP4μ*, indicating that AP-4 selectively participated in trafficking of specific proteins to the vacuolar membrane.

Wang et al. (2014) recently demonstrated, that GFP-INT1 (as well as GFP-VIT1) was partially missorted to the PM upon induction of AP1γ-adaptin deficiency. For one, the results obtained by Wang et al. (2014) are consistent with the correct sorting of GFP-INT1 to the TP of *ap4* mutants. Secondly, it is noteworthy that in the absence of AP-1 or AP-4, their respective TP-destined cargos were missorted to the PM. TP localization of GFP-SUC4 was shown to require AP-3 (Wolfenstetter et al., 2012). But in contrast to the relocation of INT1 and VIT1, or MOT2, NRAMP3 and NRAMP4 to the PM of cells depleted for AP-1 or AP-4, respectively, GFP-SUC4 localizes to the *cis*-Golgi in *ap3ß* mutants. This further contributes to the hypothesis that AP-4 and AP-1 might distribute transmembrane proteins on (partially) parallel, or at least similar routes.

TP targeting of MOT2 and INT1 (as well as VIT1) has already been shown to require a dileucine based motif (Gasber et al., 2011; Wolfenstetter et al., 2012; Wang et al., 2014), respectively. Deletion or exchange of the TP sorting motif for alanine was found to result in complete abrogation of TP localization and re-routing to the PM. The fact that the absence of the corresponding adaptor relocates these proteins to the same compartment (i.e. the PM), as the disruption of the TP-directing dileucine motif, implies that like AP-1 (Wang et al., 2014), also AP-4 participates directly in dileucine-motif dependent sorting to the TP.

However, neither depletion of AP1γ-adaptin (Wang et al., 2014), nor ko of *AP4ß* or *AP4μ* did completely abrogate TP targeting of GFP-INT1 and GFP-VIT1 (Wang et al., 2014), or NRAMP3-GFP, NRAMP4-GFP and MOT2-GFP, respectively. And in contrast to the corresponding dileucine-motif-mutants, the GFP-fusions of the native proteins were not rerouted exclusively to the PM in the absence of the respective adaptor, but also accumulated intracellularly. The fact that residual labeling of the TP by GFP-INT1 or GFP-VIT1 was occasionally still observed in AP1γ-deficient cells, was interpreted as a result of an incomplete depletion of the adaptin by bombardment with an RNAi construct against one γ-isoform in the mutant background of the second isoform (Wang et al., 2014). However, *ap4ß-1* and *ap4μ* represent complete loss-of-function mutants (see also sections 2.1 and 3.1.1), so the remaining TP localization at least of NRAMP3-GFP, NRAMP4-GFP and MOT2-GFP in these mutants must be explained differently. This suggests that an alternative pathway exists, through which at least a fraction of MOT2-, NRAMP3- and NRAMP4-GFP reaches the TP independently of AP-4. It is well established that, generally, multiple pathways to the plant TP exist and some proteins have been shown to traffic tissue-dependent via one or another (reviewed in Pedrazzini et al., 2013; Rojas-Pierce, 2013; de Marcos Lousa and Denecke, 2016). As already mentioned, AP-3 mediates one of these routes, on which SUC4 reaches the TP possibly directly from the

(*cis*-)Golgi and without transit of the TGN or the PVC (Wolfenstetter et al., 2012). However, at least in mesophyll cells, sorting of the GFP-fusions of MOT2, NRAMP3 and NRAMP4 in *ap3ß* appeared completely identical to that in WT (see section 2.4.3.2; Figure 26), which makes AP-3 an unlikely candidate for mediating their alternative route.

A possible explanation could be that the examined tonoplast localized proteins are targeted along indirect route, via the PM, at least if the major pathway is disrupted. Once the protein has reached the PM, either in a targeted manner or by a more passive bulk flow, AP-2 might in this case mediate the internalization of the protein to an endosomal compartment, possibly by recognition of the dileucine motif. From there, the proteins might be sorted further to the tonoplast, although this would likely require the participation of yet another adaptor (for example AP-1 in the absence of AP-4, or *vice versa*). Different affinities of the adaptors towards the sorting motif would, overall, also account for the distinct subcellular patterns, for example of NRAMP3-, NRAMP4-, or MOT2-GFP in *ap4* mutants. In animals, such an "indirect pathway" to the lysosomal membrane via the PM is well documented (Hunziker and Geuze, 1996; Janvier and Bonifacino, 2005; Braulke and Bonifacino, 2009; Staudt et al., 2016). Gough et al. (1999) for example demonstrated that both µ2 and µ3 are involved in sorting of the lysosomal membrane protein LAMP1 which is targeted via the PM to the lysosomal membrane. Although this partially endocytotic route to the TP has so far not been demonstrated to exist in plants, it might still be considered as a possible option. In fact, some authors even suggest that vacuolar sorting receptors might conditionally traffic via the PM (Saint-Jean et al., 2010; Wang et al., 2011). Taking this into account, AP-1 and AP-4 might also mediate consecutive sorting steps for some cargo. Since both complexes localize to the same compartment in *Arabidopsis*, i.e. the TGN/EE (Park et al., 2013; Teh et al., 2013; Fuji et al., 2016), this may initially appear contradictory. On the other hand, both complexes show only limited colocalization with one another (Fuji et al., 2016). The plant TGN is considered to fulfil a dual function as TGN/EE (Dettmer et al., 2006; Viotti et al., 2010). However, the exact nature of endosomal compartments in plants, in particular the TGN/EE, is highly discussed and several authors conclude that particular domains of the TGN/EE might actually fulfil more specific functions (Foresti and Denecke, 2008; Robinson et al., 2008; Richter et al., 2009; Gendre et al., 2015; Paez Valencia et al., 2016). It could therefore be proposed that AP-1 and AP-4 labeled subdomains of the plant TGN/EE might, in fact, represent compartments that are more specialized for the biosynthetic or the endocytotic pathway. In this scenario, cargo which is destined to the TP might be sorted for example stepwise by both complexes. Alternatively, some proteins might be preferentially targeted via one of the complexes and come in contact with the other complex only in case of leakage to the PM and successive retrieval to the more endosomal subcompartment, from where the other complex mediates the backup route.

Further experiments, for example the examination of VIT1-, NRAMP3- or NRAMP4-targeting in cells deficient for AP-4 (VIT1) or AP-1 (MOT2, NRAMP3, NRAMP4), as well as parallel comparison of AP-1 and AP-4 localization using appropriate markers specific for secretory and endocytotic TGN domains, will have to clarify whether cargo selection is specific for each complex, or whether AP-1 and AP-4 can mediate either successive or

alternative sorting steps for these proteins. Furthermore, inhibition of endocytosis could clarify, whether the native proteins are targeted via an indirect pathway *in vivo*.

3.2.3.2 Missorting of NRAMP3 and NRAMP4 might contribute to chlorosis of ap4 mutants

As described in section 2.4, it was assumed that missorting of a protein of interest would cause similar effects as a ko of the corresponding gene. A disruption of *MOT2* is known to alter molybdate levels in leaves and seeds in *Arabidopsis*, but does not result in any visible phenotype when plants are grown on soil (Gasber et al., 2011; Ide et al., 2011). Because physiological defects of *ap4* are likely to correlate to altered subcellular targeting of numerous different proteins, the missorting of MOT2 in *ap4* at least does not contradict the WT-like morphology of *mot2* mutants (Gasber et al., 2011; Ide et al., 2011). Nevertheless, it would be interesting to determine molybdate contents of *ap4* mutants, particularly in comparison to *mot2* mutants, as well as *mot2* ko plants expressing $MOT2_{LL \rightarrow AA}$ under control of the *MOT2*-promoter.

In WT plants, NRAMP3 and NRAMP4 both localize to the TP where they can mediate release of stored metal ions to the cytosol (Thomine et al., 2003; Lanquar et al., 2004, 2005). Both have been shown to transport divalent manganese (Mn^{2+}), iron (Fe^{2+}) and cadmium (Cd^{2+}) ions (Thomine et al., 2000) and both are upregulated under iron-deficiency (Lanquar et al., 2005). Since early seedling development requires remobilization of iron from the vacuole (Roschzttardtz et al., 2009), the loss of both transporters results in iron becoming trapped in the vacuole and thus in chlorosis in young plants if iron is limited, i.e. cannot be taken up from the growth medium (Lanquar et al., 2005; Mary et al., 2015). Underlining their redundant function, a single ko is compensated by the presence (and upregulation) of the other (Thomine et al., 2000, 2003, Lanquar et al., 2004, 2005; Mary et al., 2015). Uptake of iron from the cytosol for vacuolar storage in the embryo in turn is thought to depend on VIT1 (Kim et al., 2006). As already suggested by the interveinal chlorosis initially observed in the soil-grown mutants, *ap4* seedlings appeared particularly chlorotic after germination on iron-deficient medium (see section 2.3.6; Figure 16). In fact, under these conditions chlorophyll-contents were found to be comparable to those of *nramp3-1 nramp4-1* double mutants. In line with an impairment of vacuolar iron release, disruption of AP-4 was further found to interfere with correct subcellular sorting of NRAMP3- and NRAMP4-GFP. With respect to the presence and the sorting of the iron transporters VIT1, NRAMP3 and NRAMP4 in the background of different mutants, this gives rise to the following model (depicted in Figure 36):

In WT plants (grown on iron-sufficient conditions), VIT1 mediates iron uptake into the vacuole, especially for storage in seeds (Kim et al., 2006; Roschzttardtz et al., 2009). When seeds of those plants germinate under Fe-deficient conditions, the stored iron can be released from the vacuole via NRAMP3 and NRAMP4 (Lanquar et al., 2005; Mary et al., 2015). In mutants lacking NRAMP4 (or NRAMP3), NRAMP3 (or NRAMP4) compensates for the loss of its redundant homolog (Lanquar et al., 2005). Seeds of *nramp3-1 nramp4-1* double mutants germinating on iron-deficient medium cannot release iron from the vacuolar storage, resulting in chlorosis of young seedlings (Lanquar et al., 2005; Mary et

al., 2015). As just discussed, it cannot be completely excluded that TP sorting of VIT1 is also impaired in *ap4* mutants. VIT1 as well as INT1 have both been shown to be sorted, at least predominantly, by AP-1 (Wang et al., 2014) and it therefore appears likely that analogous to INT1, TP sorting of VIT1 is also at least not severely impaired in *ap4* mutants (Wang et al., 2014). Thus, in *ap4* mutants VIT1 should be able to mediate iron uptake into the vacuole if plants are grown under iron-sufficient conditions (given that PM localized iron-importers localize and function correctly, c.f. below). Since NRAMP3 and NRAMP4 partially fail to reach the TP in *ap4*, iron cannot be sufficiently released from the vacuolar storage, resulting in chlorosis. This, however, does not explain the reduced chlorophyll levels of *ap4* mutants germinated under iron sufficient conditions. Possibly, slowed vacuolar iron release upon germination might be perceived as iron-deficiency, resulting in an induction of *NRAMP3* and *NRAMP4* expression (Lanquar et al., 2005), and again in partial missorting to the PM. If functional, PM localized NRAMP3 and NRAMP4 might then counteract iron transport to sink tissues by acting as iron (re)importers.

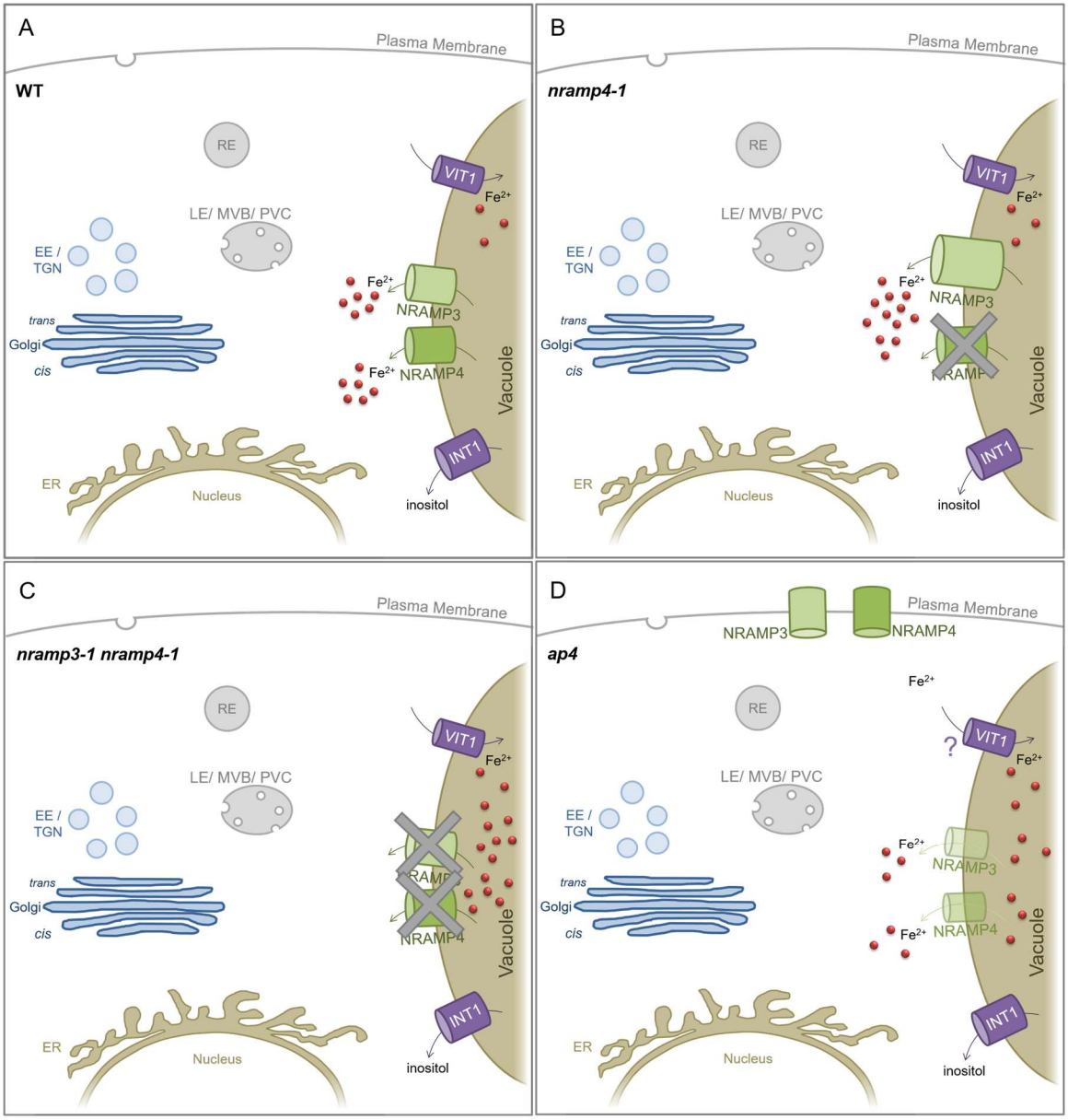

Figure 36: Iron distribution in WT and mutant with respect to localization of iron transporters.
(A) In the WT, VIT1, NRAMP3, NRAMP4 (and INT1) localize to the TP. VIT1 mediates iron uptake through the TP and storage in the vacuole. In germinating seedlings, NRAMP3 and NRAMP4 mediate iron release into the cytosol.
(B) *nramp4-1* single mutants appear WT-like, due to functional redundancy of NRAMP3 and NRAMP4.
(C) In *nramp3-1 nramp4-1* mutants, iron that has been preloaded into the vacuole by VIT1 cannot be released into the cytosol, resulting in chlorosis of *nramp3-1 nramp4-1* seedlings germinated without external iron supply.
(D) In *ap4* mutants, VIT1 is expected to be correctly sorted to the TP (via AP-1), mediating iron loading into the vacuole. NRAMP3 and NRAMP4 are partially missorted to the PM, possibly mediating uptake of iron from the apoplast (if available). Diminished presence of NRAMP3 and NRAMP4 at the TP prevents sufficient Fe^{2+} release from the vacuole in germinating seedlings.

Alterations in metal homeostasis were further reflected by a depletion of cytochrome P450 proteins in membrane fractions of *ap4ß-1* (Pertl-Obermeyer et al., 2016). According to the proteomic data, several proteins known to be regulated by iron were further found with lower relative abundance in *ap4ß-1* compared to the WT, or not detectable in the mutant in at least one experiment. For example, HEMA1, SAPX, FER1 and an uncharacterized gene (At1g68650) were recently listed among the (thirteen) most stably

down-regulated genes under iron-deficiency in a transcriptomic comparison of WT plants grown on iron-sufficient vs. -deficient conditions (Mai et al., 2016). Of two individual experiments, the corresponding proteins were also undetectable in *ap4ß-1* mutants in at least one (FER1, SAPX, HEMA) or both (At1g68650) proteomic comparisons of *ap4ß-1* with the WT, while they were detectable in the control (Pertl-Obermeyer et al., 2016; Supplementary Table 5).

3.3 Dileucine based motifs in AP-4 cargo proteins

Alanine mutagenesis revealed that post-Golgi sorting of NRAMP3-GFP and NRAMP4-GFP to the TP depends on a dileucine-based motif in the *N*-termini of the proteins (see section 2.4.3.4).

As briefly described in section 1.4.4.1, dileucine based motifs of the DXXLL type are known to bind to the VHS-domain of GGAs in animals (Takatsu et al., 2001; Misra et al., 2002; Shiba et al., 2002; and reviewed in Bonifacino and Traub, 2003; Braulke and Bonifacino, 2009). In contrast to DXXLL-type motifs, classical dileucine motifs share a [D/E]XXXL[L/I] consensus and can mediate endocytosis and/or intracellular sorting. Whereas the asparatate and both leucines are a strict prerequisite for DXXLL motifs, the acidic amino acid in the classical dileucine motif can usually be replaced by another acidic residue, and the second leucine can often be exchanged for isoleucine without affecting the functionality of the signal. In fact, particularly endocytotic motifs sometimes even accept particular non-acidic residues at position -4 from the dileucine (Bonifacino and Traub, 2003). Thus, the sorting signals of NRAMP3 and NRAMP4 do not represent DXXLL motifs, but rather correspond to dileucine motifs of the [D/E]XXXL[L/I] type.

For a better overview of the following discussion, the results are summarized in Table 2 together with already published sorting motifs of other plant transmembrane proteins.

Table 2: Summary of different dileucine-based sorting signals in TP localized transmembrane proteins of *Arabidopsis*.

Protein	Sorting motif	Adaptor	Localization in adaptor mutant	Mutant	Localization of mutant protein
VIT1	$(N)_{16}$EKQT**LL**$_{21}$[a]	AP-1 ≠ AP-3[a]	PM >> TP	AKQTAA EKQTAA AKQTLL	PM PM TP
INT1	$_{498}$NMEG**LL**E$_{505}$(C)[b]	AP-1[a] ≠ AP-3[b] ≠ AP-4[c]	PM >> TP	NMEGAAA	PM
MOT2	$(N)_2$ETTTT**PLL**$_{10}$[d]	AP-4 ≠ AP-3[c]	PM > TP > IC	ETTTTPAA	PM
NRAMP3	$(N)_5$ENNE**PLL**I$_{12}$[c]	AP-4 ≠ AP-3[c]	PM ≈ TP > IC	ENNEPAAA ENNEPALI ENNEPLAI ENNEPLLA	PM PM PM TP
NRAMP4	$(N)_5$DRER**PLL**$_{11}$[c]	AP-4 ≠ AP-3[c]	PM >> TP > IC	DRERPAA	PM
TPC1	$(N)_2$ED**PLI**$_6$[e]	≠ AP-3[e] ≠ AP-4[f]	NA	EDPAA	PM
PTR2	$(N)_5$EEEAR**PLI**$_{12}$[g]	(AP-4)[c]	(IC)	1. EEEARPAI 2. EEEARPLA 3. AAARPLI	1.-3. Internal membranes
PTR4	$(N)_5$DEERS**LL**$_{11}$[g]	NA	NA	DEERSLL-PTR1-GFP	DEERSLL redirects PTR1 to TP
PTR6	$(N)_{14}$DVEES**LL**$_{20}$[g]	(AP-4)[c]	(IC)	DVEESLL-PTR5-GFP	DVEESLL redirects PTR5 to TP
ESL1	$(N)_{10}$LEAG**LL**L$_{16}$[h]	NA	NA	1. LEAGAAA 2. AEAGLLL 3. LEAGALL 4. LEAGLAL 5. LEAGLLA	1.-4. vesicular structures and PM 5. TP

(N) or (C) denotes the position of the sorting motif in the *N*- or *C*-terminus. The precise position is indicated by subscript numbers. Amino acids are given in single-letter-code. Dileucines (or leucine-isoleucine pairs) are highlighted in bold. Proline residues directly preceding critical dileucines or leucine-isoleucine-pairs are underlined. Amino acids given in green have been shown to be dispensable for the functionality of the motif. Alanine exchange of amino acids given in red are known to alter subcellular sorting of the protein. Note that the column "adaptor" denotes altered sorting of a protein in the respective adaptor mutant and not necessarily a direct interaction. Adaptors or localizations given in brackets indicate preliminary data. IC = intracellular. Small superscript letters indicate references: [a] Wang et al., 2014; [b] Wolfenstetter et al., 2012; [c] this work; [d] Gasber et al., 2011; [e] Larisch et al., 2012; [f] Müller, 2016; [g] Komarova et al., 2012; [h] Yamada et al., 2010.

3.3.1 Tonoplast localization of NRAMP3 and NRAMP4 requires non-classical dileucine-based motifs

Dileucine based motifs have been shown to mediate TP targeting of numerous transmembrane proteins in plants (see also Table 2). VIT1 for example requires an *N*-terminal signal of the classical [D/E]XXXL[L/I]-type (EKQTLL) for sorting to the vacuolar membrane (Wang et al., 2014). Interestingly, the glutamate can be exchanged for alanine without abrogating TP localization (Wang et al., 2014). Analogously, the -4 position relative to the first critical leucine residue is occupied by an asparagine in INT1. And although the sorting motif of ESL1 (**L**EAG**LL**L) appears to include an acidic residue at -4 (underlined amino acids), Yamada et al. (2010) demonstrated that in fact the **L**XXX**LL**X peptide does account for correct sorting, whereas the glutamate or the third leucine of the leucine triplet can be exchanged for alanine without altering subcellular targeting to the TP. Also, neither the dileucine motif of MOT2 (Gasber et al., 2011), nor those identified in NRAMP3 and NRAMP4 have acidic residues at this position. Overall, the absence of acidic residues, or their substitutability with non-acidic amino acids at position -4 from the dileucine rather classifies the motifs of VIT1, INT1, ESL1, and MOT2, NRAMP3 and NRAMP4 as endocytotic signals, at least with respect to what is known from animal dileucine motifs (Bonifacino and Traub, 2003).

An extended acidic dileucine signal has recently been proposed and has particularly been implicated to act in TP sorting in plants (Komarova et al., 2012; Staudt et al., 2016). This type of dileucine motif is still characterized by the presence of critical acidic amino acids, even if the distance to the dileucine and the sum of negative charges appears to be variable to some extent. Staudt et al. (2016) recently published a review on non-classical motifs involved in lysosomal sorting in animals, where they discussed an “extended acidic dileucine signals”, characterized by the presence of more than three variable amino acids (X) between the acidic and the dileucine residues. Sorting of mammalian CLN3, a lysosomal transmembrane protein related to Batten disease, was shown to be dependent on an $EEEX_8LL$ motif positioned in a cytosolic loop of the protein (Kyttälä et al., 2003; Storch et al., 2004). Although it was initially proposed to not interact with either AP-1 or AP-3 (Storch et al., 2004), a more recent study demonstrated that sorting was in fact dependent on both complexes (Kyttälä et al., 2005).

Komarova et al. (2012) showed that a peptide of seven amino acids of PTR2 (EEARPLI) was sufficient to redirect PM proteins to the TP. Exchange of the leucine-isoleucine pair for an alanine-duplet abrogated sorting to the TP, but replacement of both glutamate residues with alanine did not. Instead, only when a third glutamate (**EEE**ARPLI) was additionally replaced, TP sorting was impaired. Hence, the authors suggested an extended $[D/E]X_{3–5}L[L/I]$ consensus to be applicable to several plant proteins, particularly PTR2 (EEEARPLI), PTR4 (DEERSLL) and PTR6 (DVEESLL), and included predictions for other plant transporters including NRAMP3 and NRAMP4, based on the presence of an *N*-terminal $[D/E]X_{3–5}L[L/I]$ and the isoelectric point of the proteins (Komarova et al., 2012, supplemental material). Yet, experimental evidence for dileucine-dependent sorting of NRAMP3 and NRAMP4 to the TP was so far not available. Moreover, the *N*-terminus of NRAMP4 contains two peptides that fit the extended $[D/E]X_{3–5}L[L/I]$ consensus. It was therefore important to

determine which single motif is required for TP localization, or if they both contribute to the targeting of NRAMP4, as this might refine the information on dileucine dependent sorting to the vacuolar membrane (see also section 3.3.5) and possibly indicate cargo preferences of plant AP complexes.

As mentioned before, neither the dileucine motif of NRAMP3, nor the signal that mediates TP sorting of NRAMP4 or MOT2 has an acidic amino acid at position -4 from the first critical leucine, but the motifs of all three proteins do correspond to the suggested consensus of an "extended acidic dileucine signal". Nevertheless, the role of the acidic residues has yet to be determined, and might clarify whether the motifs act as signals for endocytosis or direct trafficking to the TP. In fact, acidic "patches" in the sense of several consecutive acidic amino acids are not located at *N*-terminal positions of the dileucine of NRAMP3 or NRAMP4, but in that respect, it is noteworthy that both of them do have extended acidic patches closer to the first TM domain (for an alignment of the cytosolic *N*-terminal domains of NRAMP3 and NRAMP4, see section 2.4.3.4, Figure 32 or Figure 33; an alignment of the amino acid sequence of different members of the NRAMP-family is further given in the appendix, p. XI–XIII).

As presented in section 2.4.3.4 (Figure 33), only mutation of the more *N*-terminal dileucine-motif-conforming sequence of NRAMP4 abrogated TP sorting and resulted in relocation of $NRAMP4_{LL\rightarrow AA}$ to the PM. Moreover, the position of this motif corresponds to that of the TP-directing dileucine of NRAMP3. Although alanine substitution of the LI pair in the second (with respect to its distance to the *N*-terminus) putative dileucine motif of NRAMP4 resulted in increased ER-retention, TP localization was not completely abrogated, indicating that either TP sorting of this mutant is merely delayed due to improper folding, or that the affected motif is rather required for ER-release than for AP-mediated post-Golgi sorting.

The presence of the motif in the *N*-termini (and extremely close to the very *N*-terminus) might explain why constructs, in which GFP was fused to the *N*-terminus of NRAMP3 or NRAMP4 mostly failed to reach the TP (see section 2.4.3.4, Figure 31), possibly due to masking of the *N*-terminal sorting signal by the fluorophore. Similarly, Komarova et al. (2012) reported that *N*-terminal GFP impaired TP localization of PTR2, PTR4, and PTR6, which all contain *N*-terminal TP-directing dileucine motifs. Possible effects of dileucine motif positioning (in addition to the specific composition) on the cargo destination of animal proteins has already been described by Bonifacino and Traub (2003). In that respect it might be noteworthy, that *N*-terminal GFP does not impair TP targeting of the AP-1 cargo VIT1 (Kim et al., 2006; Wang et al., 2014), and neither *C*- nor *N*-terminal GFP alters TP localization of INT1, in which the dileucine is positioned close to the *C*-terminus [TP localization of an INT1-GFP fusion was published in Schneider et al. (2008)]. This suggests that AP-1 binding might confer a less stringent spatial requirement for interaction with the dileucine motifs of its cargo. It would therefore be interesting to examine in what way the functionality of the dileucine motifs, for example of NRAMP3 or NRAMP4, is affected if its position is altered.

3.3.2 AP-4 cargo might be defined by a conserved proline-dileucine or acidic patched in close vicinity of the dileucine

Larisch et al. (2012) already highlighted the presence of a conserved proline at the -1 position of dileucine-based motifs, which target several transmembrane proteins to the lysosome or vacuole (Table 2).

Interestingly, GFP-fusions of MOT2, NRAMP3 and NRAMP4, which contain a conserved proline at -1 were missorted in *ap4ß-1* and *ap4μ* mutants. In contrast, GFP-INT1, in which the -1 position is occupied by glycine, was still sorted to the TP in *ap4* protoplasts. In line with their finding that sorting of VIT1 and INT1 to the TP is AP-1 dependent, Wang et al. (2014) were also able to demonstrate an interaction between AP1γ and the (non-proline) dileucine motif of VIT1 (EKQTLL). This might indicate a preferential participation of AP-4 (or AP-1) in sorting of proteins which are targeted via a PL[L/I]-type motif (or a non-proline dileucine motif, respectively). In fact, abundance profiles of TPC1 (MED<u>P</u>LI) in organelle-specific enriched membrane fractions were found to be altered in *ap4ß-1* compared to the WT (data provided by Waltraud Schulze). On the other hand, a GFP-fusion of TPC1 was reported to localize to the TP in *Arabidopsis* mesophyll protoplasts even in the absence of AP-4 (Müller, 2016).

It must be emphasized that the confocal data obtained for GFP fusions of PTR2 (EEEAR<u>P</u>LI) and PTR6 (DVEESLL) was not quantified. Since experiments with both constructs were partially performed prior to analysis of NRAMP3- and NRAMP4-sorting and due to the fact that localization of PTR2-GFP and PTR6-GFP varied to some extent between individual experiments even in WT protoplasts (possibly due to variation in plant age, which was strictly kept constant in experiments for quantification of GFP-INT1, MOT2-GFP, NRAMP3-GFP and NRAMP4-GFP localization) the data cannot be taken as an appropriate reference for statistical analysis. But, although this observation at most reflects possible tendencies, localization of both PTR2-GFP and PTR6-GFP seemed to be affected by loss of AP-4 in most experiments. This would argue against the hypothesis that AP-4 preferentially participates in sorting of TP-localized proteins with a PL[L/I] type motif.

On the other hand, PTR2, PTR6, NRAMP3 and NRAMP4 do possess extended stretches of acidic amino acids in proximity to their dileucine motif. As discussed above, these might also be involved in TP sorting, particularly in the context of a dileucine. Although the dileucine motif of MOT2 is not accompanied by a glutamate- or aspartate-rich cluster, computational prediction (http://phosphat.uni-hohenheim.de/; Durek et al., 2009) indicates that phospho-threonines might substitute in providing negative charges in this case (see appendix, p. XIV for a prediction of phosphorylation sites in MOT2). However, patches of acidic or phosphorylatable residues further *N*-terminal to a dileucine are also present in VIT1 and INT1, so they might not affect adaptor specificity. Evaluation of the significance of acidic patches in dileucine motifs of TP transporters, therefore, requires further examination.

3.3.3 Dileucine motifs are unlikely to directly interact with AP-4

Although sorting of NRAMP3, NRAMP4 and MOT2 to the TP is clearly dependent on their dileucine motifs and requires the presence of AP-4, it is unlikely that AP-4 interacts with the dileucine motifs of its cargo directly.

Generally, AP-4 orthologs of different species have been shown to interact with tyrosine-based YXXØ-type sequences, for example that of the mammalian CD63 (Hirst et al., 1999), LAMP-1 (Stephens and Banting, 1998) or LAMP-2a (Aguilar et al., 2001), but also those of *Arabidopsis* VSR1 and VSR2 (Gershlick et al., 2014b; Fuji et al., 2016). However, the interaction between animal AP-4 and YXXØ-type motifs is often weak and the localization of these proteins is not affected by depletion of AP-4 (Simmen et al., 2002; Janvier and Bonifacino, 2005). Although a search for the AP-4 cargos identified in this study (MOT2, NRAMP3, NRAMP4, as well as PTR2 and PTR6) using the LocSigDB (King and Guda, 2007; accessible via http://genome.unmc.edu/LocSigDB/index.html) detects tyrosine-based signals (YXXΦ, i.e. Yx{2}[VILFWCM]) in all of the candidates, they occur within, or too close to predicted TM domains to be functional (see section 1.4.3.2 and references therein). Unless of course, the spatial requirements for the motifs are not as strict as assumed, or the TM prediction is erroneous.

Localization of human amyloid precursor protein (APP) on the other hand was found to be affected by AP-4 depletion (Burgos et al., 2010). If the interaction between the YKFFEE peptide of APP and the μ-subunit of AP-4 is abolished, either by depletion of AP-4 or by mutation of the sorting motif of APP, the localization of the cargo shifts from endosomes to the trans-Golgi network (TGN) (Burgos et al., 2010). The minimal motif was found to follow a YX[FYL][FL]E consensus which does not bind to the canonical binding site for tyrosine-based motifs in AP4μ (Burgos et al., 2010; Ross et al., 2014). A search for this motif in the *Arabidopsis* proteome yields approximately 400 hits (www.genome.jp/tools/motif/MOTIF2.html). Although NRAMP3 is one of them, the peptide corresponding to the query, i.e. $_{458}$YLLLE$_{462}$, occurs within a predicted transmembrane domain. As presented in section 2.4.1, the localization of human APP in *Arabidopsis* protoplasts was not found to be obviously altered in *ap4μ* compared to WT. This might, however, be attributed to the proposed dual function of the plant TGN/EE. More specific markers might be required to determine whether mutations of *AP4*-adaptins alter the TGN/EE-internal localization of human APP in *Arabidopsis.* Although, plant and animal AP-4 seem to have different affinities at least towards specific YXXØ-type signals (Gershlick et al., 2014b), which might also apply to the YKFFEE peptide of APP.

In addition, AP-4 has been implicated to mediate basolateral sorting (Simmen et al., 2002) and was shown to recognize several non-canonical sorting motifs, for example diaromatic (FXF), phenylalanine-based (FGSV) and FR motifs in the ionotropic glutamate receptor δ2 (Yap et al., 2003). However, none of the known motifs known to interact with AP-4 is present in the cytosolic domains of *Arabidopsis* NRAMP3, NRAMP4 and MOT2.

Generally, different dileucine motifs have been shown to interact with animal AP-1, AP-2 and AP-3, particularly with hemicomplexes consisting of the large γ/α/δ- and the corresponding σ1-3 subunits, respectively. In contrast, direct interactions between dileucine motifs and AP-4 have never been documented. The dileucine signal of

tyrosinase-related protein 1 (TYRP1, motif: EANQPLL) from mice, having an acidic residue is at position -5 and a proline at position -1 of the first leucine, appears highly similar to that identified in *Arabidopsis* NRAMP3, or NRAMP4. However, it also does not interact with a ε-σ4-hemicomplex, but with the AP-1 analog, γ1-σ1A (Theos et al., 2005). In fact, several dileucine motifs that have been shown to even interact promiscuously with AP-1, AP-2, and AP-3 hemicomplexes in a yeast-three-hybrid assay, did not interact with the homologous AP-4 hemicomplex (Janvier et al., 2003; Lindwasser et al., 2008; Mattera et al., 2011). Although *Arabidopsis* AP-4 was not specifically examined in their study, Wang et al. (2014) were able to demonstrate an interaction between the dileucine motif *Arabidopsis* VIT1 and the γ-adaptin of AP-1, which so far is the only plant AP complex shown to bind this type of motif. Importantly, several attempts to validate an interaction specifically between *Arabidopsis* AP-4 and NRAMP3 or NRAMP4 have failed so far. These included yeast two-hybrid and yeast three-hybrid assays (with the *N*-terminal domains of NRAMP3 or NRAMP4, and subunits of AP-4; Wollschläger, unpublished), as well as BiFC experiments (full-length NRAMP3 or NRAMP4, and subunits of AP-4; Wollschläger, unpublished).

Normal sorting of MOT2-, NRAMP3, and NRAMP4-GFP was, however, clearly impaired in AP-4 depleted *Arabidopsis* protoplasts. In summary, this suggests that either, AP-4 dependent trafficking of MOT2-, NRAMP3-, and NRAMP4-GFP (and PTR2 and PTR6) relies on another motif, or AP-4 mediates trafficking of those cargos via an indirect interaction with their dileucine motifs. A similar scenario, in which another adaptor links AP-4 to a transmembrane cargo, accounts for the polar sorting of AMPA receptors in neurons, which depends on the interaction between AP4μ and so-called transmembrane AMPA receptor regulatory proteins, although this does not occur via a dileucine-based motif (Matsuda et al., 2008; Matsuda and Yuzaki, 2009).

3.3.4 Putative accessory proteins of AP-4 in *Arabidopsis* might contribute to cargo selection and trafficking

The role of other accessory proteins in vesicle trafficking is just beginning to be illuminated in the plant system. However, several studies have suggested a role in cargo recognition for ANTH/ENTH (AP180/epsin *N*-terminal homology) domain-containing proteins like EPSINs and have already shown that these proteins are able to interact with AP complexes or cargo (Song et al., 2006; Lee et al., 2007; Song et al., 2012; Zouhar and Sauer, 2014). Recent studies have identified TEPSIN/ENTHD2 as an accessory protein of animal AP-4 (Borner et al., 2012; Mattera et al., 2015; Frazier et al., 2016). Organisms in which AP-4 is absent, interestingly also lack TEPSIN homologs (Borner et al., 2012), indicating that the protein acts specifically together with AP-4. A regular BLAST search of human TEPSIN in *Arabidopsis* gives one hit, which corresponds to the recently characterized ENTH protein modified transport to the vacuole 1 (MTV1; At3g16270) in *Arabidopsis* (Sauer et al., 2013). Both, *mtv1-1* mutants (Sauer et al., 2013), as well as *ap4* mutants (Fuji et al., 2016) have already been shown to accumulate VSR1, and the precursor form of 12S-globulin. And like AP-4 (Fuji et al., 2016), MTV1 was shown to localize to the TGN (Sauer et al., 2013). Interestingly, the results presented in this work additionally reveal a substantial overlap

between the expression pattern of *AP4μ* (section 2.2) and that of *MTV1* (Sauer et al., 2013; Figure 2), and a reduction of silique-lengths in *ap4* mutants that was also observed in *mtv1-1* (see Sauer et al., 2013 Figure 2 for the m*tv1-1* and *mtv1-1 nev/agd5/mtv4* double mutants, and section 2.3.3 of this manuscript for the *ap4* mutants). Closer inspection of the interaction between animal TEPSIN and AP-4 revealed a bivalent interaction of the ß- and ε-ear domain with its accessory protein. Mattera et al. (2015) found a conserved [GS]LFXG[ML]X[LV] and a FXF[LIMV] motif in different tepsins to be required for binding to AP4ß and AP4ε, respectively. On the other hand, Frazier et al. (2016) published a slightly shorter LFxG[ML]x[LV] motif to mediate the interaction with the ß-ear. Both, LFxG[ML]x[LV] (Frazier et al., 2016), as well as FXF[LIMV] (Mattera et al., 2015), are present in *Arabidopsis* MTV1, suggesting that it also functionally corresponds to the AP-4 accessory protein TEPSIN of animals. Each individual motif is found also in other proteins in *Arabidopsis*, and might in some cases act as a signal for recognition by AP-4. Interestingly, animal TEPSIN was found to require AP-4 for membrane recruitment (Borner et al., 2012), and this observation could be exploited to clarify whether *Arabidopsis* MTV1 fulfils similar functions to those of animal TEPSIN.

As discussed above, *Arabidopsis* mutants lacking the kinesin-like protein KIN13A show similar defects in trichome morphology as ap4 mutants. Despite the evolutionary divergence to animal kinesins, it is noteworthy that some animal kinesins have been shown to directly interact with AP complexes (Nakagawa et al., 2000; Azevedo et al., 2009; Delevoye et al., 2009; Schmidt et al., 2009). In addition, direct kinesin-cargo interactions have been reported, for example between animal kinesin family member 3B (KIF3B) and the dileucine motif containing kidney anion exchanger 1 (kAE1) (Duangtum et al., 2011). Furthermore, mutations affecting specific kinesin motor proteins, like KIF1A and KIF5A are related to hereditary spastic paraplegias in humans (Reid et al., 2002; Klebe et al., 2006; Goizet et al., 2009; Rivière et al., 2011), as are mutations in *AP4*-adaptins (see also section 3.1.1). Together this suggests that *Arabidopsis* kinesins, particularly the internal motor kinesin KIN13A, might act as intermediate or additional adaptor(s) for AP-4 or its cargo, possibly by interacting with the complex or the transmembrane protein. A yeast two-hybrid assay is currently conducted in our group to test this hypothesis (Wollschläger, unpublished).

3.3.5 Implications for sorting of other members of the NRAMP-family of metal transporters

NRAMPs mediate metal homeostasis in bacteria, archaea, yeasts, plants and animals. Interestingly, both tonoplast localized NRAMP homologs from *Arabidopsis* show an even higher sequence identity with the lysosomal NRAMP1/Slc11a1 from mouse, than to the PM localized NRAMP1 from *Arabidopsis* (50% amino acid sequence identity with MmNRAMP1 vs. less than 40% to AtNRAMP1, respectively). However, this study could clearly demonstrate that NRAMP3 and NRAMP4 from *Arabidopsis* require an *N*-terminal dileucine-based motif for sorting to the vacuolar membrane, whereas an *N*-terminal tyrosine-based (YGSI) motif of mammalian NRAMP1 was shown to redirect the

homologous NRAMP2 to the animal equivalent, i.e. the lysosomal membrane (Lam-Yuk-Tseung et al., 2006).

In plants, NRAMP homologs occur throughout all different families, even though plants generally adopt one of two principle iron-uptake mechanisms, which differ drastically from each other: Whereas many known non-graminaceous species adopt a reduction-based strategy, in which ferrous iron is reduced to the divalent cation prior to acquisition from the soil, grasses take up siderophore-chelated Fe^{3+} (Marschner et al., 1986; Kim and Guerinot, 2007; Morrissey and Guerinot, 2010). Due to their partially varying substrate specificities for different divalent metal ions like Mn^{2+}, Fe^{2+}, Zn^{2+}, Ni^{2+} and Cd^{2+}, a role for plant NRAMPs has been implicated in both phytoremediation, as well as biofortification. But although several NRAMP homologs from *Arabidopsis* and many other plant species have been analyzed with respect to their subcellular localization (Table 3), specific targeting mechanisms are hardly understood and until now, sorting motifs of plant NRAMPs had not been identified.

Table 3: Subcellular localization of members of the NRAMP family of metal transporters of different plant species.

Protein	Accession	Loc.	Method / System	Reference
AtNRAMP1	Q9SAH8	PM	GFP-fusion, *Arabidopsis*	Cailliatte et al., 2010
AtNRAMP3	Q9SNV9	TP	GFP-fusion, *Arabidopsis*	Thomin et al., 2003
AtNRAMP4	Q9FN18	TP	GFP-fusion, *Arabidopsis*	Lanquar et al., 2005
AtNRAMP6	Q9S9N8	IC	Indirect immunofluorescence detection of AtNRAMP6::HA in fixed yeast cells	Cailliatte et al., 2009
OsNRAMP1	Q0D7E4	PM	GFP-fusion, Onion	Takahashi et al., 2011
OsNRAMP3	Q653V6	PM	GFP-fusion, onion or *Arabidopsis*	Yamaji et al., 2013; Yang et al. 2013
OsNRAMP5	Q8H4H5	PM	GFP-fusion, onion or rice	Ishimaru et al. 2012; Sasaki et al., 2012
OsNRAMP6	Q2QN30	PM	GFP-fusion, rice	Peris-Peris et al., 2017
OsNRAT1	Q6ZG85	PM	GFP-fusion, onion	Xia et al., 2010
TcNRAMP3	A6YPU3	TP	GFP-fusion, *Arabidopsis*	Oomen et al., 2009
TcNRAMP4	A6YPU4	TP	GFP-fusion, *Arabidopsis*	Oomen et al., 2009
HvNRAMP5	A0A1C9ZPR6	PM	GFP-fusion, onion	Wu et al., 2016
MtNRAMP1	A0A072UZV8	PM	Indirect immunofluorescence detection of MtNramp1-HA in *Medicago*	Tejada-Jiménez et al., 2015
PtNRAMP3.1	eugene 3.02050021	IC	GFP-fusion, *Populus trichocarpa* and *Arabidopsis*	Migeon et al., 2010; Le Thi, 2015
PtNRAMP3.2	gw1.205.38.1	TP	GFP-fusion, *Populus trichocarpa* and *Arabidopsis*	Migeon et al. 2010; Le Thi, 2015

Loc.: Subcellular localization. *At*: *Arabidopsis thaliana*; *Hv*: *Hordeum vulgare* (barley); *Mt*: *Medicago trunculata* (barrel medic) *Os*: *Oryza sativa*; *Pt*: *Popolus trichocarpa (*western balsam-poplar*); Tc*: *Thlaspi caerulescens* (alpine penny-cress). Sequences of PtNRAMP3.1 and PtNRAMP3.2 can be accessed via http://genome.jgi.doe.gov/Poptr1_1/Poptr1_1.home.html. All other accession numbers refer to the UniProt ID.

Figure 37 shows an alignment of the cytosolic *N*-terminal domains of MmNRAMP1 and of the NRAMP homologs given in Table 3, in addition to the remaining homologs from *Arabidopsis* and rice, of which the subcellular localization has not been experimentally determined (the full-length alignment is given in the appendix, pp. XI–XIII). Notably, all

plant NRAMPs that have been found to localize to the vacuolar membrane share a dileucine-based motif in the cytosolic *N*-terminal domain, which suggests that dileucine-based sorting to the TP is conserved in NRAMPs of different plant species. However, sequences corresponding to a [D/E]$X_{3–5}$L[L/I] consensus are also present in NRAMP homologs that are known to localize to intracellular compartments or to the PM, which might be one reason why sorting signals for plant NRAMPs have not been identified so far.

As discussed before (section 3.3.1), the *N*-terminus of *Arabidopsis* NRAMP4 contains two putative dileucine motifs, but only mutation of the more *N*-terminal signal was sufficient to completely reroute the protein to the PM (section 2.4.3.4, Figure 33). Thus, the second putative dileucine of AtNRAMP2 is likely to correspond to this second dileucine in NRAMP4, which was shown to be unfunctional at least with respect to TP sorting. The PM localized AtNRAMP1 contains an *N*-terminal SFSNSPLI peptide. Although this doesn't fit the classical consensus sequence of dileucine motifs, two serines (at position -4 and position -6 from the leucine, underlined) have been experimentally detected as phosphoserines (http://phosphat.uni-hohenheim.de/), which might regulate its targeting for example in response to iron supply.

The results obtained in this work, together with the sequences of NRAMP homologs with known subcellular localization, furthermore allows to derive additional features that are likely to be prerequisites for targeting of plant NRAMP homologs to the tonoplast. Interestingly, OsNRAMP6 and PtNRAMP3.1, which do share an *N*-terminal peptide corresponding to the [D/E]XXXL[L/I] (or the extended [D/E]$X_{3–5}$L[L/I]) consensus (Figure 37) have recently been shown to localize to the PM (OsNRAMP6; Peris-Peris et al., 2017) or to a Golgi-associated intracellular compartment (PtNRAMP3.1; Le Thi, 2015). Identically to the sorting signals of AtNRAMP3 and AtNRAMP4, and to the putative TP directing motifs of TcNRAMP3, PtNRAMP3.2 and TcNRAMP4, position -5 from the first leucine is occupied by a conserved acidic residue. However, in contrast to the TP localized NRAMPs, OsNRAMP6 lacks the conserved proline at position -1. Furthermore, the dileucine motifs of OsNRAMP6, as well as that of NRAMP3.1 from poplar in which the proline is present, both show a greater distance from the *N*-terminus compared to the dileucine motifs of the TP localized NRAMP homologs, in which the dileucine occupies the identical position ($_{10}$LL$_{11}$).

So, in summary, the following aspects might concertedly contribute to the functionality of dileucine-based motifs for tonoplast sorting of plant NRAMPs:

1. The presence of a conserved acidic amino acid at position -5 from the first leucine.
2. The presence of a conserved proline residue preceding the first leucine.
3. The exact distance from the *N*-terminus ($_{10}$LL$_{11}$ maximum).

Overall, this corresponds to a consensus of $_{1}$MXXX[D/E]XXXPLL$_{11}$, or $_{1}$MX(0–3)[D/E]XXXPLL$_{8–11}$ (if corrected for the possibility that an even shorter distance from the *N*-terminus might be tolerated). It has been suggested, that TP targeted transporters might additionally be characterized by an overall lower isoelectric point (pI), compared to their PM homologs (Komarova et al., 2012). In fact, none of the TP localized NRAMP homologs listed in Table 3 or Figure 37, has a theoretical pI over 6.0 (see appendix p. XIII

for exact numerical values). However, based on this pI limit and the presence of an *N*-terminal dileucine-based motif, also OsNRAMP6 (pI = 5.19) and PtNRAMP3.1 (pI = 4.89) would be predicted to localize to the TP.

The putative dileucine motifs of OsNRAMP2, AtNRAMP2 and AtNRAMP5 all lack the conserved proline residue. Additionally, position -5 of AtNRAMP5 is not occupied by an acidic residue. And of all three, only the dileucine pair of OsNRAMP2 shares the conserved position of the dileucine pair. So, under the assumptions that the above-named features are all strict prerequisites for the functionality of the dileucine motif of plant NRAMP proteins for sorting to the TP, neither OsNRAMP2, nor AtNRAMP2 and AtNRAMP5 would be sorted to the TP. On the other hand, in case the proline is not essential despite its high conservation, OsNRAMP2 would be expected to localize to the TP. In turn, analysis of their subcellular localization would help to reveal the significance of the acidic, or the proline-residue, as well as of the positioning of the motif.

Figure 37: Sequence alignment of cytosolic *N*-terminal domains of NRAMP homologs.
Sequences of NRAMP homologs known to localize to the PM, TP or intracellular compartments are given in orange, green, or purple, respectively. Sequences of NRAMP homologs with unknown localization are given in black. The non-plant homolog NRAMP1 from mouse is given in dark grey. Its tyrosine-based motif is highlighted in green. Experimentally determined or putative dileucine-based motifs for sorting to the TP are highlighted in black. Other sequences that correspond to the extended [D/E]X_{3-5}L[L/I] consensus, are highlighted in grey. Yellow shading labels the beginning of the first transmembrane domain. *At*: *Arabidopsis thaliana*; *Hv*: *Hordeum vulgare* (barley); *Mt*: *Medicago trunculata* (barrel medic) *Os*: *Oryza sativa*; *Pt*: *Popolus trichocarpa (*western balsam-poplar*); Tc*: *Thlaspi caerulescens* (alpine penny-cress);.Accession numbers: AtNRAMP2 (Q9C6B2); AtNRAMP5 (Q9SN36); MmNRAMP1 (P41251); OsNRAMP2 (Q10Q65); OsNRAMP4 (Q5QN13); all others are given in Table 3.

These findings also implicate that close homology alone might not be sufficient to predict the subcellular localization of NRAMP proteins from other plants. Of course, experimental evidence is required to determine the precise role of each feature, i.e. proline, glutamate or aspartate residues and the exact position of the motif. Nevertheless, it suggests that at least those plant NRAMP proteins sharing the combined $_{1}$MXXX[D/E]XXXPLL$_{11}$ consensus are very likely to be sorted to the TP, whereas others, not fulfilling the above named features, might be targeted to the PM or to intracellular compartments, despite their close homology to the TP localized NRAMPs from *Arabidopsis*. Table 4 shows an overview of close homologs of AtNRAMP3 or AtNRAMP4 (homology of at least 70% on the amino acid level to either AtNRAMP3 or AtNRAMP4) from different plant species with an emphasis on agricultural significant crops. In addition, a rating was included to predict

subcellular sorting of each NRAMP homolog, based on the individual premises derived in this section.

Table 4: Putative dileucine-based motifs in *N*-terminal sequences of close homologs of AtNRAMP3 or AtNRAMP4.

Species	Accession	Amino acid sequence	% identity to NRAMP3 / NRAMP4	Rating
Arabidopsis thaliana	Q9SNV9	MPQLENNEPLL	100.00 / 76.74	+ + +
	Q9FN18	MSETDRERPLL	76.74 / 100.00	+ + +
Spinacia oleracea	A0A0K9RIN8	MAEPYEPLL	73.31 / 71.94	+ + 0
	A0A0K9RP80	MMESTAEFNDDDKSSESNQLL	71.72 / 69.34	- - -
Theobroma cacao	A0A061DGW0	MPPEENQVPLL	79.88 / 74.46	+ + +
Cicer arietinum	A0A1S2YS89	MSPNRREHEQPLL	75.90 / 71.71	+ + -
Capsella rubella	R0FVE1	SRKPQQETETEETQRTLQKIMSELENNEPLL	94.87 / 77.14	+ + -
Brassica rapa	M4C8P5	MSRSENDRPLL	91.91 / 76.74	+ + +
Prunus persica	M5VXT2	MPSTHDHSQPLL	80.08 / 74.65	+ + -
Phaseolus vulgaris	V7CHJ7	MPPQDRRQPLL	79.20 / 76.74	+ + +
	V7CER2	MSRNPQEQPLL	76.19 / 73.43	- + +
Citrus clementina	V4SFB6	MPPQQHEQEQDHLLPLL	78.53 / 73.81	+ + -
Daucus carota	A0A164UC12	MALPEEHQALL	77.56 / 73.99	+ - +
Cucumis melo	A0A1S3C1X3	MHPDDQQQQPLI	75.70 / 73.32	- + -
Solanum lycopersicum	Q84LR0	MPLNDEEEHHQLLADRLL	75.55 / 72.37	+ - -
Solanum tuberosum	M1CC35	MPLHDEEEHHQLLADRLL	75.40 / 71.94	+ - -
Riccinus communis	B9SG31	MPLQDHNRQPLL	80.20 / 75.65	- + -
Glycine max	I1LH97	MPPEQTQQPLL	79.20 / 75.90	- + +
	Q7X9B8	MSGSHQEQPLL	75.99 / 73.62	- + +
Lupinus angustifolius	A0A1J7HA59	MSHQPLL	75.80 / 71.09	- + 0
	A0A1J7I6J3	MSQQPLL	78.16 / 73.96	- + 0
Medicago truncatula	G7K3Y6	MSHQQPLL	79.37 / 75.30	- + 0
Populus trichocarpa	U5G4L2	MPVEENHQPLL	79.00 / 74.50	+ + +
	B9GNS0	MSSPSGGEDSKDDEKDEESNRLL	71.77 / 67.86	+ - -

Amino acid sequences are given from the initial methionine up until the first or second dileucine-pair. % identity refer to the amino acid identity between the total protein sequences (copied from the Percent Identity Matrix of an alignment created by Clustal2.1). Motifs following a consensus of [D/E]XXXPLL are given in red. If such motif occurs at the conserved distance from the *N*-terminus, the initial methionine is given in green. All other sequences corresponding to an extended [D/E]X_{3-8}L[L/I] consensus, are given in underlined letters; PLL-motifs without a preceding acidic residue are given in bold only. The rating (last column) predicts localization to the TP based on the presence of an acidic amino acid

at position -5 (+: yes, -: no), a proline at -1 (+: yes; -: no), and the distance of the dileucine pair from the *N*-terminus (+: first leucine at position 10; 0: first leucine at position ≤ 9; -: first leucine at position 11 or further) in that order.

4 Materials and methods

4.1 Materials

4.1.1 Oligonucleotides

Oligonucleotides were designed using VectorNTI (Thermo Fisher Scientific, Waltham, USA) and purchased from Sigma-Aldrich (Steinheim, D).

4.1.1.1 Primers for genotyping and analysis of transcript levels

Table 5: Primer combinations used for detection of WT- and insertion- (ko) alleles in At5g11490 (*AP4ß*) in the T-DNA line SAIL_796_A10 (*ap4ß-2*).

Amplification of allele	Primer combination	Primer sequence (5'→3')	Size of PCR product in bp
WT	AP-4g+1127f AP-4g+3205r	GAAGCAAGCCACTCTGAGGAAG CGTCAGAAAACTCAAAGGGTCC	2079
ko	LB3 AP-4g+3205r	TAGCATCTGAATTTCATAACCAATCTCGATACAC CGTCAGAAAACTCAAAGGGTCC	~ 1300
ko'	AP-4g+1127f LB3	GAAGCAAGCCACTCTGAGGAAG TAGCATCTGAATTTCATAACCAATCTCGATACAC	~ 900

PCR product sizes refer to fragments obtained using genomic DNA as the template. Ko' denotes alternative primer combinations.

Table 6: Primer combinations used for detection of *AP4ß* transcript in mutants of line SAIL_796_A10 (*ap4ß-2*).

Position relative to T-DNA insertion	Primer	Primer sequences (5'→3')	Size of amplificate in bp	
			cDNA template	Genomic contamination
5'	AP-4g+16f AP-4g+1806r	GCTTCACAGCGTTATCCGTCACC GCATACGATTGCTCTGGACTTCC	947	1791
3'	AP-4g+2193f AP-4g+4143r	CTGGAGATGGAAAAGGACTATGTGAC CGGTTGTGAATGCTTGACACG	1237	1951
traversing	AP-4g+1127f AP-4g+2477r	GAAGCAAGCCACTCTGAGGAAG CCTGTGCATACTCACCCAACATCC	817	1351

Table 7: Primer combinations used for detection of WT- and insertion- (ko) alleles in *Arabidopsis* T-DNA lines carrying an insertion in At4g24550 (*AP4μ*).

T-DNA line	Allel	Primer combination	Primer sequence (5'→3')	Size of PCR product in bp
SALK_052835	WT	AP4μg-933f AP4μg+591r	CGTGGGAAACGTACCATCTCATAATG GACATGGAAGTAGTTCACGCCATCG	1524
	ko	LBb1.3 AP4μg+591r	ATTTTGCCGATTTCGGAAC GACATGGAAGTAGTTCACGCCATCG	~ 800
	ko'	AP4μg-933f LBb1.3	CGTGGGAAACGTACCATCTCATAATG ATTTTGCCGATTTCGGAAC	~ 1000
SALK_014326 (*ap4μ*)	WT	AP4μg+613f AP4μg+1921r	GTTGCGACAACGAGAGTTAACGTGTC GTTCTATCTGAATCGAAGCTATCCAGACG	1309
	ko	LBb1.3 AP4μg+1921r	ATTTTGCCGATTTCGGAAC GTTCTATCTGAATCGAAGCTATCCAGACG	~ 1000
	ko'	AP4μg+613f LBb1.3	GTTGCGACAACGAGAGTTAACGTGTC ATTTTGCCGATTTCGGAAC	~ 600

PCR product sizes refer to fragments obtained using genomic DNA as the template. Ko' denotes alternative primer combinations.

Table 8: Primers used for detection of *AP4μ* transcript in homozygous mutants of SALK_052835 and SALK_014326 (*ap4μ*).

T-DNA line	Position relative to T-DNA insertion	Primer combination	Primer sequence (5'→3')	size of amplificate in bp (cDNA template)
SALK_052835	5'	--	--	--
	3'	AP4μg+613f AP4μg+996r	GTTGCGACAACGAGAGTTAACGTGTC GCAGCAGGATCAATAGGCTGAAGG	260
	traversing	--	--	--
SALK_014326 (*ap4μ*)	5'	AP4μg+613f AP4μg+996r	GTTGCGACAACGAGAGTTAACGTGTC GCAGCAGGATCAATAGGCTGAAGG	260
	3'	AP4μg+1078f AP4μg+1921r	GAGCCAAAAGAATGCCTGGAACTG GTTCTATCTGAATCGAAGCTATCCAGACG	343
	traversing	AP4μg+613f AP4μg+1921r	GTTGCGACAACGAGAGTTAACGTGTC GTTCTATCTGAATCGAAGCTATCCAGACG	617

Table 9: Primer combination used for amplification of *AtACT2* fragments.

Primer	Primer sequence (5'→3')	Size of amplificate in bp	
		cDNA template	genomic contamination
AtACT2g+846f	ATTCAGATGCCCAGAAGTCTTGTT	364	450
AtACT2g+1295r	GAAACATTTTCTGTGAACGATTCCT		

4.1.1.2 Oligonucleotides for cloning

Oligonucleotides for cloning of AP-4 adaptin-reporter constructs

Table 10: Oligonucleotides for cloning of *AP-4 adaptin-reporter* constructs.

Amplificate	Locus or splice variant	Primer combination	Primer sequence (5'→3')
AP4μ$_{Pro}$:AP4μ	At4g24550	AP4μ-Prom-GW-f	CACCGTTCAAGATTGGAAAAAAGAGTC
		AP4μ-GW-r	TATCCTAGCCACATAAGAATTCGCCTG
AP4μ	At4g24550.2	AP4μ-5'-BspHI-f	CCTCATGATGATCTCCCAATTCTTCG
		AP4μ-3'-BspHI-r	TCATGACTATCCTAGCCACATAAGAATTCG
		AP4μ-mut-f	GATTGTAACTTTCACGAGTCTGTTCGTCTG
		AP4μ-mut-r	CAGACGAACAGACTCGTGAAAGTTACAATC
AP4ß	At5g11490.1	AP-4ß cDNA-NcoI-F	CCATGGCTCCTCCGGCCGCTTCA
		AP-4ß cDNA-NcoI-R	CCATGGCAGGCATACCAAATTTGGAC

Oligonucleotides for cloning of AtNRAMP3- and AtNRAMP4-fragments

Table 11: Primers used for cloning of *NRAMP3*- (At2g23150.1) and *NRAMP4*- (AT5G67330.1) fragments.

Name	Primer sequence (5'→3')
AtNRAMP3-5'NcoICC-f	CCATGGCCATGCCACAACTCG
AtNRAMP3-3'NcoI-r	CCATGGCATGACTAGACTCCGCTT
AtNRAMP4-5'-PciI-f	ACATGTCGGAGACTGATAGAGAGCGTC
AtNRAMP4-3'-PciI-r	ACATGTTCTCATCATCCCTCTGTGGTTC
NRAMP3-5'NcoI-LLI/AAA-f	CCATGGCCATGCCACAACTCGAGAACAACGAGCCAGCTGCAGCCAACGAGGA
NRAMP3-5'NcoI-10L/A-f	CCATGGCCATGCCACAACTCGAGAACAACGAGCCAGCTCTAATCAA
NRAMP3-5'NcoI-11L/A-f	CCATGGCCATGCCACAACTCGAGAACAACGAGCCACTTGCAATCAA
NRAMP3-5'NcoI-12I/A-f	CCATGGCCATGCCACAACTCGAGAACAACGAGCCACTTCTAGCCAA
NRAMP4-5'PciI-LLA/AAA-f	ACATGTCGGAGACTGATAGAGAGCGTCCGGCTGCAGCATCGGA
NRAMP3-HIV/AAA-f	ACAGAGAAGGTAGCTGCCGCCAGAAACGAAGA
NRAMP3-HIV/AAA-r	TCTTCGTTTCTGGCGGCAGCTACCTTCTCTGT
NRAMP4-LIV/AAA-f	AGAAAGTTGCAGCCGCAGGAATCGACGAA
NRAMP4-LIV/AAA-r	TTCGTCGATTCCTGCGGCTGCAACTTTCT
NRAMP3-5'-NcoIC-DeltaN(30)-f	CCATGGCCTTCTCATGGAAGAAG

Primers used for cloning of other coding sequences from Arabidopsis

Table 12: Primers used for amplification of different CDS.

Gene name	Locus	Primer combination	Primer sequence (5'→3')
MTP1 (METAL TOLERANCE PROTEIN 1)	At2g46800.1	AtMTP1-mut-f AtMTP1-mut-r AtMTP1-5'-NcoI-f AtMTP1-3'-NcoI-r	CCATCACAATCATAGTCATGGGG CATGACTATGATTGTGATGGTCATGG CCATGGAGTCTTCAAGTCCCCACC CCATGGCGCGCTCGATTTGTATC
ZIF1 (ZINC INDUCED FACILITATOR 1)	At5g13740.1	AtZIF1-5'-NcoI-f AtZIF1-3'-NcoI-r	CCATGGCGGAGGAGTACAAGGAAG CCATGGCTCTTCGACTCGTCGTTAG
STP1 (SUGAR TRANSPORTER 1)	At1g11260.1	AtSTP1+1f_5'CACC AtSTP1g+2671r	CACCATGCCTGCCGGTGGAT AACATGCTTCGTTCCAGCTTGGTTA
APY1 (APYRASE 1)	At3g04080.1	AtAPY1-5'-BspHI-f AtAPY1-3'-BspHI-r	TCATGACGGCGAAGCGAGC TCATGACTGGTGAGGATACTGCTTCTATG
APY2 (APYRASE 2)	At5g18280.2	AtAPY2-5'-BspHI-f AtAPY2-3'-BspHI-r AtAPY2-mut-f AtAPY2-mut-r	TCATGATAAACATAGTTGGGAGTTACCCATC TCATGACCGGTGAGGATACGGC CTGGGTCACGATGCATCTGAGAAC GCATCGTGACCCAGCGTCCTC
MDR1 (MULTIDRUG RESISTANCE PROTEIN 11)	At3g28860.1	AtMDR1-5'-PciI-f AtMDR1-3'-PciI-r	ACATGTCGGAAACTAACACAACCGATG ACATGTTAATCCTATGTGTTTGAAGCTGTAAC
ALS1 (ALUMINUM SENSITIVE 1)	At5g39040.1	AtALS1-5'-NcoI-f AtALS1-3'-NcoI-r	CCATGGGCAACAAGAAACTGTTGAC CCATGGCCAAGGTGGTAACAGAG
SYP122 (SYNTAXIN OF PLANTS 122)	At3g52400.1	AtSYP122-5'-BspHI-f AtSYP122-3'-BspHI-r	TCATGAACGATCTTCTCTCCGGC TCATGACGCGTAGTAGCCGCC
SYP132 (SYNTAXIN OF PLANTS 132)	At5g08080.1	AtSYP132-5'-NcoI-f AtSYP132-3'-NcoI-r	CCATGGCCATGAACGATCTTCTG CCATGGCAGCACTCTTGTTTTTCC
PIP2;1 (PLASMA MEMBRANE INTRINSIC PROTEIN 2A)	At3g53420.1	AtPIP2A-GW-f AtPIP2Acds+861r	CACCATGGCAAAGGATGTGGAAG GACGTTGGCAGCACTTCTGAATGA
CAT9 (CATIONIC AMINO ACID TRANSPORTER 9)	At1g05940.1	AtCAT9-5'-NcoI-f AtCAT9-3'-NcoI-r	CCATGGGAGGCCACGAAGGT CCATGGCAGCGTCGCTTTCA

NRT1.1 (NITRATE TRANSPORTER 1.1)	At1g12110.1	AtNTR1.1-5'-PciI-f AtNTR1.1-3'-PciI-r	ACATGTCTCTTCCTGAAACTAAATCTGATGA ACATGTTATGACCCATTGGAATACTCG
PTR1 (PEPTIDE TRANSPORTER 1)	At3g54140.1	AtPTR1-5'-BspHI-f AtPTR1-3'-BspHI-r	TCATGATGATGGAAGAAAAAGATGTGTATAC TCATGACATGTGCTCGACCAACAG
PTR2 (PEPTIDE TRANSPORTER 2)	At2g02040.1	AtPTR2-B-5'-NcoI-f AtPTR2-B-3'-NcoI-r	CCATGGGTTCCATCGAAGAAGAAG CCATGGCCGACGAAGCTTTCTTTTG
PTR6 (PEPTIDE TRANSPORTER 6)	At1g62200.1	AtPTR6-5'-NcoI-f AtPTR6-3'-NcoI-r AtPTR6-mut-f AtPTR6-mut-r	CCATGGTGAATTCGAATGAAGAAGAC CCATGGCCAAAGCCTTCTTCTTTG CCAACCCTTGGAAGCTATGTACTGTAACTC GCTTCCAAGGGTTGGAAAAAGCAC

Primers used for cloning of (human) amyloid precursor protein

Table 13: Primers used for cloning of HsAPP-constructs.

Primer	Primer sequence (5'→3')
HsAPP695Ara-Linker-r	CCTTAGGCAAATTCTTAGCTTGCCTTTCTGCTTCTTCCCACT CTCTCATAACTTGTGACATTCTTTCTCTGTG
HsAPP695Ara-Linker-f	GAATTTGCCTAAGGCCGATAAGAAGGCTGTGATCCAGCATTT TCAAGAGAAGGTGGAGTCTTTGGAGCAAGAG
HsAPP695Ara-5'-PciI-f	ACATGTTGCCTGGATTGGCTCTC
HsAPP695Ara-3'-NcoI-r_wob	CCATGGCTCMATTCTGCATCTGTTC

4.1.2 Vectors

4.1.2.1 Donor and destination vectors

Table 14: Donor- and destination-vectors used in this work.

Vector	Description	Selection marker		Reference
		Bact.	Plant	
pJet1.2/blunt	Entry vector for classical cloning	AMP	--	Invitrogen™
pENTR™/D-TOPO®	Gateway entry vector	KAN	--	Invitrogen™
pCS120	$35S_{Pro}$:GFP*(NcoI)* NosT	AMP	--	Dotzauer et al., 2010
pSS87	$35S_{Pro}$:*(NcoI)*GFP NosT	AMP	--	Schneider et al., 2012b
pBASTA-GUS	(Gateway)-GUS NosT	AMP	BASTA	Rottmann et al., 2016
pBASTA-GFP	(Gateway)-GFP NosT	AMP	BASTA	Rottmann et al., 2016
pSB30	(*Asc*I)$35S_{Pro}$:*(Nco*I*)*GFP(*Spe*I/*Xba*I) NosT	AMP	--	Schneider et al., 2012b
pSS59	(*Asc*I)$35S_{Pro}$:INT1(CDS)(*Spe*I/*Xba*I) NosT	KAN	BASTA	Sabine Schneider, unpublished
pSW110	$35S_{Pro}$:*(NcoI)*C(INT1)-GFP NosT	AMP	--	Wolfenstetter et al., 2012
pAR01	$35S_{Pro}$:*(NcoI)*C(INT4)-GFP NosT	AMP	--	Reupke, 2011
pMDC43	$2x35S_{Pro}$:GFP6-(Gateway) NosT	KAN	Hyg	Curtis and Grossniklaus, 2003
pMDC83	$2x35S_{Pro}$:(Gateway)-GFP6 NosT	KAN	Hyg	Curtis and Grossniklaus, 2003
pSE35e-C	$35S_{Pro}$:(*Nco*I)RFP NosT	AMP	--	Eichhorn, 2008

Selection markers indicate resistances towards antibiotics or herbicides for selection of transformed bacteria or plants.

4.1.2.2 Generated Vectors

Table 15: Vectors encoding AP4-adaptins and AP4-reporter fusions.

Amplificate (template)	Primer combination	Entry vector	Destination vector	Resulting construct	Plasmid name
AP4μ$_{Pro}$:AP4μ (gDNA)	AP4μ-Prom-GW-f AP4μ-GW-r	pENTR™/ D-TOPO®	pBASTA-GFP pBASTA-GUS	*AP4μ$_{Pro}$:AP4μ-GFP* *AP4μ$_{Pro}$:AP4μ-GUS*	pCM147 pCM148
AP4μ (cDNA)	AP4μ-5'-BspHI-f AP4μ-3'-BspHI-r	pJET1.2/ blunt	pCS120	*35S$_{Pro}$:AP4μ-GFP*	pCM150
	AP4μ-mut-f AP4μ-mut-r		pSS87	*35S$_{Pro}$:GFP-AP4μ*	pCM151
AP4ß (cDNA)	AP-4ß cDNA-NcoI-F AP-4ß cDNA-NcoI-R	pJET1.2/ blunt	pCS120 pSS87	*35S$_{Pro}$:AP4ß-GFP* *35S$_{Pro}$:GFP-AP4ß*	pCM77 pCM78

All vectors were obtained using classical or gateway cloning. PCR fragments were obtained using the indicated primer combination and either genomic *Arabidopsis* DNA (gDNA) or complementary *Arabidopsis* DNA (cDNA) as the template. Each PCR fragment was cloned into the indicated entry vector, verified by sequencing, and recombined into GW-compatible destination vectors (pBASTA-GFP, pBASTA-GUS), or excised from the donor vector using restriction enzymes indicated by the primer name and ligated into the destination vectors (pCS120, pSS87).

Table 16: Donor- and expression vectors encoding NRAMP3 (At2g23150.1) and NRAMP4 (AT5G67330.1) fragments and *N*-terminal mutants.

Primer combination	Entry vector	Destination vector	Resulting construct	Plasmid name
AtNRAMP3-5'NcoICC-f AtNRAMP3-3'NcoI-r	pJET1.2/ blunt	pCS120	*35S$_{Pro}$:NRAMP3-GFP*	pCM210
		pSS87	*35S$_{Pro}$:GFP-NRAMP3*	pCM211
		pSB30	*(AscI)35S$_{Pro}$:NRAMP3-GFP(SpeI/XbaI)*	pCM263
		pSS59	*35S$_{Pro}$:NRAMP3-GFP*	pCM265
		pSE35e-C	*35S$_{Pro}$:NRAMP3-RFP*	pCM210R
		pSW110	*35S$_{Pro}$:NRAMP3-C(INT1)-GFP*	pCM215
AtNRAMP4-5'-PciI-f AtNRAMP4-3'-PciI-r	pJET1.2/ blunt	pCS120	*35SPro:NRAMP4-GFP*	pCM132
		pSS87	*35S$_{Pro}$:GFP-NRAMP4*	pCM133
		pSB30	*(AscI)35S$_{Pro}$:NRAMP3-GFP(SpeI/XbaI)*	pCM264
		pSS59	*35S$_{Pro}$:NRAMP3-GFP*	pCM266
		pSE35e-C	*35S$_{Pro}$:NRAMP4-RFP*	pCM132R
		pSW110	*35S$_{Pro}$:NRAMP4-C(INT1)-GFP*	pCM217
NRAMP3-5'NcoI-LLI/AAA-f AtNRAMP3-3'NcoI-r	pJET1.2/ blunt	pCS120	*35S$_{Pro}$:NRAMP3$_{LLI→AAA}$-GFP*	pCM241
AtNRAMP3-5'NcoICC-f NRAMP3-HIV/AAA-f NRAMP3-HIV/AAA-r AtNRAMP3-3'NcoI-r	pJET1.2/ blunt	pCS120	*35S$_{Pro}$:NRAMP3$_{HIV→AAA}$-GFP*	pCM243

NRAMP3-5'NcoI-10L/A-f AtNRAMP3-3'NcoI-r	pJET1.2/blunt	pCS120	*35S$_{Pro}$:NRAMP3$_{L10A}$-GFP*	pCM274
NRAMP3-5'NcoI-11L/A-f AtNRAMP3-3'NcoI-r	pJET1.2/blunt	pCS120	*35S$_{Pro}$:NRAMP3$_{L11A}$-GFP*	pCM275
NRAMP3-5'NcoI-12I/A-f AtNRAMP3-3'NcoI-r	pJET1.2/blunt	pCS120	*35S$_{Pro}$:NRAMP3$_{I12A}$-GFP*	pCM276
NRAMP4-5'PciI-LLA/AAA-f AtNRAMP4-3'-PciI-r	pJET1.2/blunt	pCS120	*35S$_{Pro}$:NRAMP4$_{LL\rightarrow AA}$-GFP*	pCM247
AtNRAMP4-5'-PciI-f NRAMP4-LIV/AAA-f NRAMP4-LIV/AAA-r AtNRAMP4-3'-PciI-r	pJET1.2/blunt	pCS120	*35S$_{Pro}$:NRAMP4$_{LIV\rightarrow AAA}$-GFP*	pCM249
AtNRAMP3-5'NcoICC-f	pJET1.2/blunt	pSW110	*35S$_{Pro}$:NRAMP3ΔC43-C(INT1)-GFP*	pCM220
AtNRAMP3-C43-3'GNcoI-r		pAR01	*35S$_{Pro}$:NRAMP3ΔC43-C(INT4)-GFP*	pCM225
AtNRAMP4-5'-PciI-f	pJET1.2/blunt	pSW110	*35S$_{Pro}$:NRAMP4ΔC50-C(INT1)-GFP*	pCM223
AtNRAMP4-C50-3'GNcoI-r		pAR01	*35S$_{Pro}$:NRAMP4ΔC50-C(INT4)-GFP*	pCM227
NRAMP3-5'-NcoIC-DeltaN(30)-f AtNRAMP3-3'NcoI-r	pJET1.2/blunt	pCS120	*35S$_{Pro}$:Met.Alα.ΔN30NRAMP3-GFP*	pCM258

All vectors were generated via classical cloning. PCR fragments were obtained using the indicated primer combination (removing stop-codons and introducing restriction sites indicated by the primer names). Each PCR fragment was cloned into the indicated entry vector, verified by sequencing, excised from the donor vector using appropriate enzymes, and ligated into the destination vectors given.

Table 17: Other donor- and expression vectors generated via classical cloning.

PCR fragment	Primer combination	Entry vector	Destination vector	Resulting construct	Plasmid name
MTP1	AtMTP1-mut-f AtMTP1-mut-r	pJET1.2/blunt	pCS120	*35S$_{Pro}$:MTP1-GFP*	pCM36
	AtMTP1-5'-NcoI-f AtMTP1-3'-NcoI-r		pSS87	*35S$_{Pro}$:GFP-MTP1*	pCM37
ZIF1	AtZIF1-5'-NcoI-f AtZIF1-3'-NcoI-r	pJET1.2/blunt	pCS120 pSS87	*35S$_{Pro}$:ZIF1-GFP* *35S$_{Pro}$:GFP-ZIF1*	pCM44 pCM45

APY1	AtAPY1-5'-BspHI-f AtAPY1-3'-BspHI-r	pJET1.2/blunt	pCS120 pSS87	*35S$_{Pro}$:APY1-GFP* *35S$_{Pro}$:GFP-APY1*	pCM67 pCM68
APY2	AtAPY2-5'-BspHI-f AtAPY2-3'-BspHI-r AtAPY2-mut-f AtAPY2-mut-r	pJET1.2/blunt	pCS120 pSS87	*35S$_{Pro}$:APY2-GFP* *35S$_{Pro}$:GFP-APY2*	pCM98 pCM99
MDR	AtMDR1-5'-PciI-f AtMDR1-3'-PciI-r	pJET1.2/blunt	pCS120 pSS87	*35S$_{Pro}$:MDR1-GFP* *35S$_{Pro}$:GFP-MDR1*	pCM100 pCM101
ALS1	AtALS1-5'-NcoI-f AtALS1-3'-NcoI-r	pJET1.2/blunt	pCS120	*35S$_{Pro}$:ALS1-GFP*	pCM79
SYP122	AtSYP122-5'-BspHI-f AtSYP122-3'-BspHI-r	pJET1.2/blunt	pCS120 pSS87	*35S$_{Pro}$:SYP122-GFP* *35S$_{Pro}$:GFP-SYP122*	pCM136 pCM137
SYP132	AtSYP132-5'-NcoI-f AtSYP132-3'-NcoI-r	pJET1.2/blunt	pCS120 pSS87	*35S$_{Pro}$:SYP132-GFP* *35S$_{Pro}$:GFP-SYP132*	pCM188 pCM189
CAT9	AtCAT9-5'-NcoI-f AtCAT9-3'-NcoI-r	pJET1.2/blunt	pCS120 pSS87	*35S$_{Pro}$:CAT9-GFP* *35S$_{Pro}$:GFP-CAT9*	pCM173 pCM174
NRT1.1	AtNRT1.1-5'-PciI-f AtNRT1.1-3'-PciI-r	pJET1.2/blunt	pCS120 pSS87	*35S$_{Pro}$:NRT1.1-GFP* *35S$_{Pro}$:GFP-NRT1.1*	pCM176 pCM177
PTR1	AtPTR1-5'-BspHI-f AtPTR1-3'-BspHI-r	pJET1.2/blunt	pCS120 pSS87	*35S$_{Pro}$:PTR1-GFP* *35S$_{Pro}$:GFP-PTR1*	pCM182 pCM183
PTR2	AtPTR2-B-5'-NcoI-f AtPTR2-B-3'-NcoI-r	pJET1.2/blunt	pCS120 pSS87	*35S$_{Pro}$:PTR2-GFP* *35S$_{Pro}$:GFP-PTR2*	pCM134 pCM135
PTR6	AtPTR6-5'-NcoI-f AtPTR6-3'-NcoI-r AtPTR6-mut-f AtPTR6-mut-r	pJET1.2/blunt	pCS120 pSS87	*35S$_{Pro}$:PTR6-GFP* *35S$_{Pro}$:GFP-PTR6*	pCM63 pCM64

PCR fragments were obtained using the indicated primer combination. *Arabidopsis* cDNA was used as the template in all PCRs. The name of the PCR fragment is given in the first column and corresponds to the name of the gene of which the CDS was amplified. Stop-codons were removed. Each PCR fragment was cloned into the indicated entry vector. Entry clones were sequenced and the insert (corresponding to the PCR fragment) excised using restriction enzymes indicated by the name of the primers and ligated into the target vectors.

Table 18: Other donor- and expression vectors generated via gateway cloning.

PCR fragment	Primer combination	Entry vector	Destination vector	Resulting construct	Plasmid name
PIP2;1	AtPIP2A-GW-f AtPIP2Acds+861r	pENTR™ /D-TOPO®	pMDC43 pMDC83	*2x35S$_{Pro}$:GFP6-PIP2;1* *2x35S$_{Pro}$:PIP2;1-GFP6*	pCM158 pCM159
STP1	AtSTP1+1f_5'CACC AtSTP1g+2671r	pENTR™/ D-TOPO®	pMDC43 pMDC83	*2x35S$_{Pro}$:GFP6-STP1* *2x35S$_{Pro}$:STP1-GFP6*	pCM156 pCM157

PCR fragments were obtained using the indicated primer combination. *Arabidopsis* cDNA was used as the template in all PCRs. The name of the PCR fragment is given in the first column and corresponds to the name of the gene of which the CDS was amplified. Stop-codons were removed. Each fragment was cloned into the indicated entry vector, verified by sequencing, and recombined into the indicated destination vectors. The amplification and cloning of STP1 was performed by Nina Danzberger yielding pND077b.

4.1.2.3 Other Vectors

Table 19: Other vectors used in this work.

Name	Vector	Selection marker (bact.)	Insert	Reference
MOT2-GFP	GFP2	AMP	*35S$_{Pro}$:MOT2-GFP*	Gasber et al., 2011
CD3-967	pBIN20	KAN	*d35S$_{Pro}$:GmMan1-mCherry*	Nelson et al., 2007
Wave13R	pNIGEL17	AMP	*UBQ10$_{Pro}$:VTI12-mCherry*	Geldner et al., 2009
Wave22R	pNIGEL17	AMP	*UBQ10$_{Pro}$:SYP32-mCherry*	Geldner et al., 2009
pSW53	pSS87	AMP	*35S$_{Pro}$:GFP-INT1*	Wolfenstetter et al., 2012
pSS74	pSEe35-C	AMP	*35S$_{Pro}$:INT4-RFP*	Wolfenstetter et al., 2012
pND077b	pENTR™/ D-TOPO®	KAN	*STP1* CDS (no stop; Gateway entry clone)	Nina Danzberger, unpublished
KR61-7 (=pEX-A2-5'APP)	pEX-A2	KAN	*HsAPP695Ara1* (*Arabidopsis* optimized HsAPP - 5' fragment)	Eurofins Genomics, Ebersberg, D
KS05-17 (=pEX-A2-3'1000 bisStop)	pEX-A2	KAN	*HsAPP695Ara1* (*Arabidopsis* optimized HsAPP - 3' fragment)	Eurofins Genomics, Ebersberg, D

4.1.3 Organisms

4.1.3.1 Escherichia coli

Original strains, untransformed

Table 20: Original *E. coli* strains.

Strain	Marker	Reference
DH5α	*deo*R, *end*A1, *gyr*A96, *hsd*R17(r_k-, m_k+), recA1, *rel*A1, *sup*E44, *thi*-1,Δ(*lac*ZYA-*arg*F)U169, Ø80*lac*/ΔM15,F-, λ-	Hanahan, 1983
DB3.1™	F-, *gyr*A462, endA1, *gln*V44Δ(sr1-recA), mcrB, mrr, *hsd*S20(r_B-, m_B-), ara14, *gal*K2, *lac*Y1, *pro*A2, *rps*L20(Sm^r), xyl5, Δleu, mtl1	Invitrogen™

Own strains

All generated plasmids (4.1.2.2) were transformed into *Escherichia coli* strain DH5α.

4.1.3.2 Agrobacterium tumefaciens

Original strains, untransformed

Table 21: Original *A. tumefaciens* strains.

Strain	Marker	Plasmid	Marker	Reference
C58C1	--	--	--	Deblaere et al., 1985
GV3101	C58C1, Rif	pMP90	Gent	Holsters et al., 1980; Koncz et al., 1992

Agrobacterium tumefaciens strains generated in this work

Table 22: *A. tumefaciens* strains generated in this work.

Name	Strain	Plasmid	Reference
A-pCM147	C58C1	pCM147	this work
A-pCM148	C58C1	pCM148	this work
A-pCM265	GV3101	pCM265	this work
A-pCM266	GV3101	pCM266	this work

4.1.3.3 Arabidopsis thaliana

Wild-type

Table 23: *Arabidopsis thaliana* WT used in this work.

Name / Ecotype	Reference
Columbia-0	*Arabidopsis* sequencing project, LEHLE SEEDS, Round Rock, USA

Lines generated in this work

Table 24: *Arabidopsis thaliana* T-DNA lines obtained via stable transformation.

Name	Background	Plasmid (construct)	Herbicide resistance
ap4μ/AP4$_{Pro}$:AP4μ-GFP	*ap4μ* (SALK_014326)	pCM147 (*AP4μ$_{Pro}$:AP4μ-GFP*)	Basta
ap4μ/AP4$_{Pro}$:AP4μ-GUS	*ap4μ* (SALK_014326)	pCM148 (*AP4μ$_{Pro}$:AP4μ-GUS*)	Basta
ap4μ/35S$_{Pro}$:NRAMP3-GFP	*ap4μ* (SALK_014326)	pCM265 (*35S$_{Pro}$:NRAMP3-GFP*)	Basta
Col-0/35S$_{Pro}$:NRAMP3-GFP	Col-0	pCM265 (*35S$_{Pro}$:NRAMP3-GFP*)	Basta
nramp3-1 nramp4-1/ 35S$_{Pro}$:NRAMP3-GFP	*nramp3-1 nramp4-1*	pCM265 (*35S$_{Pro}$:NRAMP3-GFP*)	Basta
ap4μ/35S$_{Pro}$:NRAMP4-GFP	*ap4μ* (SALK_014326)	pCM266 (*35S$_{Pro}$:NRAMP4-GFP*)	Basta
Col-0/35S$_{Pro}$:NRAMP4-GFP	Col-0	pCM266 (*35S$_{Pro}$:NRAMP4-GFP*)	Basta
nramp3-1 nramp4-1/ 35S$_{Pro}$:NRAMP4-GFP	*nramp3-1 nramp4-1*	pCM266 (*35S$_{Pro}$:NRAMP4-GFP*)	Basta

T-DNA Insertion Lines

Table 25: T-DNA insertion lines used in this work.

Name	Locus, Gene	Background	Reference
ap4μ (SALK_014326) (*gfs5-3*)	At4g24550 *AP4μ*	Col-0	NASC, Loughborough, UK (N514326); Alonso et al., 2003; Fuji et al., 2016; this work
ap4ß-2 (SAIL_796_A10) (*gfs4-3*)	At5g11490 *AP4ß*	Col-0	NASC, Loughborough, UK (N835621); Alonso et al., 2003; Müdsam, 2012; Fuji et al., 2016
ap4ß-1 (SAIL_781_H01) (*gfs4-4, ap-4ß*)	At5g11490 *AP4ß*	Col-0	NASC, Loughborough, UK (N834984); Alonso et al., 2003; Müdsam, 2012; Fuji et al., 2016; Pertl-Obermeyer et al., 2016
ap4ß-2 ap4μ	At5g11490 At4g24550	--	This work

ap3ß (SAIL_1258_G03)	At3g55480 *AP3ß*	Col-0	NASC, Loughborough, UK (N846552); Feraru et al., 2010
nramp3-1 (SALK_023049)	At2g23150 *NRAMP3*	Col-0	NASC, Loughborough, UK (N523049); Molins et al., 2013
nramp4-1 (SALK_085986)	At5g67330 *NRAMP4*	Col-0	NASC, Loughborough, UK (N585986); Molins et al., 2013
nramp3-1 nramp4-1	At2g23150 At5G67330	--	Molins et al., 2013

Other lines obtained by crossing

Table 26: Marker lines obtained in this work via crossing with *ap4ß-1*.

Name	Construct of marker plant	Reference (Marker line)
ap4ß-1 x DR5$_{Pro}$:GUS	*DR5$_{Pro}$:GUS*	Ulmasov et al., 1997
ap4ß-1 x DR5$_{Pro}$:GFP	*DR5$_{Pro}$:GFP*	Ottenschläger et al., 2003
ap4ß-1 x PIN1$_{Pro}$:PIN1-GFP	*PIN1$_{Pro}$:PIN1-GFP*	Benková et al., 2003
ap4ß-1 x PIN2$_{Pro}$:PIN2-GFP	*PIN2$_{Pro}$:PIN2-GFP*	Xu and Scheres, 2005
ap4ß-1 x PIN3$_{Pro}$:PIN3-GFP	*PIN3$_{Pro}$:PIN3-GFP*	Dello Ioio et al., 2008
ap4ß-1 x PIN7$_{Pro}$:PIN7-GFP	*PIN7$_{Pro}$:PIN7-GFP*	Blilou et al., 2005

4.1.4 Growth media for bacteria and plants

4.1.4.1 Growth media for cultivation of bacteria

Luria Broth (Luria, 1960)

Table 27: Composition of Lysogeny broth (LB-medium).

Component	Final concentration
Bacto®-Tryptone	1% (w/V)
Bacto®-Yeast Extract	0.5% (w/V)
NaCl	1% (w/V)
Agar-Agar (for solid medium only)	1.5% (w/V)

4.1.4.2 Growth media for cultivation of plants

Synthetic media for cultivation of Arabidopsis thaliana

Table 28: Composition of Murashige and Skoog (MS-medium; Murashige and Skoog, 1962).

Component	Final concentration
Murashige&Skoog Medium (including vitamins and MES 0.05%)	0.49% (w/V)
Sucrose	0–2%
pH adjusted to 5.7 with 1 M KOH	
Phytoagar	0.8% (w/V)

Table 29: Composition of ABIS medium.

Component	Final concentration
H_3PO_4	2.5 mM
KNO_3	5 mM
$MgSO_4$	2 mM
$Ca(NO_3)_2$	1 mM
Murashige and Skoog microelements (Murashige and Skoog, 1962)	1 x
Sucrose	1% (w/V)
MES	1 mM
pH adjusted to 6.1 with 1M KOH	
Phytoagar	0.7% (w/V)

For iron-sufficient medium 50 µM FeHBED was added after autoclaving (+Fe). FeHBED was prepared as a 10 mM stock solution from $FeCl_3$ (Sigma-Aldrich, Steinheim, D) and HBED [N,N'-di(2-hydroxybenzyl)ethylenediamine-N,N'diacetic acid monochloride hydrate; Strem Chemicals, Newburyport, USA]. HBED was added with a 10% excess to ensure that all Fe was chelated. To deplete the medium of iron, FeHBED was omitted and 50 µM ferrozine [3-(2-pyridyl)-5,6-bis(4-phenyl-sulfonic acid)-1,2,4-triazine] was added to chelate any residual iron (-Fe).

Cultivation soil for Arabidopsis thaliana

- 65% composted soil (type “P”, Fruhstorfer Erde, Archut, Lauterbach, D)
- 25% sand
- 15% lava granules

4.1.4.3 Antibiotic and herbicide stock solution

Table 30: Antibiotic and herbicide stock solutions.

Antibiotic	Stock concentration	Final concentration
Ampicillin	100 mg/mL	100 µg/mL
Kanamycin	50 mg/mL	50 µg/mL
Streptomycin	20 mg/mL	20 µg/mL
Spectinomycin	50 mg/mL	50 µg/mL
Rifampicin	50 mg/mL	50 µg/mL
Gentamycin	25 mg/mL	25 µg/mL
Glufosinate-ammonium	12 mg/mL	12 µg/mL

Antibiotics were prepared as aqueous solution, sterile filtered, and added to autoclaved media.

4.1.5 Solutions and buffers

4.1.5.1 Solutions for alkaline lysis procedure

S1	50 mM	Tris/HCl (from 1 M stock at pH 7.5)
	10 mM	EDTA (from 0.5 M stock at pH 8.0)
	100 µg/mL	RNAse A
	stored at 4 °C	
S2	0.2 M	NaOH
	1% (w/V)	SDS
	stored at RT	
S3	2.8 M	KAc
	adjusted to pH 5.1 with HAc	
	stored at 4 °C	

4.1.5.2 Solutions and buffers for transformation of protoplasts from **A. thaliana**

Digestion buffer	0.03% (w/V)	Pectolyase Y23
	0.75% (w/V)	Cellulase YC
	in MCP, freshly prepared for each experiment	
MaMg-buffer	400 mM	Sorbitol
	15 mM	$CaCl_2$ (or $MgCl_2$)
	5 mM	MES
	adjusted to pH 5.6 with KOH	

MCP	500 mM	Sorbitol
	1 mM	$CaCl_2$
	10 mM	MES adjusted to pH 5.6–6.0 with KOH
PEG-CMS-buffer	400 mM	Sorbitol
	100 mM	$Ca(NO_3)_2$
	40% (w/V)	PEG 4000
	adjusted to pH 8.0 with KOH over several days	
W5-buffer	154 mM	NaCl
	125 mM	$CaCl_2$
	5 mM	KCl
	5 mM	Glucose
	1.5 mM	MES
	adjusted to pH 5.6 with KOH	
Sorbitol for Barley	400 mM	Sorbitol
	30 mM	KCl
	20 mM	HEPES
	adjusted to pH 7.2 with KOH	
Lysis buffer	200 mM	Sorbitol
	20 mM	EDTA
	10 mM	HEPES
	adjusted to pH 8.0 with KOH	
	10%	Ficoll (dissolved at 4°C)

4.1.5.3 Other solutions and buffers

Ethidium bromide (EtBr) stock solution	10 mg/mL in H_2O	
Loading Dye (10x)	100 mM	EDTA (from 0.5 M stock at pH 8.0)
	60%	Glycerol
	0.25%	Bromophenol blue
	0.25%	Xylene xyanol
TE-buffer	10 mM	Tris / HCl (from 1 M stock at pH 7.5)
	1 mM	EDTA (from 0.5 M stock at pH 8.0)
TAE	40 mM	Tris
	20 mM	HAc
	1 mM	EDTA (at pH 8.0)

Agarose Gel	1% (w/V)	Agarose
	heated in TAE to dissolve agarose	
DNA-Extraction buffer	200 mM	Tris / HCl (from 1 M stock at pH 8.0)
	250 mM	NaCl
	25 mM	EDTA (from 0.5 M stock at pH 8.0)
	0.5% (w/V)	SDS
Sterilisation solution for seeds	1 : 1 dilution of DanKlorix and H_2O	
	0.05% (w/V)	Tween 20
Alexander stain (for pollen)	10 ml	Ethanol
	1 ml	Malachite green (1% (w/V) in ethanol)
	5	Fuchsin acid (1% in H_2O)
	0.5 mL	Orange G (1% in H_2O)
	5 g	Phenol
	5g	Chloral hydrate
	2 ml	Acetic acid
	25 mL	Glycerol
	50 mL	ddH_2O
	stored in the dark at 4 °C	
PBS/EGTA or PBST/EGTA	139 mM	KCl
	10 mM	K_2HPO_4
	2 mM	KH_2PO_4
	0.1% (V/V)	Triton X-100 (for PBST only)
	pH adjusted to 7.3–7.4 with HCl	
	50 mM	EGTA (from 0.5 M stock adjusted to pH 7.5 with KOH)

4.1.6 Consumables, Chemicals and Enzymes

- 325PCellulose (AA Packaging Limited, Preston, UK)
- Adhesion Miscroscope Slides, Histobond (Marienfeld, Lauda-Königshofen, D)
- Agar-Agar (Difco Laboratories, Detroit, USA)
- Agarose (Invitrogen, Darmstadt, D)
- Bacto® Peptone (Difco Laboratories, Detroit, USA)
- Bacto® Tryptone (Difco Laboratories, Detroit, USA)
- Bacto® Yeast Extract (Difco Laboratories, Detroit, USA)
- Basta® (Bayer AG, Leverkusen, D)
- Bovine serum albumin - fraction V (BSA) (New England Biolabs, Frankfurt, D)
- Calf Intestine Alkaline Phosphatase (CIP) (Roche, Mannheim, D)
- Cellulase (Serva-Elektrophoresis, Heidelberg, D)
- CloneJET™ PCR Cloning Kit (Fermentas, St.Leon-Rot, D)

- DanChlorix (Colgate-Palmolive, Hamburg, D)
- Deoxynucleotide Triphosphates (dNTPs) (Fermentas, St.Leon-Rot, D)
- ExTaq (TaKaRa Shuzo co., Ltd., Shiga, JP)
- FastGene Optima HotStart Ready Mix (Nippon Genetics Europe, Düren, D)
- Ficoll (Fluka, Taufkirchen, D)
- Gateway® LR Clonase™ II Enzyme Mix (Invitrogen, Darmstadt, D)
- Gentamycin (Duchefa, Haarlem, NL)
- High capacity RNA-to-cDNA Master Mix (applied biosystems, Foster City, USA)
- innuPREP DOUBLEpure Kit (analytikjena, Jena, D)
- Lamda DNA [(dam-, dcm-), λ-DNA digested with *Cla*I was used as DNA-size-standard for gel-electrophoresis] (New England Biolabs, Frankfurt, D)
- Leukopor Tape (BSN medical, Hamburg, D)
- Ligase, T4 DNA-Ligase (New England Biolabs, Frankfurt, D)
- Murashige & Skoog medium incl. vitamins/MES (Duchefa, Haarlem, NL)
- NEB buffer system for enzymatic digestion of DNA (New England Biolabs, Frankfurt, D)
- NEB Thermopol buffer for Taq-DNA-polymerase (New England Biolabs, Frankfurt, D)
- NEB-Taq-DNA-Polymerase (New England Biolabs, Frankfurt, D)
- NucleoBond® Kit AX 100 for plasmid purification (Macherey-Nagel, Düren, D)
- pENTR™/D-TOPO®-Cloning-Kit (Invitrogen, Darmstadt, D)
- Pectolyase Y-23 from *Aspergillus japonicus* (MP Biomedicals, Eschwede, D)
- Phusion™ High-Fidelity DNA-Polymerase (New England Biolabs, Frankfurt, D)
- Phusion™ Hot-Start High-Fidelity DNA-Polymerase (New England Biolabs, Frankfurt, D)
- Phytagar (Duchefa, Haarlem, NL)
- Proteinase K (Invitrogen, Darmstadt, D)
- Restriction enzymes (New England Biolabs, Frankfurt; and Fermentas, St. Leon-Rot; D)
- SeaPlaque® GTG® agarose, low melting temperature agarose (BioWhittaker Molecular Applications, Rockwell, USA)
- Square pots for *Arabidopsis* cultivation (Pöppelmann- TEKU®, Lohne, D)
- Silwet (Lehle Seeds, Round Rock, USA)
- ThermoTube™ PCR-Reactiontubes, 0.2 ml, ultra thin (Peqlab, Erlangen, D)
- TOPO® Cloning Kit (Invitrogen, Darmstadt, D)
- Triton X-100 (Serva, Heidelberg, D)
- Trizol® Reagent (Invitrogen, Darmstadt, D)
- TaKaRa Ex Taq™ Kit (TAKARA BIO INC., Otsu, JP)
- X-Gal (5-Brom-4-Chlor-3-indolyl-β-D-galaktopyranosid) (Applichem, Darmstadt, D)

Standard laboratory consumables (reaction tubes, petri dishes, pipette tips etc.) were purchased from Sarstedt AG & Co (Nümbrecht, D), Greiner (Nürtingen, D) or Roth

(Karlsruhe, D). Chemicals not listed, were purchased from Merck (Darmstadt, D), Roth (Karlsruhe, D) or Sigma-Aldrich (Steinheim, D).

4.1.7 Instruments

- Benchtop Centrifuge 5417C (Eppendorf, Hamburg, D)
- Confocal Laser Scanning Microscope Leica TCS SP5 (Leica, Wetzlar, D)
- LAS AF Version 2.7.29586 (Leica, Wetzlar, D)
- Cooling Centrifuge Avanti J-25 (Beckman Instruments, Palo Alto, USA)
- Diaphragm vacuum pump (Vacuumbrand, Wertheim, D)
- Digital Camera Sony α500 DSLR-A500L (Sony, Tokio, JP)
- HPLC: DIONEX ICS 3000 (Dionex, Idstein, D)
- Nanophotometer P330 (Implen, Munic, D)
- PCR-Machine T3000 Thermocycler (Biometra, Göttingen, D)
- PCR-Machine T-Gradient (Biometra, Göttingen, D)
- Platform Shaker (New Brunswick Scientific, Nürtingen, D)
- Speed Vac Eppendorf Concentrator 5301 (Eppendorf, Mississauga, CAN)
- Thermocabinet Function line (Heraeus instruments, Hanau, D)
- Thermomixer 5436 (Eppendorf, Hamburg, D)
- Thermomixer compact (Eppendorf, Hamburg, D)
- TissueLyser II (QIAGEN, Hilden, D)
- UV/Visible Spectrophotometer Ultrospec 2100 Pro (Biochrome LTD., Cambridge, UK)

4.1.8 Software

- ImageJ 1.44p (Schneider et al., 2012a)
- FiJi (Schindelin et al., 2012)
- LAS AF Version 2.7.29586 (Leica, Wetzlar, D)
- Microsoft Office 2010, and 365 (Microsoft Corporation, Remond, USA)
- Vector NTI Advance v11.5.2 (Lu and Moriyama, 2004)

4.1.9 Websites

- BLAST: Basic Local Alignment Search Tool (https://blast.ncbi.nlm.nih.gov/Blast.cgi)
- eFP browser (http://bar.utoronto.ca/efp/cgi-bin/efpWeb.cgi)
- Expasy Compute pI/Mw tool (http://web.expasy.org/compute_pi/)
- Genevestigator (https://www.genevestigator.ethz.ch)
- GenomeNet Database Resources - MOTIF Search (http://www.genome.jp/tools/motif/MOTIF2.html)
- JGI genome portal (for sequences of PtNRAMP3.1 and PtNRAMP3.2)

(http://genome.jgi.doe.gov/Poptr1_1/Poptr1_1.home.html)

- NASC - The European *Arabidopsis* Stock Centre (*Arabidopsis* photograph collection) (http://arabidopsis.info/InfoPages?template=photopage;web_section=germplasm)
- LocSigDB - A catalog of protein sorting signals (http://genome.unmc.edu/LocSigDB/index.html)
- Phenopsis DB (*Arabidopsis thaliana* phenotyping database) (http://bioweb.supagro.inra.fr/phenopsis/)
- PhosPhAt 4.0 - The *Arabidopsis* Protein Phosphorylation Site Database (Heazlewood et al., 2008; Durek et al., 2009) http://phosphat.uni-hohenheim.de/
- Protter - interactive protein feature visualization (http://wlab.ethz.ch/protter/start/)
- RARGE: RIKEN *Arabidopsis* Genome Encyclopedia (http://rarge-v2.psc.riken.jp/)
- RIKEN *Arabidopsis* Phenome Information Database (http://rarge-v2.psc.riken.jp/phenome/) (Kuromori et al., 2006)
- Standardardized kinesin nomenclature (https://labs.cellbio.duke.edu/Kinesin/Nomenclature_Details.html)
- TAIR: The Arabidosis Information Resource (http://www.arabidopsis.org/)
- T-DNA Express: *Arabidopsis* Gene Mapping Tool (http://signal.salk.edu/cgi-bin/tdnaexpress)
- TMHMM Server v. 2.0: Prediction of transmembrane helices in proteins (http://www.cbs.dtu.dk/services/TMHMM/)

4.2 Methods

4.2.1 Growth of organisms

4.2.1.1 Bacteria

Cultivation

E. coli were cultivated at 37 °C, *A. tumefaciens* at 29 °C in liquid or on solid LB-medium (4.1.4.1) with appropriate antibiotics (4.1.4.3). When grown in liquid medium, the tubes or flasks were constantly shaken or spun to guarantee optimal mixing and air supply.

Preparation of long-term cultures

In a sterile 2 mL screw-cap micro tube, 200 µL of an 80% glycerol (aq) solution were added to 800 µL of the appropriate ONC to obtain a final concentration of 15% glycerol. The suspension was mixed thoroughly, frozen on liquid N_2 and stored at -80 °C.

4.2.1.2 Plants

Growth on soil

Non-sterile *Arabidopsis* seeds were distributed on thoroughly wetted cultivation soil (4.1.4.2). Pots were initially covered with cling film to inhibit the material from drying. Seeds were stratified at 4 °C in the dark for three days prior to further cultivation. Generally, seedlings were cultivated under SD-conditions (8 h light / 16 h dark, ca. 22 °C, 60% humidity) for four to six weeks, and cultivated further under LD-conditions (16 h light / 8 h dark, ca. 22 °C, 60% humidity) until full maturity.

Growth on synthetic medium

If seedlings were to be cultivated on synthetic medium (MS or ABIS medium; 4.1.4.2), seeds were sterilized according to the following protocol: a small spatula's tip worth of seeds was transferred to a 1.5 mL eppendorf tube. From this step on, the tubes were only opened under sterile conditions. 1 mL of sterilisation solution (4.1.5) was added and the samples inverted approximately every second for 4–5 min. The seeds were collected by centrifugation at 14000 rpm for 10 sec. The liquid was decanted and the seeds were washed three times with 1 mL ddH_2O, inverted and vortexed very briefly, centrifuged for 10 s at 14000 rpm and the water removed. After the final washing step, 1 mL sterile 0.1% agarose solution was added and the seeds distributed by snipping the tube. Seeds were applied to plates containing the solid medium using disposable sterile pipettes and stratified on the plates for three days at 4 °C in the dark. Seedlings on synthetic medium were cultivated under LD-conditions.

4.2.2 DNA extraction and modification

4.2.2.1 Isolation of genomic DNA from Arabidopsis thaliana

Genomic DNA was extracted using the „Quick Preparation"-method (p.114, Dissertation Pommerrenig, B., 2007). The pellet was dissolved in 100 µL ddH_2O and stored at 4 °C. Approximately 1 µL of this solution was used, if the gDNA was to serve as a template for PCR (with a total reaction volume of 20 µL).

4.2.2.2 Isolation of RNA

Approximately 50 mg plant material (usually leaves) were weighed, frozen in liquid N_2 and pulverized (TissueLyser II; QIAGEN). RNA was extracted from plant material using the trizol-reagent TRIZOL® Reagent (Invitrogen, Darmstadt, D) according to the manufacturer's instructions. The product was resuspended in 50 µL DEPC H_2O and stored at -20 °C.

4.2.2.3 Preparation of plasmid DNA

Plasmid DNA was generally obtained via alkaline lysis (for buffers and solutions see section 4.1.5). To obtain small amounts of plasmid DNA (mini plasmid DNA preparation), for example for restriction digests, ~ 1.5 mL of an *E. coli* ONC were pelleted and resuspended in 150 µL S1. Cells were lysed by adding 200 µL S2 and proteins precipitated by neutralization with 150 µL S3. After centrifugation, DNA was precipitated from the clear lysate by addition of 800 µL ethanol and subsequent centrifugation. The DNA was then washed with 70% ethanol, dried, and solved in 50 µL ddH_2O.
To obtain transfection-grade plasmid DNA (highly purified DNA with concentrations of > 1 mg/mL; "midi plasmid DNA preparation"), DNA was isolated and purified by alkaline lysis followed by anion-exchange chromatography. The NucleoBond Midi Kit AX 100 (MACHEREY-NAGEL, Düren, D) was used according to the manufacturer's instructions using 100 mL ONC culture of the appropriate *E. coli* strain as source material. If DNA was to be used for transformation of *Arabidopsis* mesophyll protoplasts (4.2.3), the product was dissolved in ddH_2O (usually 100 µL), yielding a final concentration of ≥ 1 µg/µL DNA.

4.2.2.4 Amplification of DNA-fragments via polymerase chain reaction (PCR)

To amplify DNA fragments for cloning, Phusion® High-Fidelity DNA Polymerase (Thermo Fisher Scientific, Waltham, USA) was used due to its low error rate. For genotypic analyses, or detection of transcript and the like, TaKaRa Ex Taq™, Phire Hot Start II polymerase (Thermo Fisher Scientific, Waltham, USA), or FastGene Optima HotStart Ready Mix (Nippon Genetics Europe, Düren, D) was used. The PCR conditions were based on the manufacturer's information and optimized if necessary. The annealing-temperature was chosen according to the melting temperature (T_m) of the primers and the time for elongation was set to match the expected size of the product.

Table 31: Standard PCR reaction for PCR with Phusion Polymerase.

Component	20 µL reaction	Final concentration
5x Phusion GC Buffer	4 µL	1x
10 µM forward primer	0.5 µL	0.25 µM
10 µM reverse primer	0.5 µL	0.25 µM
10 mM dNTPs	0.4 µL	0.5 µM
Template-DNA	--	20–100 ng
Phusion Polymerase [20U/µl]	0.2 µL	0.02 U/µL
ddH_2O	ad 20 µL	--

Table 32: Standard cycling protocol for PCR with Phusion Polymerase.

Cycle Step	Temperature	Duration	Cycles
Initial denaturation	98 °C	30 s	1
Denaturation	98 °C	5–10 s	40
Annealing	Primer dependent	30 s	
Extension	72 °C	15–30 s/1 kb	
Final extension	72° C 10 °C	5–10 min hold	1

Table 33: Standard PCR reaction for PCR with ExTaq Polymerase.

Component	20 µL reaction	Final concentration
ExTaq buffer	2 µL	1x
10 µM forward primer	1 µL	0.5 µM
10 µM reverse primer	1 µL	0.5 µM
10 mM dNTPs	2 µL	1 µM
Template-DNA	--	1–100 ng
ExTaq polymerase	0.1 µL	--
ddH_2O	ad 20 µL	--

Table 34: Standard cycling protocol for PCR with ExTaq Polymerase.

Cycle Step	Temperature	Duration	Cycles
Initial denaturation	98 °C	1 min	1
Denaturation	98 °C	30 s	40
Annealing	Primer dependent	15 s	
Extension	72 °C	1 min/1 kb	
Final extension	72° C 10 °C	5 min hold	1

Table 35: Standard reaction for PCR with Phire II Polymerase.

Component	20 µL reaction	Final concentration
5x Phire Reaction buffer	4 µL	1x
10 µM forward primer	1 µL	0.5 µM
10 µM reverse primer	1 µL	0.5 µM
10 mM dNTPs	1.6 µL	0.8 µM
Template-DNA	--	1–100 ng
Phire II Polymerase	0.1 µL	--
ddH_2O	ad 20 µL	--

Table 36: Standard cycling protocol for PCR with Phire II Polymerase.

Cycle Step	Temperature	Duration	Cycles
Initial denaturation	98 °C	2 min	1
Denaturation	98 °C	5 s	40
Annealing	Primer dependent	5 s	
Extension	72 °C	10–20 s /1 kb	
Final extension	72° C 10 °C	1 min hold	1

Table 37: Standard PCR reaction for PCR with Fast-Gene Optima.

Component	10 µL reaction	Final concentration
2x Fast-Gene Optima HotStart Ready Mix with dye	5 µL	1x
10 µM forward primer	0.5 µL	0.5 µM
10 µM reverse primer	0.5 µL	0.5 µM
10 mM dNTPs	1.6 µL	0.8 µM
Template-DNA	--	< 50 ng
ddH_2O	ad 10 µL	--

Table 38: Standard cycling protocol for a PCR with Fast-Gene-Optima.

Cycle Step	Temperature	Duration	Cycles
Initial denaturation	95 °C	3 min	1
Denaturation	95 °C	15 s	40
Annealing	60° C	1 s	
Extension	72 °C	1 min /1 kb	
Final extension	72° C 10 °C	5 min hold	1

4.2.2.5 Reverse-transcription

Reverse transcription was performed to obtain cDNA from isolated RNA, using the High Capacity RNA-to-cDNA Master Mix (Invitrogen™), or the QuantiTect Reverse Transcription Kit (Qiagen, Hilden, D) according to the manufacturer's instruction. 0.5–1 µg RNA was used for each reaction. The product was stored at -20 °C.

4.2.2.6 PCR-based genotyping and transcript detection

Generally, PCR-based genotyping was performed to identify mutants among different T-DNA lines, by detecting the presence of an insertion-allele and/or the corresponding WT allele via amplification of characteristic genomic fragments using specifically selected primer combinations (see sections 2.1 and 4.1.1.1). To detect the WT allele in any given T-DNA line, forward and reverse primers were chosen to flank the T-DNA insertion site, binding up- and downstream of the insertion within the genomic sequence of the affected gene, respectively, yielding a PCR fragment of known size in the absence of the T-DNA insertion. The corresponding insertion allele could then be detected by combining either the genomic forward primer or the genomic reverse with a T-DNA specific primer binding within the right- or left-border sequence of the T-DNA. Depending on the orientation of the T-DNA insertion within the gene, a PCR with the appropriate combination of genomic and T-DNA primer yields a product only in the presence of the insertion.
Transcript was detected via PCR, using cDNA (obtained via reverse transcription of plant RNA) as the template. Primers were designed to bind exon-specific sequences. To account for variances in cDNA concentrations of different samples and to identify false negatives, a fragment corresponding to *AtACT2*-transcript was amplified from each cDNA sample. If necessary, template volumes were adjusted in subsequent reactions, until the amount of reference product obtained from the individual cDNAs was comparable between samples. The same template volume was then used in the PCRs performed to detect the fragments of interest. Primer combinations were further selected to span intron-sequences, to detect potential contamination with genomic DNA (yielding additional fragments of larger size).

4.2.2.7 Site directed mutagenesis

Introduction of point mutations was achieved via site directed mutagenesis in two subsequent steps. Primers spanning the site of mutagenesis were designed to match the desired DNA-sequence (black arrows with mutation indicated in red). In the first step, fragment1 (F1) was obtained in a PCR using the forward (solid black arrow) and the reverse mutagenesis primer in PCR 1a. Fragment2 (F2) was obtained in PCR 1b with the forward mutagenesis primer and the reverse primer. In the second step (PCR 2), equimolar amounts of F1 and F2 containing the altered DNA-sequence were used as the template. A PCR with the forward and reverse primer yielded the desired product.

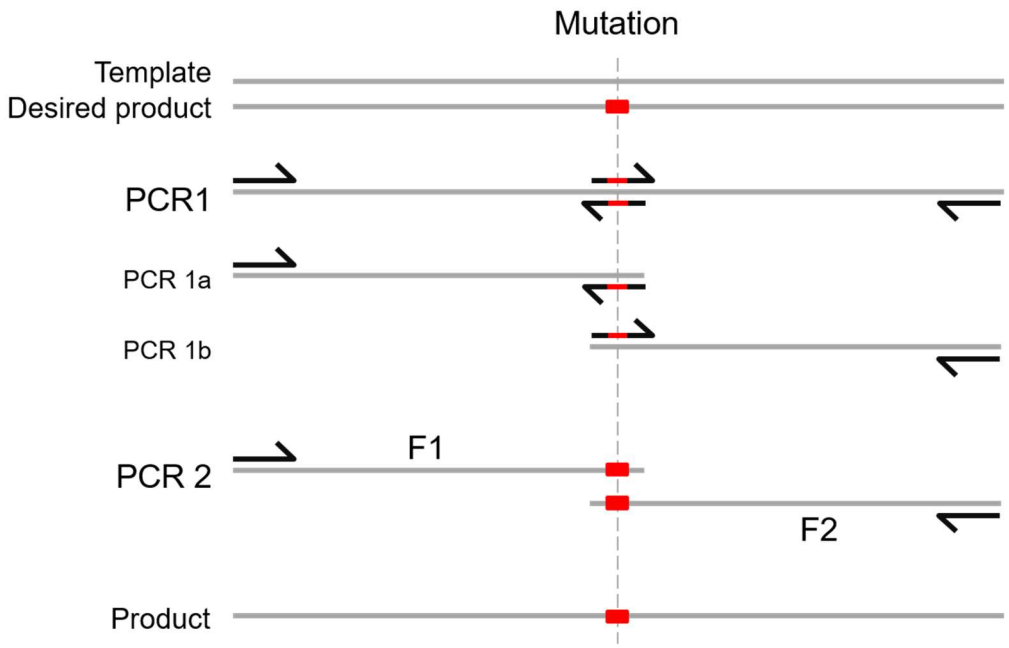

Figure 38: Schematic representation of different steps to introduce mutations via site-directed mutagenesis (SDM). Solid black arrows indicate the forward and reverse primer, respectively. Black arrows with red stripe indicate (partially or fully complementary) forward (pointing to the right) and reverse (pointing to the left) mutagenesis primers matching the mutated sequence. Grey bars represent DNA corresponding to template sequence, the red box indicates the mutation to be introduced. Fragment1 (F1) and fragment2 (F2) represent fragments obtained in the first step (PCR1 = two individual PCRs: PCR 1a and PCR 1b).

4.2.2.8 Agarose gel electrophoresis and DNA extraction from agarose gel

DNA fragments were separated by agarose gel electrophoresis in a horizontal electrophoresis chamber (PEQLAB, Erlangen, D). Most agarose gels, i.e. those used to separate DNA fragments > 300 bp, were obtained by heating 1% (w/V) agarose (Invitrogen, Darmstadt, D) in TAE-buffer (4.1.5.3) until dissolved. If necessary, the agarose concentration was increased (to 2%) or decreased (to 0.8%) to separate smaller or larger DNA fragments, respectively. Ethidium bromide (4.1.5) was added to the slightly cooled agarose-solution (for a final concentration of ~0.03 µg/mL) before the gel had set, to later label DNA for documentation under ultra-violet light. Samples were mixed with 10x loading dye to yield a 1x final concentration. To estimate the size of separated DNA-fragments, an appropriate DNA electrophoresis size standard (Table 39) was loaded to the gels.

Table 39: Size standards used for DNA electrophoresis.

Name	Size of DNA fragments / (bp)
λ_{ClaI}	354, 537, 621, 657, 973, 1112, 1701, 1804, 1915, 2014, 2614, 3673, 4396, 6262, 10496, 11385
100 bp	100, 200, 300, 500, 800, 1000, 1500

Purification of DNA from agarose gel slices was performed according to the manufacturer's protocol of innuPREP DOUBLEpure Kit (analytikjena, Jena, D). DNA was eluted with ddH_2O.

4.2.2.9 DNA sequencing

Sequencing of DNA, e.g. of fragments obtained via PCR to determine T-DNA insertion sites and to validate the correct sequence of inserts in donor-vectors, was performed at GATC Biotech GmbH (Constance, D).

4.2.2.10 Generation of donor vectors for classical cloning

Donor vectors for classical cloning were usually generated in the background of pJet1.2/blunt using the CloneJET PCR Cloning Kit (Fermentas, St. Leon-Rot, D). A typical reaction is given below.

Table 40: Standard reaction for cloning of PCR fragments into pJET1.2/blunt.

Component	10 µL reaction
2x reaction buffer	5 µL
pJet1.2/blunt	0.5 µL (= 25 ng)
PCR product	30 ng (for fragments between 800 and 2500 kb), or up to 4 µL
T4 Ligase	0.5 µL
ddH_2O	ad 10 µL

The mixture was incubated for 30 min at RT prior to transformation into chemically competent *E. coli* (DH5α).

4.2.2.11 Test restrictions and preparative digests

Enzymatic digests of DNA with restriction endonucleases was used to validate the correct makeup of obtained plasmids and for classical cloning steps. Standard reaction mixtures for test-restrictions of plasmids and for preparative digests are given below. Enzymes and compatible buffer systems were purchased from New England Biolabs (Frankfurt, D). Reaction mixtures were incubated at 37 °C for 1 h for test-digests. Incubation time was prolonged to at least 1.5 h (or over-night) for preparative digests.

Table 41: Reaction mixture for digests with restriction endonucleases.

Component	Test-digest (20 µL total volume)	Preparative digest (50 µL total volume)
10X Enzyme Buffer	2 µL	5 µL
Enzymes (5–20 U/µL)	0.2–0.4 µL of each (depending on the enzyme concentration, buffer dependent activity and number of cutting sites) (1 µL max. in total)	3 µL max. in total
Bovine serum albumin (BSA) (20mg/ml)	0.2 µL (depending on enzymes used)	0.5 µL (depending on enzymes used)
Plasmid DNA obtained via alkaline lysis	3–5 µL (depending on expected fragment sizes)	Up to 20 µL
ddH_2O	ad 20 µL	ad 50 µL

4.2.2.12 Dephosphorylation and ligation of DNA-fragments

Restriction endonucleases cut DNA at specific, often palindromic, sequences. Depending on the enzyme used, the DNA is cleaved to leave specific sticky or blunt ends. For classical cloning, cut DNA can be ligated to other DNA-fragments with compatible ends.

To avoid self-religation of DNA-fragments generated by restriction digest with a single enzyme (or different enzymes leaving compatible ends), e.g. of linearized vectors (pCS120$_{NcoI}$, pSS87$_{NcoI}$), such fragments were dephosphorylated. Treatment with calf intestine alkaline phosphatase (CIP) removed 3‘- and 5‘-phosphate groups of the linearized vector prior to ligation to the desired DNA fragment.

Following restriction digest (of the vector), enzymes were inactivated. This process depends on the particular restriction enzyme, but was usually achieved by heat application (20 min incubation at 65 °C). After briefly cooling the mixture on ice, 10x CIP buffer and CIP were added (e.g. 2 µL buffer and 1 µL CIP for 20 µL of a digest preparation) and the mixture was incubated at 37 °C for 40 min. The linearized and dephosphorylated vector was then purified from an agarose gel to additionally test for the presence of (or to remove residual) undigested vector.

To connect DNA fragments with compatible ends, the following reaction was prepared:

Table 42: Standard reaction for ligation of DNA vectors.

Component	Volume required for 10 µL total reaction
10x T4 ligase buffer (NEB, Frankfurt/Main)	1 µL
Vector (digested, dephosphorylated, purified)	50 ng
Insert (digested, purified)	See below
T4 Ligase (NEB, Frankfurt/Main)	0.5 µL
ddH_2O	ad 10 µL

Reactions were prepared to yield either equimolar (1:1) concentrations of insert and vector or higher concentrations of the insert (3:1). Empty vector controls were usually

performed only once for each newly prepared dephosphorylated vector. The amount of insert required for 1:1 reactions was calculated according to the following formula, where m(vector) = 50 ng:

$$\frac{m(vector) \times size\ of\ insert\ [bp]}{size\ of\ vector\ [bp]} = m(insert)\ [ng]$$

The reaction was incubated at RT for 2h (or at 16 °C over-night, or at 4 °C for 48 h), before chemically competent *E. coli* were transformed with the whole preparation.

4.2.2.13 Gateway cloning

To generate constructs in the background of pENTR/D-TOPO, or of the expression vectors pBasta-GUS, pBasta-GFP, pMDC43 and pMDC83 (4.1.2.1), the Gateway (GW) system (Invitrogen, Darmstadt, D) was used according to manufacturer's instructions. A PCR-product was created with appropriate primers (4.1.1.2 and 4.2.2.4), and purified by agarose gel electrophoresis followed by extraction from the gel (4.2.2.8).
The PCR fragment was cloned into pENTR/D-TOPO using the pENTR/D-TOPO cloning kit (Life technologies, Darmstadt, D). Briefly, 0.1–0.5 µL eluate [c(DNA) ≈ 10–30 ng/µL], 0.5 µL salt solution, 0.5 µL TOPO reagent and ddH_2O (ad 2.5 µL) were incubated for 30 min at RT. The reaction mixture was then used to transform a 100 µL aliquot of chemically competent *E. coli* DH5α. Transformed cells were selected by incubation on LB-plates supplemented with kanamycin. Insertion of the PCR fragment was confirmed by restriction digest (of plasmid DNA obtained from individual clones) with suitable enzymes, and verified by DNA-sequencing.
Expression vectors were obtained via an LR-reaction using the Gateway LR Clonase™ II enzyme mix (Life technologies, Darmstadt, D). Donor vectors (i.e. pENTR/D-TOPO containing the desired insert) were digested with suitable enzymes to remove the KAN^R for generation of expression vectors carrying the same selection marker (i.e. pMDC vectors, section 4.1.2.1). The entry clone fragment for further cloning steps was then purified from an agarose gel. Undigested entry-DNA (for generation of expression vectors selectable via their AMP^R), as well as destination vectors obtained by alkaline lysis of an appropriate *E. coli* strain were generally purified according to the manufacturer's protocol of innuPREP DOUBLEpure Kit (analytikjena) prior to the following steps. For the LR reaction 25–75 ng Entry DNA were combined with 75 ng destination vector and TE buffer (10 mM Tris/HCl pH 8.0, 1 mM EDTA) to a final volume of 4 µL. 1 µL LR Clonase™ II was added and the mixture was incubated at 25 °C for 1 h. The reaction was then terminated by addition of 0.5 µL proteinase K followed by incubation at 37 °C for 10 min. Chemically competent DH5α *E. coli* cells were transformed with the reaction mixture and selected on LB medium supplemented with antibiotics suitable for the respective expression vector. Presence and orientation of the desired construct were verified by restriction digests with appropriate enzymes.

4.2.3 Transformation of organisms

4.2.3.1 Escherichia coli

Preparation of chemically competent E. coli

The OD_{600} of a 4 mL ONC of *E. coli* (DH5α) in LB-medium was measured. According to this value, 100 mL of LB-medium were inoculated to obtain an OD_{600} of 0.1. The cell suspension was incubated at 37 °C until the OD_{600} had increased to 0.4–0.6. At that point, cells were harvested by centrifugation at 3500 rpm for 10 min. The cell pellet was re-suspended in 40 mL of cold aqueous 50 mM $CaCl_2$ solution and stored on ice for 30 min. The mixture was again centrifuged at 3500 rpm for 10 min. The supernatant was decanted and the cells re-suspended in 5 mL of cold aqueous 50 mM $CaCl_2$ solution, and incubated on ice for 10 min. 1.67 mL of 80% glycerol were added, before the mixture was distributed in aliquots, frozen on liquid N_2 and stored at -80 °C.

Transformation of E. coli

100 µL of chemically competent *E. coli* (DH5α strain) were combined with 10 µL plasmid DNA (in case of entry vectors) or 3–8 µL plasmid DNA (in case of expression vectors) in a 1.5 mL reaction tube and incubated on ice for 15–30 min. Transformation was achieved by heat shock application at 42 °C for 40 sec. 800 µL LB-medium were added, and the mixture was shaken at 37 °C for 1 h. Cells were harvested via centrifugation at 14000 rpm for 15 sec, followed by removal of approximately 800 µL of the supernatant and re-suspension in the remaining liquid. The cell suspension was then plated on medium containing the appropriate antibiotic for selection and incubated at 37 °C ON.

4.2.3.2 Agrobacterium tumefaciens

Preparation of chemically competent A. tumefaciens

The preparation of competent *Agrobacteria* was performed according to Höfgen und Willmitzer (1988). The cell suspension was distributed in aliquots and stored at -80 °C.

Transformation of A. tumefaciens

The transformation was performed based on the protocol of Höfgen und Willmitzer (1988). 500 µL competent *Agrobacteria* were thawed on ice. After the addition of 1–2 µg plasmid DNA, the cells were first kept on ice for 5 min, secondly immersed in liquid N_2 for 5 min and lastly heated to 37 °C for 5 min. 1 mL LB-medium was then added and incubated at 28 °C for 4 h. Cells were harvested via centrifugation, followed by removal of most of the supernatant, leaving 100 µL for resuspension of the bacteria. The cells were then plated on medium containing the appropriate antibiotic and incubated at 29 °C for two days.

4.2.3.3 Arabidopsis thaliana

Stable transformation

To stably transform *Arabidopsis thaliana*, the floral-dip-method was used (Clough and Bent, 1998). To achieve optimal conditions for the *Agrobacteria*, the plants were covered with cling film for 1–2 days after dipping and cultivated in the green house until seed maturation.

Transient transformation of mesophyll protoplasts

Mesophyll protoplast were isolated (Drechsel et al., 2011), and polyethylene glycol-mediated transformation was performed as previously described (Abel and Theologis, 1994). Transformed cells were incubated for 24–72 h in the dark at 22 °C prior to confocal analysis. Osmotic lysis of protoplasts was conducted according to Schneider et al. (2012b). Buffer compositions are given in section 4.1.5.

3 mL MCP buffer were diluted with 6 mL H_2O in a glass petri dish (~ 90 mm diameter). The lower epidermis of leaves from four- to six-week-old *Arabidopsis* plants was scratched with sand paper and kept in the diluted MCP scratched-side-down to avoid drying. Usually, if leaves were placed closely side by side to cover the whole petri dish, the procedure yielded enough cells for at least four individual transformations. Diluted MCP was exchanged for 5–7 mL digestion buffer and the petri dish was gently shaken for approximately 1.5 h (in the dark), to obtain protoplasts by enzymatic removal of the cell wall. Skeleted leaves were washed with 10 mL MCP and the protoplast suspension (from digestion and washing step) was carefully filtered through a 100 µm nylon mesh (pre-wetted with MCP). To avoid bursting of the protoplasts, cells were sedimented in the centrifuge with the break switched-off and at low acceleration (100 *g* ≈ 700 rpm). The protoplasts were then resuspended in 40 mL MaMg buffer, sedimented again and resuspended in ~ 500 µL of the supernatant. The suspension was adjusted (with MaMg) to yield a concentration of about 5000 protoplasts per µL.

For transformation, 150 µL of the protoplast suspension was transferred to a 13 mL round bottom reaction tube and gently mixed with 25 µg plasmid DNA (in ddH_2O, c(DNA) ≥ 1 µg/µL) and 150 µL PEG-CMS. Following 30 min of incubation at RT, W5 buffer was added stepwise to allow for adjustment of the cells to the osmotic value of the washing solution (300µL, 500 µl, 1 ml, and 2 ml of W5 buffer added in 5 min intervals). Buffer was removed after centrifugation at 80 *g* for 3 min, and cells were washed and sedimented again in 3 mL W5, prior to resuspension in 2 mL W5 supplemented with 25 µg/mL gentamycin or 100 µg/mL ampicillin. Transformed cells were incubated for 24–72 h in the dark at 22 °C prior to confocal analysis.

If protoplasts were to be lysed, protoplasts were sedimented and resuspended in sorbitol for barley. To remove the PM, ~ 13 µL of the cell suspension were directly mounted onto a microscope slide and 13 µL lysis buffer were added prior to analysis.

4.2.4 Plant physiological methods

4.2.4.1 ß-Glucuronidase assay of transgenic Arabidopsis

GUS-staining was used to examine promoter activities of *Arabidopsis* transformed with *promoter:GUS* or *promoter:gene-GUS* constructs. The plant material was submerged in GUS staining solution in appropriate vessels. The material was vacuum infiltrated for 1 min to allow the staining solution to penetrate the tissue and incubated at 37 °C for several hours or over-night. The staining solution was then removed and the tissue was cleared by washing several times with 70 % ethanol. Samples were stored in 70 % ethanol until further examination.

4.2.4.2 Isolation of Arabidopsis leaf trichomes

Trichomes were isolated according to the protocol given in Marks et al. (2008). Collected trichomes can easily be stained or simply observed under a microscope (without having to account for strong background caused by the chlorophyll in the leaf etc.)
About 1g of *Arabidopsis* leaves were collected in a 50-mL-tube (kept on ice). A pinch of 250–500 µm glass beads (~ 0.2 g), and 20 mL pre-chilled PBS/EGTA (or PBST/EGTA) were added. The tube was vortexed for 30 s, then put back on ice for 30 s. Vortexing and cooling was repeated three more times (storage for another 30 min to ON in the fridge was sometimes found to increase final trichome yield). The material was strained through a wide nylon mesh (500 µm), tube and leaves were rinsed with another 20 mL of the isolation-solution, strained, and the liquid (containing the trichomes) was collected. The tube was centrifuged for 5 min at 100 *g* (≈ 700 rpm) (break switched-off), the supernatant was removed, and trichomes washed with 20 mL of PBS. After centrifugation (5 min at 100 *g*), most of the supernatant was removed and the trichomes resuspended in the remaining liquid (~ 0.5–1 mL depending on amount of trichomes) by gently agitating the tube.

4.2.4.3 Preparation of plant material for HPLC analysis

Arabidopsis plants for HPLC analysis were cultivated solely under SD-conditions. To guarantee for constant parameters and comparable results, plants of different genotypes were cultivated side-by-side (checkerboard arrangement) and kept at the same position in the growth chamber throughout growth. Plant material was harvested at the same time for each experiment, i.e. after 5 hours of light. To measure sugar concentrations in source tissue, plants were grown for seven weeks; three fully lightened rosette leaves of comparable size were collected per plant (~ 50–100 mg plant material). To analyze sugar concentration in seedlings (representing sink tissue), plants were grown for 19 days before all aerial parts were collected (seedlings were cut shortly above the soil). 9–16 seedlings per sample were collected to obtain the required amount of at least 20 mg plant material. The leaves or seedlings were put in 1.5 mL screw cap micro tubes, weighed (the fresh-weight was noted), frozen in liquid N_2 and stored at -20 °C until further extraction. This in turn was achieved by adding 0.5–0.8 mL 80 % EtOH (the exact amount was noted)

and shaking at 80 °C for 1 h. Afterwards, the samples were slowly cooled down in the switched-off thermo-block for 15 min. Solids were then removed by centrifugation at 4 °C and 14.000 rpm for 5 min. 400–750 µL of the supernatant (exact amount noted) was transferred to a new reaction vessel and dried completely by evaporating the liquid using the SpeedVac at 45 °C. The dried material was then dissolved in 250 µL ddH_2O. 125 µL of this solution were later used for measurements.

4.2.4.4 Analyses of seedling development on MS-plates

For the analyses of root lengths, hypocotyl growth (section 2.3.1), and chlorophyll content (section 2.3.6), seedlings were cultivated on synthetic medium (see also sections 4.1.4.2). The specific medium is indicated for individual experiments in the results section. Generally, seeds of different genotypes were arranged alternatingly and in varying order on several plates to minimize positional effects during growth. After stratification (4 °C for two days), plates were transferred to the growth chamber, and kept under LD-conditions for the duration the experiments. If growth of etiolated hypocotyls was to be analyzed, plates were wrapped in aluminum foil, and kept vertically in a cubicle in the same growth chamber. For analyses of root growth, plates were kept vertically; for all other experiments, plates were kept horizontally. For measurement of root lengths or hypocotyls, images of all seedlings were captured at the indicated time point and lengths of roots or hypocotyls were determined using ImageJ (Schneider et al., 2012a).

4.2.4.5 Pollen germination assays

Pollen germination medium was prepared according to Rodriguez-Enriquez et al. (2013) as given below.

Table 43: Pollen germination medium (Rodriguez-Enriquez et al., 2013).

Reagent	Final concentration
$CaCl_2$	1 mM
$Ca(NO_3)_2$	1 mM
KCl	1 mM
Amicase	0.03% (w/V)
myo-Inositol	0.01% (w/V)
Ferric ammonium citrate $(NH_4)_5[Fe(C_6H_4O_7)_2]$	0.01% (w/V)
γ-Aminobutyric acid (GABA)	10 mM
Spermidine	0.1 mM
Boric acid $(B(OH)_3)$	0.01% (w/V)
Sucrose	250 mM

The pH was adjusted to 8.0 with KOH. 0.5 % (w/V) low-melt agarose (SeaPlaque® GTG® agarose; BioWhittaker Molecular Applications, Rockwell, USA) was added and the mixture was heated briefly in the microwave. Aliquots of 1 mL each were kept at -20 °C and liquefied prior to use by shaking at 63 °C for ~ 10 min.
To prepare a sample, 250 µL re-melted pollen germination medium was pipetted on a histobond slide forming a small rectangle (~ 1.5 x 2 cm) and briefly left to cool at RT.

Another 250 µL melted medium was added on top of the cooled gel yielding a flat rectangle of gel. Cellulose membrane (325PCellulose; AA Packaging Limited, Preston, UK) cut into a ~ 1.2 x 1.7 cm rectangle was then carefully put on the medium. The membrane tends to roll up when it gets in contact with the medium, so two diagonal edges were fixed with forceps until the membrane held its shape on the gel. The slides were prepared freshly for each experiment and kept in dark chambers prior to use. Wetted tissues were placed in the chambers to yield a high humidity necessary for pollen germination. The membrane was pollinated by gently pinching a flower (sepals opened for ~ 1–2 days) with forceps to release the anthers and to expose the pollen, and carefully stroking over the cellulose. The pollinated slide was then placed in the dark chamber and incubated at 25 °C. Images of pollen tubes were taken after 2.5 h of incubation to measure pollen tube length, or after 4.5 h to determine the pollen germination rate (section 2.3.3). Lengths of germinated pollen tubes were measured using ImageJ 1.47, as previously described (Schneider et al., 2012a).

4.2.4.6 Measurement of pigment contents in seedlings

For determination of chlorophyll contents (section 2.3.6), seedlings were grown on ABIS medium under Fe-sufficient and Fe-deficient conditions for four days under LD-conditions. Samples were prepared as described (Mary et al., 2015). Briefly, for each sample, 15 seedlings were put in an eppendorf tube together with a small metal bead and frozen in liquid N_2. The bead was added to help pulverization of the plant material, which was achieved by shaking on a tissue lyzer for 2 min. Pigments were extracted in 1 mL ethanol by shaking for 30 min at RT. Samples were centrifuged for 5 min at 14.000 rpm and 900 µL of the supernatant was used for the measurement. The pigment content was determined spectrophotometrically from the absorbance measured at 632, 649 and 665 nm to (Ritchie, 2008). Absorbance coefficients of Chlorophyll a, b and c in ethanol according to Ritchie (2008) are given below.

Table 44: Absorbance coefficients of chlorophyll *a*, chlorophyll *b*, chlorophyll *c* and total chlorophyll in ethanol at 632, 649 and 665 nm according to Ritchie (2008) in g m^{-3} cm A^{-1}.

	E632 nm	E649 nm	E665 nm	"+/-%Chl"
Chl *a*	-0.9394 ± 0.0085	-4.2774 ± 0.0025	13.3914 ± 0.0015	0.009
Chl *b*	-4.0937 ± 0.0162	25.6865 ± 0.0048	-7.3430 ± 0.0029	0.0171
Chl *c*	28.5073 ± 0.0091	-9.9940 ± 0.0027	-1.9749 ± 0.0016	0.0096
Total Chl	23.4742 ± 0.0166	11.4096 ± 0.0049	4.0735 ± 0.0029	0.0175

4.2.4.7 Alexander stain

For examination of pollen viability (section 2.3.3), pollen was stained as described (Alexander, 1969). The composition of the staining solution is given in 4.1.5.3. *Arabidopsis* pollen were incubated in a drop of the staining solution mounted on a cover slip for approximately 2 min, before the solution was removed, the pollen washed with a few drops of ddH_2O, and the coloration observed under a microscope.

4.2.4.8 Staining with propidium iodide and FM4-64

Seedlings were carefully removed from the growth medium (usually ½ strength MS) to avoid cell damage. To fluorescently label the cell wall, plant material was incubated in a drop (~ 30 µL) of a 42 µg/mL propidium iodide solution (on a microscope slide) for approximately 3–5 min. The material was then briefly washed with H_2O prior to microscopic analysis.
To stain cells with the styryl dye FM4-64, samples were directly mounted on a microscope slide with ~30 µL of an aqueous FM4-64 (10 µM) solution prior to microscopic analysis.

4.2.5 Confocal microscopy and image analysis

Fluorescence was detected using a TCS SP5 confocal laser scanning microscope (Leica Microsystems, Mannheim, D). Image preparation and processing was done using LAS AF Version 2.7.29586 (Leica, Wetzlar, D), or FiJi (Schindelin et al., 2012). Excitation wavelengths and corresponding detector settings for different fluorophores, or fluorescent dyes used in this work are given below. Images in this work are displayed in false-colors as indicated.

Table 45: Excitation wavelengths and settings used to detect emission of different fluorophores and dyes.

Fluorescent marker	Excitation / [nm]	Detector range / [nm]
GFP	488	495–548
RFP	561	590–640
mCherry	561	587–643
Chlorophyll	488	654–732
FM4-64	561	652–709
Propidium iodide	488	620–732

Quantification of colocalization of GFP- and RFP-signals was performed with the Coloc2 plug-in in Fiji. Single channel images (RFP and corresponding GFP) were merged, a color-threshold (Otsu, 1979) applied, and a mask was created from the thresholded image. Colocalization was then quantified in the raw image, limited to the area (i.a. the pixels) determined by the mask. Results are presented as scatterplots with the linear Pearson correlation coefficient (r_p) and the nonlinear Spearman correlation coefficient (r_s), ranging from -1.0 to +1.0 for perfect exclusion to perfect colocalization, respectively. At least five independent images were analyzed per colocalization study (note that this applies only to those experiments, for which r_p, r_s and scatterplot are given). One representative image and the corresponding scatterplot is shown, respectively.

4.2.6 Cloning strategies

4.2.6.1 Generation of AP4µ$_{Pro}$:AP4µ-reporter lines

To generate *AP4µ$_{Pro}$:AP4µ-reporter* plants and complement *ap4µ* mutants, appropriate vectors were generated using the Gateway technology (Invitrogen™). First, a genomic fragment (*AP4µ$_{Pro}$:AP4µ*) was amplified using *Arabidopsis* Col-0 DNA as the template (and

adding 5'CACC for cloning into the entry vector pENTR™/D-TOPO®). Primers were designed to amplify a fragment comprising 1800 bp upstream of the start-ATG of *AP4μ* (At4g24550.2) together with the genomic sequence of *AP4μ* up to the last exon, omitting the stop-codon (primers AP4μ-Prom-GW-f and AP4μ-GW-r; see section 4.1.1.2). The fragment was cloned into pENTR™/D-TOPO® (Invitrogen, Darmstadt, D), verified by sequencing, and recombined (LR-reaction, see section 4.2.2.13) into the GW-compatible destination vectors pBASTA-GFP and pBASTA-GUS (Rottmann et al., 2016), yielding the plasmids pCM147 (*AP4μ$_{Pro}$:AP4μ-GFP*) and pCM148 (*AP4μ$_{Pro}$:AP4μ-GUS*). *Ap4μ* mutants were transformed via floral dip with *Agrobacterium tumefaciens* Smith & Townsend strain GV3101 (Holsters et al., 1980; Clough and Bent, 1998; see section 4.2.3). Seeds of *ap4μ* transformed with pCM147 or pCM148 were planted on soil and selected via their Basta-resistance. Since the constructs were to be analyzed with respect their ability to complement mutant phenotypes, 24 surviving seedlings of each line were cultivated further to later obtain *ap4μ* mutants with homozygous single insertions of the respective construct. Seeds obtained from the T3 generation, homozygous for a single insertion of the pCM147 or pCM148 construct were used in further experiments, and are herein referred to as *ap4μ/AP4μ$_{Pro}$:AP4μ-GFP* or *ap4μ/AP4μ$_{Pro}$:AP4μ-GUS*, respectively.

4.2.6.2 Generation of vectors for transient overexpression in Arabidopsis mesophyll protoplasts

Generation of *N*- and *C*-terminal GFP-fusions, e.g. for examination of subcellular targeting of AP-4 cargo candidates in WT and *ap4* mutant protoplasts, usually comprised the following steps (depicted in Figure 39): To generate vectors via classical cloning, the coding sequence of any gene of interest was amplified from *Arabidopsis* cDNA via PCR (section 4.2.2.4), removing the stop-codon and introducing restriction sites for excision of the insert from the donor vector via enzymatic digest with *Nco*I, *Pci*I, or *Bsp*HI (to allow for ligation into the destination vectors pSS87 and pCS120 via their compatible *Nco*I-site). Any internal restriction sites for the same enzyme were removed via site-directed mutagenesis (e.g. if flanking *Pci*I-sites had to be introduced to a CDS containing an internal *Pci*I-site). Primer sequences used are given in section 4.1.1.2.

The amplified fragment was cloned into an appropriate entry vector (generally pJET1.2/blunt; section 4.2.2.10), and the plasmid was used to transform chemically competent *E. coli* (4.2.3.1). Positive clones were selected via their antibiotic resistance and appropriate test digests. The correct sequence of the insert was confirmed via DNA sequencing (GATC Biotech GmbH, Constance, D). The insert was then excised from the donor vector (section 4.2.2.11), yielding "sticky ends" compatible to the unique *Nco*I-site of pSS87 and pCS120. Ligation of the insert to the linearized and dephosphorylated (section 4.2.2.12) destination vectors then yielded 5' or 3' fusions of the desired CDS to the open reading frame of the reporter (usually *GFP*). *E. coli* were then again transformed with the respective plasmid(s), cultivated on appropriate selection medium, plasmid DNA of individual clones isolated, and the correct orientation of the insert tested via test-digest with appropriate enzymes. Some vectors for transient overexpression were generated

analogously, but via Gateway cloning (indicated in the appropriate paragraph in section 4.1.1.2, and 4.1.2.2). Protocols are given in section 4.2.2.13. The plasmid was finally purified (from an individual clone; for midi plasmid DNA preparation see section 4.2.2.3) and used to transform mesophyll protoplasts (section 4.2.3.3) to study the subcellular sorting in WT or mutant cells via confocal microscopy (section 4.2.5).

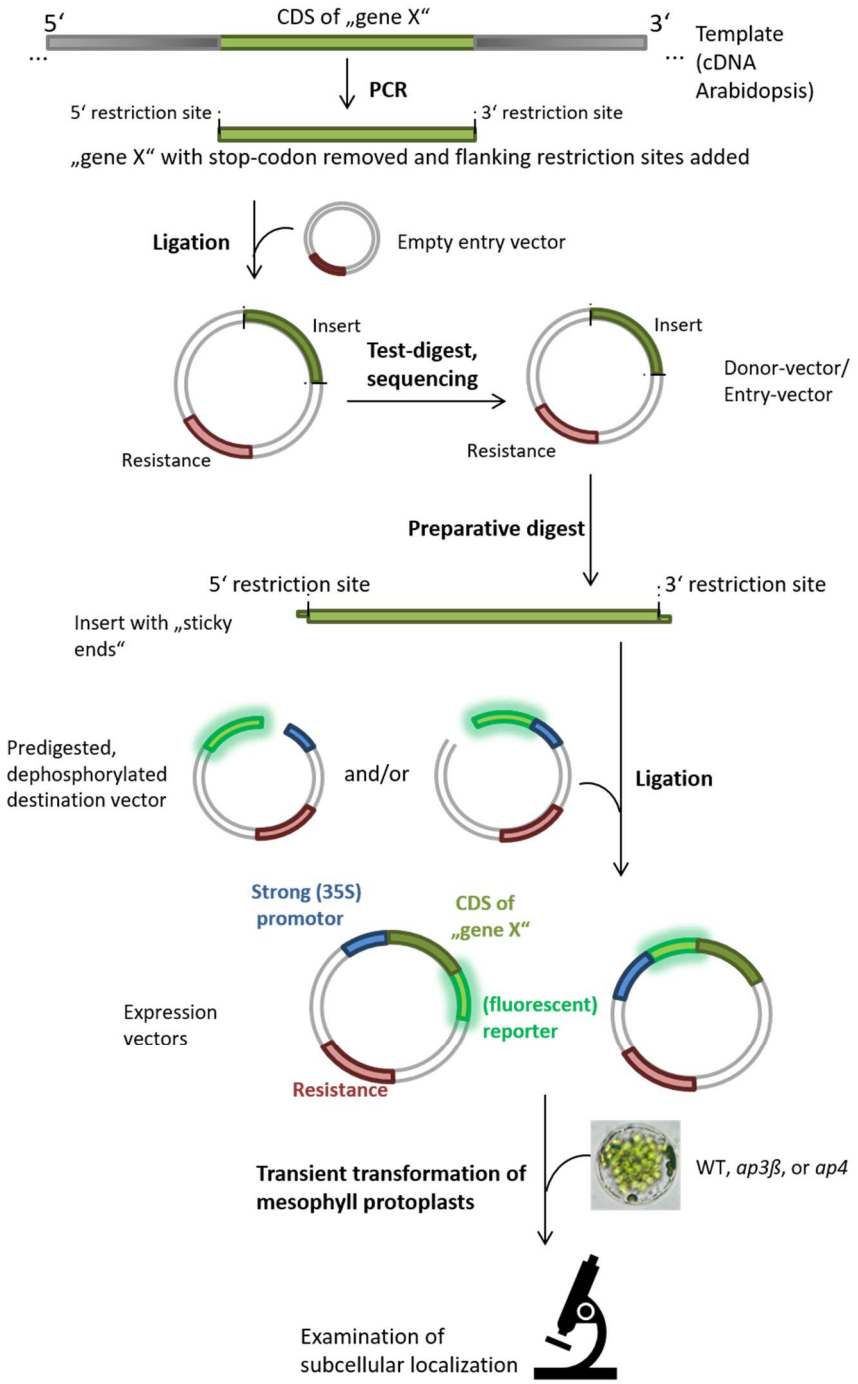

Figure 39: Workflow for generation of vectors used to study subcellular sorting in *Arabidopsis* mesophyll protoplasts. The coding sequence of the gene of interest was generally amplified from *Arabidopsis* cDNA, removing the stop-codon and introducing restriction sites (compatible to a unique site of the destination vectors). The amplified fragment was cloned into an appropriate entry vector. Positive clones were selected via their antibiotic resistance and appropriate test digests, and the sequence of the insert validated (GATC Biotech GmbH, Constance, D). The insert was excised from the donor vector, yielding "sticky ends". The insert was then ligated into the linearized and dephosphorylated

destination vectors to yield 5’ or 3’ fusions to the open reading frame of the reporter (usually *GFP*). The obtained plasmids were finally used to transform mesophyll protoplasts to study the subcellular sorting in WT or mutant cells.

4.2.6.3 Cloning strategy for 35S$_{Pro}$:HsAPP-GFP

To obtain fluorophore-fusions of human amyloid precursor protein for transient overexpression in *Arabidopsis*, two synthetic 1000 bp fragments of *HsAPP* were ordered from Eurofins genomics. *De novo* synthesis of the CDS by Eurofins further allowed for codon optimization for expression in *Arabidopsis*, and was designed to simultaneously mutate internal *Pci*I- and *Nco*I-sites without alteration of the resulting amino acid sequence. For codon optimization, codons used with a frequency of < 0.15 in *Arabidopsis* were automatically exchanged for the most frequent codon of the respective amino acid. Since high order homopolymers were to be avoided for synthesis, a lysine-triplet-coding 5’-AAA AAA AAA-3’ was exchanged for 5’-AAA AAG AAA-3’, thereby maintaining the resulting amino acid sequence and avoiding synthesis of a homohexamer. The 5’ **ATG** CTC (coding for the initial methionine and leucine) was further exchanged for 5’ **ATG** TTG to later allow for easier insertion of a 5’ *Pci*I-site (A˅C**ATG**T), without alteration of the amino acid sequence. Both the 5’ and 3’ fragments were delivered in the background of the vector pEX-A2, yielding the vectors pEX-A2-5’APP (KR61-7) and pEX-A2-3'1000bisStop (KS05-17), respectively. The complete CDS was then obtained via PCR, as depicted in Figure 40. First, the 5’ fragment was amplified from pEX-A2-5’APP using the primers HsAPP695Ara-5'-PciI-f and HsAPP695Ara-Linker-r and the 3’ fragment was amplified from pEX-A2-3'1000bisStop using the primers HsAPP695Ara-Linker-f and HsAPP695Ara-3'-NcoI-r_wob (primer sequences are given in 4.1.1.2). Next, combination of both fragments in a PCR using the primers HsAPP695Ara-5'-PciI-f and HsAPP695Ara-3'-NcoI-r_wob yielded the complete fragment. Using a wobble base in the reverse primer resulted in an APP fragment with or without a stop-codon. The PCR product(s) were cloned into pJET1.2/blunt. Clones containing the insert were selected via restriction digest with *Pci*I and *Nco*I. The sequence and presence or absence of a stop-codon was determined via sequencing (GATC Biotech GmbH, Constance, D). The HsAPP-encoding fragment was subsequently excised from the respective donor vector (via the added *Pci*I and *Nco*I restriction sites) and ligated into pSS87 (with stop-codon) or pCS120 (without stop-codon) via the unique *Nco*I-site of the destination vectors), to obtain *N*- and *C*-terminal *GFP*-fusions for transient expression in *Arabidopsis* protoplasts

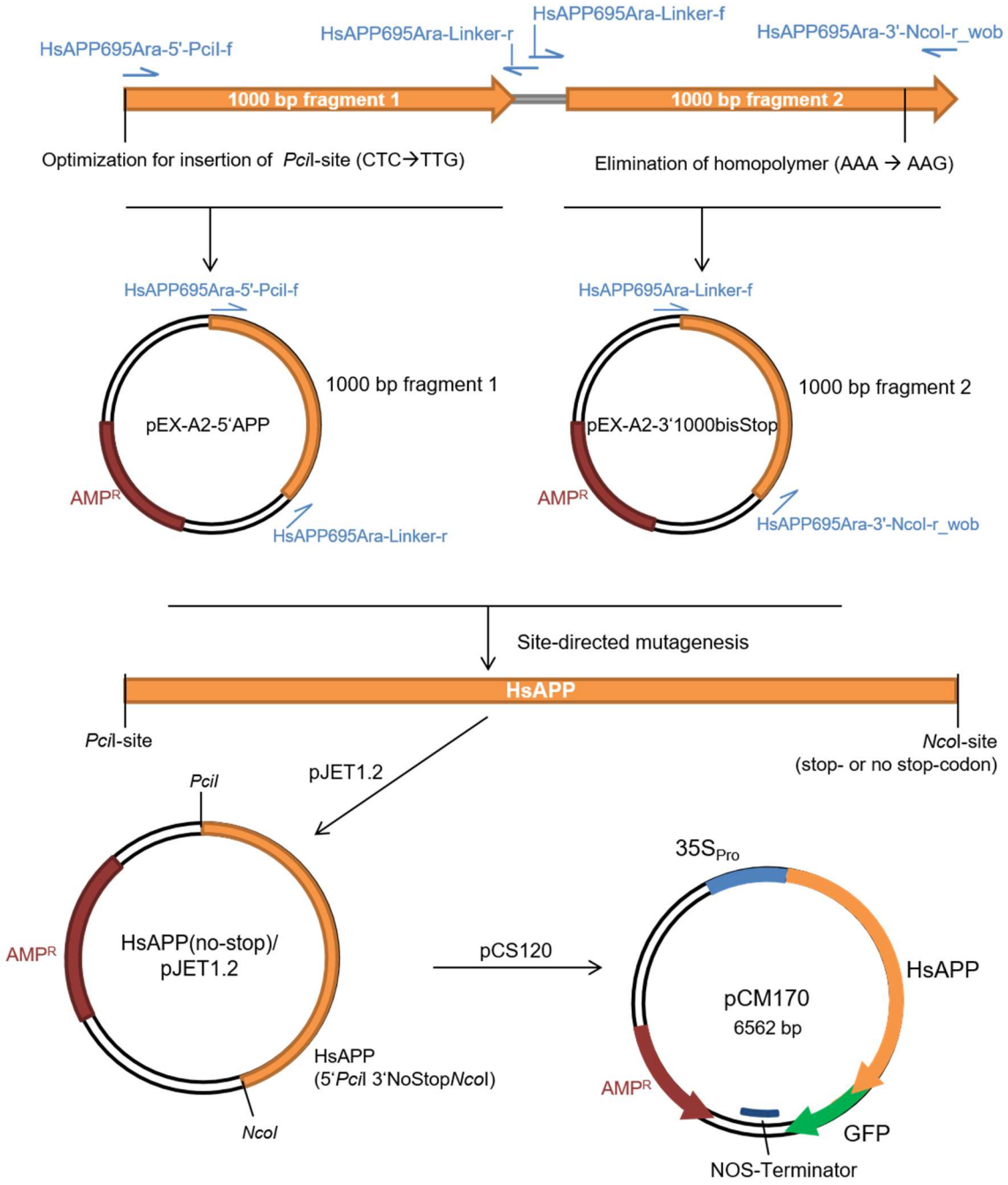

Figure 40: **Cloning strategy for pCM170 ($35S_{Pro}$:HsAPP-GFP).**
Two 1000 bp fragments of the coding sequence of HsAPP were codon-optimized for expression in *Arabidopsis* (further modifications, all without alteration of the resulting amino acid sequence, are indicated), synthesized de novo, and delivered as separate plasmids (Eurofins Genomics). The complete CDS was obtained in consecutive PCRs (site-directed mutagenesis): the 5' fragment was amplified from pEX-A2-5'APP, and the 3' fragment was amplified from pEX-A2-3'1000bisStop using the indicated primers. Next, combination of both fragments in a PCR using the primers HsAPP695Ara-5'-PciI-f and HsAPP695Ara-3'-NcoI-r_wob yielded the complete fragment. PCR product(s) were cloned into pJET1.2/blunt. Clones containing the insert were selected via test-digest, followed by sequencing (to discriminate between variants with and without stop-codon). The HsAPP-encoding fragment (without stop-codon) was excised from the donor vector and ligated into pCS120, yielding pCM170 *($35S_{Pro}$:HsAPP-GFP)*. (The donor vector containing HsAPP including the stop-codon and subsequent steps, i.e. ligation into pSS87, are not depicted.)

4.2.6.4 Cloning of NRAMP3 and NRAMP4 fragments

The full-length CDS of *NRAMP3*, or *NRAMP4* was amplified from *Arabidopsis* cDNA, using the primers AtNRAMP3-5'NcoICC-f and AtNRAMP3-3'NcoI-r, or AtNRAMP4-5'-PciI-f and AtNRAMP4-3'-PciI-r. This removed the stop-codon and introduced flanking *Nco*I (*NRAMP3*) or *Pci*I-sites (*NRAMP4*) for later cloning steps. The PCR fragments were cloned in pJET1.2/blunt. Individual clones were tested for the presence of the insert via test-digest and the sequence was confirmed by sequencing. The fragment encoding NRAMP3, or NRAMP4 was then excised from the corresponding donor vector (via enzymatic digest with *Nco*I, or *Pci*I, respectively) and purified. The fragments were ligated into different destination vectors (linearized by enzymatic digest with *Nco*I and dephosphorylated). Ligation to pCS120 yielded pCM210 (*35S$_{Pro}$:NRAMP3-GFP*) and pCM132 (35S$_{Pro}$:NRAMP3-GFP) for GFP-fusions to the *C*-terminus of NRAMP3 or NRAMP4; ligation to pSS87 yielded pCM211 (*35S$_{Pro}$:GFP-NRAMP3*) or pCM133 (*35S$_{Pro}$:GFP-NRAMP4*) for GFP-fusions to the *N*-terminus of NRAMP3 or NRAMP4; ligation to pSE35e-C yielded pCM210R, or pCM132R for RFP-fusions to the *C*-terminus of NRAMP3 or NRAMP4; and ligation to pSW110 yielded pCM215 (*35S$_{Pro}$:NRAMP3-C(INT1)-GFP*) or pCM217 (*35S$_{Pro}$:NRAMP4-C(INT1)-GFP*) for GFP-fusions to the *C*-terminus of NRAMP/INT1 chimaera, in which the *C*-terminus of INT1 was added to the endogenous *C*-terminus of NRAMP3 or NRAMP4, respectively.

To generate vectors for stable overexpression (*35S$_{Pro}$*) of NRAMP3-GFP or NRAMP4-GFP in *Arabidopsis*, *NRAMP3*- or *NRAMP4*-coding fragments (obtained via digest of the corresponding pJet1.2 donor vector) were initially ligated to the unique *Nco*I-site of pSB30, which is similar to pCS120, but contains a unique *Asc*I-site 5' of the *35S$_{Pro}$*-sequence, and a unique *Spe*I-/*Xba*I-site 3' of the *Nos*-terminator (in turn 3' of the *GFP* CDS). Ligation to pSB30 yielded pCM263 [(*Asc*I)*35S$_{Pro}$:NRAMP3-GFP*(*Spe*I/*Xba*I)], and pCM264 [(*Asc*I)*35S$_{Pro}$:NRAMP4-GFP*(*Spe*I/*Xba*I)]. From these vectors, the *35S$_{Pro}$:NRAMP3-GFP*, or *35S$_{Pro}$:NRAMP4-GFP* fragment was isolated via enzymatic digest of the corresponding vector with *Asc*I and *Spe*I (pCM263), or with *Asc*I and *Xba*I (pCM264), followed by agarose gel electrophoresis and extraction of the respective fragment from the gel.

pSS59 is a vector suited for *Agrobacterium*-mediated transformation of *Arabidopsis*. Its original insert [*35S$_{Pro}$:AtINT1(CDS)NosT*] was removed from the vector via restriction with *Asc*I (cleaving 5' of its *35S$_{Pro}$*-sequence) and *Spe*I (cutting 3' of *NosT*). The remaining vector-fragment was purified and dephosphorylated. *35S$_{Pro}$:NRAMP3-GFP* or *35S$_{Pro}$:NRAMP4-GFP* fragments obtained by restrictive digest of pCM263 or pCM264 could then be ligated to the pSS59-vector-fragment to obtain the plasmids pCM265 and pCM266, respectively. Those plasmids are then suited for stable transformation of *Arabidopsis* to finally drive overexpression of *NRAMP3-GFP*, or *NRAMP4-GFP* in WT, *nramp3-1 nramp4-1*, and *ap4μ*.

Other fluorophore-fusions of NRAMP3 or NRAMP4 were generated by amplification of *NRAMP*-fragments or -mutants with the primers given in Table 11, using pCM210 (*35S$_{Pro}$:NRAMP3-GFP*) or pCM132 (*35S$_{Pro}$:NRAMP4-GFP*) as the template. Fragments were again cloned into pJET1.2/blunt, before the insert was isolated from a single clone and ligated to destination vectors indicated in Table 16.

References

Abel, S. and Theologis, A. (1994). Transient transformation of *Arabidopsis* leaf protoplasts: a versatile experimental system to study gene expression. Plant J. **5**: 421–427.

Abou Jamra, R. et al. (2011). Adaptor protein complex 4 deficiency causes severe autosomal-recessive intellectual disability, progressive spastic paraplegia, shy character, and short stature. Am. J. Hum. Genet. **88**: 788–795.

Aguilar, R.C., Boehm, M., Gorshkova, I., Crouch, R.J., Tomita, K., Saito, T., Ohno, H., and Bonifacino, J.S. (2001). Signal-binding specificity of the μ4 subunit of the adaptor protein complex AP-4. J. Biol. Chem. **276**: 13145–13152.

Ahmed, S.U., Rojo, E., Kovaleva, V., Venkataraman, S., Dombrowski, J.E., Matsuoka, K., and Raikhel, N. V (2000). The plant vacuolar sorting receptor AtELP is involved in transport of NH2-terminal propeptide-containing vacuolar proteins in *Arabidopsis thaliana*. J. Cell Biol. **149**: 1335–1344.

Alexander, M.P. (1969). Differential staining of aborted and nonaborted pollen. Stain Technol. **44**: 117–122.

Alonso, J.M. et al. (2003). Genome-wide insertional mutagenesis of *Arabidopsis thaliana*. Science **301**: 653–657.

Anderberg, H.I., Danielson, J.Å., and Johanson, U. (2011). Algal MIPs, high diversity and conserved motifs. BMC Evol. Biol. **11**: 110.

Ang, A., Taguchi, T., Francis, S., Fölsch, H., and Murrells, L. (2004). Recycling endosomes can serve as intermediates during transport from the Golgi to the plasma membrane of MDCK cells. J. Cell Biol. **167**: 531–543.

Antonny, B., Beraud-Dufour, S., Chardin, P., and Chabre, M. (1997). N-terminal hydrophobic residues of the G-protein ADP-ribosylation factor-1 insert into membrane phospholipids upon GDP to GTP exchange. Biochemistry **36**: 4675–4684.

Augustin, R., Riley, J., and Moley, K.H. (2005). GLUT8 contains [DE]XXXL[LI] sorting motif and localizes to a late endomosal/lysosomal compartment. Traffic **6**: 1196–1212.

Azevedo, C., Burton, A., Ruiz-Mateos, E., Marsh, M., and Saiardi, A. (2009). Inositol pyrophosphate mediated pyrophosphorylation of AP3B1 regulates HIV-1 Gag release. Proc. Natl. Acad. Sci. U.S.A. **106**: 21161–21166.

Bai, H., Doray, B., and Kornfeld, S. (2004). GGA1 interacts with the adaptor protein AP-1 through a WNSF sequence in its hinge region. J. Biol. Chem. **279**: 17411–17417.

Bar, M. and Avni, A. (2009). EHD2 inhibits ligand-induced endocytosis and signaling of the leucine-rich repeat receptor-like protein LeEix2. Plant J. **59**: 600–611.

Barberon, M., Zelazny, E., Robert, S., Conejero, G., Curie, C., Friml, J., and Vert, G. (2011). Monoubiquitin-dependent endocytosis of the iron-regulated transporter 1 (IRT1) transporter controls iron uptake in plants. Proc. Natl. Acad. Sci. U.S.A **108**: E450-8.

Barois, N. and Bakke, O. (2005). The adaptor protein AP-4 as a component of the clathrin coat machinery: a morphological study. Biochem. J. **385**: 503–510.

Bassham, D.C., Brandizzi, F., Otegui, M.S., and Sanderfoot, A.A. (2008). The secretory system of *Arabidopsis*. Arabidopsis Book: e0116.

Bauer, P., Leshinsky-Silver, E., Blumkin, L., Schlipf, N., Schröder, C., Schicks, J., Lev, D., Riess, O., Lerman-Sagie, T., and Schöls, L. (2012). Mutation in the AP4B1 gene cause

hereditary spastic paraplegia type 47 (SPG47). Neurogenetics **13**: 73–76.

Benková, E., Michniewicz, M., Sauer, M., Teichmann, T., Seifertová, D., Jürgens, G., and Friml, J. (2003). Local, efflux-dependent auxin gradients as a common module for plant organ formation. Cell **115**: 591–602.

Besserer, A. et al. (2012). Selective regulation of maize plasma membrane aquaporin trafficking and activity by the SNARE SYP121. Plant Cell **24**: 3463–3481.

Béthune, J., Wieland, F., and Moelleken, J. (2006). COPI-mediated transport. J. Membr. Biol. **211**: 65–79.

Blilou, I., Xu, J., Wildwater, M., Willemsen, V., Paponov, I., Friml, J., Heidstra, R., Aida, M., Palme, K., and Scheres, B. (2005). The PIN auxin efflux facilitator network controls growth and patterning in *Arabidopsis* roots. Nature **433**: 39–44.

Boehm, M., Aguilar, R.C., and Bonifacino, J.S. (2001). Functional and physical interactions of the adaptor protein complex AP-4 with ADP-ribosylation factors (ARFs). EMBO J. **20**: 6265–6276.

Boehm, M. and Bonifacino, J.S. (2001). Adaptins: the final recount. Mol. Biol. Cell **12**: 2907–2920.

Boehm, M. and Bonifacino, J.S. (2002). Genetic analyses of adaptin function from yeast to mammals. Gene **286**: 175–186.

Bonifacino, J.S. (2004). The GGA proteins: adaptors on the move. Nat. Rev. Mol. Cell Biol. **5**: 23–32.

Bonifacino, J.S. and Glick, B.S. (2004). The mechanisms of vesicle budding and fusion. Cell **116**: 153–166.

Bonifacino, J.S. and Traub, L.M. (2003). Signals for sorting of transmembrane proteins to endosomes and lysosomes. Annu. Rev. Biochem. **72**: 395–447.

Le Borgne, R., Griffiths, G., and Hoflack, B. (1996). Mannose 6-phosphate receptors and ADP-ribosylation factors cooperate for high affinity interaction of the AP-1 Golgi assembly proteins with membranes. J. Biol. Chem. **271**: 2162–2170.

Borgne, R.L. and Hoflack, B. (1998). Mechanisms of protein sorting and coat assembly: Insights from the clathrin-coated vesicle pathway. Curr. Opin. Cell Biol. **10**: 499–503.

Borner, G.H.H., Antrobus, R., Hirst, J., Bhumbra, G.S., Kozik, P., Jackson, L.P., Sahlender, D. a, and Robinson, M.S. (2012). Multivariate proteomic profiling identifies novel accessory proteins of coated vesicles. J. Cell Biol. **197**: 141–160.

Bouchard, R., Bailly, A., Blakeslee, J.J., Oehring, S.C., Vincenzetti, V., Lee, O.R., Paponov, I., Palme, K., Mancuso, S., Murphy, A.S., Schulz, B., and Geisler, M. (2006). Immunophilin-like TWISTED DWARF1 modulates auxin efflux activities of *Arabidopsis* P-glycoproteins. J. Biol. Chem. **281**: 30603–30612.

Brandizzi, F. and Barlowe, C. (2013). Organization of the ER-Golgi interface for membrane traffic control. Nat. Rev. Mol. Cell Biol. **14**: 382–92.

Braulke, T. and Bonifacino, J.S. (2009). Sorting of lysosomal proteins. Biochim. Biophys. Acta **1793**: 605–614.

Burgos, P. V, Mardones, G. a, Rojas, A.L., DaSilva, L.L.P., Prabhu, Y., Hurley, J.H., and Bonifacino, J.S. (2010). Sorting of the Alzheimer's disease amyloid precursor protein mediated by the AP-4 complex. Dev. Cell **18**: 425–436.

Cai, Y., Jia, T., Lam, S.K., Ding, Y., Gao, C., San, M.W.Y., Pimpl, P., and Jiang, L. (2011). Multiple cytosolic and transmembrane determinants are required for the trafficking of SCAMP1 via an ER-Golgi-TGN-PM pathway. Plant J. **65**: 882–896.

Cailliatte, R., Lapeyre, B., Briat, J.-F., Mari, S., and Curie, C. (2009). The NRAMP6 metal

transporter contributes to cadmium toxicity. Biochem. J. **422**: 217–228.

Cailliatte, R., Schikora, A., Briat, J.-F.F., Mari, S., and CURIE, C. (2010). High-affinity manganese uptake by the metal transporter NRAMP1 is essential for *Arabidopsis* growth in low manganese conditions. Plant Cell **22**: 904–917.

De Camilli, P., Chen, H., Hyman, J., Panepucci, E., Bateman, A., and Brunger, A.T. (2002). The ENTH domain. FEBS Lett. **513**: 11–18.

Chen, H., Zou, Z., Sarratt, K.L., Pylayeva, Y., Giancotti, F.G., Zhou, D., Zhang, M., Sebzda, E., Hammer, D.A., and Kahn, M.L. (2006). *In vivo* β1 integrin function requires phosphorylation-independent regulation by cytoplasmic tyrosines. Genes Dev. **20**: 927–932.

Chen, W.W.-J.W., Goldstein, J.L., and Brown, M.S. (1990). NPXY, a sequence often found in cytoplasmic tails, is required for coated-pit mediated internalization of the low density lipoprotein receptor. J. Biol. Chem. **265**: 3116–3123.

Chevalier, A.S., Bienert, G.P., and Chaumont, F. (2014). A new LxxxA motif in the transmembrane Helix3 of maize aquaporins belonging to the plasma membrane intrinsic protein PIP2 group is required for their trafficking to the plasma membrane. Plant Physiol. **166**: 125–38.

Chevalier, A.S. and Chaumont, F. (2014). Trafficking of plant plasma membrane aquaporins: multiple regulation levels and complex sorting signals. Plant Cell Physiol. **56**: 819–829.

Chiu, T.Y., Christiansen, K., Moreno, I., Lao, J., Loqué, D., Orellana, A., Heazlewood, J.L., Clark, G., and Roux, S.J. (2012). AtAPY1 and AtAPY2 function as golgi-localized nucleoside diphosphatases in *Arabidopsis thaliana*. Plant Cell Physiol. **53**: 1913–1925.

Choy, R.W.-Y., Cheng, Z., and Schekman, R. (2012). Amyloid precursor protein (APP) traffics from the cell surface via endosomes for amyloid β (Aβ) production in the trans-Golgi network. Proc. Natl. Acad. Sci. U.S.A. **109**: E2077–E2082.

Cline, M.G. (1997). Concepts and terminology of apical dominance. Am. J. Bot. **84**: 1064–1069.

Clough, S.J. and Bent, A.F. (1998). Floral dip: a simplified method for *Agrobacterium*-mediated transformation of *Arabidopsis thaliana*. Plant J. **16**: 735–743.

Cockcroft, S., Thomas, G.M., Fensome, A., Geny, B., Cunningham, E., Gout, I., Hiles, I., Totty, N.F., Truong, O., and Hsuan, J.J. (1994). Phospholipase D: a downstream effector of ARF in granulocytes. Science **263**: 523–526.

Costaguta, G., Stefan, C.J., Bensen, E.S., Emr, S.D., and Payne, G.S. (2001). Yeast Gga coat proteins function with clathrin in Golgi to endosome transport. Mol. Biol. Cell **12**: 1885–1896.

Crump, C., Xiang, Y., Thomas, L., and Gu, F. (2001). PACS-1 binding to adaptors is required for acidic cluster motif-mediated protein traffic. EMBO J.

Curtis, M.D. and Grossniklaus, U. (2003). A gateway cloning vector set for high-throughput functional analysis of genes in planta. Plant Physiol. **133**: 462–469.

Van Damme, D., Coutuer, S., De Rycke, R., Bouget, F.-Y., Inzé, D., and Geelen, D. (2006). Somatic cytokinesis and pollen maturation in *Arabidopsis* depend on TPLATE, which has domains similar to coat proteins. Plant Cell **18**: 3502–3518.

Van Damme, D., Gadeyne, A., Vanstraelen, M., Inze, D., Van Montagu, M.C.E., De Jaeger, G., Russinova, E., and Geelen, D. (2011). Adaptin-like protein TPLATE and clathrin recruitment during plant somatic cytokinesis occurs via two distinct pathways. Proc.

Natl. Acad. Sci. U.S.A **108**: 615–620.

daSilva, L.L.P., Foresti, O., and Denecke, J. (2006). Targeting of the plant vacuolar sorting receptor BP80 is dependent on multiple sorting signals in the cytosolic tail. Plant Cell **18**: 1477–1497.

Davis, C.G., Lehrman, M.A., Russell, D.W., Anderson, R.G.W., Brown, M.S., and Goldstein, J.L. (1986). The J. D. mutation in familial hypercholesterolemia: Amino acid substitution in cytoplasmic domain impedes internalization of LDL receptors. Cell **45**: 15–24.

Deblaere, R., Bytebier, B., de Greve, H., Deboeck, F., Schell, J., van Montagu, M., and Leemans, J. (1985). Efficient octopine Ti plasmid-derived vectors for *Agrobacterium*-mediated gene transfer to plants. Nucleic Acids Res. **13**: 4777–4788.

Delevoye, C., Hurbain, I., Tenza, D., Sibarita, J.-B.B., Uzan-Gafsou, S., Ohno, H., Geerts, W.J.C.C., Verkleij, A.J., Salamero, J., Marks, M.S., and Raposo, G. (2009). AP-1 and KIF13A coordinate endosomal sorting and positioning during melanosome biogenesis. J. Cell Biol. **187**: 247–264.

Dell'Angelica, E.C. (2009). AP-3-dependent trafficking and disease: the first decade. Curr. Opin. Cell Biol. **21**: 552–559.

Dell'Angelica, E.C., Klumperman, J., Stoorvogel, W., and Bonifacino, J.S. (1998). Association of the AP-3 adaptor complex with clathrin. Science **280**: 431–434.

Dell'Angelica, E.C., Mullins, C., and Bonifacino, J.S. (1999). AP-4, a novel protein complex related to clathrin adaptors. J. Biol. Chem. **274**: 7278–7285.

Dell'Angelica, E.C., Ohno, H., Ooi, C.E., Rabinovich, E., Roche, K.W., and Bonifacino, J.S. (1997). AP-3: An adaptor-like protein complex with ubiquitous expression. EMBO J. **16**: 917–928.

Deng, Z.Y., Liu, L.T., Li, T., Yan, S., Kuang, B.J., Huang, S.J., Yan, C.J., and Wang, T. (2015). OsKinesin-13A is an active microtubule depolymerase involved in glume length regulation via affecting cell elongation. Sci. Rep. **5**: 9457.

Desbrosses-Fonrouge, A.-G., Voigt, K., Schröder, A., Arrivault, S., Thomine, S., and Krämer, U. (2005). *Arabidopsis thaliana* MTP1 is a Zn transporter in the vacuolar membrane which mediates Zn detoxification and drives leaf Zn accumulation. FEBS Lett. **579**: 4165–4174.

Dettmer, J., Hong-Hermesdorf, A., Stierhof, Y.-D., and Schumacher, K. (2006). Vacuolar H^+-ATPase activity is required for endocytic and secretory trafficking in *Arabidopsis*. Plant Cell **18**: 715–730.

Dietel, K. (2012). Charakterisierung pflanzlicher AP-Complexe.

Domagalska, M. a and Leyser, O. (2011). Signal integration in the control of shoot branching. Nat. Rev. Mol. Cell Biol. **12**: 211–21.

Donaldson, J.G. and Jackson, C.L. (2000). Regulators and effectors of the ARF GTPases. Curr. Opin. Cell Biol. **12**: 475–482.

Doray, B., Ghosh, P., Griffith, J., Geuze, H.J., and Kornfeld, S. (2002). Cooperation of GGAs and AP-1 in packaging MPRs at the trans-Golgi network. Science **297**: 1700–1703.

Doray, B., Knisely, J.M., Wartman, L., Bu, G., and Kornfeld, S. (2008). Identification of acidic dileucine signals in LRP9 that interact with both GGAs and AP-1/AP-2. Traffic **9**: 1551–1562.

Doray, B., Lee, I., Knisely, J., Bu, G., and Kornfeld, S. (2007). The γ/σ1 and α/σ2 hemicomplexes of clathrin adaptors AP-1 and AP-2 harbor the dileucine recognition site. Mol. Biol. Cell **18**: 1887–1896.

Dotzauer, D., Wolfenstetter, S., Eibert, D., Schneider, S., Dietrich, P., and Sauer, N. (2010). Novel PSI Domains in Plant and Animal H+-Inositol Symporters. Traffic **11**: 767–781.

Downes, B.P., Stupar, R.M., Gingerich, D.J., and Vierstra, R.D. (2003). The HECT ubiquitin-protein ligase (UPL) family in *Arabidopsis*: UPL3 has a specific role in trichome development. Plant J. **35**: 729–742.

Drakakaki, G. and Dandekar, A. (2013). Protein secretion: How many secretory routes does a plant cell have? Plant Sci. **203**–**204**: 74–78.

Drechsel, G., Bergler, J., Wippel, K., Sauer, N., Vogelmann, K., and Hoth, S. (2011). C-terminal armadillo repeats are essential and sufficient for association of the plant U-box armadillo E3 ubiquitin ligase SAUL1 with the plasma membrane. J. Exp. Bot. **62**: 775–785.

Duangtum, N., Junking, M., Sawasdee, N., Cheunsuchon, B., Limjindaporn, T., and Yenchitsomanus, P. thai (2011). Human kidney anion exchanger 1 interacts with kinesin family member 3B (KIF3B). Biochem. Biophys. Res. Commun. **413**: 69–74.

Duden, R., Griffiths, G., Frank, R., Argos, P., and Kreis, T.E. (1991). ß-COP, a 110 kd protein associated with non-clathrin-coated vesicles and the golgi complex, shows homology to ß-adaptin. Cell **64**: 649–665.

Dunkel, M., Latz, A., Schumacher, K., Mü Ller, T., Becker, D., Hedrich, R., Müller, T., Becker, D., and Hedrich, R. (2008). Targeting of vacuolar membrane localized members of the TPK channel family. Mol. Plant **1**: 938–949.

Durek, P., Schmidt, R., Heazlewood, J.L., Jones, A., MacLean, D., Nagel, A., Kersten, B., and Schulze, W.X. (2009). PhosPhAt: The *Arabidopsis thaliana* phosphorylation site database. An update. Nucleic Acids Res. **38**: D828–D834.

Ebine, K., Inoue, T., Ito, J., Ito, E., Uemura, T., Goh, T., Abe, H., Sato, K., Nakano, A., and Ueda, T. (2014). Plant vacuolar trafficking occurs through distinctly regulated pathways. Curr. Biol. **24**: 1375–1382.

Eichhorn, S. (2008). Herstellung von RFP-Reporterkonstrukten für die subzelluläre Lokalisation von AtINT1- und AtINT4-Transportern in *Arabidopsis thaliana*.

Enami, K., Ichikawa, M., Uemura, T., Kutsuna, N., Hasezawa, S., Nakagawa, T., Nakano, A., and Sato, M.H. (2009). Differential expression control and polarized distribution of plasma membrane-resident SYP1 SNAREs in *Arabidopsis thaliana*. Plant Cell Physiol. **50**: 280–289.

Fan, L., Hao, H., Xue, Y., Zhang, L., Song, K., Ding, Z., Botella, M.A., Wang, H., and Lin, J. (2013). Dynamic analysis of *Arabidopsis* AP2 σ subunit reveals a key role in clathrin-mediated endocytosis and plant development. Development **140**: 3826–3837.

Feraru, E. and Friml, J. (2008). PIN Polar Targeting. Plant Physiol. **147**: 1553–1559.

Feraru, E., Paciorek, T., Feraru, M.I., Zwiewka, M., De Groodt, R., De Rycke, R., Kleine-Vehn, J., and Friml, J.J. (2010). The AP-3 β adaptin mediates the biogenesis and function of lytic vacuoles in *Arabidopsis*. Plant Cell **22**: 2812–2824.

Fiedler, K., Veit, M., Stamnes, M.A., and Rothman, J.E. (1996). Bimodal interaction of coatomer with the p24 family of putative cargo receptors. Science **273**: 1396.

Flessner, L.B. and Moley, K.H. (2009). Similar [DE]XXXL[LI] motifs differentially target GLUT8 and GLUT12 in Chinese hamster ovary cells. Traffic **10**: 324–333.

Folkers, U., Berger, J., and Hülskamp, M. (1997). Cell morphogenesis of trichomes in *Arabidopsis*: differential control of primary and secondary branching by branch initiation regulators and cell growth. Development **124**: 3779–3786.

Foresti, O. and Denecke, J. (2008). Intermediate organelles of the plant secretory pathway: Identity and function. Traffic **9**: 1599–1612.

Frazier, M.N., Davies, A.K., Voehler, M., Kendall, A.K., Borner, G.H.H., Chazin, W.J., Robinson, M.S., and Jackson, L.P. (2016). Molecular basis for the interaction between AP4 β4 and its accessory protein, tepsin. Traffic **17**: 400–415.

Friml, J. (2010). Subcellular trafficking of PIN auxin efflux carriers in auxin transport. Eur. J. Cell Biol. **89**: 231–235.

Fuji, K., Shimada, T., Takahashi, H., Tamura, K., Koumoto, Y., Utsumi, S., Nishizawa, K., Maruyama, N., and Hara-Nishimura, I. (2007). *Arabidopsis* vacuolar sorting mutants (green fluorescent seed) can be identified efficiently by secretion of vacuole-targeted green fluorescent protein in their seeds. Plant Cell **19**: 597–609.

Fuji, K., Shirakawa, M., Shimono, Y., Kunieda, T., Fukao, Y., Koumoto, Y., Takahashi, H., Hara-Nishimura, I., and Shimada, T. (2016). The adaptor complex AP-4 regulates vacuolar protein sorting at the trans-Golgi network by interacting with VACUOLAR SORTING RECEPTOR1. Plant Physiol. **170**: 211–219.

Fujikura, U., Elsaesser, L., Breuninger, H., Sánchez-Rodríguez, C., Ivakov, A., Laux, T., Findlay, K., Persson, S., and Lenhard, M. (2014). AtKinesin-13A modulates cell-wall synthesis and cell expansion in *Arabidopsis thaliana* via the THESEUS1 pathway. PLoS Genet. **10**: e1004627.

Fujimoto, M. and Tsutsumi, N. (2014). Dynamin-related proteins in plant post-Golgi traffic. Front. Plant Sci. **5**: 408.

Gadeyne, A. et al. (2014). The TPLATE adaptor complex drives clathrin-mediated endocytosis in plants. Cell **156**: 691–704.

Gasber, A., Klaumann, S., Trentmann, O., Trampczynska, A., Clemens, S., Schneider, S., Sauer, N., Feifer, I., Bittner, F., Mendel, R.R., and Neuhaus, H.E. (2011). Identification of an *Arabidopsis* solute carrier critical for intracellular transport and inter-organ allocation of molybdate. Plant Biol. **13**: 710–718.

Geldner, N., Dénervaud-Tendon, V., Hyman, D.L., Mayer, U., Stierhof, Y.D., and Chory, J. (2009). Rapid, combinatorial analysis of membrane compartments in intact plants with a multicolor marker set. Plant J. **59**: 169–178.

Gendre, D., Jonsson, K., Boutté, Y., and Bhalerao, R.P. (2015). Journey to the cell surface—the central role of the trans-Golgi network in plants. Protoplasma **252**: 385–398.

Gershlick, D.C., Lousa, C.D.M., Farmer, L., and Denecke, J. (2014a). Routes to and from the plasma membrane: bulk flow versus signal mediated endocytosis. Plant Signal. Behav. **9**: e972813.

Gershlick, D.C., Lousa, C.D.M., Foresti, O., Lee, A.J., Pereira, E. a, DaSilva, L.L.P., Bottanelli, F., and Denecke, J. (2014b). Golgi-dependent transport of vacuolar sorting receptors is regulated by COPII, AP1, and AP4 protein complexes in tobacco. Plant Cell **26**: 1308–1329.

Goizet, C., Boukhris, A., Mundwiller, E., Tallaksen, C., Forlani, S., Toutain, A., Carriere, N., Paquis, V., Depienne, C., Durr, A., Stevanin, G., and Brice, A. (2009). Complicated forms of autosomal dominant hereditary spastic paraplegia are frequent in SPG10. Hum. Mutat. **30**: E376–E385.

Gough, N.R., Zweifel, M.E., Martinez-Augustin, O., Aguilar, R.C., Bonifacino, J.S., and Fambrough, D.M. (1999). Utilization of the indirect lysosome targeting pathway by lysosome-associated membrane proteins (LAMPs) is influenced largely by the C-

terminal residue of their. J. Cell Sci. **112**: 4257–4269.

Grunewald, W. and Friml, J. (2010). The march of the PINs: developmental plasticity by dynamic polar targeting in plant cells. EMBO J. **29**: 2700–2714.

Gu, F., Crump, C.., and Thomas, G. (2001). Trans-Golgi network sorting. Cell. Mol. Life Sci. **58**: 1067–1084.

Guo, X., Mattera, R., Ren, X., Chen, Y., Retamal, C., González, A., and Bonifacino, J.S. (2013). The adaptor protein-1μ1B subunit expands the repertoire of basolateral sorting signal recognition in epithelial cells. Dev. Cell **27**: 353–366.

ter Haar, E., Harrison, S.C., and Kirchhausen, T. (2000). Peptide-in-groove interactions link target proteins to the beta-propeller of clathrin. Proc. Natl. Acad. Sci. U.S.A. **97**: 1096–1000.

Hachez, C., Besserer, A., Chevalier, A.S., and Chaumont, F. (2013). Insights into plant plasma membrane aquaporin trafficking. Trends Plant Sci. **18**: 344–352.

Hanahan, D. (1983). Studies on transformation of *Escherichia coli* with plasmids. J. Mol. Biol. **166**: 557–580.

Hanton, S.L., Bortolotti, L.E., Renna, L., Stefano, G., and Brandizzi, F. (2005a). Crossing the divide - Transport between the endoplasmic reticulum and Golgi apparatus in plants. Traffic **6**: 267–277.

Hanton, S.L., Renna, L., Bortolotti, L.E., Chatre, L., Stefano, G., and Brandizzi, F. (2005b). Diacidic motifs influence the export of transmembrane proteins from the endoplasmic reticulum in plant cells. Plant Cell **17**: 3081–3093.

Harter, C. and Mellman, I. (1992). Transport of the lysosomal membrane glycoprotein lgp120 (lgp-A) to lysosomes does not require appearance on the plasma membrane. J. Cell Biol. **117**: 311–325.

Haydon, M.J. and Cobbett, C.S. (2007). A novel major facilitator superfamily protein at the tonoplast influences zinc tolerance and accumulation in *Arabidopsis*. Plant Physiol. **143**: 1705–1719.

Haydon, M.J., Kawachi, M., Wirtz, M., Hillmer, S., Hell, R., and Kramer, U. (2012). Vacuolar nicotianamine has critical and distinct roles under iron deficiency and for zinc sequestration in *Arabidopsis*. Plant Cell **24**: 724–737.

He, G., Gupta, S., Yi, M., Michaely, P., Hobbs, H.H., and Cohen, J.C. (2002). ARH is a modular adaptor protein that interacts with the LDL receptor, clathrin, and AP-2. J. Biol. Chem. **277**: 44044–44049.

Heazlewood, J.I., Durek, P., Hummel, J., Selbig, J., Weckwerth, W., Walther, D., and Schulze, W.X. (2008). PhosPhAt : A database of phosphorylation sites in *Arabidopsis thaliana* and a plant-specific phosphorylation site predictor. Nucleic Acids Res. **36**: D1015–D1021.

Hicke, L. and Dunn, R. (2003). Regulation of membrane protein transport by ubiquitin and ubiquitin-binding proteins. Annu. Rev. Cell Dev. Biol. **19**: 141–172.

Hicke, L. and Riezman, H. (1996). Ubiquitination of a yeast plasma membrane receptor signals its ligand- stimulated endocytosis. Cell **84**: 277–287.

Hirst, J. et al. (2011). The fifth adaptor protein complex. PLoS Biol. **9**: e1001170.

Hirst, J., Borner, G.H.H., Antrobus, R., Peden, A.A., Hodson, N.A., Sahlender, D.A., and Robinson, M.S. (2012). Distinct and overlapping roles for AP-1 and GGAs revealed by the “knocksideways” system. Curr. Biol. **22**: 1711–1716.

Hirst, J., Bright, N.A., Rous, B., and Robinson, M.S. (1999). Characterization of a fourth adaptor-related protein complex. Mol. Biol. Cell **10**: 2787–802.

Hirst, J., Schlacht, A., Norcott, J.P., Traynor, D., Bloomfield, G., Antrobus, R., Kay, R.R., Dacks, J.B., and Robinson, M.S. (2014). Characterization of TSET, an ancient and widespread membrane trafficking complex. eLife **2014**: 1–18.

Hofgen, R. and Willmitzer, L. (1988). Storage of competent cells for *Agrobacterium* transformation. Nucleic Acids Res. **16**: 9877.

Hofmann, K. and Falquet, L. (2001). A ubiquitin-interacting motif conserved in components of the proteasomal and lysosomal protein degradation systems. Trends Biochem. Sci. **26**: 347–350.

Holsters, M., Silva, B., Van Vliet, F., Genetello, C., De Block, M., Dhaese, P., Depicker, A., Inzé, D., Engler, G., Villarroel, R., Van Montagu, M., and Schell, J. (1980). The functional organization of the nopaline *A. tumefaciens* plasmid pTiC58. Plasmid **3**: 212–230.

Honda, A., Nogami, M., Yokozeki, T., Yamazaki, M., Nakamura, H., Watanabe, H., Kawamoto, K., Nakayama, K., Morris, A.J., Frohman, M.A., and Kanaho, Y. (1999). Phosphatidylinositol 4-phosphate 5-kinase alpha is a downstream effector of the small G protein ARF6 in membrane ruffle formation. Cell **99**: 521–532.

Hong, W. (2005). SNAREs and traffic. Biochim. Biophys. Acta **1744**: 120–144.

Höning, S., Ricotta, D., Krauss, M., Späte, K., Spolaore, B., Motley, A., Robinson, M., Robinson, C., Haucke, V., and Owen, D.J. (2005). Phosphatidylinositol-(4,5)-bisphosphate regulates sorting signal recognition by the clathrin-associated adaptor complex AP2. Mol. Cell **18**: 519–531.

Höning, S., Sosa, M., Hille-Rehfeld, A., and von Figura, K. (1997). The 46-kDa mannose 6-phosphate receptor contains multiple binding sites for clathrin adaptors. J. Biol. Chem. **272**: 19884–19890.

Horgan, C.P. and McCaffrey, M.W. (2011). Rab GTPases and microtubule motors. Biochem. Soc. Trans. **39**: 1202–1206.

Hülskamp, M. (2004). Plant trichomes: a model for cell differentiation. Nat. Rev. Mol. Cell Biol. **5**: 471–480.

Hülskamp, M., Miséra, S., and Jürgens, G. (1994). Genetic dissection of trichome cell development in *Arabidopsis*. Cell **76**: 555–566.

Hunziker, W. and Geuze, H.J. (1996). Intracellular trafficking of lysosomal membrane proteins. Bioessays **18**: 379–389.

Hunziker, W., Harter, C., Matter, K., and Mellman, I. (1991). Basolateral sorting in MDCK cells requires a distinct cytoplasmic domain determinant. Cell **66**: 907–20.

Hurley, J.H. (2008). ESCRT complexes and the biogenesis of multivesicular bodies. Curr. Opin. Cell Biol. **20**: 4–11.

Hwang, I. and Robinson, D.G. (2009). Transport vesicle formation in plant cells. Curr. Opin. Plant Biol. **12**: 660–669.

Ide, Y., Kusano, M., Oikawa, A., Fukushima, A., Tomatsu, H., Saito, K., Hirai, M.Y., and Fujiwara, T. (2011). Effects of molybdenum deficiency and defects in molybdate transporter MOT1 on transcript accumulation and nitrogen/sulphur metabolism in *Arabidopsis thaliana*. J. Exp. Bot. **62**: 1483–1497.

Inoue, H. and Randazzo, P.A. (2007). Arf GAPs and their interacting proteins. Traffic **8**: 1465–1475.

Dello Ioio, R., Nakamura, K., Moubayidin, L., Perilli, S., Taniguchi, M., Morita, M.T., Aoyama, T., Costantino, P., and Sabatini, S. (2008). A genetic framework for the control of cell division and differentiation in the root meristem. Science **322**: 1380–

1384.

Ishimaru, Y., Takahashi, R., Bashir, K., Shimo, H., Senoura, T., Sugimoto, K., Ono, K., Yano, M., Ishikawa, S., Arao, T., Nakanishi, H., and Nishizawa, N.K. (2012). Characterizing the role of rice NRAMP5 in manganese, iron and cadmium transport. Sci. Rep. **2**: 286.

Jacobsen, S.E. (1993). Mutations at the SPINDLY locus of *Arabidopsis* alter gibberellin signal transduction. Plant Cell **5**: 887–896.

Janvier, K. and Bonifacino, J.S. (2005). Role of the endocytic machinery in the sorting of lysosome-associated membrane proteins. Mol. Biol. Cell **16**: 4231–4242.

Janvier, K., Kato, Y., Boehm, M., Rose, J.R., Martina, J.A., Kim, B.Y., Venkatesan, S., and Bonifacino, J.S. (2003). Recognition of dileucine-based sorting signals from HIV-1 Nef and LIMP-II by the AP-1 γ-σ1 and AP-3 δ-σ3 hemicomplexes. J. Cell Biol. **163**: 1281–1290.

Johanson, U., Karlsson, M., Johansson, I., Gustavsson, S., Sjö, S., Fraysse, L., Weig, A.R., and Kjellbom, P. (2001). The complete set of genes encoding Major Intrinsic Proteins in *Arabidopsis* provides a framework for a new nomenclature for Major Intrinsic Proteins in plants. Plant Physiol. **126**: 1358–1369.

Johnson, M.A., Von Besser, K., Zhou, Q., Smith, E., Aux, G., Patton, D., Levin, J.Z., and Preuss, D. (2004). *Arabidopsis* hapless mutations define essential gametophytic functions. Genetics **168**: 971–982.

Jones, B.G., Thomas, L., Molloy, S.S., Thulin, C.D., Fry, M.D., Walsh, K.A., and Thomas, G. (1995). Intracellular trafficking of furin is modulated by the phosphorylation state of a casein kinase II site in its cytoplasmic tail. EMBO J. **14**: 5869–5883.

Jones, D.H., Morris, J.B., Morgan, C.P., Kondo, H., Irvine, R.F., and Cockcroft, S. (2000). Type I phosphatidylinositol 4-phosphate 5-kinase directly interacts with ADP-ribosylation factor 1 and is responsible for phosphatidylinositol 4,5-bisphosphate synthesis in the Golgi compartment. J. Biol. Chem. **275**: 13962–13966.

Jost, M., Simpson, F., Kavran, J.M., Lemmon, M.A., and Schmid, S.L. (1998). Phosphatidylinositol-4,5-bisphosphate is required for endocytic coated vesicle formation. Curr. Biol. **8**: 1399–1404.

Jürgens, G. (2004). Membrane trafficking in plants. Annu. Rev. Cell Dev. Biol. **20**: 481–504.

Kang, H. and Hwang, I. (2014). Vacuolar sorting receptor-mediated trafficking of soluble vacuolar proteins in plant cells. Plants (Basel) **3**: 392–408.

Kasai, K., Takano, J., Miwa, K., Toyoda, A., and Fujiwara, T. (2011). High boron-induced ubiquitination regulates vacuolar sorting of the BOR1 borate transporter in *Arabidopsis thaliana*. J. Biol. Chem. **286**: 6175–6183.

Keller, P. and Simons, K. (1997). Post-Golgi biosynthetic trafficking. J. Cell Sci. **110**: 3001–3009.

Kim, S.A. and Guerinot, M. Lou (2007). Mining iron: Iron uptake and transport in plants. FEBS Lett. **581**: 2273–2280.

Kim, S.A., Punshon, T., Lanzirotti, A., Li, L., Alonso, J.M., Ecker, J.R., Kaplan, J., and Guerinot, M. Lou (2006). Localization of iron in *Arabidopsis* seed requires the vacuolar membrane transporter VIT1. Science **314**: 1295–1298.

Kim, S.Y., Xu, Z.-Y., Song, K., Kim, D.H., Kang, H., Reichardt, I., Sohn, E.J., Friml, J., Jürgens, G., and Hwang, I. (2013). Adaptor protein complex 2-mediated endocytosis is crucial for male reproductive organ development in *Arabidopsis*. Plant Cell **25**: 2970–2985.

King, B.R. and Guda, C. (2007). ngLOC: an n-gram-based Bayesian method for estimating the subcellular proteomes of eukaryotes. Genome Biol. **8**: 68.

Kirchhausen, T. (1999). Adaptors for clathrin-mediated traffic. Annu. Rev. Cell Dev. Biol. **15**: 705–732.

Kitagawa, K., Kurinami, S., Oki, K., Abe, Y., Ando, T., Kono, I., Yano, M., Kitano, H., and Iwasaki, Y. (2010). A novel kinesin 13 protein regulating rice seed length. Plant Cell Physiol. **51**: 1315–1329.

Kitakura, S., Vanneste, S., Robert, S., Löfke, C., Teichmann, T., Tanaka, H., and Friml, J. (2011). Clathrin mediates endocytosis and polar distribution of PIN auxin transporters in *Arabidopsis*. Plant Cell **23**: 1920–1931.

Klebe, S., Azzedine, H., Durr, A., Bastien, P., Bouslam, N., Elleuch, N., Forlani, S., Charon, C., Koenig, M., Melki, J., Brice, A., and Stevanin, G. (2006). Autosomal recessive spastic paraplegia (SPG30) with mild ataxia and sensory neuropathy maps to chromosome 2q37.3. Brain **129**: 1456–1462.

Kobae, Y., Uemura, T., Sato, M.H., Ohnishi, M., Mimura, T., Nakagawa, T., and Maeshima, M. (2004). Zinc transporter of *Arabidopsis thaliana* AtMTP1 is localized to vacuolar membranes and implicated in zinc homeostasis. Plant Cell Physiol. **45**: 1749–1758.

Komarova, N.Y., Meier, S., Meier, A., Grotemeyer, M.S., and Rentsch, D. (2012). Determinants for *Arabidopsis* peptide transporter targeting to the tonoplast or plasma membrane. Traffic **13**: 1090–1105.

Koncz, C., Németh, K., Rédei, G.P., and Schell, J. (1992). T-DNA insertional mutagenesis in *Arabidopsis*. Plant Mol. Biol. **20**: 963–976.

Křeček, P., Skůpa, P., Libus, J., Naramoto, S., Tejos, R., Friml, J., and Zažímalová, E. (2009). The PIN-FORMED (PIN) protein family of auxin transporters. Genome Biol. **10**: 249.

Kreis, T.E., Lowe, M., and Pepperkok, R. (1995). COPs regulating membrane traffic. Annu. Rev. Cell Dev. Biol. **11**: 677–706.

Krouk, G. et al. (2010). Nitrate-regulated auxin transport by NRT1.1 defines a mechanism for nutrient sensing in plants. Dev. Cell **18**: 927–937.

Kuromori, T., Wada, T., Kamiya, A., Yuguchi, M., Yokouchi, T., Imura, Y., Takabe, H., Sakurai, T., Akiyama, K., Hirayama, T., Okada, K., and Shinozaki, K. (2006). A trial of phenome analysis using 4000 Ds-insertional mutants in gene-coding regions of *Arabidopsis*. Plant J. **47**: 640–651.

Kyttälä, A., Ihrke, G., Vesa, J., Schell, M.J., and Luzio, J.P. (2003). Two motifs target Batten disease protein CLN3 to lysosomes in transfected nonneuronal and neuronal cells. Mol. Biol. Cell **15**: 1313–1323.

Kyttälä, A., Yliannala, K., Schu, P., Jalanko, A., and Luzio, J.P. (2005). AP-1 and AP-3 facilitate lysosomal targeting of Batten disease protein CLN3 via its dileucine motif. J. Biol. Chem. **280**: 10277–10283.

Lam-Yuk-Tseung, S., Picard, V., and Gros, P. (2006). Identification of a tyrosine-based motif (YGSI) in the amino terminus of Nramp1 (Slc11a1) that is important for lysosomal targeting. J. Biol. Chem. **281**: 31677–31688.

Lam, S.K., Siu, C.L., Hillmer, S., Jang, S., An, G., Robinson, D.G., and Jiang, L. (2007). Rice SCAMP1 defines clathrin-coated, trans-Golgi-located tubular-vesicular structures as an early endosome in tobacco BY-2 Cells. Plant Cell **19**: 296–319.

Lanoix, J., Ouwendijk, J., Chung-Chih, L., Stark, A., Love, H.D., Ostermann, J., and Nilsson,

T. (1999). GTP hydrolysis by ARF1 mediates sorting and concentration of Golgi resident enzymes into functional COPI vesicles. EMBO J. **18**: 4935–4948.

Lanquar, V., Lelièvre, F., Barbier-Brygoo, H., and Thomine, S. (2004). Regulation and function of AtNRAMP4 metal transporter protein. Soil Sci. Plant Nutr. **50**: 1141–1150.

Lanquar, V., Lelièvre, F., Bolte, S., Hamès, C., Alcon, C., Neumann, D., Vansuyt, G., Curie, C., Schröder, A., Krämer, U., Barbier-Brygoo, H., and Thomine, S. (2005). Mobilization of vacuolar iron by AtNRAMP3 and AtNRAMP4 is essential for seed germination on low iron. EMBO J. **24**: 4041–4051.

Larisch, N., Schulze, C., Galione, A., and Dietrich, P. (2012). An N-terminal dileucine motif directs two-pore channels to the tonoplast of plant cells. Traffic **13**: 1012–1022.

Larkin, J.C., Young, N., Prigge, M., and Marks, M.D. (1996). The control of trichome spacing and number in *Arabidopsis*. Development **122**: 997–1005.

Lee, G.-J., Kim, H., Kang, H., Jang, M., Lee, D.W., Lee, S., and Hwang, I. (2007). EpsinR2 interacts with clathrin, adaptor protein-3, AtVTI12, and phosphatidylinositol-3-phosphate. Implications for EpsinR2 function in protein trafficking in plant cells. Plant Physiol. **143**: 1561–1575.

Lee, H.K., Cho, S.K., Son, O., Xu, Z., Hwang, I., and Kim, W.T. (2009). Drought stress-induced Rma1H1, a RING membrane-anchor E3 ubiquitin ligase homolog, regulates aquaporin levels via ubiquitination in transgenic *Arabidopsis* plants. Plant Cell **21**: 622–641.

Legendre-Guillemin, V., Wasiak, S., Hussain, N.K., Angers, A., and McPherson, P.S. (2004). ENTH/ANTH proteins and clathrin-mediated membrane budding. J. Cell Sci. **117**: 9–18.

Letourneur, F. and Klausner, R.D. (1992). A novel di-leucine motif and a tyrosine-based motif independently mediate lysosomal targeting and endocytosis of CD3 chains. Cell **69**: 1143–1157.

Levkowitz, G., Waterman, H., Ettenberg, S.A., Katz, M., Tsygankov, A.Y., Alroy, I., Lavi, S., Iwai, K., Reiss, Y., Ciechanover, A., Lipkowitz, S., and Yarden, Y. (1999). Ubiquitin ligase activity and tyrosine phosphorylation underlie suppression of growth factor signaling by c-Cbl/Sli-1. Mol. Cell **4**: 1029–1040.

Li, R., Raikhel, N. V, and Hicks, G.R. (2012). Chemical effectors of plant endocytosis and endomembrane trafficking. In Endocytosis in Plants, J. Šamaj, ed, pp. 37–62.

Li, X., Wang, X., Yang, Y., Li, R., He, Q., Fang, X., Luu, D.-T., Maurel, C., and Lin, J. (2011). Single-molecule analysis of PIP2;1 dynamics and partitioning reveals multiple modes of *Arabidopsis* plasma membrane aquaporin regulation. Plant Cell **23**: 3780–97.

Lin, R. and Wang, H. (2005). Two homologous ATP-binding cassette transporter proteins, AtMDR1 and AtPGP1, regulate Arabidopsis photomorphogenesis and root development by mediating polar auxin transport. Plant Physiol. **138**: 949–964.

Lindwasser, O.W., Smith, W.J., Chaudhuri, R., Yang, P., Hurley, J.H., and Bonifacino, J.S. (2008). A diacidic motif in human immunodeficiency virus type 1 Nef is a novel determinant of binding to AP-2. J. Virol. **82**: 1166–1174.

Liu, X., Wu, J., Clark, G., Lundy, S., Lim, M., Arnold, D., Chan, J., Tang, W., Muday, G.K., Gardner, G., and Roux, S.J. (2012). Role for apyrases in polar auxin transport in *Arabidopsis*. Plant Physiol. **160**: 1985–1995.

Lu, G. and Moriyama, E.N. (2004). Vector NTI, a balanced all-in-one sequence analysis suite. Brief. Bioinformatics **5**: 378–388.

Lu, L., Lee, Y.-R.J., Pan, R., Maloof, J.N., and Liu, B. (2005). An internal motor kinesin is

associated with the Golgi apparatus and plays a role in trichome morphogenesis in *Arabidopsis*. Mol. Biol. Cell **16**: 811–823.

Luria, S.E. (1960). The bacterial protoplasm: composition and organization. Bact. **1**: 1–34.

Luschnig, C. and Vert, G. (2014). The dynamics of plant plasma membrane proteins: PINs and beyond. Development **141**: 2924–2938.

Luu, D.T., Martiniãre, A., Sorieul, M., Runions, J., and Maurel, C. (2012). Fluorescence recovery after photobleaching reveals high cycling dynamics of plasma membrane aquaporins in *Arabidopsis* roots under salt stress. Plant J. **69**: 894–905.

Mai, H.-J., Pateyron, S., and Bauer, P. (2016). Iron homeostasis in *Arabidopsis thaliana*: transcriptomic analyses reveal novel FIT-regulated genes, iron deficiency marker genes and functional gene networks. BMC Plant Biol. **16**: 211.

Malhotra, V., Serafini, T., Orci, L., Shepherd, J.C., and Rothman, J.E. (1989). Purification of a novel class of coated vesicles mediating biosynthetic protein transport through the Golgi stack. Cell **58**: 329–336.

de Marcos Lousa, C. and Denecke, J. (2016). Lysosomal and vacuolar sorting: not so different after all! Biochem. Soc. Trans. **44**: 891–897.

Marcusson, E.G., Horazdovsky, B.F., Cereghino, J.L., Gharakhanian, E., and Emr, S.D. (1994). The sorting receptor for yeast vacuolar carboxypeptidase Y is encoded by the VPS10 gene. Cell **77**: 579–586.

Marks, M.D., Betancur, L., Gilding, E., Chen, F., Bauer, S., Wenger, J.P., Dixon, R.A., and Haigler, C.H. (2008). A new method for isolating large quantities of Arabidopsis trichomes for transcriptome, cell wall and other types of analyses. Plant J. **56**: 483–492.

Marks, M.D., Wenger, J.P., Gilding, E., Jilk, R., and Dixon, R.A. (2009). Transcriptome analysis of *Arabidopsis* wild-type and *gl3-sst sim* trichomes identifies four additional genes required for trichome development. Mol. Plant **2**: 803–822.

Marks, M.S., Woodruff, L., Ohno, H., and Bonifacino, J.S. (1996). Protein targeting by tyrosine- and di-leucine-based signals: Evidence for distinct saturable components. J. Cell Biol. **135**: 341–354.

Marschner, H., Romheld, V., and Kissel, M. (1986). Different strategies in higher plants in mobilization and uptake of iron. J. Plant Nutr. **9**: 695–713.

Mary, V., Schnell Ramos, M., Gillet, C., Socha, A.L., Giraudat, J., Agorio, A., Merlot, S., Clairet, C., Kim, S.A., Punshon, T., Guerinot, M. Lou, and Thomine, S. (2015). Bypassing iron storage in endodermal vacuoles rescues the iron mobilization defect in the *natural resistance associated-macrophage protein3natural resistance associated-macrophage protein4* double mutant. Plant Physiol. **169**: 748–759.

Mathur, J., Spielhofer, P., Kost, B., and Chua, N. (1999). The actin cytoskeleton is required to elaborate and maintain spatial patterning during trichome cell morphogenesis in *Arabidopsis thaliana*. Development **126**: 5559–5568.

Matsuda, S., Miura, E., Matsuda, K., Kakegawa, W., Kohda, K., Watanabe, M., and Yuzaki, M. (2008). Accumulation of AMPA receptors in autophagosomes in neuronal axons lacking adaptor protein AP-4. Neuron **57**: 730–745.

Matsuda, S. and Yuzaki, M. (2008). AP-4: Autophagy-four mislocalized proteins in axons. Autophagy **4**: 815–816.

Matsuda, S. and Yuzaki, M. (2009). Polarized sorting of AMPA receptors to the somatodendritic domain is regulated by adaptor protein AP-4. Neurosci. Res. **65**: 1–5.

Mattera, R., Boehm, M., Chaudhuri, R., Prabhu, Y., and Bonifacino, J.S. (2011). Conservation and diversification of dileucine signal recognition by adaptor protein (AP) complex variants. J. Biol. Chem. **286**: 2022–2030.

Mattera, R., Guardia, C.M., Sidhu, S.S., and Bonifacino, J.S. (2015). Bivalent motif-ear interactions mediate the association of the accessory protein tepsin with the AP-4 adaptor complex. J. Biol. Chem. **290**: 30736–30749.

Maurel, C. (2007). Plant aquaporins: Novel functions and regulation properties. FEBS Lett. **581**: 2227–2236.

Maurel, C., Boursiac, Y., Luu, D.-T., Santoni, V., Shahzad, Z., and Verdoucq, L. (2015). Aquaporins in plants. Physiol. Rev. **95**: 1321–1358.

Maxfield, F.R. and McGraw, T.E. (2004). Endocytic recycling. Nat. Rev. Mol. Cell Biol. **5**: 121–132.

McMahon, H.T. and Boucrot, E. (2011). Molecular mechanism and physiological functions of clathrin-mediated endocytosis. Nat. Rev. Mol. Cell Biol. **12**: 517–533.

McMahon, H.T. and Mills, I.G. (2004). COP and clathrin-coated vesicle budding: Different pathways, common approaches. Curr. Opin. Cell Biol. **16**: 379–391.

Meyer, D.M., Crottet, P., Maco, B., Degtyar, E., Cassel, D., and Spiess, M. (2005). Oligomerization and dissociation of AP-1 adaptors are regulated by cargo signals and by ArfGAP1-induced GTP hydrolysis. Mol. Biol. Cell **16**: 4745–4754.

Migeon, A., Blaudez, D., Wilkins, O., Montanini, B., Campbell, M.M., Richaud, P., Thomine, S., and Chalot, M. (2010). Genome-wide analysis of plant metal transporters, with an emphasis on poplar. Cell. Mol. Life Sci. **67**: 3763–3784.

Miller, S.E., Collins, B.M., McCoy, A.J., Robinson, M.S., and Owen, D.J. (2007). A SNARE–adaptor interaction is a new mode of cargo recognition in clathrin-coated vesicles. Nature **450**: 570–574.

Miller, S.E., Sahlender, D.A., Graham, S.C., Höning, S., Robinson, M.S., Peden, A.A., and Owen, D.J. (2011). The molecular basis for the endocytosis of small R-SNAREs by the clathrin adaptor CALM. Cell **147**: 1118–1131.

Misra, S., Puertollano, R., Kato, Y., Bonifacino, J.S., and Hurley, J.H. (2002). Structural basis for acidic-cluster-dileucine sorting-signal recognition by VHS domains. Nature **415**: 933–937.

Molins, H., Michelet, L., Lanquar, V., Agorio, A., Giraudat, J., Roach, T., Krieger-Liszkay, A., and Thomine, S. (2013). Mutants impaired in vacuolar metal mobilization identify chloroplasts as a target for cadmium hypersensitivity in *Arabidopsis thaliana*. Plant Cell Environ. **36**: 804–817.

Montpetit, A., Côté, S., Brustein, E., Drouin, C.A., Lapointe, L., Boudreau, M., Meloche, C., Drouin, R., Hudson, T.J., Drapeau, P., and Cossette, P. (2008). Disruption of AP1S1, causing a novel neurocutaneous syndrome, perturbs development of the skin and spinal cord. PLoS Genet. **4**: e1000296.

Moreno-De-Luca, A., Helmers, S.L., Mao, H., Burns, T.G., Melton, A.M.A., Schmidt, K.R., Fernhoff, P.M., Ledbetter, D.H., and Martin, C.L. (2011). Adaptor protein complex-4 (AP-4) deficiency causes a novel autosomal recessive cerebral palsy syndrome with microcephaly and intellectual disability. J. Med. Genet. **48**: 141–144.

Morris, S.M. and Cooper, J.A. (2001). Disabled-2 colocalizes with the LDLR in clathrin-coated pits and interacts with AP-2. Traffic **2**: 111–123.

Morrissey, J. and Guerinot, M. Lou (2010). Iron uptake and transport in plants: The good, the bad, and the ionome. Chem. Rev. **109**: 4553–4567.

Mucha, E., Hoefle, C., Hückelhoven, R., and Berken, A. (2010). RIP3 and AtKinesin-13A – A novel interaction linking Rho proteins of plants to microtubules. Eur. J. Cell Biol. **89**: 906–916.

Müdsam, C. (2012). Analysis of adaptor protein mediated vesicle transport in *Arabidopsis thaliana*.

Müdsam, C., Wollschläger, P., Sauer, N., Schneider, S. (2018). Sorting of *Arabidopsis* NRAMP3 and NRAMP4 depends on adaptor protein complex AP4 and a dileucine-based motif. Traffic (*Accepted for publication: 16 March 2018*). doi:10.1111/tra.12567.

Müller, N. (2016). Localization and regulation of two-pore channels in *Arabidopsis thaliana*.

Murashige, T. and Skoog, F. (1962). A revised medium for rapid growth and bio assays with tobacco tissue cultures. Physiol Plant **15**: 473–497.

Najmabadi, H. et al. (2011). Deep sequencing reveals 50 novel genes for recessive cognitive disorders. Nature **478**: 57–63.

Nakagawa, T., Setou, M., Seog, D.-H.D., Ogasawara, K., Dohmae, N., Takio, K., and Hirokawa, N. (2000). A novel motor, KIF13A, transports mannose-6-phosphate receptor to plasma membrane through direct interaction with AP-1 complex. Cell **103**: 569–581.

Nakatsu, F., Hase, K., and Ohno, H. (2014). The role of the clathrin adaptor AP-1: Polarized sorting and beyond. Membranes (Basel). **4**: 747–763.

Nakatsu, F. and Ohno, H. (2003). Adaptor protein complexes as the key regulators of protein sorting in the post-Golgi network. Cell Struct. Funct. **28**: 419–429.

Nelson, B.K., Cai, X., and Nebenführ, A. (2007). A multicolored set of in vivo organelle markers for co-localization studies in *Arabidopsis* and other plants. Plant J. **51**: 1126–1136.

Nie, Z. and Randazzo, P.A. (2006). Arf GAPs and membrane traffic. J. Cell Sci. **119**: 1203–1211.

Nielsen, M.S., Madsen, P., Christensen, E.I., Nykjær, A., Gliemann, J., Kasper, D., Pohlmann, R., and Petersen, C.M. (2001). The sortilin cytoplasmic tail conveys Golgi-endosome transport and binds the VHS domain of the GGA2 sorting protein. EMBO J. **20**: 2180–2190.

Niihama, M., Takemoto, N., Hashiguchi, Y., Tasaka, M., and Morita, M.T. (2009). ZIP genes encode proteins involved in membrane trafficking of the TGN/PVC/vacuoles. Plant Cell Physiol. **50**: 2057–2068.

Noh, B., Murphy, A.S., and Spalding, E.P. (2001). Multidrug Resistance–like genes of *Arabidopsis* required for auxin transport and auxin-mediated development. Plant Cell **13**: 2441–2454.

Oda, Y. and Fukuda, H. (2013). Rho of plant GTPase signaling regulates the behavior of *Arabidopsis* kinesin-13A to establish secondary cell wall patterns. Plant Cell **25**: 4439–4450.

Ohno, H. (2006). Physiological roles of clathrin adaptor AP complexes: Lessons from mutant animals. J. Biochem. **139**: 943–948.

Ohno, H., Stewart, J., Fournier, M.C., Bosshart, H., Rhee, I., Miyatake, S., Saito, T., Gallusser, A., Kirchhausen, T., and Bonifacino, J.S. (1995). Interaction of tyrosine-based sorting signals with clathrin-associated proteins. Science **269**: 1872–1875.

Ohno, H., Tomemori, T., Nakatsu, F., Okazaki, Y., Aguilar, R.C., Foelsch, H., Mellman, I.,

Saito, T., Shirasawa, T., and Bonifacino, J.S. (1999). μ1B, a novel adaptor medium chain expressed in polarized epithelial cells. FEBS Lett. **449**: 215–220.

Ooi, C.E., Dell'Angelica, E.C., and Bonifacino, J.S. (1998). ADP-ribosylation factor 1 (ARF1) regulates recruitment of the AP-3 adaptor complex to membranes. J. Cell Biol. **142**: 391–402.

Oomen, R.J.F.J., Wu, J., Lelièvre, F., Blanchet, S., Richaud, P., Barbier-Brygoo, H., Aarts, M.G.M., and Thomine, S. (2009). Functional characterization of NRAMP3 and NRAMP4 from the metal hyperaccumulator *Thlaspi caerulescens*. New Phytol. **181**: 637–650.

Oppenheimer, D.G., Herman, P.L., Sivakumaran, S., Esch, J., and Marks, M.D. (1991). A myb gene required for leaf trichome differentiation in *Arabidopsis* is expressed in stipules. Cell **67**: 483–493.

Otsu, N. (1979). A threshold selection method from gray-level histograms. IEEE Trans Syst Man Cybern Syst **9**: 62–66.

Ottenschläger, I., Wolff, P., Wolverton, C., Bhalerao, R.P., Sandberg, G., Ishikawa, H., Evans, M., and Palme, K. (2003). Gravity-regulated differential auxin transport from columella to lateral root cap cells. Proc. Natl. Acad. Sci. U.S.A. **100**: 2987–2991.

Owen, D.J. and Evans, P.R. (1998). A structural explanation for the recognition of tyrosine-based endocytotic signals. Science **282**: 1327–1332.

Paez Valencia, J., Goodman, K., and Otegui, M.S. (2016). Endocytosis and endosomal trafficking in plants. Annu. Rev. Plant Biol. **67**: 309–335.

Park, M., Song, K., Reichardt, I., Kim, H., Mayer, U., Stierhof, Y.-D., Hwang, I., and Jürgens, G. (2013). *Arabidopsis* μ-adaptin subunit AP1M of adaptor protein complex 1 mediates late secretory and vacuolar traffic and is required for growth. Proc. Natl. Acad. Sci. U.S.A. **110**: 10318–10323.

Pearse, B.M. and Robinson, M.S. (1990). Clathrin, adaptors, and sorting. Annu. Rev. Cell Biol. **6**: 151–171.

Pedrazzini, E., Komarova, N.Y., Rentsch, D., and Vitale, A. (2013). Traffic routes and signals for the tonoplast. Traffic **14**: 622–628.

Perazza, D., Herzog, M., Hu, M., Brown, S., Dorne, A.-M., and Bonneville, J.-M. (1999). Trichome cell growth in *Arabidopsis thaliana* can be derepressed by mutations in at least five genes. Genetics **152**: 461–476.

Peris-peris, C., Serra-cardona, A., Campo, S., and Arin, J. (2017). Two NRAMP6 isoforms function as iron and manganese transporters and contribute to disease resistance in rice. Mol. Plant Microbe Interact. **30**: 385–398.

Pertl-Obermeyer, H., Wu, X.N., Schrodt, J., Müdsam, C., Obermeyer, G., and Schulze, W.X. (2016). Identification of cargo for adaptor protein complexes AP-3 and AP-4 by sucrose gradient profiling. Mol. Cell. Proteomics **15**: 2877–2889.

Pesch, M. and Hülskamp, M. (2011). Role of TRIPTYCHON in trichome patterning in *Arabidopsis*. BMC Plant Biol. **11**: 130.

Piccirillo, R., Palmisano, I., Innamorati, G., Bagnato, P., Altimare, D., and Schiaffino, M. V. (2006). An unconventional dileucine-based motif and a novel cytosolic motif are required for the lysosomal and melanosomal targeting of OA1. J. Cell Sci. **119**: 2003–2014.

Piper, R.C. and Luzio, J.P. (2007). Ubiquitin-dependent sorting of integral membrane proteins for degradation in lysosomes. Curr. Opin. Cell Biol. **19**: 459–465.

Pommerrenig, B. (2007). Molekularbiologische Untersuchungen des Leitgewebes und der

Stressphysiologie des Breitwegerichs.

Pond, L., Kuhn, L.A., Teyton, L., Schutze, M.P., Tainer, J.A., Jackson, M.R., and Peterson, P.A. (1995). A role for acidic residues in Di-leucine motif-based targeting to the endocytic pathway. J. Biol. Chem. **270**: 19989–19997.

Praefcke, G.J.K. and McMahon, H.T. (2004). The dynamin superfamily: universal membrane tubulation and fission molecules? Nat. Rev. Mol. Cell Biol. **5**: 133–47.

Prak, S., Hem, S., Boudet, J., Viennois, G., Sommerer, N., Rossignol, M., Maurel, C., and Santoni, V. (2008). Multiple phosphorylations in the C-terminal tail of plant plasma membrane aquaporins: role in subcellular trafficking of AtPIP2;1 in response to salt stress. Mol. Cell. Proteomics **7**: 1019–1030.

Puertollano, R., Aguilar, R.C., Gorshkova, I., Crouch, R.J., and Bonifacino, J.S. (2001a). Sorting of mannose 6-phosphate receptors mediated by the GGAs. Science **292**: 1712–1716.

Puertollano, R., Randazzo, P.A., Presley, J.F., Hartnell, L.M., and Bonifacino, J.S. (2001b). The GGAs promote ARF-dependent recruitment of Clatrin to the TGN. Cell **105**: 93–102.

Puertollano, R., Van Der Wel, N.N., Greene, L.E., Eisenberg, E., Peters, P.J., and Bonifacino, J.S. (2003). Morphology and dynamics of clathrin/GGA1-coated carriers budding from the trans-Golgi network. Mol. Biol. Cell **14**: 1545–1557.

Rajasekaran, A.K., Humphrey, J.S., Wagner, M., Miesenbock, G., Le Bivic, A., Bonifacino, J.S., and Rodriguez-Boulan, E. (1994). TGN38 recycles basolaterally in polarized Madin-Darby canine kidney cells. Mol. Biol. Cell **5**: 1093–1103.

Ramachandran, R. (2011). Vesicle scission: Dynamin. Semin. Cell Dev. Biol. **22**: 10–17.

Randazzo, P.A., Terui, T., Sturch, S., Fales, H.M., Ferrige, A.G., and Kahn, R.A. (1995). The myristoylated amino terminus of ADP-ribosylation factor1 is a phospholipid- and GTP-sensitive switch. J. Biol. Chem. **270**: 14809–14815.

El Refy, A., Perazza, D., Zekraoui, L., Valay, J.G., Bechtold, N., Brown, S., Hülskamp, M., Herzog, M., and Bonneville, J.M. (2003). The *Arabidopsis* KAKTUS gene encodes a HECT protein and controls the number of endoreduplication cycles. Mol. Genet. Genomics **270**: 403–414.

Reid, E., Kloos, M., Ashley-Koch, A., Hughes, L., Bevan, S., Svenson, I.K., Graham, F.L., Gaskell, P.C., Dearlove, A., Pericak-Vance, M. a, Rubinsztein, D.C., and Marchuk, D. a (2002). A kinesin heavy chain (KIF5A) mutation in hereditary spastic paraplegia (SPG10). Am. J. Hum. Genet. **71**: 1189–1194.

Ren, X., Farías, G.G., Canagarajah, B.J., Bonifacino, J.S., and Hurley, J.H. (2013). Structural basis for recruitment and activation of the AP-1 clathrin adaptor complex by Arf1. Cell **152**: 755–767.

Reupke, A. (2011). Studien zur subzellulären Lokalisation von Saccharosetransportproteinen aus *Arabidopsis thaliana*.

Richter, S., Geldner, N., Schrader, J., Wolters, H., Stierhof, Y.-D., Rios, G., Koncz, C., Robinson, D.G., and Jürgens, G. (2007). Functional diversification of closely related ARF-GEFs in protein secretion and recycling. Nature **448**: 488–492.

Richter, S., Voß, U., and Jürgens, G. (2009). Post-Golgi traffic in plants. Traffic **10**: 819–828.

Ritchie, R.J. (2008). Universal chlorophyll equations for estimating chlorophylls a, b, c, and d and total chlorophylls in natural assemblages of photosynthetic organisms using acetone, methanol, or ethanol solvents. Photosynthetica **46**: 115–126.

Rivière, J.B. et al. (2011). KIF1A, an axonal transporter of synaptic vesicles, is mutated in hereditary sensory and autonomic neuropathy type 2. Am. J. Hum. Genet. **89**: 219–301.

Robinson, D.G., Brandizzi, F., Hawes, C., and Nakano, A. (2015). Vesicles versus tubes: Is endoplasmic reticulum-Golgi transport in plants fundamentally different from other eukaryotes? Plant Physiol. **168**: 393–406.

Robinson, D.G., Jiang, L., and Schumacher, K. (2008). The endosomal system of plants: Charting new and familiar territories. Plant Physiol. **147**: 1482–1492.

Robinson, D.G. and Neuhaus, J.M. (2016). Receptor-mediated sorting of soluble vacuolar proteins: Myths, facts, and a new model. J. Exp. Bot. **67**: 4435–4449.

Robinson, D.G. and Pimpl, P. (2014). Receptor-mediated transport of vacuolar proteins: A critical analysis and a new model. Protoplasma **251**: 247–264.

Robinson, M.S. (2004). Adaptable adaptors for coated vesicles. Trends Cell Biol. **14**: 167–174.

Robinson, M.S. (2015). Forty years of clathrin-coated vesicles. Traffic **16**: 1210–1238.

Robinson, M.S.M. and Bonifacino, J.J.S. (2001). Adaptor-related proteins. Curr. Opin. Cell Biol. **13**: 444–453.

Rodriguez-Enriquez, M.J., Mehdi, S., Dickinson, H.G., and Grant-Downton, R.T. (2013). A novel method for efficient in vitro germination and tube growth of *Arabidopsis thaliana* pollen. New Phytol. **197**: 668–679.

Rohde, G., Wenzel, D., and Haucke, V. (2002). A phosphatidylinositol (4,5)-bisphosphate binding site within μ2-adaptin regulates clathrin-mediated endocytosis. J. Cell Biol. **158**.

Rohrer, J., Schweizer, A., Russell, D., and Kornfeld, S. (1996). The targeting of lamp1 to lysosomes is dependent on the spacing of its cytoplasmic tail tyrosine sorting motif relative to the membrane. J. Cell Biol. **132**: 565–576.

Rojas-Pierce, M. (2013). Targeting of tonoplast proteins to the vacuole. Plant Sci. **211**: 132–136.

Ron, M. and Avni, A. (2004). The receptor for the fungal elicitor ethylene-inducing xylanase is a member of a resistance-like gene family in tomato. Plant Cell **16**: 1604–1615.

Roschzttardtz, H., Conéjéro, G., Curie, C., and Mari, S. (2009). Identification of the endodermal vacuole as the iron storage compartment in the *Arabidopsis* embryo. Plant Physiol. **151**: 1329–38.

Ross, B.H., Lin, Y., Corales, E.A., Burgos, P. V., and Mardones, G.A. (2014). Structural and functional characterization of cargo-binding sites on the μ4-subunit of adaptor protein complex 4. PLoS One **9**: e88147.

Roth, A. and Davis, N. (1996). Ubiquitination of the yeast a-factor receptor. J. Cell Biol. **134**: 661–674.

Rothman, J.E. and Wieland, F.T. (1996). Protein sorting by transport vesicles. Science **272**: 227–234.

Rottmann, T., Zierer, W., Subert, C., Sauer, N., and Stadler, R. (2016). STP10 encodes a high-affinity monosaccharide transporter and is induced under low-glucose conditions in pollen tubes of *Arabidopsis*. J. Exp. Bot. **67**: 2387–2399.

Rous, B.A., Reaves, B.J., Ihrke, G., Briggs, J.A.G., Gray, S.R., Stephens, D.J., Banting, G., and Luzio, J.P. (2002). Role of adaptor complex AP-3 in targeting wild-type and mutated CD63 to lysosomes. Mol. Biol. Cell **13**: 1071–1082.

Saint-Jean, B., Seveno-Carpentier, E., Alcon, C., Neuhaus, J.-M., and Paris, N. (2010). The cytosolic tail dipeptide Ile-Met of the pea receptor BP80 is required for recycling from the prevacuole and for endocytosis. Plant Cell **22**: 2825–37.

Sancho-Andrés, G., Soriano-Ortega, E., Gao, C., Bernabé-Orts, J.M., Narasimhan, M., Müller, A., Tejos, R., Jiang, L., Friml, J., Aniento, F., and Marcote, M.J. (2016). Sorting motifs involved in the trafficking and localization of the PIN1 auxin efflux carrier. Plant Physiol. **171**: pp.00373.

Sandoval, I. V., Martínez-Arca, S., Valdueza, J., Palacios, S., and Holman, G.D. (2000). Distinct reading of different structural determinants modulates the dileucine-mediated transport steps of the lysosomal membrane protein LIMPII and the insulin-sensitive glucose transporter GLUT4. J. Biol. Chem. **275**: 39874–39885.

Santolini, E., Puri, C., Salcini, A.E., Gagliani, M.C., Pelicci, P.G., Tacchetti, C., and Di Fiore, P.P. (2000). Numb is an endocytic protein. J. Cell Biol. **151**: 1345–1351.

Santoni, V., Verdoucq, L., Sommerer, N., Vinh, J., Pflieger, D., and Maurel, C. (2006). Methylation of aquaporins in plant plasma membrane. Biochem. J. **400**: 189–197.

Sasaki, A., Yamaji, N., Yokosho, K., and Ma, J.F. (2012). Nramp5 is a major transporter responsible for manganese and cadmium uptake in rice. Plant Cell **24**: 2155–2167.

Sauer, M., Delgadillo, M.O., Zouhar, J., Reynolds, G.D., Pennington, J.G., Jiang, L., Liljegren, S.J., Stierhof, Y.-D., De Jaeger, G., Otegui, M.S., Bednarek, S.Y., and Rojo, E. (2013). MTV1 and MTV4 encode plant-specific ENTH and ARF GAP proteins that mediate clathrin-dependent trafficking of vacuolar cargo from the trans-Golgi network. Plant Cell **25**: 2217–2235.

Schellmann, S., Schnittger, A., Kirik, V., Wada, T., Okada, K., Beermann, A., Thumfahrt, J., Jürgens, G., and Hülskamp, M. (2002). TRYPTICON and CAPRICE mediate lateral inhibition during trichome and root hair patterning in Arabidopsis. EMBO J. **21**: 5036–5046.

Scheuring, D., Künzl, F., Viotti, C., San Wan Yan, M., Jiang, L., Schellmann, S., Robinson, D.G., and Pimpl, P. (2012). Ubiquitin initiates sorting of Golgi and plasma membrane proteins into the vacuolar degradation pathway. BMC Plant Biol. **12**: 164.

Schiller, M., Massalski, C., Kurth, T., and Steinebrunner, I. (2012). The *Arabidopsis* apyrase AtAPY1 is localized in the Golgi instead of the extracellular space. BMC Plant Biol. **12**: 123.

Schindelin, J. et al. (2012). Fiji: an open source platform for biological image analysis. Nat. Methods **9**: 676–682.

Schmid, S.L. (1997). Clathrin-coated vesicle formation and protein sorting: an integrated process. Annu. Rev. Biochem. **66**: 511–548.

Schmidt, M.R., Maritzen, T., Kukhtina, V., Higman, V.A., Doglio, L., Barak, N.N., Strauss, H., Oschkinat, H., Dotti, C.G., and Haucke, V. (2009). Regulation of endosomal membrane traffic by a Gadkin/AP-1/kinesin KIF5 complex. Proc. Natl. Acad. Sci. U.S.A **106**: 15344–15349.

Schneider, C. a, Rasband, W.S., and Eliceiri, K.W. (2012a). NIH Image to ImageJ: 25 years of image analysis. Nat. Methods **9**: 671–675.

Schneider, S., Beyhl, D., Hedrich, R., and Sauer, N. (2008). Functional and physiological characterization of *Arabidopsis* INOSITOL TRANSPORTER1, a novel tonoplast-localized transporter for *myo*-inositol. Plant Cell **20**: 1073–1087.

Schneider, S., Hulpke, S., Schulz, A., Yaron, I., Höll, J., Imlau, A., Schmitt, B., Batz, S., Wolf, S., Hedrich, R., and Sauer, N. (2012b). Vacuoles release sucrose via tonoplast-

localised SUC4-type transporters. Plant Biol. **14**: 325–336.

Schneider, S., Schneidereit, A., Konrad, K.K., Hajirezaei, M.-R., Gramann, M., Hedrich, R., and Sauer, N. (2006). Arabidopsis INOSITOL TRANSPORTER4 mediates high-affinity H+ symport of *myo*-inositol across the plasma membrane. Plant Physiol. **44**: 1–10.

Schwab, B., Mathur, J., Saedler, R.R., Schwarz, H., Frey, B., Scheidegger, C., and Hülskamp, M. (2003). Regulation of cell expansion by the DISTORTED genes in *Arabidopsis thaliana*: Actin controls the spatial organization of microtubules. Mol. Genet. Genomics **269**: 350–360.

Scott, G.K., Gu, F., Crump, C.M., Thomas, L., Wan, L., Xiang, Y., and Thomas, G. (2003). The phosphorylation state of an autoregulatory domain controls PACS-1-directed protein traffic. EMBO J. **22**: 6234–6244.

Seeger, M. and Payne, G.S. (1992). A role for clathrin in the sorting of vacuolar proteins in the Golgi complex of yeast. EMBO J. **11**: 2811–2818.

Setta-Kaffetzi, N. et al. (2014). AP1S3 mutations are associated with pustular psoriasis and impaired toll-like receptor 3 trafficking. Am. J. Hum. Genet. **94**: 790–797.

Shiba, T., Takatsu, H., Nogi, T., Matsugaki, N., Kawasaki, M., Igarashi, N., Suzuki, M., Kato, R., Earnest, T., Nakayama, K., and Wakatsuki, S. (2002). Structural basis for recognition of acidic-cluster dileucine sequence by GGA1. Nature **415**: 937–941.

Shih, W., Gallusser, A., and Kirchhausen, T. (1995). A clathrin-binding site in the hinge of the β2 chain of mammalian AP-2 complexes. J. Biol. Chem. **270**: 31083–31090.

Shimada, T., Fuji, K., Tamura, K., Kondo, M., Nishimura, M., and Hara-Nishimura, I. (2003). Vacuolar sorting receptor for seed storage proteins in *Arabidopsis thaliana*. Proc. Natl. Acad. Sci. U.S.A **100**: 16095–16100.

Simmen, T., Honing, S., Icking, A., Tikkanen, R., and Hunziker, W. (2002). AP-4 binds basolateral signals and participates in basolateral sorting in epithelial MDCK cells. Nat. Cell Biol. **4**: 154–159.

Smith, M.J., Hardy, W.R., Murphy, J.M., Jones, N., and Pawson, T. (2006). Screening for PTB domain binding partners and ligand specificity using proteome-derived NPXY peptide arrays. Mol. Cell. Biol. **26**: 8461–8474.

Song, J., Lee, M.H., Lee, G.-J., Yoo, C.M., and Hwang, I. (2006). *Arabidopsis* EPSIN1 plays an important role in vacuolar trafficking of soluble cargo proteins in plant cells via interactions with clathrin, AP-1, VTI11, and VSR1. Plant Cell **18**: 2258–2274.

Song, K., Jang, M., Kim, S.Y., Lee, G.-J., Lee, G.-J., Kim, D.H., Lee, Y., Cho, W., and Hwang, I. (2012). An A/ENTH domain-containing protein functions as an adaptor for clathrin-coated vesicles on the growing cell plate in *Arabidopsis* root cells. Plant Physiol. **159**: 1013–1025.

Sorieul, M., Santoni, V., Maurel, C., and Luu, D.T. (2011). Mechanisms and effects of retention of over-expressed aquaporin AtPIP2;1 in the endoplasmic reticulum. Traffic **12**: 473–482.

Spang, A. (2013). Retrograde traffic from the Golgi to the endoplasmic reticulum. Cold Spring Harb Perspect Biol **5**: a013391.

Stamnes, M.A. and Rothman, J.E. (1993). The binding of AP-1 clathrin adaptor particles to Golgi membranes requires ADP-ribosylation factor, a small GTP-binding protein. Cell **73**: 999–1005.

Staudt, C., Puissant, E., and Boonen, M. (2016). Subcellular trafficking of mammalian lysosomal proteins: an extended view. Int. J. Mol. Sci. **18**: 47.

Steinebrunner, I., Wu, J., Sun, Y., Corbett, A., and Roux, S.J. (2003). Disruption of apyrases inhibits pollen germination in *Arabidopsis*. Plant Physiol. **131**: 1638–1647.

Stephens, D.J. and Banting, G. (1998). Specificity of interaction between adaptor-complex medium chains and the tyrosine-based sorting motifs of TGN38 and lgp120. Biochem. J. **335**: 567–572.

Stephens, D.J., Crump, C.M., Clarke, A.R., and Banting, G. (1997). Serine 331 and tyrosine 333 are both involved in the interaction between the cytosolic domain of TGN38 and the μ2 subunit of the AP2 clathrin adaptor complex. J. Biol. Chem. **272**: 14104–14109.

Storch, S., Pohl, S., and Braulke, T. (2004). A dileucine motif and a cluster of acidic amino acids in the second cytoplasmic domain of the batten disease-related CLN3 protein are required for efficient lysosomal targeting. J. Biol. Chem. **279**: 53625–53634.

Strous, G.J., van Kerkhof, P., Govers, R., Ciechanover, A., and Schwartz, A.L. (1996). The ubiquitin conjugation system is required for ligand-induced endocytosis and degradation of the growth hormone receptor. EMBO J. **15**: 3806–3812.

Szul, T. and Sztul, E. (2011). COPII and COPI traffic at the ER-Golgi interface. Physiology **26**: 348–364.

Taguchi, T. (2013). Emerging roles of recycling endosomes. J. Biochem. **153**: 505–510.

Taheri, A., Gao, P., Yu, M., Cui, D., Regan, S., Parkin, I., and Gruber, M. (2015). A landscape of hairy and twisted: hunting for new trichome mutants in the Saskatoon *Arabidopsis* T-DNA population. Plant Biol. **17**: 384–394.

Takahashi, R., Ishimaru, Y., Nakanishi, H., and Nishizawa, N.K. (2011). Role of the iron transporter OsNRAMP1 in cadmium uptake and accumulation in rice. Plant Signal. Behav. **6**: 1813–1816.

Takano, J., Tanaka, M., Toyoda, A., Miwa, K., Kasai, K., Fuji, K., Onouchi, H., Naito, S., and Fujiwara, T. (2010). Polar localization and degradation of *Arabidopsis* boron transporters through distinct trafficking pathways. Proc. Natl. Acad. Sci. U.S.A. **107**: 5220–5225.

Takatsu, H., Katoh, Y., Shiba, Y., and Nakayama, K. (2001). Golgi-localizing, γ-adaptin ear homology domain, ADP-ribosylation factor-binding (GGA) proteins interact with acidic dileucine sequences within the cytoplasmic domains of sorting receptors through their Vps27p/Hrs/STAM (VHS) domains. J. Biol. Chem. **276**: 28541–28545.

Tamura, K., Shimada, T., Ono, E., Tanaka, Y., Nagatani, A., Higashi, S.I., Watanabe, M., Nishimura, M., and Hara-Nishimura, I. (2003). Why green fluorescent fusion proteins have not been observed in the vacuoles of higher plants. Plant J. **35**: 545–555.

Tanigawa, G., Orci, L., Amherdt, M., Ravazzola, M., Helms, J.B., and Rothman, J.E. (1993). Hydrolysis of bound GTP by ARF protein triggers uncoating of Golgi-derived COP-coated vesicles. J. Cell Biol. **123**: 1365–1371.

Tarpey, P.S. et al. (2006). Mutations in the gene encoding the Sigma 2 subunit of the adaptor protein 1 complex, AP1S2, cause X-linked mental retardation. Am. J. Hum. Genet. **79**: 1119–1124.

Teh, O.K., Shimono, Y., Shirakawa, M., Fukao, Y., Tamura, K., Shimada, T., and Hara-Nishimura, I. (2013). The AP-1 μ adaptin is required for KNOLLE localization at the cell plate to mediate cytokinesis in *Arabidopsis*. Plant Cell Physiol. **54**: 838–847.

Tejada-Jiménez, M., Castro-Rodríguez, R., Kryvoruchko, I., Lucas, M.M., Udvardi, M., Imperial, J., and González-Guerrero, M. (2015). *Medicago truncatula* natural resistance-associated macrophage protein1 is required for iron uptake by rhizobia-

infected nodule cells. Plant Physiol. **168**: 258–272.

Theos, A.C. et al. (2005). Functions of adaptor protein (AP)-3 and AP-1 in tyrosinase sorting from endosomes to melanosomes. Mol. Biol. Cell **16**: 5356–5372.

Le Thi, V.A. (2015). Characterization of poplar metal transporters to improve rehabilitation of metal polluted soils.

Thomine, S., Lelièvre, F., Debarbieux, E., Schroeder, J.I., and Barbier-Brygoo, H. (2003). AtNRAMP3, a multispecific vacuolar metal transporter involved in plant responses to iron deficiency. Plant J. **34**: 685–695.

Thomine, S., Wang, R., Ward, J.M., Crawford, N.M., and Schroeder, J.I. (2000). Cadmium and iron transport by members of a plant metal transporter family in *Arabidopsis* with homology to Nramp genes. Proc. Natl. Acad. Sci. U.S.A. **97**: 4991–4996.

Traub, L.M. and Kornfeld, S. (1997). The trans-Golgi network: a late secretory sorting station. Curr. Opin. Cell Biol. **9**: 527–533.

Tse, Y., Mo, B., Hillmer, S., Zhao, M., and Lo, S. (2004). Identification of multivesicular bodies as prevacuolar compartments in *Nicotiana tabacum* BY-2 cells. Plant Cell **16**: 672–693.

Uemura, T., Kim, H., Saito, C., Ebine, K., Ueda, T., Schulze-Lefert, P., and Nakano, A. (2012). Qa-SNAREs localized to the trans-Golgi network regulate multiple transport pathways and extracellular disease resistance in plants. Proc. Natl. Acad. Sci. U.S.A **109**: 1784–1789.

Ulmasov, T., Hagen, G., and Guilfoyle, T.J. (1997). ARF1, a transcription factor that binds to auxin response elements. Science **276**: 1865–1868.

Verkerk, A.J.M.H. et al. (2009). Mutation in the AP4M1 gene provides a model for neuroaxonal injury in cerebral palsy. Am. J. Hum. Genet. **85**: 40–52.

Viotti, C. et al. (2010). Endocytic and secretory traffic in *Arabidopsis* merge in the trans-Golgi network/early endosome, an independent and highly dynamic organelle. Plant Cell **22**: 1344–1357.

Viotti, C. (2014). ER and vacuoles: never been closer. Front. Plant Sci. **5**: 20.

Vitale, A. (1999). The endoplasmic reticulum - gateway of the secretory pathway. Plant Cell **11**: 615–628.

Wan, L., Molloy, S.S., Thomas, L., Liu, G., Xiang, Y., Rybak, S.L., and Thomas, G. (1998). PACS-1 defines a novel gene family of cytosolic sorting proteins required for trans-Golgi network localization. Cell **94**: 205–216.

Wang, H., Zhuang, X.H., Hillmer, S., Robinson, D.G., and Jiang, L.W. (2011). Vacuolar sorting receptor (VSR) proteins reach the plasma membrane in germinating pollen tubes. Mol. Plant **4**: 845–853.

Wang, J.-G., Li, S., Zhao, X.-Y., Zhou, L.-Z., Huang, G.-Q., Feng, C., and Zhang, Y. (2013). HAPLESS13, the *Arabidopsis* µ1 adaptin, is essential for protein sorting at the trans-Golgi network/early endosome. Plant Physiol. **162**: 1897–1910.

Wang, X., Cai, Y., Wang, H., Zeng, Y., Zhuang, X., Li, B., and Jiang, L. (2014). Trans-Golgi network-located AP1 gamma adaptins mediate dileucine motif-directed vacuolar targeting in *Arabidopsis*. Plant Cell **26**: 4102–4118.

Wang, Y.Y.J., Wang, J., Sun, H.Q.H., Martinez, M., Sun, Y.X.Y., Macia, E., Kirchhausen, T., Albanesi, J.P., Roth, M.G., and Yin, H.L. (2003). Phosphatidylinositol 4 phosphate regulates targeting of clathrin adaptor AP-1 complexes to the Golgi. Cell **114**: 299–310.

Waters, M.G., Serafini, T., and Rothman, J.E. (1991). "Coatomer": a cytosolic protein

complex containing subunits of non-clathrin-coated Golgi transport vesicles. Nature **349**: 248–251.

Watson, P. and Stephens, D.J. (2005). ER-to-Golgi transport: Form and formation of vesicular and tubular carriers. Biochim. Biophys. Acta **1744**: 304–315.

Wei, L., Zhang, W., Liu, Z., and Li, Y. (2009). AtKinesin-13A is located on Golgi-associated vesicle and involved in vesicle formation/budding in *Arabidopsis* root-cap peripheral cells. BMC Plant Biol. **9**: 138.

Williams, M.A. and Fukuda, M. (1990). Accumulation of membrane glycoproteins in lysosomes requires a tyrosine residue at a particular position in the cytoplasmic tail. J. Cell Biol. **111**: 955–966.

Winter, V. and Hauser, M.-T.M. (2006). Exploring the ESCRTing machinery in eukaryotes. Trends Plant Sci. **11**: 115–123.

Wolf, C., Hennig, M., Romanovicz, D., and Steinebrunner, I. (2007). Developmental defects and seedling lethality in apyrase *AtAPY1* and *AtAPY2* double knockout mutants. Plant Mol. Biol. **64**: 657–672.

Wolfenstetter, S. (2012). Analysen zur subzellulären Verteilung von Zucker- und Zuckeralkoholtransportern in *Arabidopsis thaliana*.

Wolfenstetter, S., Wirsching, P., Dotzauer, D., Schneider, S., and Sauer, N. (2012). Routes to the tonoplast: The sorting of tonoplast transporters in *Arabidopsis* mesophyll protoplasts. Plant Cell **24**: 215–232.

Wu, D., Yamaji, N., Yamane, M., Kashino-Fujii, M., Sato, K., and Feng Ma, J. (2016). The HvNNRAMP5 transporter mediates uptake of cadmium and manganese, but not iron. Plant Physiol. **172**: 1899–1910.

Wu, G., Lewis, D.R., and Spalding, E.P. (2007a). Mutations in *Arabidopsis* multidrug resistance-like ABC transporters separate the roles of acropetal and basipetal auxin transport in lateral root development. Plant Cell **19**: 1826–1837.

Wu, J., Steinebrunner, I., Sun, Y., Butterfield, T., Torres, J., Arnold, D., Gonzalez, A., Jacob, F., Reichler, S., and Roux, S.J. (2007b). Apyrases (nucleoside triphosphate-diphosphohydrolases) play a key role in growth control in *Arabidopsis*. Plant Physiol. **144**: 961–975.

Xia, J., Yamaji, N., Kasai, T., and Ma, J.F. (2010). Plasma membrane-localized transporter for aluminum in rice. Proc. Natl. Acad. Sci. U.S.A **107**: 18381–18385.

Xiang, L. and Van Den Ende, W. (2013). Trafficking of plant vacuolar invertases: from a membrane-anchored to a soluble status. Understanding sorting information in their complex N-terminal motifs. Plant Cell Physiol. **54**: 1263–1277.

Xiang, L., Etxeberria, E., and Van Den Ende, W. (2013). Vacuolar protein sorting mechanisms in plants. FEBS J. **280**: 979–993.

Xu, J. and Scheres, B. (2005). Dissection of *Arabidopsis* ADP-ribosylation factor1 function in epidermal cell polarity. Plant Cell **17**: 525–536.

Yamada, K., Osakabe, Y., Mizoi, J., Nakashima, K., Fujita, Y., Shinozaki, K., and Yamaguchi-Shinozaki, K. (2010). Functional analysis of an *Arabidopsis thaliana* abiotic stress-inducible facilitated diffusion transporter for monosaccharides. J. Biol. Chem. **285**: 1138–1146.

Yamaji, N., Sasaki, A., Xia, J.X., Yokosho, K., and Ma, J.F. (2013). A node-based switch for preferential distribution of manganese in rice. Nat. Commun. **4**: 1306–1313.

Yamaoka, S., Shimono, Y., Shirakawa, M., Fukao, Y., Kawase, T., Hatsugai, N., Tamura, K., Shimada, T., and Hara-Nishimura, I. (2013). Identification and dynamics of

Arabidopsis Adaptor Protein-2 complex and its involvement in floral organ development. Plant Cell **25**: 2958–2969.

Yang, M., Zhang, W., Dong, H., Zhang, Y., Lv, K., Wang, D., and Lian, X. (2013). OsNRAMP3 is a vascular bundles-specific manganese transporter that is responsible for manganese distribution in rice. PLoS One **8**: e83990.

Yap, C.C., Murate, M., Kishigami, S., Muto, Y., Kishida, H., Hashikawa, T., and Yano, R. (2003). Adaptor protein complex-4 (AP-4) is expressed in the central nervous system neurons and interacts with glutamate receptor δ2. Mol. Cell. Neurosci. **24**: 283–295.

Yoshinari, A., Kasai, K., Fujiwara, T., Naito, S., and Takano, J. (2012). Polar localization and endocytic degradation of a boron transporter, BOR1, is dependent on specific tyrosine residues. Plant Signal. Behav. **7**: 46–49.

Young, P., Deveraux, Q., Beal, R.E., Pickart, C.M., and Rechsteiner, M. (1998). Characterization of two polyubiquitin sites in the 26S protease subunit 5a. J. Biol. Chem. **273**: 5461–5467.

Zelazny, E., Borst, J.W., Muylaert, M., Batoko, H., Hemminga, M.A., and Chaumont, F. (2007). FRET imaging in living maize cells reveals that plasma membrane aquaporins interact to regulate their subcellular localization. Proc. Natl. Acad. Sci. U.S.A. **104**: 12359–12364.

Zelazny, E., Miecielica, U., Borst, J.W., Hemminga, M.A., and Chaumont, F. (2009). An N-terminal diacidic motif is required for the trafficking of maize aquaporins ZmPIP2;4 and ZmPIP2;5 to the plasma membrane. Plant J. **57**: 346–355.

Zhu, Y., Doray, B., Poussu, A., Lehto, V.P., and Kornfeld, S. (2001). Binding of GGA2 to the lysosomal enzyme sorting motif of the mannose 6-phosphate receptor. Science **292**: 1716–1718.

Zimmermann, R., Eyrisch, S., Ahmad, M., and Helms, V. (2011). Protein translocation across the ER membrane. Biochim. Biophys. Acta **1808**: 912–924.

Zouhar, J. and Sauer, M. (2014). Helping hands for budding prospects: ENTH/ANTH/VHS accessory proteins in endocytosis, vacuolar transport, and secretion. Plant Cell **26**: 1–13.

Zwiewka, M., Feraru, E., Möller, B., Hwang, I., Feraru, M.I., Kleine-Vehn, J., Weijers, D., and Friml, J. (2011). The AP-3 adaptor complex is required for vacuolar function in *Arabidopsis*. Cell Res. **21**: 1711–1722.

Appendix

Vector maps

Vectors used for classical cloning

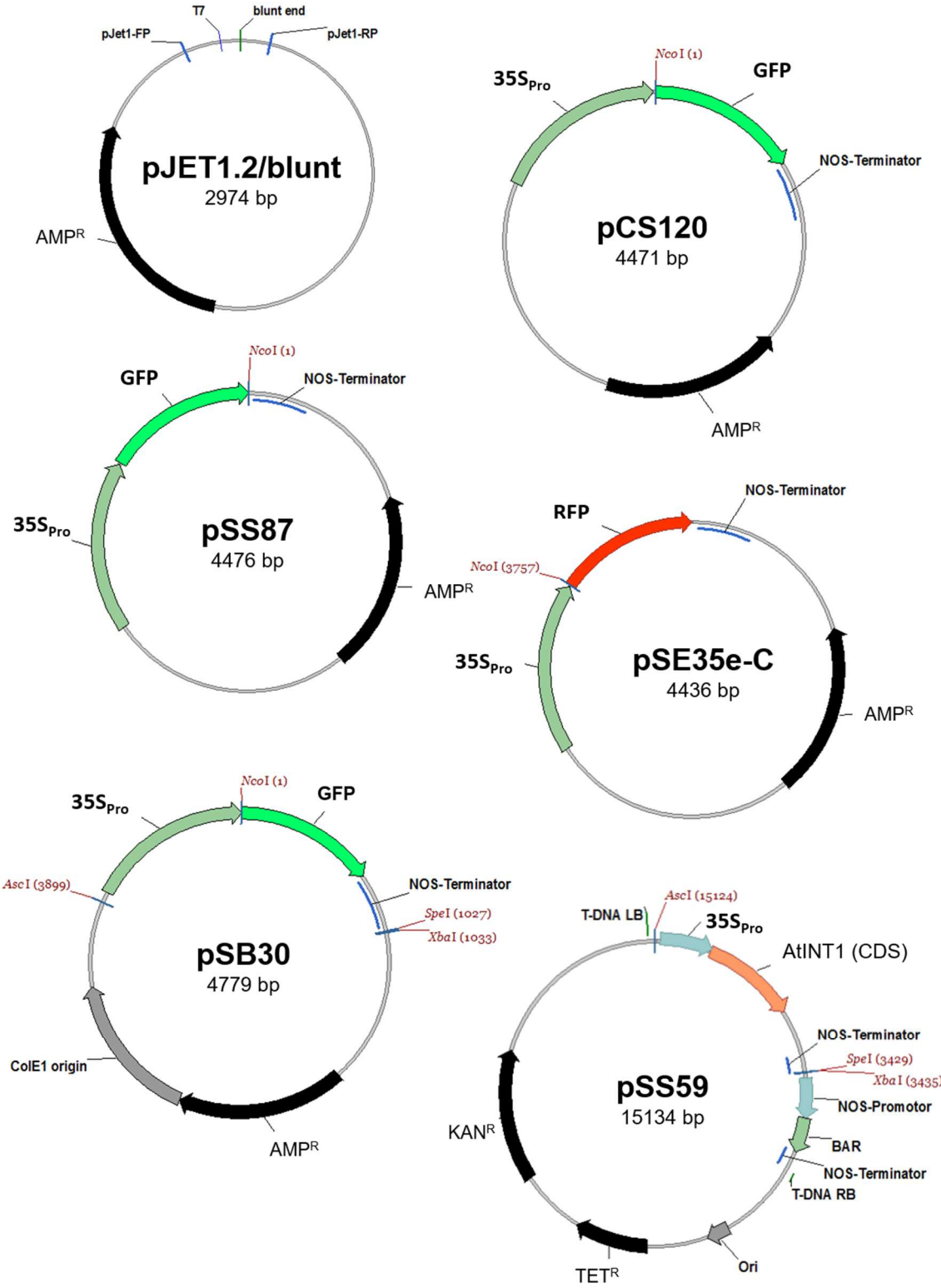

Gateway vectors

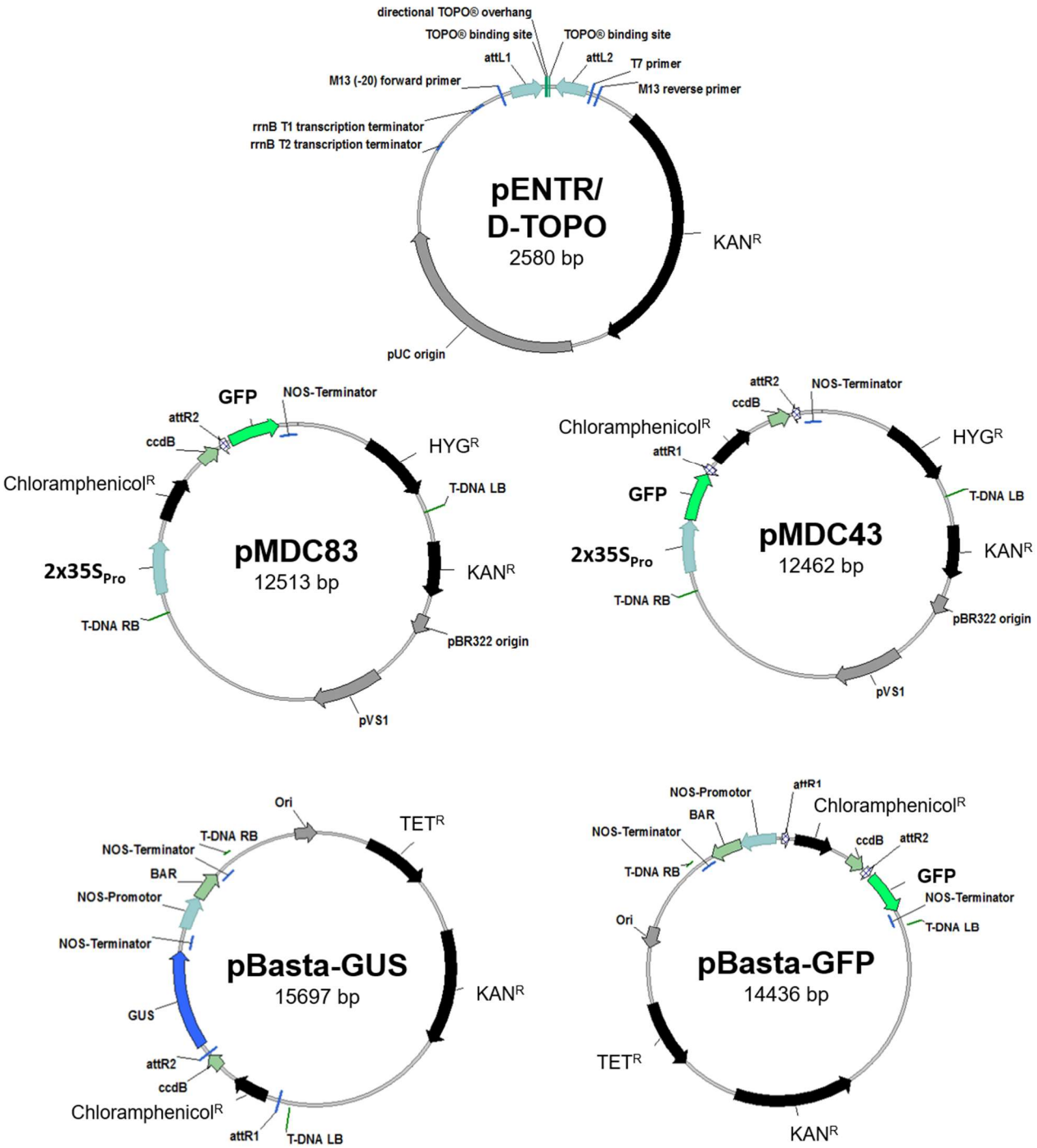

Alignment and pIs of MmNRAMP1 and plant NRAMP homologs

Sequences of NRAMP homologs known to localize to the PM, TP or intracellular compartments are given in orange, green, or purple, respectively. Sequences of NRAMP homologs with unknown localization are given in black. The non-plant homolog NRAMP1 from mouse is given in dark grey. Its tyrosine-based motif is highlighted in green. Other sequences corresponding to the consensus of a tyrosine-based motif (YXXΦ, with Φ being M, I, L, Y, W, F, or V) are underlined (except if positioned in a predicted transmembrane domain). Experimentally determined or putative dileucine-based motifs for sorting to the TP are highlighted in black. Other sequences that correspond to the extended [D/E]X_{3-5}L[L/I] consensus, are highlighted in grey (if not positioned within a predicted transmembrane domain). Yellow shading labels approximate position of transmembrane domains. XX below the alignment indicates the position of the non-TP-directing LI peptide of AtNRAMP4. *At*: *Arabidopsis thaliana*; *Hv*: *Hordeum vulgare* (barley); *Mt*: *Medicago truncatula* (barrel medic) *Os*: *Oryza sativa*; *Pt*: *Popolus trichocarpa (*western balsam-poplar*); Tc*: *Thlaspi caerulescens* (alpine penny-cress). Accession numbers are given after the last amino acid of each protein, followed by the theoretical pI. Sequences of PtNRAMP3.1 and PtNRAMP3.2 were accessed via http://genome.jgi.doe.gov/Poptr1_1/Poptr1_1.home.html. All other accession numbers refer to the UniProt ID.

```
CLUSTAL O(1.2.4) multiple sequence alignment

OsNRAMP4    ----------MEEGAK-IGREHEQQQQQHGR---VNGSGRVAAVGGGS---GGGGDEIEIEVAAAAGASPSRQ----HGG-LHGDVQAPTWKRFLAHVGPGFVISIAYLDPSNLQTDLVA 98
OsNRAT1     ------------------------MEGTGE---MREVGRETLHGG---------VVQSVSETDEYKEKTIDS------EKDGQFRVQPRWRKFLAHVGPGALVAIGFLDPSNLETDMQA 77
OsNRAMP3    ----------------------MSGPMQRSSQ---PQFISS--VERN-------------NQSNGPGTPLIDS----IDVDQIVIPEKNSWKNLFSYIGPGFLVSIAYIDPGNFETDLQA 76
AtNRAMP1    ----------------------MA--ATGSGR---SQFISS----SG-------------GNRSFSNSPLIEN----SDSNQIIVSEKKSWKNFFAYLGPGFLVSIAYIDPGNFETDLQA 72
AtNRAMP6    ---------------------------------MAAETA----SG-------------SNRSISNSPLIEN----SDSNQILVPEKKSWKNFFSYLGPGFLVSIAYIDPGNFETDLQS 64
MtNRAMP1    ----------------------MAHQEVNNGS---NNRIVAVNVTPS---------------------STPSYN----HDDS-SKQDQKPGWKKFLAYVGPGFLVSLAYLDPGNMETDLQA 70
OsNRAMP1    ----------------------MGV-------------------TKA-------------EAVAGDGGKVVDD----IEAL-ADLRKEPAWKRFLSHIGPGFMVCLAYLDPGNMETDLQA 61
HvNRAMP5    ----------------------MEIEREAPGS---ERGR-SWRANPA-------------AAQDAQGEKKFGD------GD-ETFVKEPAWKRFLSHVGPGFMVSLAYLDPGNLETDLQA 74
OsNRAMP5    ----------------------MEIERESS-E---RGSI-SWRASAA-------------HDQ---DAKKLDA------DD-QLLMKEPAWKRFLAHVGPGFMVSLAYLDPGNLETDLQA 70
MmNRAMP1    ---------------MIS-DKSPPRLSRPSPGGSSLPGP-APQPAPCRETYLSEKI--------------------PIPSADQGTFSLRKLWAFTGPGFLMSIAFLDPGNIESDLQA 81
AtNRAMP5    ----------MTGST--VSRQENSPKRPNDSNGEFKRLLVPETSQPEEDELHESPPENQILNVE------------EDRDKTYDSVPPFSWAKLWKFTGPGFLMSIAFLDPGNIEGDLQA 96
OsNRAMP2    ----------------MASRDLAESLLPVGGG-AATATATATAHDEYDERAYDSDDKVSIAVSD------SDSED-GGGGGGGDAMRPAFSWRKLWRFTGPGFLMCIAFLDPGNLEGDLQA 96
OsNRAMP6    MAPLPAAATATASSAATPADDEAHSLLPSTP-------SNEEDDDDLEERAYEATEKVIVSISDFPDADDDEEESGLATSTAASGIPPFSWRKLWLFTGPGFLMSIAFLDPGNLEGDLQA 113
AtNRAMP4    -------------------------MSETDR--ERPLL------ASEERAYEETEKVLIVGID------EEEDA--DYDDDPGNSPKFSWKKLWLFTGPGFLMSIAFLDPGNLESDLQA 78
TcNRAMP4    -------------------------MSETER--ERPLL------ASEERAYEETEKVHIVGVD------EEDDA--NYD-ELGNAPRFSWKKLWLFTGPGFLMSIAFLDPGNLESDLQA 77
AtNRAMP2    ----------MENDVKENLEEEEDRLLPPPP-----PSQSLPSTDSESEAAFETNEKILIVDFE------SPDDP-----TTGDTPPPFSWRKLWLFTGPGFLMSIAFLDPGNLEGDLQA 94
AtNRAMP3    -------------------------MPQLEN--NEPLLINE--EEEEETAYDETEKVHIVRNE------E--EDDLEHGVGCGGAPPFSWKKLWLFTGPGFLMSIAFLDPGNLEGDLQA 82
TcNRAMP3    -------------------------MSRLEN--DRPLLIDRIDEEEEETAYDETEKVHIVRDE------DDNERDLEYGVGCGGAPPFSWRKLWLFTGPGFLMSIAFLDPGNLEGDLQS 86
PtNRAMP3.1  ------------------------MPSPEED--PQPLL-----KDQEETAYDSDGKVLSFGID------YDTES-----GGSTVVPSFSWRKLWLFTGPGFLMCIAFLDPGNLEGDLQA 77
PtNRAMP3.2  -------------------------MPVEEN--YQPLL-----QEEEERAYDSDEKVLIIGVD------SDTES-----GGSTVLPPFSWKKLWLFTGPGFLMSIAFLDPGNLEGDLQA 76
                                                                          XX                              .:  . *** ::.:.::**.*:: *: :

OSNRAMP4    GSSHRYSLLWVLLFGFIFVLTVQSLAANLGIITGRHLAELCMGEYPKYVKYCLWLLAELGVIAATIPGVLGTALAYNMLL--HIPFWAGVLACGACTFLILGLQGYGARKMEFTISVLML 216
OsNRAT1     GADFKYELLWVILVGMVFALLIQTLAANLGVKTGRHLAELCREEYPHYVNIFLWIIAELAVISDDIPEVLGTAFAFNILL--KIPVWAGVILTVFSTLLLLGVQRFGARKLEFIIAAFMF 195
OsNRAMP3    GAQYKYELLWIILIASCAALIIQSLAARLGVVTGKHLAEHCRAEYPKATNFILWILAELAVVACDIPEVIGTAFALNMLF--KIPVWCGVLITGLSTLMLLLLQQYGVRKLEFLIAILVS 194
AtNRAMP1    GAHYKYELLWIILVASCAALVIQSLAANLGVVTGKHLAEQCRAEYSKVPNFMLWVVAEIAVVACDIPEVIGTAFALNMLF--SIPVWIGVLLTGLSTLILLALQKYGVRKLEFLIAFLVF 190
AtNRAMP6    GAQYKYELLWIILVASCAALVIQSLAANLGVVTGKHLAEHCRAEYSKVPNFMLWVVAEIAVVACDIPEVIGTAFALNMLF--NIPVWIGVLLTGLSTLILLALQQYGIRKLEFLIAFLVF 182
MtNRAMP1    GANHGYELLWIILIGLIFACIIQSLAANLGVCTGKHLSEICKAEYPWFVKYCLWILAELAVIAADIPEVIGTAFALNILF--HVPVWGGVLLTGCSTLLFLGLQRFGVRKLELLISILVF 188
OsNRAMP1    GANHKYELLWVILIGLIFALIIQSLSANLGVVTGRHLAELCKTEYPVWVKTCLWLLAELAVIASDIPEVIGTGFAFNLLF--HIPVWTGVLIAGSSTLLLLGLQRYGVRKLEVVVALLVF 179
HvNRAMP5    GANHRYELLWVILIGLIFALIIQSLAANLGVVTGKHLAEICKSEYPKPVMICLWLLAEVAVIAADIPEVIGTAFAFYLLF--RIPVWIGVLITGSSTLLLLGLQRYGVRKLEFLISMLVF 192
MmNRAMP1    GAVAGFKLLWVLLWATVLGLLCQRLAARLGVVTGKDLGEVCHLYYPKVPRILLWLTIELAIVGSDMQEVIGTAISFNLLSAGRIPLWDGVLITIVDTFFFLFLDNYGLRKLEAFFGLLIT 201
```

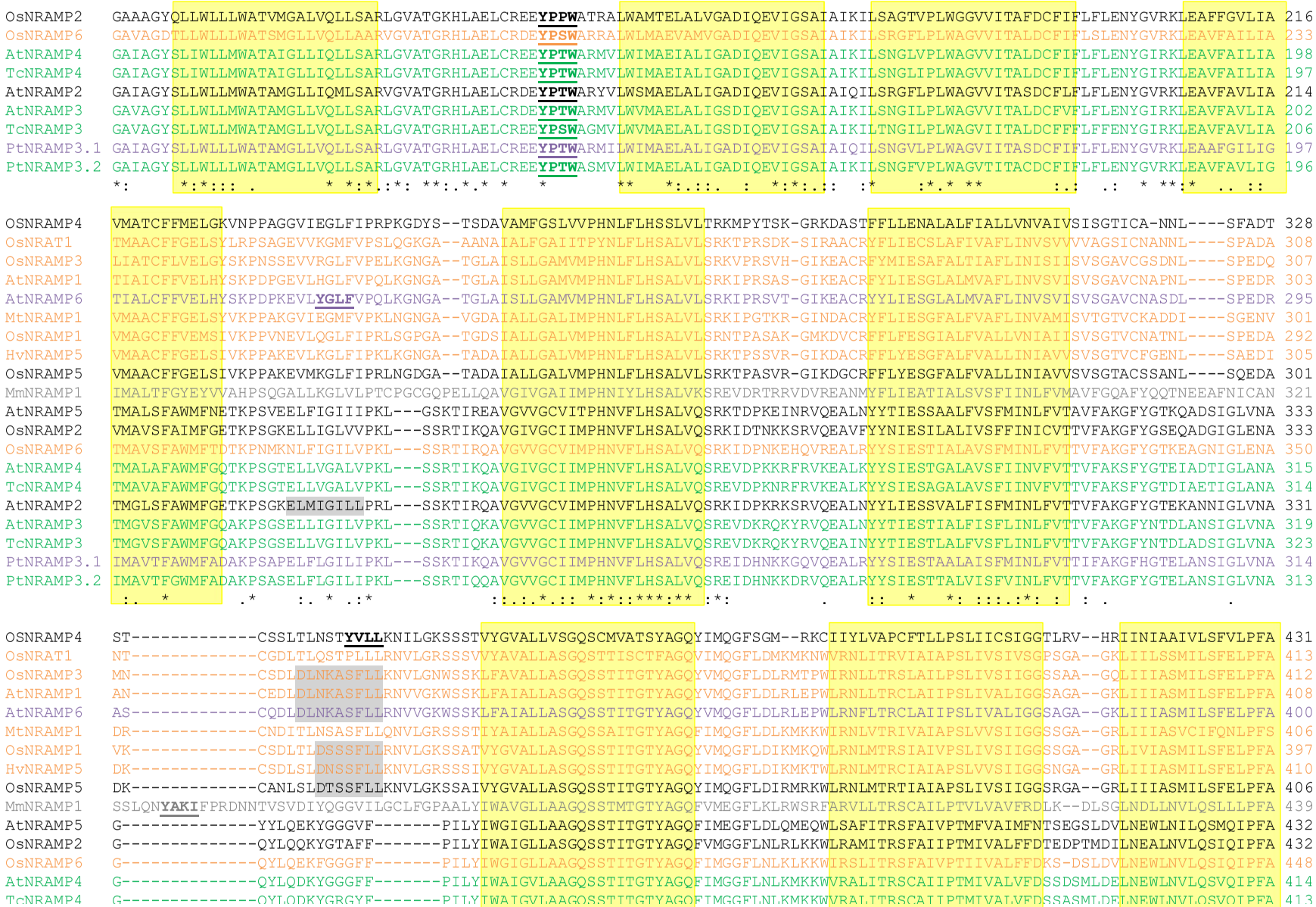
OsNRAMP2 GAAAGYQLLWLLLWATVMGALVQLLSARLGVATGKHLAELCREEYPPWATRALWAMTELALVGADIQEVIGSAIAIKILSAGTVPLWGGVVITAFDCFIFLFLENYGVRKLEAFFGVLIA 216
OsNRAMP6 GAVAGDTLLWLLLWATSMGLLVQLLAARVGVATGRHLAELCRDEYPSWARRALWLMAEVAMVGADIQEVIGSAIAIKILSRGFLPLWAGVVITALDCFIFLSLENYGVRKLEAVFAILIA 233
AtNRAMP4 GAIAGYSLIWLLMWATAIGLLIQLLSARLGVATGRHLAELCREEYPTWARMVLWIMAEIALIGADIQEVIGSAIAIKILSNGLVPLWAGVVITALDCFIFLFLENYGIRKLEAVFAILIA 198
TcNRAMP4 GAIAGYSLIWLLMWATAIGLLIQLLSARLGVATGRHLAELCREEYPTWARMVLWIMAEIALIGADIQEVIGSAIAIKILSNGLIPLWAGVVITALDCFIFLFLENYGIRKLEAVFAILIA 197
AtNRAMP2 GAIAGYSLLWLLMWATAMGLLIQMLSARVGVATGRHLAELCRDEYPTWARYVLWSMAELALIGADIQEVIGSAIAIQILSRGFLPLWAGVVITASDCFLFLFLENYGVRKLEAVFAVLIA 214
AtNRAMP3 GAVAGYSLLWLLMWATAMGLLVQLLSARLGVATGRHLAELCRDEYPTWARMVLWVMAELALIGSDIQEVIGSAIAIKILSNGILPLWAGVVITALDCFVFLFLENYGIRKLEAVFAVLIA 202
TcNRAMP3 GAVAGYSLLWLLMWATAMGLLVQLLSARLGVATGRHLAELCREEYPSWAGMVLWVMAELALIGSDIQEVIGSAIAIKILTNGILPLWAGVIITALDCFFFLFFENYGIRKLEAVFAVLIA 206
PtNRAMP3.1 GAIAGYSLLWLLLWATAMGLLVQLLSARLGVATGRHLAELCREEYPTWARMILWIMAELALIGADIQEVIGSAIAIQILSNGVLPLWAGVIITASDCFIFLFLENYGVRKLEAAFGILIG 197
PtNRAMP3.2 GAIAGYSLLWLLLWATAMGLLVQLLSARLGVATGRHLAELCREEYPTWASMVLWIMAELALIGADIQEVIGSAIAIKILSNGFVPLWAGVTITACDCFIFLFLENYGVRKLEAVFAVLIG 196
OSNRAMP4 VMATCFFMELGKVNPPAGGVIEGLFIPRPKGDYS--TSDAVAMFGSLVVPHNLFLHSSLVLTRKMPYTSK-GRKDASTFFLLENALALFIALLVNVAIVSISGTICA-NNL----SFADT 328
OsNRAT1 TMAACFFGELSYLRPSAGEVVKGMFVPSLQGKGA--AANAIALFGAIITPYNLFLHSALVLSRKTPRSDK-SIRAACRYFLIECSLAFIVAFLINVSVVVVAGSICNANNL----SPADA 308
OsNRAMP3 LIATCFLVELGYSKPNSSEVVRGLFVPELKGNGA--TGLAISLLGAMVMPHNLFLHSALVLSRKVPRSVH-GIKEACRFYMIESAFALTIAFLINISIISVSGAVCGSDNL----SPEDQ 307
AtNRAMP1 TIAICFFVELHYSKPDPGEVLHGLFVPQLKGNGA--TGLAISLLGAMVMPHNLFLHSALVLSRKIPRSAS-GIKEACRFYLIESGLALMVAFLINVSVISVSGAVCNAPNL----SPEDR 303
AtNRAMP6 TIALCFFVELHYSKPDPKEVLYGLFVPQLKGNGA--TGLAISLLGAMVMPHNLFLHSALVLSRKIPRSVT-GIKEACRYYLIESGLALMVAFLINVSVISVSGAVCNASDL----SPEDR 295
MtNRAMP1 VMAACFFGELSYVKPPAKGVIEGMFVPKLNGNGA--VGDAIALLGALIMPHNLFLHSALVLSRKIPGTKR-GINDACRYFLIESGFALFVAFLINVAMISVTGTVCKADDI----SGENV 301
OsNRAMP1 VMAGCFFVEMSIVKPPVNEVLQGLFIPRLSGPGA--TGDSIALLGALVMPHNLFLHSALVLSRNTPASAK-GMKDVCRFFLFESGIALFVALLVNIAIISVSGTVCNATNL----SPEDA 292
HvNRAMP5 VMAACFFGELSIVKPPAKEVLKGLFIPKLKGNGA--TADAIALLGALVMPHNLFLHSALVLSRKTPSSVR-GIKDACRFFLYESGFALFVALLINIAVVSVSGTVCFGENL----SAEDI 305
OsNRAMP5 VMAACFFGELSIVKPPAKEVMKGLFIPRLNGDGA--TADAIALLGALVMPHNLFLHSALVLSRKTPASVR-GIKDGCRFFLYESGFALFVALLINIAVVSVSGTACSSANL----SQEDA 301
MmNRAMP1 IMALTFGYEYVVAHPSQGALLKGLVLPTCPGCGQPELLQAVGIVGAIIMPHNIYLHSALVKSREVDRTRRVDVREANMYFLIEATIALSVSFIINLFVMAVFGQAFYQQTNEEAFNICAN 321
AtNRAMP5 TMALSFAWMFNETKPSVEELFIGIIIPKL---GSKTIREAVGVVGCVITPHNVFLHSALVQSRKTDPKEINRVQEALNYYTIESSAALFVSFMINLFVTAVFAKGFYGTKQADSIGLVNA 333
OsNRAMP2 VMAVSFAIMFGETKPSGKELLIGLVVPKL---SSRTIKQAVGIVGCIIMPHNVFLHSALVQSRKIDTNKKSRVQEAVFYYNIESILALIVSFFINICVTTVFAKGFYGSEQADGIGLENA 333
OsNRAMP6 TMAVSFAWMFTDTKPNMKNLFIGILVPKL---SSRTIRQAVGVVGCVIMPHNVFLHSALVQSRKIDPNKEHQVREALRYYSIESTIALAVSFMINLFVTTVFAKGFYGTKEAGNIGLENA 350
AtNRAMP4 TMALAFAWMFGQTKPSGTELLVGALVPKL---SSRTIKQAVGIVGCIIMPHNVFLHSALVQSREVDPKKRFRVKEALKYYSIESTGALAVSFIINVFVTTVFAKSFYGTEIADTIGLANA 315
TcNRAMP4 TMAVAFAWMFGQTKPSGTELLVGALVPKL---SSRTIKQAVGIVGCIIMPHNVFLHSALVQSREVDPKNRFRVKEALKYYSIESAGALAVSFIINVFVTTVFAKSFYGTDIAETIGLANA 314
AtNRAMP2 TMGLSFAWMFGETKPSGKELMIGILLPRL---SSKTIRQAVGVVGCVIMPHNVFLHSALVQSRKIDPKRKSRVQEALNYYLIESSVALFISFMINLFVTTVFAKGFYGTEKANNIGLVNA 331
AtNRAMP3 TMGVSFAWMFGQAKPSGSELLIGILVPKL---SSRTIQKAVGVVGCIIMPHNVFLHSALVQSREVDKRQKYRVQEALNYYTIESTIALFISFLINLFVTTVFAKGFYNTDLANSIGLVNA 319
TcNRAMP3 TMGVSFAWMFGQAKPSGSELLVGILVPKL---SSRTIQKAVGVVGCIIMPHNVFLHSALVQSREVDKRQKYRVQEAINYYTIESTLALFVSFLINLFVTTVFAKGFYNTDLADSIGLVNA 323
PtNRAMP3.1 IMAVTFAWMFADAKPSAPELFLGILIPKL---SSKTIKQAVGVVGCIIMPHNVFLHSALVQSREIDHNKKGQVQEALRYYSIESTAALAISFMINLFVTTIFAKGFHGTELANSIGLVNA 314
PtNRAMP3.2 IMAVTFGWMFADAKPSASELFLGILIPKL---SSRTIQQAVGVVGCIIMPHNVFLHSALVQSREIDHNKKDRVQEALRYYSIESTTALVISFVINLFVTTVFAKGFYGTELANSIGLVNA 313
OsNRAMP4 ST----------CSSLTLNSTYVLLKNILGKSSSTVYGVALLVSGQSCMVATSYAGQYIMQGFSGM--RKCIIYLVAPCFTLLPSLIICSIGGTLRV--HRIINIAAIVLSFVLPFA 431
OsNRAT1 NT----------CGDLTLQSTPLLLRNVLGRSSSVVYAVALLASGQSTTISCTFAGQVIMQGFLDMKMKNWVRNLITRVIAIAPSLIVSIVSGPSGA--GKLIILSSMILSFELPFA 413
OsNRAMP3 MN----------CSDLDLNKASFLLKNVLGNWSSKLFAVALLASGQSSTITGTYAGQYVMQGFLDLRMTPWIRNLLTRSLAILPSLIVSIIGGSSAA--GQLIIIASMILSFELPFA 412
AtNRAMP1 AN----------CEDLDLNKASFLLRNVVGKWSSKLFAIALLASGQSSTITGTYAGQYVMQGFLDLRLEPWLRNLLTRCLAIIPSLIVALIGGSAGA--GKLIIIASMILSFELPFA 408
AtNRAMP6 AS----------CQDLDLNKASFLLRNVVGKWSSKLFAIALLASGQSSTITGTYAGQYVMQGFLDLRLEPWLRNFLTRCLAIIPSLIVALIGGSAGA--GKLIIIASMILSFELPFA 400
MtNRAMP1 DR----------CNDITLNSASFLLQNVLGRSSSTIYAIALLASGQSSAITGTYAGQFIMQGFLDLKMKKWIRNLVTRIVAIAPSLVVSIIGGSSGA--GRLIIIASVCIFQNLPFS 406
OsNRAMP1 VK----------CSDLTLDSSSFLLRNVLGKSSATVYGVALLASGQSSTITGTYAGQYVMQGFLDIKMKQWLRNLMTRSIAIVPSLIVSIIGGSSGA--GRLIVIASMILSFELPFA 397
HvNRAMP5 DK----------CSDLSLDNSSFLLKNVLGRSSSIVYGVALLASGQSSTITGTYAGQYIMQGFLDIKMKTWLRNLMTRCIAIAPSLVVSIIGGSNGA--GRLIIIASMILSFELPFA 410
OsNRAMP5 DK----------CANLSLDTSSFLLKNVLGKSSAIVYGVALLASGQSSTITGTYAGQYIMQGFLDIRMRKWLRNLMTRTIAIAPSLIVSIIGGSRGA--GRLIIIASMILSFELPFA 406
MmNRAMP1 SSLQNYAKIFPRDNNTVSVDIYQGGVILGCLFGPAALYIWAVGLLAAGQSSTMTGTYAGQFVMEGFLKLRWSRFARVLLTRSCAILPTVLVAVFRDLK--DLSGLNDLLNVLQSLLLPFA 439
AtNRAMP5 G----------YYLQEKYGGGVF-------PILYIWGIGLLAAGQSSTITGTYAGQFIMEGFLDLQMEQWLSAFITRSFAIVPTMFVAIMFNTSEGSLDVLNEWLNILQSMQIPFA 432
OsNRAMP2 G----------QYLQQKYGTAFF-------PILYIWAIGLLASGQSSTITGTYAGQFVMGGFLNLRLKKWLRAMITRSFAIIPTMIVALFFDTEDPTMDILNEALNVLQSIQIPFA 432
OsNRAMP6 G----------QYLQEKFGGGFF-------PILYIWGIGLLAAGQSSTITGTYAGQFIMGGFLNLKLKKWIRSLITRSFAIVPTIIVALFFDKS-DSLDVLNEWLNVLQSIQIPFA 448
AtNRAMP4 G----------QYLQDKYGGGFF-------PILYIWAIGVLAAGQSSTITGTYAGQFIMGGFLNLKMKKWVRALITRSCAIIPTMIVALVFDSSDSMLDELNEWLNVLQSVQIPFA 414
TcNRAMP4 G----------QYLQDKYGRGYF-------PILYIWAIGVLAAGQSSTITGTYAGQFIMGGFLNLKMKKWVRALITRSCAIIPTMIVALVFDSSASMLDELNEWLNVLQSVQIPFA 413


AtNRAMP2 G----------QYLQEKFGGGLL-------PILYIWGIGLLAAGQSSTITGTYAGQFIMGGFLNLRLKKWMRAVITRSCAIVPTMIVAIVFNTSEASLDVLNEWLNVLQSVQIPFA 430
AtNRAMP3 G----------QYLQEKYGGGVF-------PILYIWAIGLLAAGQSSTITGTYAGQFIMGGFLNFKMKKWLRALITRSCAIIPTIIVALVFDSSEATLDVLNEWLNVLQSIQIPFA 418
TcNRAMP3 G----------QYLQDKYGGGLF-------PILYIWGIGLLAAGQSSTITGTYAGQFIMGGFLNFRMKKWMRALITRSCAIIPTIIVALVFDSSEATLDVLNEWLNVLQSIQIPFA 422
PtNRAMP3.1 G----------QYLQDKYGGGFF-------PILYIWGIGLLAAGQSSTITGTYAGQFIMGGFLNLGLKKWLRALITRSCAIIPTIIVALVFDTSEDSLDVLNEWLNMLQSIQIPFA 413
PtNRAMP3.2 G----------QYLQDKYGGGFF-------PILYIWGIGLLAAGQSSTITGTYAGQFIMGGFLNLRLKKWLRALITRSCAIIPTMIVALVFDTSEDSLDVLNEWLNVLQSIQIPFA 412
OSNRAMP4 LIPLIKFSSSCTNIGPYKNATSIIRIAWILSLVIIGINIYFFCTSFVAWLVHSDLPRVVNAIISSLVFPFMAAYIAALIYLAFRKVNLSDPFPTNSVSGEIEV----------QHIQ 538
OsNRAT1 LIPLLKFCNSSKKVGPLKESIYTVVIAWILSFALIVVNTYFLVWTYVDWLVHNNLPKYANGLISVVVFALMAAYLVAVVYLTFRKDTVATYVPVPERAQAQVEAGGTPVVDASAADEDQP 533
OsNRAMP3 LVPLLKFTSSRTKMGQHTNSKAISVITWGIGSFIVVINTYFLITSFVKLLLHNGLSTVSQVFSGIFGFLGMLIYMAAILYLVFRKNRKATLPLLEGDSTV-RI--VGRDTATE-GEGSLG 528
AtNRAMP1 LVPLLKFTSCKTKMGSHVNPMAITALTWVIGGLIMGINIYYLVSSFIKLLIHSHMKLILVVFCGILGFAGIALYLAAIAYLVFRKNRVATS--LLIS----------R-DSQNVE 510
AtNRAMP6 LVPLLKFTSSKTKMGSHANSLVISSVTWIIGGLIMGINIYYLVSSFIKLLLHSHMNLVAIVFLGVLGFSGIATYLAAISYLVLRKNRESSSTHFLDF----------S-NSQTEE 504
MtNRAMP1 LPSAYVYILNIIQIT---------- 421
OsNRAMP1 LIPLLKFSSSSNKMGENKNSIYIVGFSWVLGFVIIGINIYFLSTKLVGWILHNALPTFANVLIGIVLFPLMLLYVVAVIYLTFRKDTVKF-VSRRELQAGDDT--EKAQVATCVADEHSK 514
HvNRAMP5 LIPLLKFSSSSSKMGPHKNSIYIIVFSWTLGLMLIGINVYFLSTSFMGWLINSSLPTYAKVLVGVVVCPLMLVYLVAVVYLTFRKDTVVTFVADSCKADA------EKAAGGSGEDDDEP 524
OsNRAMP5 LIPLLKFSSSKSKMGPHKNSIYIIVFSWFLGLLIIGINMYFLSTSFVGWLIHNDLPKYANVLVGAAVFPFMLVYIVAVVYLTIRKDSVVTFVADSSLAAVVDA--EKADAGDLAVDDDEP 524
MmNRAMP1 VLPILTFTSMPAVMQEFANGRMSKAITSCIMALVCAINLYFVISYLPS--------LPHPAYFG-LVALFAIGYLGLTAYL---------AWTCCIAHGATFL------THS--SHKHFL 533
AtNRAMP5 VIPLLTMVSNEHIMGVFKIGPSLEKLAWTVAVFVMMINGYLLLDFFMA--------EVEGFLVGFLVFGGVVGYISFIIYLVSYRSSQSSSWSSLEMSERVVS------TET-------- 530
OsNRAMP2 LIPLITLVSKEQVMGSFVVGPITKVISWIVTVFLMLINGYLILSFYAT--------EVRGALVRSSLCVVLAVYLAFIVYLIMRNTSLYSRLRSAMTKST---------- 524
OsNRAMP6 LIPLITLVSKEKVMGVFKIGRNTQAVTWTVATLLITINGYLLLDFFSS--------EIRGLLSGSILCVAVLAYASFVLYLILRGTELPNQIITTIRKSFS---------- 541
AtNRAMP4 VIPLLCLVSNEQIMGSFKIQPLVQTISWIVAALVIAINGYLMVDFFSG--------AATNLILLVPVIIFAIAYVVFVLYLISRGLTY-TPWQLVASSHKEPQ------RDD--E----- 512
TcNRAMP4 VIPLLCLVSNEQIMGSFKIQPLVQTISWIVAALVISINGYLMVDFFSG--------AAKSVVLLVLVIIFAVAYVLFVLYLISRGLTY-TPCN---------- 497
AtNRAMP2 LLPLLTLVSKEEIMGDFKIGPILQRIAWTVAALVMIINGYLLLDFFVS--------EVDGFLFGVTVCVWTTAYIAFIVYLISHSNFFPSPWSSSSIELPKRV------SVS--NS---- 530
AtNRAMP3 LIPLLCLVSKEQIMGSFKIGPLYKTIAWLVAALVIMINGYLLLEFFSN--------EVSGIVYTGFVTLFTASYGAFILYLIARGITF-TPWPFKAESSH---------- 509
TcNRAMP3 LIPLLCLVSKERIMGSFKIGPLCQTIAWLVAALVIMINGYLLIEFFSS--------EVSGIVYTGFVTVFTALYGAFIVYLIARGINF-TPWRPKAESS---------- 512
PtNRAMP3.1 LIPLLCLVSKEQIMGTFTVGPILKMVSWLVAALVMLINGYLLLDFFSN--------EVTGVVFTTVVCAFTGAYVTFIIYLISREVTI-STWYCPT---------- 500
PtNRAMP3.2 LIPLLCLVSKEQIMGTFKIGPILKMVAWLVAALVMVINGYLLLDFFFN--------EVTGVAFTTVVCGFTGAYVAFIIYLISRGFT---------- 491
OsNRAMP4 IQEKQEDLG-VHL---------- 550 Q5QN13 8.48
OsNRAT1 AP-YRKDLADASM---------- 545 Q6ZG85 7.00
OsNRAMP3 HL-PREDISSMQLPQQRTASDLD- 550 Q653V6 8.33
AtNRAMP1 TL-PRQDIVNMQLPCRVSTSDVD- 532 Q9SAH8 8.86
AtNRAMP6 TL-PREDIANMQLPNRVAVIGDLN 527 Q9S9N8 8.03
MtNRAMP1 ---------- 421 A0A072UZV8 8.27
OsNRAMP1 EP-P--------V---------- 518 Q0D7E4 7.58
HvNRAMP5 VP-YREDLADIPLPAHSTRDMQ-- 545 A0A1C9ZPR6 6.67
OsNRAMP5 LP-YRDDLADIPLPR--------- 538 Q8H4H5 6.76
MmNRAMP1 YGLPNEEQGGVQGSG--------- 548 P41251 7.52
AtNRAMP5 ---------- 530 Q9SN36 4.84
OsNRAMP2 ---------- 524 Q10Q65 6.17
OsNRAMP6 ---------- 541 Q2QN30 5.19
AtNRAMP4 ---------- 512 Q9FN18 4.99
TcNRAMP4 ---------- 497 A6YPU4 5.46
AtNRAMP2 ---------- 530 Q9C6B2 5.06
AtNRAMP3 ---------- 509 Q9SNV9 5.11
TcNRAMP3 ---------- 512 A6YPU3 5.05
PtNRAMP3.1 ---------- 500 eugene3.02050021 4.89

Prediction of phosphorylation sites in MOT2

Putative phosphorylation sites in the amino acid sequence of *Arabidopsis* MOT2 (accession: Q0WP36), as computed via The Arabidopsis Protein Phosphorylation Site Database (PhosPhAt 4.0; http://phosphat.uni-hohenheim.de/; Durek et al., 2010). Predicted phosphorylation hotspots in the amino acid sequence of MOT2 are highlighted in grey. Predicted phospho-serines, -threonine, and -tyrosines are highlighted in green. For each predicted phosphorylated residue, the position and score (rounded to second decimal) is given below the sequence.

```
METTTTPLLP GDRSRCGWLR RRLRLKNPLS SELSGAVGDL GTFIPIVLTL 50
TLVSNLDLST TLIFTGFYNI ATGLLFDIPM PVQPMKSIAA VAVSESPHLT 100
PSQIAAAGAS TAATLLLLGA TGAMSFLYNI IPLPVVRGVQ LSQGLQFAFT 150
AIKYVRFNYD TATLKPSSSP RIWLGLDGLI LALAALLFII LSTGSGNDRE 200
AEDGDLAETS SNESQSRRRR LRLLSSIPSA LIVFALGLVL CFIRDPSIFK 250
DLKFGPSKFH ILRISWDDWK IGFLRAAIPQ IPLSVLNSVI AVCKLSNDLF 300
DKELSATTVS ISVGVMNLIG CWFGAMPVCH GAGGLAGQYR FGARSGLSVI 350
FLGIGKLIVG LVFGNSFVRI LSQFPIGILG VLLLFAGIEL AMASKDMNSK 400
EDSFIMLVCA AVSMTGSSAA LGFGCGVVLYLLLKLRTLDCSSVTLFSRSSDE 450
SQVDSEAAPRDV*

S30:  0.30
S96:  1.31 T100: 2.50
T114: 0.23
Y154: 0.04 T163: 0.57 S169: 1.15 T193: 0.13 S195: 0.51
T209: 0.57 S211: 0.89 S214: 0.39
T415: 0.24 S417: 0.01 T444: 0.63
S457: 0.14
```

List of abbreviations and symbols

°C	degree Celsius
A. tumefaciens	*Agrobacterium tumefaciens*
AMP	ampicillin
AP	adaptor protein
ATP	adenosine triphosphate
BiFC	bimolecular fluorescence complementation
bp	base pair(s)
BSA	bovine serum albumin
Ca^{2+}	calcium-ion
CCV	clathrin coated vesicle
cDNA	complementary DNA
CDS	coding sequence
CIP	calf intestine alkaline phosphatase
Col-0	Columbia-0 (*Arabidopsis thaliana* ecotype)
COP	COAT PROTEIN
C-terminus	carboxy terminus
C(INT1)	*C*-terminus of AtINT1 (amino acids 469-509)
C(INT4)	*C*-terminus of AtINT4 (amino acids 550-582)
cf.	*conferre* (compare)
D	Germany
Da	Dalton
ddH_2O	double-distilled Millipore water
DEPC	diethyl pyrocarbonate
DNA	deoxyribonucleic acid
dNTP	deoxynucleoside triphosphate
E. coli	*Escherichia coli*

e.g.	*exempli gratia* (for example)
EDTA	ethylenediaminetetraacetic acid
EE	early endosome
EGTA	ethylene glycol-bis(β-aminoethyl ether)-N,N,N',N'-tetraacetic acid
ER	endoplasmic reticulum
EtBr	ethidium bromide
f	forward
FW	fresh weight
gDNA	genomic DNA
GFP	GREEN FLUORESCENT PROTEIN
GTP	guanosine triphosphate
GUS	ß-glucuronidase
h	hour
HAc	acetic acid
HBED	N,N'-di(2-hydroxybenzyl)ethylenediamine-N,N'diacetic acid monochloride hydrate
HEPES	4-(2-hydroxyethyl)-1-piperazineethanesulfonic acid
Hs	Homo sapiens
Hyg	Hygromycin
H^+	Proton
H_2O	millipore water
i.e.	id est
INT	inositol transporter
KAc	potassium acetate
KAN	kanamycin
kb	kilo base pairs
kDa	kilo Dalton
ko	knockout
LB-medium	Lysogeny broth / Luria broth
LB	left border
LD	long-day (16h light / 8h dark cycle)
LE	late endosome
M	molar concentration; mol/L (or single letter abbreviation for methionine)
max.	maximum
MES	2-(N-morpholino)ethanesulfonic acid
mg	milligram
mM	millimolar
Mm	Mus musculus
min	minute
mL	milliliter
MOT	molybdate transporter
MVB	multivesicular body
ng	nanogram
N-terminus	amino terminus
NRAMP	natural resistance-associated macrophage protein
OD	optical density
ON	over night
ONC	over-night culture
PBS	phosphate buffered saline
PCR	polymerase chain reaction
PEG	polyethylene glycol
PIP	plasma membrane intrinsic protein
PM	plasma membrane
Pro	promoter
PTR	peptide transporter
PVC	prevacuolar compartment
r	reverse
r_P	Pearson's correlation coefficient

r_S	Spearman's rank correlation
R	resistance
RNA	ribonucleic acid
RNase	ribonuclease
rpm	rounds per minute
RFP	RED FLUORESCENT PROTEIN
RT	room temperature
s	second
SD	short-day (8h light / 16h dark cycle)
SDS	sodium dodecyl sulfate
Spec	spectinomycin
ST	sialyl transferase
Strep	Streptomycin
SUC	sucrose transporter
SYP	syntaxin of plants
Spec	spectinomycin
TAIR	The Arabidopsis Information Resource
TE	Tris-EDTA
TET	tetracycline
TGN	*trans*-Golgi network
TM	transmembrane-
TP	tonoplast
TPC1	two-pore channel 1
Tris	2-Amino-2-hydroxymethyl-propane-1,3-diol
Tween	polyoxyethylene sorbitan monolaurate
T-DNA	transfer DNA
USA	United States of America
V	volume (if not referring to valine)
w	weight
WT	wild-type
α	alpha
β	beta
γ	gamma
δ	delta
ε	epsilon
λ	phage Lambda DNA
ζ	zeta
μ	mu
µL	microliter
µM	micromolar
σ	sigma

Abbreviations for amino acids: Three- and single-letter code

Amino acid	Three-letter code	Single-letter code	Amino acid	Three-letter code	Single- letter code
Glycine	Gly	G	Tryptophan	Trp	W
Proline	Pro	P	Histidine	His	H
Alanine	Ala	A	Lysine	Lys	K
Valine	Val	V	Arginine	Arg	R
Leucine	Leu	L	Glutamine	Gln	Q
Isoleucine	Ile	I	Asparagine	Asn	N

Methionine	Met	M	Glutamic Acid	Glu	E
Cystein	Cys	C	Aspartic Acid	Asp	D
Phenylalanine	Phe	F	Serine	Ser	S
Tyrosine	Tyr	Y	Threonine	Thr	T

Φ : bulky, hydrophobic amino acid, i.e. methionine, phenylalanine, leucine, isoleucine or valine
X : any amino acid
- : gap of indeterminate length

List of figures

List of tables

List of publications

Publications that resulted from this work:

Pertl-Obermeyer, H., Wu, X.N., Schrodt, J., Müdsam, C., Obermeyer, G., and Schulze, W.X. (2016). Identification of cargo for adaptor protein complexes AP-3 and AP-4 by sucrose gradient profiling. Mol. Cell. Proteomics **15:** 2877–2889**.**
doi: 10.1074/mcp.M116.060129

Müdsam, C., Wollschläger, P., Sauer, N., Schneider, S. (2017). AP4 dependent sorting of *Arabidopsis* NRAMP3 and NRAMP4 requires a dileucine-based motif. Traffic (*in revision*).

Declaration

Ich versichere, dass ich diese Arbeit ohne fremde Hilfe und ohne Benutzung anderer als der angegebenen Quellen angefertigt habe. Diese Arbeit hat in gleicher oder ähnlicher Form noch keiner anderen Prüfungsbehörde vorgelegen und ist von dieser nicht als Teil einer Prüfungsleistung angenommen worden. Ausführungen, die wörtlich oder sinngemäß aus anderen Arbeiten übernommen wurden, sind als solche gekennzeichnet.

Erlangen, July 2017 . . . . . .

Christina Müdsam